MINISTRY OF EDUCATION AND SCIENCE, YOUTH AND SPORT OF UKRAINE

Odessa I. I. Mechnikov National University

ФОТОЭЛЕКТРОНИКА

PHOTOELECTRONICS
INTER-UNIVERSITIES SCIENTIFIC ARTICLES

Founded in 1986

Number 21

Odessa
2012

«PHOTOELECTRONICS»
№ 2 1 – 2 0 1 2

INTER-UNIVERSITIES SCIENTIFIC ARTICLES

Founded in 1986

Certificate of State Registration KB № 15953

«ФОТОЭЛЕКТРОНИКА»
№ 21–2012

МЕЖВЕДОМСТВЕННЫЙ НАУЧНЫЙ СБОРНИК

Основан в 1986 г.

Свидетельство о Государственной регистрации КВ № 15953

UDC 621.315.592:621.383.51:537.221

The results of theoretical and experimental studies in problems of the semiconductor and microelectronic devices physics, opto- and qantum electronics, quantum optics, spectroscopy and photophysics of nucleus, atoms, molecules and solids are presented in the issue. New directions in the photoelectronics, stimulated by problems of the super intense laser radiation interaction with nuclei, atomic systems and substance, are considered. Scientific articles «Photoelectronics» collection abstracted in ВИНИТИ and «Джерело».

The issue is introduced to the List of special editions of the Ukrainian Higher Certification Commission in physics-mathematics and technical sciences.

For lecturers, scientists, post-graduates and students.

У збірнику наведено результати теоретичних і експериментальних досліджень з питань фізики напівпровідників та мікроелектронних приладів, опто- та квантової електроніки, квантової оптики, спектроскопії та фотофізики ядра, атомів, молекул та твердих тіл. Розглянуто нові напрямки розвитку фотоелектроніки, пов'язані із задачами взаемодії надінтенсивного лазерного випромінювання з ядром, атомними системами, речовиною.

Збірник включено до Переліку спеціальних видань ВАК України з фізико-математичних та технічних наук. Збірник «Photoelectronics» реферується у ВІНІТІ (Москва) та «Джерело» (Київ).

Для викладачів, наукових працівників, аспіранітв, студентів.

В сборнике приведены результаты теоретических и экспериментальных исследований по вопросам физики полупроводников и микроэлектронных приборов, опто- и квантовой электроники, квантовой оптики, спектроскопии и фотофизики ядра, атомов, молекул и твердых тел. Рассмотрены новые направления развития фотоэлектроники, связанные с задачами взаимодействия сверхинтенсивного лазерного излучения с ядром, атомными системами, веществом.

Сборник включен в Список специальных изданий ВАК Украины по физико-математическим и техническим наукам. Сборник «Photoelectronics» реферируется в ВИНИТИ (Москва) и «Джерело» (Киев).

Для преподавателей, научных работников, аспирантов, студентов.

Address of editorial board:
Odessa I. I. Mechnikov National University 42, Pasteur str., Odessa, 65026, Ukraine
e-mail: wadz@mail.ru, tel.: +38-0482-7266356.
Information is on the site: http://www.photoelectronics.onu.edu.ua

TABLE OF CONTENTS:

UDC 548:539.32, 534.222.2

A. P. Onanko, O. V. Lyashenko, G. T. Prodayvoda, S. A. Vyzhva, Y. A. Onanko

Taras Shevchenko Kyiv national university, Volodymyrs'ka str., 64, Kiev, 01601, Ukraine,
e-mail: onanko@univ.kiev.ua

INFLUENCE MECHANICAL TREATMENT, ELECTRICAL CURRENT, CHANGING OF DEFECT STRUCTURE ON INELASTIC CHARACTERISTICS OF Si + SiO_2 WAFER-PLATES, GeSi AND SiO_2

The method is created for nondestructive control of structure defects in semiconductors plates, which determines the integral density of structure defects, their distribution and the broken layer from the internal friction difference of free elastic vibrations on neighboring harmonics f_1 and f_2. The dislocation density and the broken layer are measured from the curve of dependence for plates Si + SiO_2. The results of influencing of direct and variable electrical current at simultaneous influence of ultrasonic deformation on internal friction and the elastic module of crystal GeSi after cutting and polishing were studied. The decreasing of elastic module and the raise of internal friction was obtained under condition when the critical value of the electrical current is exceeded.

Introduction

Internal friction (IF) depends essentially from nature and density of structure defects. IF depends on different relaxation processes, that connected with plate defect structure. The local heterogeneities are the factor, which gains strength the influence of direct current I on state of impurities in GeSi. The measuring of amplitude dependent IF (ADIF) can be used as the highly sensitive control method of nanoplastic deformation GeSi crystals. The measuring of ADIF allows to fix the moment of tearing away of dislocation segments L_C from stops. Therefore the purpose of this work was a study of influence of electrical current I on tearing away from the stops of dislocation segments L_C during simultaneous ultrasound deformation σ_{US} GeSi crystals with orientation [111] after mechanical cutting and polishing.

Experiment

For measuring of the temperature dependences of IF $Q^{-1}(T)$ and elastic module E(T) of mono crystal GeSi of orientation [111] with sizes 2x2x16 mm^3 with the dislocation density $N_d \approx 10^8$ m^{-2} after cutting and polishing the methods of complete piezoelectric oscillator on frequency $f \approx 118$ kHz and bending resonance vibrations on frequency $f \approx 1$ kHz during alternative deformation $\varepsilon \approx 10^{-6}$ in vacuum $P \approx 10^{-3}$ Pa were used [1-3]. The measuring error of IF was $\Delta Q^{-1}/Q^{-1} \approx 10\%$ and the elastic module relative changing was $\Delta E/E_o \approx 0{,}1\%$. The temperature dependencies of IF $Q^{-1}(T)$ and elastic module E(T) experimentally simultaneously were measured, that are allowed more exactly to determine the critical deformation amplitude ε_σ^*, at which the dislocation segments average length $\bar{L}_C$ tear off from stops — point defects. The high exactness of the elastic module E measuring, especially its relative changing, is conditioned the high exactness of determination resonance frequency specimen oscillation f.

The method of determining the integral density structure defects mono crystal discs Si + SiO_2 — plates, which were element of metal- dielectric-semiconductor (MDS) — structure at manufacturing the big integral schemes (BIS) for industrial express operation technology control of structure perfection of multilayer epitaxial structures and the increase of reliability valid p-n crossing was created.

The method and the machinery were developed for nondestructive for the control of the structure defects semiconductors plates, which permit on IF difference ΔQ^{-1} free elastic vibrations on neighboring harmonics f_1 and f_2 to determine the integral density of structure defects N_d, their distribution and the broken layer h_b. It is necessary take into account attenuation, arising as a result of absorption of elastic mechanical vibrations energy – IF and of fastening of plate at examination the vibrations of disks with recording of their structure imperfections. In developed acoustic machinery for operation control at manufacture of semiconductor devices the research plate - disk with thickness h » 500 μm and diameter D = 100÷200 mm fasten off in centre and electrostatic method in it are excited the elastic umbrella vibrations. The measuring of difference IF $\Delta Q^{-1} = Q^{-1}_1 - Q^{-1}_2$ on different frequencies f_1 and f_2 takes to minimum measuring error. The method and the machinery were developed – machinery, that generate elastic bending vibrations in disk for study of free elastic vibrations in disks Si + SiO_2 – plates, which are fastened in centre. The principle of machinery work is consisting. The variable voltage U gives to the disk and capacitive gage, which is on distance d = 50÷100 μm. Resonance elastic bending free vibrations, umbrella type, are excited at coincidence of frequency electrical value with own frequency f ≈ 1 kHz. The capacitive gage is for generation and receiving of free vibrations of disk. Own frequency f vibrations of disk and IF are determined with help electronic frequency meter and amplitude discriminator, which makes way for the value in given amplitude interval from A_1 to A_2.

Results and discussion

The research results of elastic US wave's absorption are on imperfections of crystal structure after mechanical, temperature and radiation treatments. There are studied the kinetics of structure defects annealing. This method may be used for the control of structure defects Si, Si + SiO_2, GaAs plates after technological mechanical, temperature and radiation treatments. The measuring results are presented on fig. 1 and fig. 2. The dependence of IF difference ΔQ^{-1} in Si + SiO_2 plate with orientation (111), diameter D ≈ 60 mm and thickness h ≈ 500 μm on neighboring harmonics f_1 and f_2 from the dislocation density N_d is presented on fig. 1. The integral dislocation density after different treatments changes in limits $N_d = 10^2 \div 10^5$ sm^{-2} on fig. 1.

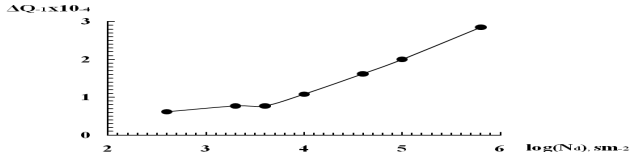

Fig. 1. Dependence of internal friction difference ΔQ^{-1} of Si + SiO_2 plate with orientation (111) from the dislocation density N_d

IF difference $\Delta Q^{-1} = Q^{-1}_1 - Q^{-1}_2$ on different frequencies f_1 and f_2 deposit on vertical axis, and on horizontal – dislocation density N_d. The dislocation density N_d was determined by standard etch-pit method for construction of the calibration graphic. Specimens Si + SiO_2 were washing in alcohol and in distilled water before etching. The using of method layer-specific polishing, which alternate with chemical etching at T = 290 K in Sirtl etching agent $Cr_2O_3 : H_2O : HF = 1 : 2 : 3$, allow to observed, that US treatment (UST) hardens the layer, which ranges from surface on depths h » 100000 nm. The etch pits for vacancy clusters V-V-V were disappeared on this depth. The etch pits were oval, rounded form, which connected with presence in near-surface crystal layers vacancy clusters, coagulants of diffuse impurities on surface Si specimens after UST. The dependence of difference IF ΔQ^{-1} Si plate with diameter D ≈ 60 mm and thickness h ≈ 500 μm on neighboring harmonics f_1 and f_2 from the broken layer depth h_b, that was created by the polishing of Si plates with help of diamond pastes with different grain was studied. The broken layer depth h_b were measured by roentgen method. The IF difference ΔQ^{-1} Si plate with diameter D ≈ 60 mm and thickness h ≈ 500 μm on neighboring harmonics f_1 and f_2 linear increases with the broken layer depth h_b can see from fig. 2. The broken layer depth is presents on curve fig. 2 and was changing in limits h_b = 1000÷3000 nm.

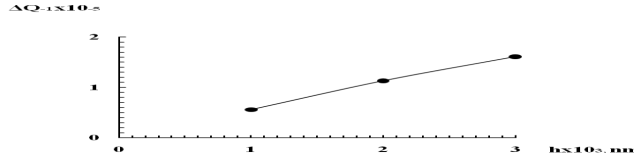

Fig. 2. Dependence of internal friction difference ΔQ^{-1} of Si + SiO_2 plate with orientation (111) from the broken layer h_b

The solution of differential equation of round disks vibrations under action of periodical external force allow to get circular resonance frequency of disc free vibrations [1]:

$$\omega = \frac{\beta}{R^2}\sqrt{\frac{D}{\rho h}}. \quad (1)$$

It is necessary take into account that the attenuation arise as a result of the attaching of plate and absorption of mechanical vibrations energy – IF at examination of resonance frequency ω. IF обусловлено different relaxation processes, that connected with plates defect structure. The account of dispersion of elastic mechanical vibrations energy of Si+SiO_2 plate on the structure defects results in expression for frequency of disk free vibrations [1]:

$$\omega = \sqrt{\frac{D\beta^2}{\rho h R^4} - 2\pi^2\left(\frac{Q^{-1}}{T}\right)^2}, \quad (2)$$

where cylindrical inflexibility of disc *D*, determined through the elastic module E, plate thickness h and Puasson coefficient μ:

$$D = \frac{Eh^3}{12(1-\mu)^2}, \quad (3)$$

$$\mu = \frac{(\frac{1}{2}V_{\updownarrow}{}^2 - V_{\leftrightarrow}{}^2)}{(V_{\updownarrow}{}^2 - V_{\leftrightarrow}{}^2)} \quad (4)$$

where $V_{\updownarrow}$ — longitudinal velocity US of elastic wave, $V_{\leftrightarrow}$ — quick shear velocity US of elastic wave. β — is dimensionless coefficient, the value of which depends on the number of key circumferences, ρ – the specific density of plate, R — the disk radius, Q^{-1} — IF, T — the disk vibrations period. The measuring of vibrations resonance frequency f allow to determine the elastic module E plate (without attenuation recording) on formula [1]:

$$E = \frac{12\rho\omega^2 R^4(1-\mu)^2}{\beta^2 h^2}. \quad (5)$$

IF was measured in regime of free attenuate vibrations on formula [4,5]:

$$Q^{-1} = \frac{\ln\left(\frac{A_1}{A_2}\right)}{\pi N}, \quad (6)$$

where A_1 and A_2 – upper and lower discrimination level accordingly, N — number of free vibrations at amplitude decreasing from A_1 to A_2.

The parameters of vibrations on neighboring harmonics f_1 and f_2 were measured for exclusion of contribution in IF, which depend on the attaching of plate — disk in centre. The changing from first harmonic f_1 to second f_2 without transposition the plate allow to except the instrumental errors, which connected with it fastening in centre. The measured losses of mechanical vibrations energy of plate consist from two summands: own IF plates Q^{-1}_p and IF instrumental losses Q^{-1}_o, which connected with fastening of plate. The difference of measured loss mechanical vibrations energy on two neighboring harmonics f_1 and f_2 is equal the difference of values IF on this frequencies $\Delta Q^{-1} = Q^{-1}_1 - Q^{-1}_2$, and instrumental losses are reduced. There was a small value of IF background in SiO_2 $Q_o^{-1} \approx 2\cdot10^{-6}$ to T < 385 K. In comparison of results on the same Si + SiO_2 plate on propose method h_b = 7000±1000 nm and with standard roentgen method h_b = 6000±5000 nm, at that productivity of experiment increase on two order.

The influence of the external fields (electrical and magnetic) is possible to explain on IF within the framework of string dislocation mechanism of elastic vibrations attenuation in GeSi, designing the motion of the charged dislocations in these fields. Will consider GeSi crystal with orientation [111], which periodic mechanical tension $\tau = \tau_0 e^{i\omega_0 t}$ is added to, and which is under the combined influence of external electric field $\vec{E}$ and external magnetic field $\vec{B}$. If dislocation segment $\xi(x, y)$, that are vibrated under the act of tension τ, is charged, additional forces will operate on it $\vec{F}_e = e\rho(\xi)\vec{E}$ and $\vec{F}_m = e\rho(\xi)[\frac{\partial \xi}{\partial t}, \vec{B}]$, where $\rho(\xi)$ - is the distribution function of electrical charge density on the dislocation segment.

The system of equations, which describes the movement of the charged dislocation under act of the mechanical, electrical **E** and magnetic **B** fields, within the framework of string dislocation model acquires the following kind:

$$M\frac{\partial^2\xi}{\partial t^2} = V_d\frac{\partial^2\xi}{\partial x^2} - Q\frac{\partial\ \xi}{\partial t} + b\tau - b\tau_a - N_j\frac{\partial U}{\partial\xi} + \\ + e\rho(\xi)E + e\rho(\xi)[\frac{\partial\ \xi}{\partial t}, B], \quad (7)$$

$$\frac{\partial^2\tau}{\partial y^2} - \frac{\rho}{G}\frac{\partial^2\tau}{\partial t^2} = \rho b\frac{\partial^2}{\partial t^2} < \int_0^\infty\ [\int_0^l\ \xi(x)dx]N(l)dl >, \quad (8)$$

where $\left(M\cdot\frac{\partial^2\xi}{\partial\ t^2}\right)$ — inertial force, $M \approx \rho b^2$ — effective mass of unit of dislocation length, ρ — crystal density, b — Byurgers vector, t — time, $\left(V_d\cdot\frac{\partial^2\xi}{\partial x^2}\right)$ — force which is conditioned effective strain of bended dislocation line, $V_d \approx G b^2$ for screw dislocations and $V_d \approx \frac{Gb^2}{(1-\mu)}$ for line dislocations, G — the displacement module, $\left(Q\cdot\frac{\partial\ \xi}{\partial\ t}\right)$ — the force of the viscid braking, Q — damping constant or coefficient viscid braking, $b\tau$ — external force, which operates on unit of dislocation length, $b\tau_a$ — force, which operates on unit of dislocation length and tensions is conditioned, which arise up as a result of potential pattern of crystalline grate, $\left(N_j\cdot\frac{\partial U}{\partial\xi}\right)$ — force, which operates on unit of dislocation length from the side of point defects, which co-operate with dislocation and located on dislocation line with the density $N_j(x)$, $U(\xi)$ — potential energy of co-operation, l – length of dislocation segment, $N(l)$ — the distributing function of dislocation segments for lengths, which is conditioned $N_j(x)$.

Practically interesting is a case, when the external electrical and magnetic fields are periodic, that: $E = E_0 e^{i\omega_E t}$, $B = B_0 e^{i\omega_M t}$. When the variable electrical current density $J^{\sim}$ is the same ultrasonic (US) frequency $\omega_J = \omega_{US}$. Examinations for influence of $J^{\sim}$ on IF $Q^{-1}(J^{\sim})$ on fig. 3 and elastic module $E(J^{\sim})$ on fig. 4.

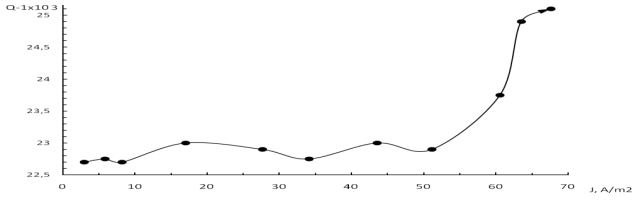

Fig. 3. Current dependence internal friction $Q^{-1}(J)$ in GeSi of orientation [111] with the dislocation density $N_d \approx 10^8$ m^{-2} after cutting and polishing from variable electrical current with frequency equal US frequency $\omega_I = \omega_{US}$ at T = 296 K and constant amplitude US deformation $\varepsilon_{US} \approx 2\cdot10^{-6}$

The variable electrical current J˜, which flowed through the sample, was in the phase with the voltage, which applied on piezoelectric vibrator to make ultrasonic strain σ_{US}.

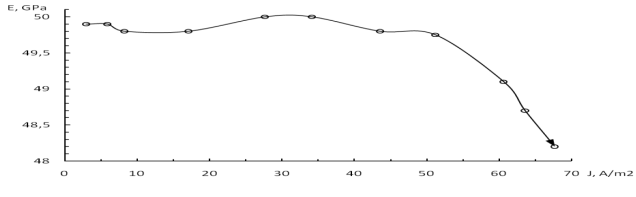

Fig. 4. Current dependence elastic module $E_{111}(J)$ of GeSi after cutting and polishing from variable electrical current with $\omega_I = \omega_{US}$ at T = 296 K and constant amplitude US deformation $\varepsilon_{US} \approx 2\cdot10^{-6}$

As one can see from fig. 5, for variable electrical current $J^{\sim}$ when the critical value $J^*_{\sigma} \approx 60\cdot10^3$ A/m^2 realized the raise of IF $Q^{-1}(J^{\sim})$ with simultaneous the decrease the value of elastic module $E(J^{\sim})$ is observed at the subsequent increase of variable current.

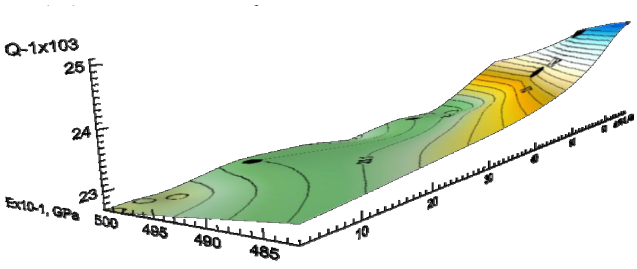

Fig. 5. Current dependence internal friction $Q^{-1}(J)$ and elastic module $E_{111}(J)$ (indicatory surface of inelasticity-elasticity body) GeSi after cutting and polishing from variable electrical current with frequency equal ultrasound frequency $\omega_I = \omega_{US}$ at T = 296 K

For explanation of correlation $Q^{-1}(J)$ and E(J) one can see equations (7) and (8). Compare the equations (7) and (8) with the experimental results on fig. 3, fig. 4 and fig. 5 made conclusion, that the influence performance of electrical current on IF $Q^{-1}(J^{\sim})$ and elastic module $E(J^{\sim})$ sharply increasing, when variable electrical current with frequency equal US frequency $\omega_J = \omega_{US}$.

The increasing of IF $Q^{-1}(J)$ is related to that the electrons of certain energy co-operate with the dislocation segments L_C, which vibrate under the action of US deformation ε_{US}, and assist in their tearing away from stops – point defects. The changing of absolute value US deformation amplitude ε_{0US} did not influence on quality motion of IF dependence from the electrical current $Q^{-1}(J)$, although here US deformation amplitude changed to $\varepsilon_{0US} \approx 4 \cdot 10^{-6}$, at the same time at temperatures to T < 470 K there was ANDIF. The diminishing of critical value current J_{σ}^{*} at the increase of temperature testifies that the thermofluctuations vibrations of dislocation segments L_C grow with temperature T growth, which in same allows the lesser stream of electrons to tear away dislocations from stops. The changing of steepness of curves dependences IF from the current $Q^{-1}(J)$ during constant US deformation on fig. 3 can be consider as an indicator of tearing-fixing away of dislocations. An eloped direct and reverse motions of dependence IF from the current $Q^{-1}(J)$ represents the absence of irreversible changes of dislocation structure in the process of measuring IF. 3D atomic-force microscopy (AFM) of microstructure image of GeSi with orientation (111) is represented on fig. 6.

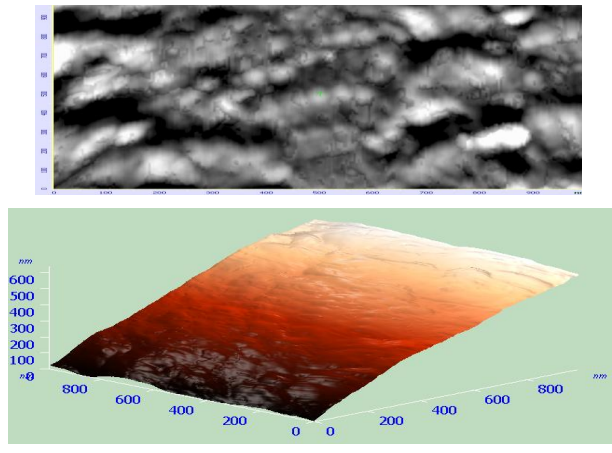

Fig. 6. 3D atomic-force microscopy of microstructure image of GeSi with orientation (111) (1x1 mkm)

The shallow dispersion fleshy plain surface, the intergrowth of little islands are observed, their configuration are rounded. The crystal sites have the fragmentary structure, which formed from weakly disorient one from another islands.

The single-row chain of impurity atoms under super-plane can't provide all relaxation of dislocation elastic field σ_i [6,7].The impurity atoms Si accumulate in planes, which perpendicular to dislocation line, to full compensation of it's field σ_i [8-10]. The beginning of temperature dependence IF $Q^{-1}(J,\varepsilon,T)$ correspond to peripheral atoms Si going out of stopper atmosphere, that reduce attaching effect of dislocation segments L_C. The resorption of atmospheres around stoppers take place at further increasing of temperature. The increase of length between stoppers – the increasing of the middle effective dislocation segments length L_C begins after completion this process. When the resorption of impurity atmospheres near the stoppers finished, IF $Q^{-1}(J,\varepsilon,T)$ intensive decrease with temperature increasing. The values of critical amplitude deformation ε_{σ}^{*} are stabilizing at temperature T, which correspond to full absence of fixing centres. It's showed, that inelastic Q^{-1} and elastic E characteristics are essentially depended from morphology of surface layer. 3D atomic-force microscopy (AFM) of microstructure image of Si + SiO_2 with orientation (100) is represented on fig. 7.

AFM are testified the presence of wafer-plate relief. There are many defects at film from abroad the influence of wafer-plate, which formed at increasing of islands. The structure defects don't to skin over in time at first growth stages at little film thickness h ≤ 1000 nm.

Conclusion

Thus, the studying of structure defects influence on attenuation of elastic vibrations in Si + SiO_2 plates allow to estimate the degree of crystal structure perfection. The maximal error of definition of dislocation density N_d don't exceed 1,5÷2 twice, that in combination with small measured time allow to use the modify method for experiment. The integral dislocation density in limit $N_d = 10^6 \div 10^9$ m^{-2} and broken layer depths in limit $h_b = 0 \div 40000$ nm were measured from calibrating curves for Si + SiO_2 plates. The measuring of IF background Q^{-1}_0 after different heat, mechanical, radiation treatments gives information about the changing of the thermoelastic strains fields σ_i in Si+SiO_2, GeSi plates. The growth of IF maximums heights Q_M^{-1} testifies the growth of structural defects concentration, and the broadening of IF maximums ΔQ_M^{-1} represents the relaxation processes of structural defects new type.

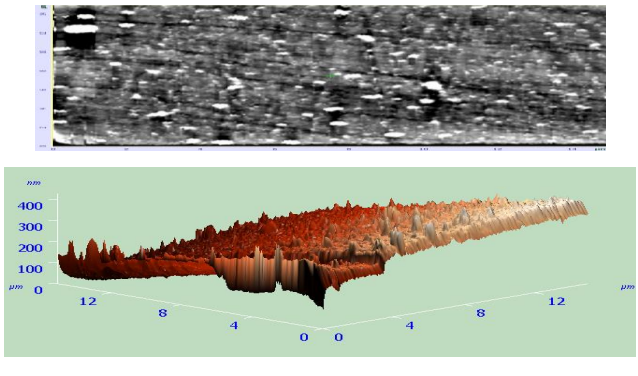

Fig. 7. 3D atomic-force microscopy of microstructure image of Si + SiO_2 type KDB-6.0 with orientation (100) (15x15 mkm)

It is found out in crystal GeSi with orientation [111] the influence of direct J and variable electric current $J^{\sim}$ on growth of IF $Q^{-1}(J)$ and on the simultaneous diminishing of absolute value of the elastic module E(J), that may be related to that the electrons of certain energy co-operate with dislocation segments L_C under US deformation ε_{US} and is instrumental in their tearing off from points defects. It is obtained, that at presence of variable electrical current with the same frequency and phase, as the strain, that leads to US deformation ε_{US}, the critical value of variable current $J^{*\sim}_{\sigma}$ is nearly by an order of magnitude lesser, than in case of direct current J^{*}_{σ} , which is necessary to observe the same IF $Q^{-1}(J)$ raise at increasing of direct current. It is suggested the highly sensitive method of nanoplasticity deformation control of GeSi crystals by measuring of amplitude dependent IF.

References

1. *Landau L. D., Liphshic E. M.* Theory of elasticity. — M.: Nauka, 1999 — P. 364 .
2. *Lyashenko O. V. , Onanko A. P., Veleschuk V. P. et al*. Structural defects relaxation during complex thermal and dynamical mechanic processing of CdTe // Photoelectronics. — 2008. — № 17. — P. 10-13.
3. *Onanko A. P.* Influence of hydrogen on directional surface of inelastic-elastic body $Ti_{0.5}Al_{0.5}$ alloy // Metalphysics and new technology. — 2011. — V. 33, № 2. — P. 253-261.
4. *Novik A., Berri B.* Relaxation phenomena in crystals. — M.: Atomizdat, 1995. — P.472 .
5. *Nikanorov S. P., Kardashev B. K.* Elasticity and dislocation inelasticity of crystals. — M.: Nauka, 1995. — P.253 .
6. *Shpak A. P., Kunickiy Y. A., Karbovskiy V. L.* Clusters and nanostructure materials. — Kyiv: Academy periodic, 2001. — P.588 .
7. *Molodkin V. B., Nizkova A. I., Shpak A. P. et al.* Difractometria nanosize defects and geterolayers in crystals. — Kyiv: Academy periodic, 2005. — P.364 .
8. *Azarenkov N. A., Beresnev V. M., Pogrebnyak A. D.* Structure and properties of protective covering and modify materials layers. — Charkov: CNU, 2007. — P.560 .

9. V*laskina S. I., Svechnikov G. S., Smintina V. A.* Films of silicon carbide. — Odesa: Astroprint, 2007. — P.104 .

10. *Smintina V. A.* Physics-chemical phenomena on solid state surface. — Odesa: Astroprint, 2009. — P.191

.

UDC 548:539.32, 534.222.2

Onanko A. P., Lyashenko O. V., Prodayvoda G. T., Vyzhva S. A., Onanko Y. A.

INFLUENCE MECHANICAL TREATMENT, ELECTRICAL CURRENT, CHANGING OF DEFECT STRUCTURE ON INELASTIC CHARACTERISTICS of Si + SiO_2 wafer-plates, GeSi and SiO_2.

Abstract

The method is created for nondestructive control of structure defects in semiconductors plates, which determines the integral density of structure defects, their distribution and the broken layer from the internal friction difference of free elastic vibrations on neighboring harmonics f_1 and f_2. The dislocation density and the broken layer are measured from the curve of dependence for wafer-plates Si + SiO_2. The results of influencing of direct and variable electrical current at simultaneous influence of ultrasonic deformation on internal friction and the elastic module of crystal GeSi after cutting and polishing were studied. The decreasing of elastic module and the raise of internal friction was obtained under condition when the critical value of the electrical current is exceeded.

Keywords: semiconductor wafer-plate, structure defects, ultrasound deformation, internal friction, elastic module.

УДК 548:539.32, 534.222.2

Онанко А. П., Ляшенко О. В., Продайвода Г. Т., Вижва С. А., Онанко Ю. А.

ВПЛИВ МЕХАНІЧНОЇ ОБРОБКИ, ЕЛЕКТРИЧНОГО ТОКУ, ЗМІНИ ДЕФЕКТНОЇ СТРУКТУРИ НА НЕПРУЖНІ характеристики підкладок Si + SiO_2, GeSi и SiO_2

Резюме

Для неруйнівного контролю структурних дефектів напівпровідникових пластин розроблена методика, що дозволяє по різниці внутрішнього тертя вільних пружних коливань на сусідніх гармоніках f_1 і f_2 визначати інтегральну щільність структурних дефектів, їх розподіл і глибину порушеного шару. Для підкладок Si + SiO_2 зміряна інтегральна щільність дислокацій і глибина порушеного шару по градуювальній кривій. Розглянутий вплив постійного і змінного електричного току при одночасній дії ультразвукової деформації на внутрішнє тертя і модуль пружності монокристала GeSi після різання і шліфування. Виявлено зменшення модуля пружності і зростання внутрішнього тертя досягши критичної величини електричного току.

Ключові слова: напівпровідникова підкладка, структурні дефекти, ультразвукова деформація, внутрішнє тертя, модуль пружності.

УДК 548:539.32, 534.222.2

Онанко А. П., Ляшенко О. В., Продайвода Г. Т., Выжва С. А., Онанко Ю.

ВЛИЯНИЕ МЕХАНИЧЕСКОЙ ОБРАБОТКИ, ЭЛЕКТРИЧЕСКОГО ТОКА, ИЗМЕНЕНИЯ ДЕФЕКТНОЙ СТРУКТУРЫ НА НЕУПРУГИЕ характеристики подложек Si + SiO_2, GeSi и SiO_2

Резюме

Для неразрушающего контроля структурных дефектов полупроводниковых пластин разработана методика, позволяющая по разности внутреннего трения свободных упругих колебаний на соседних гармониках f_1 и f_2 определять интегральную плотность структурных дефектов, их распределение и глубину нарушенного слоя. Для подложек Si + SiO_2 измерена интегральная плотность дислокаций и глубина нарушенного слоя по градуировочной кривой. Рассмотрено влияние постоянного и переменного электрического тока при одновременном действии ультразвуковой деформации на внутреннее трение и модуль упругости монокристалла GeSi после резки и шлифовки. Обнаружено уменьшение модуля упругости и рост внутреннего трения при достижении критической величины электрического тока.

Ключевые слова: полупроводниковая подложка, структурные дефекты, ультразвуковая деформация, внутреннее трение, модуль упругости.

UDC 54.03

V. S. Grinevych, V. A. Smyntyna, L. M. Filevska,

Odessa I. I. Mechnikov National University, 2 Dvoryanskaya str., Odessa 65082, Ukraine
e-mail: grinevich@onu.edu.ua, lfilevska@gmail.com

INFLUENCE OF A PRECURSOR PROPERTIES ON THE SURFACE MORPHOLOGY OF NANOSCALE TIN DIOXIDE FILMS

The work presents the results of the nanosize tin dioxide films' surface morphology investigation which is dependent on the precursor complex's technological properties used for their production. The used precursors differ only due to the technology of their preparation at the final stage. This defines the presence of the bound water in their composition. The water acts as a looser at the thermal decomposition which gives the possibility to obtain the nanosized films with nano grains of different sizes dependently on the precursor's type.

INTRODUCTION

Thin films of oxide materials with nano-sized grains are widely used as sensors in modern gas analyzers, the transparent electrodes for solar cells, catalysts of the oxidation processes [1-3]. The well-known production method for nano-size tin dioxide, as well as other metal oxides, for sensitive elements of sensors are liquid-phase chemical methods: sol-gel method, chemical precipitation from solution, etc. [4,5] The basic process for such technologies is the decomposition of thermally unstable tin compounds to form tin dioxide as the final product. The small number of such compounds, as well as limited and contradictory literature data on their physical and chemical properties causes the necessity for selection of a suitable precursor for nanosized tin dioxide.

In [6] we have proposed a technique for obtaining SnO_2 films based on the method of chemical precipitation from solution using polyvinyl acetate (PVA) as structuring agents. The films investigated in the present work were obtained by this method. Complex based on Bis(acetylacetonato)dichlorotin (BADCT) served as a precursor of tin dioxide. According to [7] this compound ($Sn(C_5H_7O_2)_2Cl_2$) was firstly obtained in 1903. In the literature [8-10] obtaining BADCT was reported using chloroform or dry toluene [9] as a solvent. The peculiarity of our method is using of water as a solvent. Characterization of BADCT obtained by our method is shown in [11].

In [12] it was reported on preparation of ZrO_2 thin films using such compounds, namely, zirconium acetylacetonate. Using a BADCT based complex prepared by our original method gives a thin transparent film of tin dioxide with nano-sized grains [13]. Precursor complexes necessary for comparative studies were obtained by two methods, differing only at the latest technological stage: the drying process. A comparative study of these precursor complexes were fulfilled using thermogravimetric methods [13]. Supposedly the different drying processes determine conservation of water molecules in the precursor complex which influences the structure and morphology of the resulting film. The principal goal of the present work is the investigation of the mentioned precursor's peculiarities influence on the surface morphology of the obtained tin dioxide films.

METHODS OF FILMS PRODUCTION AND INVESTIGATIONS

Samples for the investigation were prepared by the technique described in [6]. Bis(acetylacetonato)dichlorotin (BADCT) was used as a tin dioxide precursor [11]. Initially it was a preparation of the precursor: the production solution N1 was prepared of 50 ml (0,5 mol) of

acetilaceton dissolved in 250 ml of the distilled water and then put away for 24 hours for full dissolution. Next, the production solution N2 was prepared of 14ml (0,12 mol) of tin tetrachloride and 50 ml of cold (2-5°) distilled water. Further, the production solutions N1 and N2 were mixed adding 5 ml of 20% of aqueous NH_3 solution. The mixture obtained was being mixed for two hours by the magnetic mixer which resulted in deposition of thick white sediment. 600 ml of distilled water was added to it. After 10-15 minutes of settling the upper layer was decanted. The sediment was separated by the vacuum filtering by the Shott filter (residue pressure P = 500 mm Hg) then washed by the distilled water and dried up at 20-25°C during 3 days. Finally, it was washed by benzyl and dried up for 5-6 hours at 60°C: complex N1 in the air, and complex N2 — in vacuum.

This difference of these two complexes has become their principle production peculiarity which was investigated in the present work due to its influence on the topology properties of the films.

Freshly prepared BADCT was dissolved in acetone at different concentrations, then equal volumes of each solution were mixed with the same volumes of Polyvinlyacetate (PVAC) solutions in acetone prepared at different PVAC concentrations. The mixtures were then sprayed onto the microscope cover glass of 22 mm x22 mm size. Samples were kept at room temperature for about 15 minutes to allow the removal of acetone prior to annealing them at 600 °C for 6 hours in air for the thermal decomposition of organic components of the film (BADCT and PVAC) and subsequent removal of decay products. Removal of organic components was confirmed by our thermogravimetric studies of the precursor [11] and by the data [14] on the PVAC decomposition at temperatures above 200 °C, particularly in the presence of catalytic oxides (tin dioxide in our case). After annealing, the tin dioxide film was left on the substrate. PVAC was employed to structurize the film during the removal of its decay products.

The tin dioxide layer's surface morphology was investigated by the industrial Atom Force microscope (AFM) Nano Scope 111a (Digital instruments, USA). The measurements were fulfilled by siliceous probe with a nominal radius ~10 nm (the production firm NT-MDT, Russia) in a regime of periodical contacts (Tapping Mode™). The investigated surface area was in the interval of 500x500 nm^2 to 45x45 mkm^2.

RESULTS AND DISCUSSION

Figure 1 shows the AFM-image of the tin dioxide films surface morphology obtained from the precursor complex number 1. The higher points at Fig. 1, correspond to the lighter parts of the snapshot, the dark parts reflects the deeper zones. Amount of precursor in the initial solution was 1 and 5 wt %.

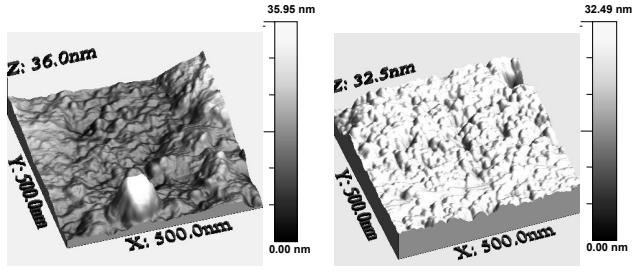

a b

Fig. 1. AFM-images of the surface morphology of tin dioxide films obtained from precursor complex number 1. The content of the precursor in the original solution: a — 1 wt %, b — 5 wt %.

As it can be seen from the images obtained for the complex number one, the film of tin dioxide has a well-developed surface and structured at a nanoscale. The minimal grains' size, visible in the images is in the interval from 10 to 15 nm. One may notice that the films' thickness visually evaluated increases with the precursor's concentration increasing.

Figure 2 shows the AFM-images of the surface of tin dioxide films obtained from precursor complex number 2 (dried in vacuum). As in the previous case, the precursor's content in the initial solution was 1 and 5 wt%.

As it can be clearly seen at the figures, the films have developed surfaces and are composed of agglomerate groups of different sizes, mostly of columnar structure. The crystallites grain sizes in the films (precursor number 2) is an average from 200 nm (at lower concentrations) to 500 nm and more (with a greater concentration of the precur-

sor), which is in strict correspondence with AFM image scaling. Consequently, there is a definite dependence of the morphology and grain sizes in the films on the concentration of the initial solutions for films obtained. The high concentrations of tin dioxide precursor in the films gave the larger crystallites.

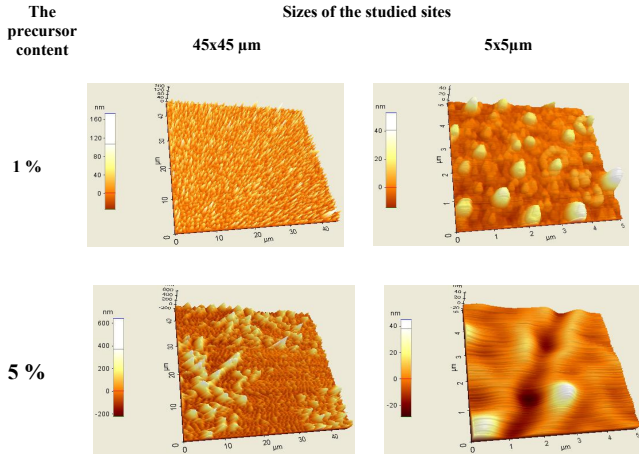

Fig. 2. AFM-images of the surfaces of tin dioxide films obtained from precursor complex number
2. The precursor content and the sizes of the studied sites are indicated.

The images of Figures 1 and 2 comparison shows that the hydrated precursor (complex number 1) gives films with smaller grain size of 10-20 nm. At the same time, the grain sizes of the films obtained from a complex number 2 (anhydrous DHDAO) were 200-500 nm. Hence, the present studies support the idea that a complex of hydrated precursor is preferable in production of tin dioxide films of smaller (nanoscale) grain size, and therefore the more developed surface morphology.

CONCLUSION

The studies of tin dioxide films' surface morphology obtained from two different precursor complexes had established a significant effect of even small differences in the process of obtaining of tin dioxide precursor on the morphology of the surface and structure.

It was found that differences in the drying process used in the production of precursor complexes' films are the significant factor in the topological features of the films. The main feature which defines this influence is the bound water in the precursor's composition.

At the complex thermal decomposition, the water, which is in its composition acts as a loosener, which allows to obtain tin dioxide films with nanograins of different sizes, depending on the precursor's type. Consequently, the use of a complex containing a hydrated precursor (№ 1) should be preferable in obtaining nano-sized tin dioxide films with a well-developed surface, thus providing high sensitivity of its physical parameters to the environmental changes and, and therefore, widely used as sensors.

References

1. M. Batzill, U. Diebold. Progress in Surface Science, 79, 2005, p. 47-154.
2. D. S. Ginley, H. Hosono, D. C. Paine (Eds.), Handbook of Transparent Conductors, Springer Science+Business Media, New York, 2010.
3. J. Huang and Q. Wan. Gas Sensors Based on Semiconducting Metal Oxide One-Dimensional Nanostructures Sensors 2009, 9, 9903-9924; doi:10.3390/s91209903.
4. J. Gong, Q. Chen. Sol-Gel Prepared Single Wall Carbon Nanotube SnO_2 Thin Film for Micromachined Gas Sensor// Nanotech. — 2004. — Vol. 3. — P. 232-235.
5. В. В. Иванов, И. А. Сидорак, А. А. Шубин, Л. Т. Денисова. Получение порошков SnO_2 разложением термически нестабильных соединений // Journal of Siberian Federal University. Engineering & Technologies. — 2010. — Vol. 2, №3. — P. 189–213.
6. Filevskaya L. N., Smyntyna V. A., Grinevich V. S. Morphology of nanostructured SnO_2 films prepared with polymers employment// Photoelectronics. — 2006. — № 15. — P. 11-14.
7. Alexander G. Stepanov. A new general method for the preparation of bis(acetylacetonato)dihalogenotin(IV) by action of molecular oxygen on tin(II)

halides in acetylacetone// Journal of Organomet. Chem. — 1989. — .Vol. 361, № 2 — P. 157-159.; W. Dilthey.// Ber. Deut. Chem. Ges. — 1903. — T. 36, 923-930.
8. Ueeda R., Kawasaki Y., Tanaka T., Okawara R. Organometal complexes: II. Organotin and organolead bis(acetylacetonates)// J. Organomet. Chem. — 1966. — Vol.5, № 2 — P. 194-197.
9. G. T. Morgan, H. D.K. Drew, J. Chem. Soc. — 1924. — Vol.125. — P. 372-381.
10. Shahzadi, S. Ali and G.-X. Jin. Synthesis, Characterization and Crystal Structure of Bis(acetylacetonato) dichlorotin(IV)// J. Iranian Chem. Soc. — 2006. — T. 3,№ 4. — C. 323-326.
11. B. Ulug, H. M. Turkdemir, A. Ulug, O. Buyukgungor, M. B. Yucel, V. A. Smyntyna, V. S. Grinevich, L. N. Filevskaya. Structure, spectroscopic and thermal characterization of bis(acetylacetonato)dichlorotin (IV) synthesized in aqueous solution Укр. Хим. Журн. 2010. Т. 76, № 7, 12-17
12. Борило Л.П. Синтез и физико-химические закономерности формирования золь-гель методом тонкопленочных и дисперсных наноматериалов оксидных систем элементов III-V групп. Автореферат диссертации на соискание ученой степени доктора химических наук. — Томск.2003. — 29 с.
13. В. С. Гриневич, В. А. Смынтына, С. Н. Савин, Л. Н. Филевская, Б. Улуг, М. Халук Туркдемир, А. Улуг, С. Ялткая. Термогравиметрические исследования комплексов прекурсора для получения наноразмерных пленок двуокиси олова. Sensor Electronics and Microsystem Technologies. T. 2 (8) 2/2011, 69-75.
14. H. F. Mark., N. G. Gaylord, N. M. Bikales, (Eds.) Encyclopedia of Polymer Science and Technology, vol.14, Thermogravimetric Analysis to Wire and Cable Coverings, Interscience Publishers, New York, 1971, p.149.

UDC 54.03

V. S. Grinevych, V. A. Smyntyna, L. M. Filevska

INFLUENCE OF A PRECURSOR PROPERTIES ON THE SURFACE MORPHOLOGY OF NANOSCALE TIN DIOXIDE FILMS

Abstract.

The work presents the results of the nanosize tindioxide films' surface morphology investigation which is dependent on the precursor complex's technological properties used for their production. The used precursors differ only due to the technology of their preparation at the final stage. This defines the presence of the bound water in their composition. The water acts as a looser at the thermal decomposition which gives the possibility to obtain the nanosized films with nano grains of different sizes dependently on the precursor's type.

Keywords: tin dioxide, Bis(acetylacetonato)dichlorotin, thin films, surface morphology.

УДК 54.03

В. С. Гриневич, В. А. Смынтына, Л. Н. Филевская

ВЛИЯНИЕ ОСОБЕННОСТЕЙ ПРЕКУРСОРА НА МОРФОЛОГИЮ ПОВЕРХНОСТИ НАНОРАЗМЕРНЫХ ПЛЕНОК ДИОКСИДА ОЛОВА

Аннотация.

В работе представлены результаты исследований морфологии поверхности наноразмерных пленок двуокиси олова в зависимости от особенностей получения комплексов прекурсора для их полученияИспользованные прекурсоры различаются только особенностями приготовления на последнем этапе, что определяет различное содержание в их составе связанной воды. При термическом разложении комплекса вода в его составе выполняет функцию разрыхления, что позволяет получать пленки двуокиси олова с нанозернами разного размера в зависимости от типа прекурсора.

Ключевые слова. двуокись олова, дихлордиацетилацетонат олова, тонкие пленки, морфология поверхности.

УДК 54.03

В. С. Гріневич, В. А. Сминтина, Л. М. Філевська

ВПЛИВ ОСОБЛИВОСТЕЙ ПРЕКУРСОРУ НА МОРФОЛОГІЮ ПОВЕРХНІ НАНОРОЗМІРНИХ ПЛІВОК ДІОКСИДУ ОЛОВА

Анотація.

У роботі представлені результати досліджень морфології поверхні нанорозмірних плівок двоокису олова в залежності від особливостей отримання комплексів прекурсора для їх отримання. Використані прекурсори розрізняються тільки особливостями приготування на останньому етапі, що визначає різний зміст у їх складі зв'язаної води. При термічному розкладанні комплексу вода в його складі виконує функцію розпушення, що дозволяє отримувати плівки діоксиду олова з нанозернами різного розміру в залежності від типу прекурсора.

Ключові слова: двоокис олова, діхлордіацетілацетонат олова, тонкі плівки, морфологія поверхні.

UDC 621.315.592

K. D. Kardashev [1] , *D. L. Kardashev* [2]
[1] A.S. Popov Odessa National Academy of Telecommunications,
tel. 7236118, E-mail: konstantinkardashev@gmail.com
[2] Odessa National Maritime Academy, tel. 7332339,
Email: dkardashev@mail.ru

LOCAL DENSITY OF STATES OF ELECTRONS IN GRAPHEN

The local density of states of electrons in a graphen calculation provided based on a Green's function method for Bethe lattice approximation.

A rapid development of nanotechnologies requires at least qualitative theoretical research of physical properties of newly synthesized materials. Precise mathematical description of energy and oscillatory specters of such materials is well enough problematic due to multiplicity of their structure and composition. That is why, in a recent time theoretical interpretation of experimental data can only be made on a base of highly simplified model calculation, which, though, must correctly represent main features of these data.

Among the shared concepts in the theory of electron structure in a disordered materials, the preferences should be given to approximations based on a Green's functions calculation, as these functions are directly related with the density of states and doesn't require introduction of long-range order concepts.

For determination of local density of states of electron (LDSE) in hexagonal monolayer (graphen) we'll use Green's function method with semi-empirical single-electron tight-binding Hamiltonian included all important two center interactions between nearest atoms. Structure of graphen is being modeled with a Bethe lattice, holding hexagonal arrangement of neighboring atoms. As the basis for tight-binding Hamiltonian we'll chose one s- and two p_x, p_y – atomic orbitals.

According to Sletter-Coster notation [1], parameters of interaction in a two center approximation have a look:

$$E_s = \langle S_0 | \hat{H} | S_0 \rangle; \quad E_p = \langle P_0 | \hat{H} | P_0 \rangle$$

$$; \quad U = \langle S_0 | \hat{H} | S_i \rangle;$$

$$V = \langle P_{0x} | \hat{H} | P_{ix} \rangle; \quad X = \langle S_0 | \hat{H} | P_{ix} \rangle;$$

$$W = \langle P_{0y} | \hat{H} | P_{iy} \rangle \qquad (1)$$

here subscript 0 related with the central atom, *i* – with its nearest neighbors. In a nodal representation the Hamiltonian's matrix has block structure. Each block of 3x3 dimensionality (according to number of basis functions), represents a matrix of interactions of nearby atoms. According to accepted notations (1) it can be written as

$$\underline{H_0} = \begin{bmatrix} E_s & 0 & 0 \\ 0 & E_p & 0 \\ 0 & 0 & E_p \end{bmatrix};$$

$$\underline{H_0} = \begin{bmatrix} U & X & 0 \\ -X & V & 0 \\ 0 & 0 & W \end{bmatrix} \qquad (2)$$

It is easily can be shown that other matrices of interaction can be gained from (2) with the help of symmetry transformations

$$H_{0i} = L_j^{-1} H_{0j} L_j \,, \tag{3}$$

where

$$L_{\theta} = \begin{bmatrix} -1 & 0 & 0 \\ 0 & -\cos\theta & \sin\theta \\ 0 & -\sin\theta & -\cos\theta \end{bmatrix}; \tag{4}$$

$$L_{\theta} = \begin{bmatrix} -1 & 0 & 0 \\ 0 & -\cos\theta & -\sin\theta \\ 0 & \sin\theta & -\cos\theta \end{bmatrix}$$

here q – a valence angle.

It is obviously that:

$$L_{ij} = L_j^{-1}; \;\; L_{ij} L_j = -L_k \;\; ; \tag{5}$$

$$i, j, k, l = 1,...,3$$

The Green's function for i^{th} node can be calculated from the Dyson's equation:

$$(E_i - H_i) G_j = I_j + \sum_{k=1}^{3} H_k G_k \tag{6}$$

where I_{ij} – identity matrix, and the summing provided for nearest neighbors. Let us interested in a density of states for central, 0^{th}, atom. Then, (6) will represent an infinite sequence of equations:

$$(E - H_0) G_0 = I + \sum_k H_{0k} G_{k0}$$

$$(E - H_0) G_{k0} = H_{0k}^T G_0 + \sum_{k' \neq k} H_{0k'} G_{k'0} \tag{7}$$

This sequence can be closed only if we'll use two basic properties of the Bethe lattice: first, each node of the lattice can be transformed into another by a finite number of transformations; secondly, any two nearest nodes are bonded only with each other. This fact allows us to introduce so-called transfer matrices:

$$\Phi_{L(\nu)} = G_0 G_0^{-1} \;; \quad \Phi_{L(\mu)} = G_0 G_0^{-1} \;; \tag{8}$$

$$L(\nu), L(\mu) = 1,2,3$$

Substituting (8) in to system (7), for 0^{th} atom we'll have:

$$G_0 = \left[E - H_0 - \Sigma\right]^{-1}, \tag{9}$$

where, a self-energy part is:

$$\Sigma = \sum_{\nu} H_{0\nu} \Phi_{L(\nu)} \tag{10}$$

and the transfer matrices can be determined from the equations:

$$\Phi_{L(\nu)} = \left[E_\nu - H_\nu - \widetilde{\Sigma} + H_\mu^T \Phi_{L(\nu)}\right]^{-1} H_\mu^T \tag{11}$$

$$\widetilde{\Phi}_{L(\mu)} = \left[E_\mu - H_\mu - \Sigma + H_\mu \Phi_{L(\nu)}\right]^{-1} H_\mu \tag{12}$$

here $\widetilde{\Sigma} = \sum_{\lambda} H_\lambda^T \widetilde{\Phi}_{L(\lambda)}$. For homopolar Bethe lattice the transfer matrices $\Phi_{L(\nu)}$ and $\widetilde{\Phi}_{L(\mu)}$ are related with each other by the transposition operation. Thus it will be sufficient to solve only one of these two matrix equations. We chose the second one. For different bonds the transfer matrices can be transformed into each other by the same symmetry operations as for the interaction matrices, so:

$$\Phi_1 = \begin{bmatrix} u & x & 0 \\ -x & v & 0 \\ 0 & 0 & w \end{bmatrix}; \tag{13}$$

$$\Phi_2 = L_2^{-1} \Phi_1 L_2 \;; \quad \Phi_3 = L_3^{-1} \Phi_1 L_{143} \;.$$

Equation (12) can be rearranged as

$$\left[E - H_0 - \Sigma + H_0 \Phi_1\right] \widetilde{\Phi}_1 = H_0 \tag{14}$$

or, multiplying (14) from the right on H_0^T, we'll obtain a matrix equation for determination of transfer matrix:

$$Z_1 = H_0\,\Phi_1$$
$$(\varepsilon - \Sigma + Z_A)Z_A^T = H_0\,H_0^T \qquad (15)$$

here $\varepsilon = \boldsymbol{E} - H_0$.

In a common case it is a quite difficult to solve equations (15). Analytical solution can be found if we neglect ppπ interaction between p-orbitals of neighboring atoms:

$$G_0^s = \frac{1}{\Sigma_s} \qquad \text{and} \qquad G_0^p = \frac{1}{\Sigma_p} \qquad (16)$$

$$\Sigma_s = \frac{\varepsilon_s \pm \sqrt{\varepsilon_s^2 - 4(9(U^2+X^2)-\varepsilon_s^2)(2-9\varphi^2)}}{2(2-9\varphi^2)} \qquad (17)$$

$$\Sigma_p = \frac{-\varepsilon_p \pm \sqrt{\varepsilon_p^2 - (9(V^2+X^2)-\varepsilon_p^2)(2-9\varphi^2)}}{2-9\varphi^2} \qquad (18)$$

where

$$= \delta^2\,\frac{\varepsilon_s^2\varepsilon_p^2 - \gamma \pm \sqrt{(\varepsilon_s^2\varepsilon_p^2 - 2\gamma)^2 - 4\delta^2}}{\Delta} \qquad (19)$$

and used the notations

$$\begin{aligned}
&\gamma = \varepsilon_s^2(9(X^2+V^2)-\varepsilon_p^2) + \\
&+ \varepsilon_p^2(9(9(X^2+U^2)-\varepsilon_s^2) - 9\delta, \\
&\qquad \delta = 3X(U-V), \\
&\Delta = \gamma^2 - 16\varepsilon_s^2\varepsilon_p^2(9(X^2+V^2) - \\
&- 4\varepsilon_p^2)(9(X^2+U^2)-\varepsilon_s^2, \\
&\qquad \varepsilon_s = E - E_s,\ \varepsilon_p = E - E_p
\end{aligned} \qquad (20)$$

It is easy to ensure that function $j^2(E)$ approaches zero if sps (X=0) –interactions can be neglected. In this case we obtain known solution for Bethe lattice with single-parametric tight-binding Hamiltonian, set in basis of single s-orbital function per each atom.

Let us remind that partial density of states determined as imaginary parts of Green's function G_0^s and G_0^p and the total local density of states of electron is the sum of these partials.

On a figure 1 represented LDSE of hexagonal monolayer (solid curve) calculated by equations (16) – (20) and tetrahedrally coordinated structure (dashed curve)[2].

It is well enough seen that energy spectrum of hexagonal structure, unlike the tetrahedral, doesn't have forbidden gap, i.e. the graphite monolayer has a metallic type of conductivity. Consequently, as it was mentioned in [3], the most significant properties of electron sub-system of solids are determined by the short-range order. Note that represented graphs have qualitative character. All calculations are provided to establish the influence of geometry of nearest atomic arrangement on an electron energy spectrum.

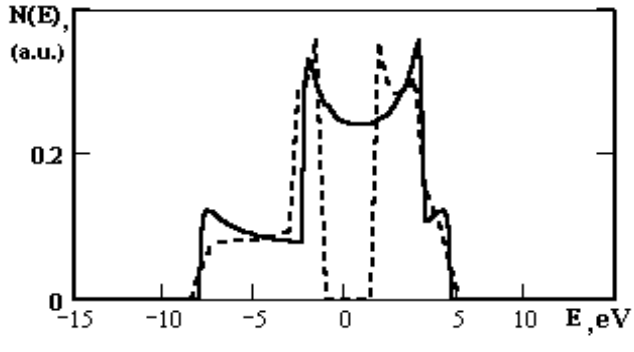

Figure 1 — LDSE of tetrahedral [2](dashed) and hexagonal (solid line) structures

References

[1]. Joannopolus J. D. Theory of fluctuations and localized states in amorphous tetrahedrally bonded solids// *Phys.Rev.B*, — 1997,Vol.16, № 6, — P. 2764-2774.

[2]. Kardashev D. L. Electron density of states and neutral vacancy levels in an amorphous covalent semiconductors //*Phys. and chem.of solid state*. — 2009. — № 4. — P. 643-646.

[3]. Madan A., Shaw M. *The Physics and applications of amorphous semiconductors*// Mir, Moscow, 1999. — P. 195-330.

UDC 621.315.592

K. D. Kardashev, D. L. Kardashev

LOCAL DENSITY OF STATES OF ELECTRONS IN GRAPHEN

Abstract

The local density of states of electrons in a graphen calculation provided based on a Green's function method for Bethe lattice approximation.

Key word: density of states, Green function, graphen.

УДК 621.315.592

К. Д. Кардашев, Д. Л. Кардашев

ЛОКАЛЬНАЯ ПЛОТНОСТЬ ЭЛЕКТРОННЫХ СОСТОЯНИЙ ГРАФЕНА

Резюме

В данной работе рассчитана локальная плотность электронных состояний графена методом функций Грина на основе приближения решетки Бете.Ж

Ключевые слова: плотность состояния, функция Грина, графен.

УДК 621.315.592

К. Д. Кардашев, Д. Л. Кардашев

ЛОКАЛЬНА ГУСТИНА ЕЛЕКТРОННИХ СТАНІВ ГРАФЕНУ

Резюме

У данній роботі розрахована густина електронних станів графену методом функцій Гріна на основі наближення гратки Бете.

Ключові слова: густина стану, функія Гріна, графен.

UDC 539.84

T. B. Tkach
Odessa State Environmental University, 15, Lvovskaya str., Odessa, Ukraine
e-mail: quantper@mail.ru

OPTIMIZED RELATIVISTIC MODEL POTENTIAL METHOD AND QUANTUM DEFECT APPROXIMATION IN THEORY OF RADIATIVE TRANSITIONS IN SPECTRA OF MULTICHARGED IONS

The combined relativistic model potential approach and relativistic many-body perturbation theory with the zeroth order optimized one-particle approximation are used for calculation of the Li-like ions energies and oscillator strengths of radiative transitions from ground state to low-excited and Rydberg states. New element in our scheme is an implementation of optimized relativistic model potential and quantum defect approximation) approach to energy approach frames. Comparison of calculated oscillator strengths with available theoretical and experimental (compillated) data is performed.

1. Introduction

The research on the spectroscopic and structural properties of highly ionized atoms has a fundamental importance in many fields of atomic physics (spectroscopy, spectral lines theory), astrophysics, plasma physics, laser physics and so on. It should be mentioned that the correct data on radiative decay widths, probabilities and oscillator strengths of atomic transitions are needed in astrophysics and laboratory, thermonuclear plasma diagnostics and in fusion research. In this light, an special interest attracts studying the spectral characteristics of the He-, Li etc like ions. There have been sufficiently many reports of calculations and compilation of energies and oscillator strengths for the Li-like ions and other alkali-like ions (see, for example, [1–19]). Particularly, Martin and Wiese have undertaken a critical evaluation and compilation of the spectral parameters for Li-like ions (Z=3-28) [1,2]. The results of the high-precision non-relativistic calculations of the energies and oscillator strengths of $1s22s_j 1s22p$ for Li-like systems up to $Z = 50$ are presented in Refs. [9-17]. The Hylleraas-type variational method and the $1/Z$ expansion method have been used. Chen Chao and Wang Zhi-Wen [14] listed the nonrelativistic dipole-length, -velocity, -acceleration oscillator strengths for 1s22s–1s22p transitions of LiI isoelectronic sequence calculated within a full core plus correlation method with using multiconfiguration interaction wave functions. Fully variational nonrelativistic Hartree-Fock wave functions were used by Bièmont in calculating 1s2n2L (n<8=s,p,d,f; 3<Z<22) Li-like states [16]. In many papers the Dirac-Fock (DF) method, model potential, quantum defect approximation in the different realizations have been used for calculating the energies and oscillator strengths of the Li-like and similar ions (see Refs.[3-6,16-30]). The consistent QED calculations of the energies, ionization potentials, hyperfine structure constants for the Li-like ions are performed in Refs. [18,19]. However, for Li-like ions with higher Z, particularly, for their high-excited (Rydberg) states, there are not enough precise data available in literatures. In our paper the optimized relativistic model potential (ORMP) [26-29] combined with the relativistic energy approach [3-5] and many-body perturbation theory (PT) [19,29] with zeroth order optimized 1-particle representation [4,21-24] are used for calculation the Li-like ions (Z=11-42,69,70) energies and oscillator strengths of radiative transitions from ground state to low-excited and Rydberg states. The key feature of the presented basis theory is an implementation of the relativistic model potential

(quantum defect approach) to the frames of energy approach for studying spectral parameters of Rydberg multi-electron ions. The comparison of calculated oscillator strengths with available theoretical and experimental (compillated) data is performed.

2. The theoretical method

In the relativistic energy approach [3,4,22-24] the imaginary part of electron energy shift of an atom is directly connected with the radiation transition probability. An approach, using the Gell-Mann and Low formula is used in treating the relativistic atom. The total energy shift of the state is usually presented as (see, for example, [3,4,24] and also [21]):

$$\Delta E = \mathrm{Re}\Delta E + i\,\Gamma/2 \qquad (1)$$

where Γ is interpreted as the level width and decay possibility $P = \Gamma$. The imaginary part of electron energy of the system, which is defined in the lowest PT order as [3]:

$$\mathrm{Im}\Delta E(B) = -\frac{e^2}{4\pi} \sum_{\substack{\alpha>n>f \\ [\alpha<n\le f]}} V^{|\omega_{\alpha n}|}_{\alpha n \alpha n} \qquad (2)$$

where $\sum_{\alpha>n>f}$ for electron and $\sum_{\alpha<n\le f}$ for vacancy. The matrix element is determined as follows:

$$V^{|\omega|}_{ijkl} = \iint dr_1 dr_2 \Psi^*_i(r_1)\Psi^*_j(r_2)\frac{\sin|\omega|r_{12}}{r_{12}} \qquad (3)$$

$$(1-\alpha_1\alpha_2)\Psi^*_k(r_2)\Psi^*_l(r_1)$$

The separated terms of the sum in (3) represent the contributions of different channels and a probability of the dipole transition is:

$$\Gamma_{\alpha_n} = \frac{1}{4\pi}\cdot V^{|\omega_{\alpha_n}|}_{\alpha_n\alpha_n} \qquad (4)$$

The corresponding oscillator strength: $gf = \lambda^2_g \cdot \Gamma_{\alpha n}/6.67\cdot 10^{15}$, where g is the degeneracy degree, λ is a wavelength in angstrems (Å). Under calculating the matrix elements (3) one should use the angle symmetry of the task and write the expansion for potential $\sin|\omega|r_{12}/r_{12}$ on spherical functions as follows [3,4]:

$$\frac{\sin|\omega|r_{12}}{r_{12}} = \frac{\pi}{2\sqrt{r_1 r_2}}\sum_{\lambda=0}^{\infty}(\lambda)J_{\lambda+1/2}(|\omega|r_1)J_{\lambda+1/2}(|\omega|r_2)P_\lambda(\cos r_1 r_2) \qquad (5)$$

where J is the Bessel function of first kind and $(\lambda)= 2\lambda + 1$. This expansion corresponds to usual multipole one for radiative probability. Substitution of expansion (5) to matrix element of interaction gives [3,4]:

$$V^{\omega}_{1234} = [(j_1)(j_2)(j_3)(j_4)]^{1/2}\sum_{\mu}(-1)^{\mu}\begin{pmatrix} j_1 & j_3 & \lambda \\ m_1 & -m_3 & \mu \end{pmatrix} \times \mathrm{In}\ Q_\lambda(1234),$$

$$Q_\lambda = Q^{Qul}_\lambda + Q^{B}_\lambda, \qquad (6)$$

where j_i is the total single electron momentum, m_i – the projections; Q^{Qul}_λ is the Coulomb part of interaction, Q^{B}_λ – the Breit part. The Coulomb part Q^{Qul}_λ is expressed in terms of radial integrals R_λ, angular coefficients S_λ:

$$Q^{\mathrm{Qul}}_\lambda = \frac{1}{Z}\{R_l(1243)S_\lambda(1243) + R_\lambda(\tilde{1}243)S_\lambda(\tilde{1}243) + R_\lambda(1\tilde{2}43)S_\lambda(1\tilde{2}43) + R_\lambda(\tilde{1}\tilde{2}43)S_\lambda(\tilde{1}\tilde{2}43)\}. \qquad (7)$$

The different items in (7) include large and small components of the Dirac functions; the sign «~» means that in (7) the large radial component f_i is to be changed by the small g_i one and the moment l_i is to be changed by $\tilde{l}_i = l_i - 1$ for the Dirac number æ> 0 and l_i+1 for æ<0. The Breit interaction part is defined by similar way (see [3-5,21,24]. The relativistic wave functions are calculated by solution of the Dirac equation with the potential, which includes the «outer electron-ionic core» potential and polarization potential [21]. In order to describe interaction of the outer electron with the He-like core the simplified Ivanova-Ivanov type model potential [3] is used. The calibration of the single model potential parameter has been performed on the basis of the special ab initio procedure within relativistic energy approach [22] (see also [4,5,21]). In Ref.[22] the lowest order multielectron effects, in particular, the gauge dependent radiative contribution Im dE_{ninv} for the certain class of the photon propagator calibration is treated. This value is considered to be the typical representative of the electron correlation effects, whose minimization is a reasonable criterion in the searching for the optimal

one-electron basis of the relativistic many-body PT. The minimization of functional Im dE_{ninv} leads to integral-differential equation that can be solved using one of the standard codes. Therefore, it provides the construction of the optimized 1-particle representation and thus ORMP scheme [27-29]. The same procedure is used in generalization of the relativistic quantum defect approximation (QDA). Usually, the most exact version of the QDA is provided by using the empirical data in order to determine the quantum defect values for different state. The above described approach allows to generalize the QDA and get a new ab initio optimized QDA (OQDA) scheme, satisfying a principle of minimization for the gauge dependent radiative contributions to Im δE_{ninv} for the certain class of the photon propagator calibration. A relativistic quantum defect is usually defined as (see, for example, [30]:

$$\mu_\chi(E_n) = n - \nu_n + \gamma - |\chi|, \tag{8}$$

where χ is he Dirac quantum number, and

$$\gamma = \sqrt{\chi^2 - (\alpha z)^2}\,,\ \nu_n = \frac{z\varepsilon}{\lambda},\ \lambda = \sqrt{-E_n(1+\varepsilon)}\,,\ \varepsilon = 1 + \alpha^2 E_n\,. \tag{9}$$

In the non-relativistic limit (i.e. the fine structure constant $\alpha \to 0$) expression (8) transfers to the well known non-relativistic expression for quantum defect:

$$\mu_l^{\text{R}}(E_n) = n - n^* = n - \frac{z}{\sqrt{-2E_n}}\,, \tag{10}$$

where n is the principal quantum number, n^* is an effective quantum number, E_n is an electron energy and z is a charge of a core (ion).

3. Results

We applied the above described approach to calculating the energies and oscillator strengths of transitions in spectra of the Li-like ions (Z=11-42,69,70). All calculations are performed on the basis of the numeral code Superatom. There are considered the radiative transitions from ground state to the low-excited and Rydberg states, particularly, $2s_{1/2} - np_{1/2,3/2}$, $np_{1/2,3/2}$-$nd_{3/2,5/2}$ (n=2-12). To test the obtained results, we compare our calculation data on the oscillator strengths values for some Li-like ions with the known theoretical and compillated data [1,2,6-17,25]. As example, in table 1,2 we list our oscillator strengths values (ORMP and OQDA) for $2s_{1/2}$–$2p_{1/2,3/2}$ transitions in Li-like ions S^{13+},Ca^{17+},Fe^{23+},Zn^{27+},Zr^{37+}, Mo^{39+}, Sn^{47+}, Tm^{66+}, Yb^{67+} . The DF calculation data by Zilitis [6] and the "best" compillated (experimental) data [1,2] for the some low-Z Li-like ions are listed in tables 1,2 for comparison too. It should be reminded that the experimental data on the oscillator strengths for many (especially, high-Z) Li-like ions are absent. In a whole, there is a physically reasonable agreement between the listed data. The important features of the approach used are using the optimized one-particle representation and account for the polarization effect. Letus note that an estimate of the gauge-noninvariant contributions (the difference between the oscillator strengths values calculated with using the transition operator in the form of «length» and «velocity») is about 0.3%. It means that the results are practically equal within schemes with using the different photon propagator gauges (such as Coulomb, Babushkin, Landau). In table 3 we present the our oscillator strengths values (ORMP and OQDA) for the $2s_{1/2}$ – np_j (n=3-12, j=1/2,3/2) transitions in spectrum of the Li-like Ca^{17+}.

Table 1. Oscillator strengths of the $2s_{1/2} - 2p_{1/2}$ transitions in Li-like ions.

	DF	Exp.	Our data: ORMP	Our data: OQDA
Ion	$2s_{1/2}$–$2p_{1/2}$	$2s_{1/2}$–$2p_{1/2}$	$2s_{1/2}$–$2p_{1/2}$	$2s_{1/2}$–$2p_{1/2}$
S^{13+}	0.0299	0.030	0.0301	0.0303
Ca^{17+}	0.0234	0.024	0.0236	0.0238
Fe^{23+}	0.0177	0.018	0.0179	0.0181
Zn^{27+}	0.0153	–	0.0156	0.0158
Zr^{37+}	0.0114	–	0.0118	0.0121
Mo^{39+}	–	0.011	0.0110	0.0114
Sn^{47+}	0.0092	–	0.0095	0.0099
Tm^{66+}	–	–	0.0072	0.0076
Yb^{67+}	0.0067	–	0.0069	0.0073

Table 2. Oscillator strengths of the $2s_{1/2} - 2p_{3/2}$ transitions in Li-like ions.

	DF	Exp.	Our data: ORMP	Our data: OQDA
Ion	$2s_{1/2}$–$2p_{3/2}$	$2s_{1/2}$–$2p_{3/2}$	$2s_{1/2}$–$2p_{3/2}$	$2s_{1/2}$–$2p_{3/2}$
S^{13+}	0.0643	0.064	0.0641	0.0643
Ca^{17+}	0.0542	0.054	0.0541	0.0544
Fe^{23+}	0.0482	0.048	0.0481	0.0484
Zn^{27+}	0.0477	–	0.0475	0.0479
Zr^{37+}	0.0543	–	0.0540	0.0544
Mo^{39+}	–	0.056	0.0558	0.0562
Sn^{47+}	0.0686	–	0.0684	0.0688
Tm^{66+}	–	–	01140	01145
Yb^{67+}	0.1170	–	0.1167	0.1172

Table 3. Oscillator strengths of the $2s_{1/2} - np_{1/2}$ transitions in Ca^{17+}.

Transition	QDA	DF	Exp.	Our data: ORMP	Our data: OQDA
$2s_{1/2}$–$3p_{1/2}$	–	–	0.123	0.122	0.127
$2s_{1/2}$–$3p_{3/2}$	–	–	0.241	0.243	0.248
$2s_{1/2}$–$4p_{1/2}$	–	–	–	0.029	0.032
$2s_{1/2}$–$8p_{1/2}$	2.54[a]	2.53[a]	–	2.55[a]	2.55[a]
$2s_{1/2}$–$10p_{1/2}$	1.24[a]	1.24[a]	–	1.25[a]	1.25[a]
$2s_{1/2}$–$12p_{1/2}$	0.70[a]	0.698[a]	–	0.71[a]	0.71[a]

Note: [a] ($10^{-3}gf$).

The standard QDA, DF oscillator strengths calculation results by Zilitis and some experimental data by Martin-Weiss [1,2,6,24] are listed in table 3 too. The QDA oscillator strengths data become more exact with the growth of the principal quantum number. At the same time the accuracy of the DF data may be decreased. The agreement between the Martin-Weiss data and our results for the transitions between low-lying terms is sufficiently good.

References

1. Martin G. A. and Wiese W. L., Atomic oscillator-strength dis-tributions in spectral series of the lithium isoelectronic sequence// Phys. Rev. A. — 1999. — Vol.13. — P. 699–714.
2. Martin G. A. and Wiese W. L., Tables of critically evaluated oscillator strengths for lithium isoelectronic sequence// Journ. of Phys. Chem. Ref. Data. — 1996. — Vol.5. — P. 537-570.
3. Ivanov L. N., Ivanova E. P., Extrapolation of atomic ion energies by model potential method: Na-like spectra// Atom. Dat.Nuc.Dat.Tab.— 1999. — Vol.24. — P. 95-121.
4. Glushkov A. V., Ivanov L. N., Ivanova E. P., Generalized energy approach in relativistic theory of atom// Autoionization Pheno-mena in Atoms. — M.: Moscow State Univ. — 1999.
5. Glushkov A. V., Advanced relativistic energy approach to radia-tive decay processes in multielectron atoms and multicharged ions//Adv.in Theory of Quantum Systems in Chem. and Phys., Ser.: Frontiers in Theor. Phys. and Chem. (Springer). — 2012 — Vol.26. — P. 131-152.
6. Zilitis V. A., Determination of the energies and oscillator stren-gths of Li-like ions//Opt. Spectr. — 1999. — Vol.55. — P. 215-218.
7. Froese Fischer C., Breit–Pauli energy levels, lifetimes, and transition probabilities for the beryllium-like to neon-like sequences//Atom.Dat.Nucl. Dat. Tabl. — 2004. — Vol.87. — P.1-184.
8. Barnett R., Johnson E., Lester W. Jr., Quantum Monte Carlo determination of the lithium 2S-2P oscillator strength: Higher precision//Phys. Rev. A.— 1995. — Vol.51. — P. 2049-2052.
9. Zong-Chao Yan and Drake G. W. F., Theoretical lithium 2S-2P and 2P-3D oscillator strengths//Phys. Rev. A. — 1995. —Vol. 52. — P.R4316-4319.
10. Lianhua Qu, Zhiwen Wang and Baiwen Li, Theory of oscillator strength of the lithium isoelectronic sequence//J. Phys.

B: At. Mol. Opt. Phys. — 1998. — Vol. 31. — P. 3601-3612.
11. Kunisz M. D., Coulomb approximation oscillator strengths for some transitions in rare earths//Acta Phys. Polon.— 1999. —Vol.a62. — P. 285-296.
12. Xiaoxu Guan and Baiwen Li, Energies and oscillator strengths of lithium in a strong magnetic field//Phys. Rev. A. — 2001. — Vol. 63. — P.043413.
13. Khetselius O. Yu, Relativistic perturbation theory calculation of hyperfine structure parameters for some heavy-element isotopes//Int. Journ. Quant. Chem. — 2009. — Vol. 109. — P. 3330-3335.
14. Chen Chao, Wang Zhi-Wen, Oscillator strengths for 2s2–2p2P transitions of lithium isoelectronic sequence NaIX-CaXVIII// Com.Theor.Phys. — 2005. — Vol. 43. — P. 305-312.
15. Hu Mu-Hong, Wang Zhi-Wen, Oscillator strengths for 2S–nP transitions of lithium isoelectronic sequence from Z = 11 to 20//Chinese Phys. B. — 2009. — Vol.18. — P. 2244-2258.
16. Bièmont E., Theoretical oscillator strengths in the lithium isoelectronic sequence (3 <= Z <= 22)// Astr. and Astrophys. Suppl. Ser. — 1999. — Vol. 27. — P. 489-494.
17. Zhi-Wen Wang and Ye Li , Calculations of the transition energies and oscillator strengths for Cu^{26+} ion// Journ. of Atom. Mol. Sci.- 2010. — Vol. 1.— P. 62-67.
18. Yerokhin V., Artemyev A., Shabaev V. M., QED treatment of electron correlation in Li-like ions//Phys.Rev.A.— 2007. — Vol.75. — P.062501.
19. Glushkov A. V., Ambrosov S. V., Loboda A. V., Gurnitskaya E. P., Khetselius O.Yu., QED calculation of heavy multicharged ions with account for the correlation, radiative and nuclear effects// Recent Advances in Theor. Phys. and Chem. Systems (Springer).— 2006.— Vol. 15.— P. 285-300.
20. Safronova U. I., Safronova A. S., Hamasha S., Beiersdorfer P., Relativistic many-body calculations of multipole (E1,M1,E2,M2) transition wavelengths and rates of 31-141′ ex-cited and ground states in Ni-like ions//Atom.Dat.Nuc. Dat.Tab. — 2006. — Vol.92. — P. 47–104
21. Glushkov A. V., Relativistic quantum theory. Quantum, mecha-nics of atomic systems.-Odessa: Astroprint, 2008. — 700P.
22. Glushkov A. V., Ivanov L. N. Radiation Decay of Atomic States: atomic residue and gauge non-invariant contributions // Phys. Lett.A.— 1992. — Vol. 170, N1.— P. 33-38.
23. Ivanova E. P., Glushkov A. V. Theoretical investigation of spectra of multicharged ions of F-and Ne-like isoelectronic sequences//J.Quant.Spectr.Rad.Tr. — 1999. — Vol. 36. — P. 127-145.
24. Ivanova E. P., Grant I. P., Oscillator strength anomalies in Ne isoelectronic sequence with applications to X-ray laser modeling//J.Phys.B. — 1998. — Vol. 31.— P. 2871-2883.
25. Schweizer W., Faßbinder P. and Gonzalez-Ferez R., Model potentials for alkali metal atoms and Li-like ions 1999 Atom. Dat.Nucl.Dat.Tabl. — 1999. — Vol.72. — P. 33-55
26. Zelentsova T. N., Perelygina T. B., Thermal photoionization of the Rydberg atoms by the blackbody radiation: New relativistic approach// Sensor Electr. and Microsyst. Techn.— 2009.— № 4.— P. 5-11.
27. Svinarenko A. A., Nikola L. V., Prepelitsa G. P., Tkach T., Mischenko E., The Auger (autoionization) decay of excited states in spectra of multicharged ions: Relativistic theory//Spectral Lines Shape. — 2010. — Vol.16. — P. 94-98
28. Zelentsova T. N., Tkach T. B., Shakhman A. N., Serga I. N., Energy approach to positron collisional excitation and ionization of multielectron Rydberg atoms//Photoelectronics. — 2010. — № 19. — P. 99-102.

29. Malinovskaya S., Glushkov A., Khetselius O., Perelygina T., Svinarenko A., Loboda A., Lopatkin Y., Nikola L., Generalized energy approach to calculating electron collision cross-sections for multicharged ions in plasma: Debye shielding model//Int. Journ.Quant. Chem. — 2011. — Vol. 111. — P. 288-296.
30. Zilitis V. A., Determination of Rydberg *D* and *F* energy levels of Cs-like ions by method of interpolation of relativistic quantum defects//Opt.Spectr. — 2012. — Vol. 113. — P. 231-234.

UDC 539.84

T. B. Tkach

OPTIMIZED RELATIVISTIC MODEL POTENTIAL METHOD AND QUANTUM DEFECT APPROXIMATION IN THEORY OF RADIATIVE TRANSITIONS IN SPECTRA OF MULTICHARGED IONS

Abstract. The combined relativistic model potential approach and relativistic many-body perturbation theory with the zeroth order optimized one-particle approximation are used for calculation of the Li-like ions energies and oscillator strengths of radiative transitions from ground state to low-excited and Rydberg states. New element in our scheme is an implementation of optimized relativistic model potential and quantum defect approximation) approach to energy approach frames. Comparison of calculated oscillator strengths with available theoretical and experimental (compillated) data is performed.

Key words: optimized model potential approach, oscillator strengths, radiative transition

УДК 539.84

Т. Б. Ткач

ОПТИМИЗИРОВАННЫЙ РЕЛЯТИВИСТСКИЙ МЕТОД МОДЕЛЬНОГО ПОТЕНЦИАЛА И МЕТОД КВАНТОВОГО ДЕФЕКТА В ТЕОРИИ РАДИА-ЦИОННЫХ ПЕРЕХОДОВ В СПЕКТРАХ МНОГОЗАРЯДНЫХ ИОНОВ

Резюме. Комбинированный релятивистский метод модельного потенциала и метод теории возмущений с оптимизированным 1-частичным нулевым приближением использованы для вычисления энергий и сил осцилляторов радиационных переходов из основного состояния в низколежащие и ридберговские состояния в спектрах Li-подобных ионов. Основная особенность нового подхода заключается в имплементации оптимизированного релятивистского приближения модельного потенциала (квантового дефекта) в рамки энергетического подхода. Выполнен анализ и сравнение полученных данных для сил осцилляторов с имеющимися теоретическими и экспериментальными данными.

Ключевые слова: оптимизированный метод модельного потенциала, силы осцилляторов, радиационные переходы

UDC 621.315.592

Yu. A. Nitsuk, Yu. F. Vaksman, Yu. N. Purtov

I. I. Mechnikov Odessa National University
e-mail: nitsuk@onu.edu.ua

OPTICAL ABSORPTION AND DIFFUSION OF COBALT IN ZnS SINGLE CRYSTALS

ZnS:Co single crystals obtained by diffusion doping are investigated. The spectra of optical density in the energy range 0.3-3.8 eV are investigated. On absorption edge shift of investigated crystals the cobalt concentration is calculated. Nature of optical transitions determining optical properties of ZnS:Co single crystals in the visible and IR-region of spectrum is identified.

The diffusion profile of the Co dopant is determined via measurement of the relative optical density of the crystals in the visible spectral region. The Co diffusivities in the ZnS crystals at 1170-1270 K are calculated. The Co diffusivity at 1270 K equals 10^{-9} cm^2/s.

INTRODUCTION

Cobalt-doped ZnS single crystals have found a wide application as generating media and passive gates of lasers emitting in the IR region. In [1,2], the possibility of the use of Co^{2+}:ZnS as the efficient passive gate and active media for lasers emitting in the region of 1.5-2.1 and 0.7-0.8 μm is shown. The diffusion doping with Co has a number of advantages compared with doping during growth, among which we can distinguish the main ones, namely, the possibility of controlling the impurity concentration and doping profile.

In this study, the procedure of diffusion doping is realized, which allows one to obtain ZnS:Co single crystals with a specified concentration of Co impurity. The structure of the optical absorption spectra in the visible and infrared wavelength regions is studied and identified. The maximum concentration of the Co impurity is determined by means of the magnitude of the shift of the absorption edge. The analysis of the profile of the relative optical density allowed us to determine the diffusivity of Co in the ZnS crystals.

The goals of this study are development of a procedure of diffusion doping of the ZnS crystals with Co, identification of the optical absorption spectra, and determination of diffusivity of Co in ZnS crystals.

EXPERIMENTAL

The samples under study are obtained by diffusion doping with Co of starting pure ZnS single crystals. Undoped crystals are obtained via the free growth on a single crystal ZnS (111) substrate. A detailed description of this growth method and main characteristics of the ZnS crystals are presented in [3]. Selection of temperature profiles and design of the growth chamber excluded the possibility of contact of the crystal with chamber walls. The dislocation density in obtained crystals was no higher than 10^4 cm^{-2}. The crystals were doped via diffusion of impurity from metal powderlike Co in He+Ar atmosphere. In order to avoid etching of crystals, powderlike ZnS in the ratio 1:1 was added to the Co powder. Crystals were annealed in evacuated quartz cells at temperatures from 1170 to 1270 K (see Table 1). The duration of the diffusion process was 10 h. After annealing the ZnS:Co crystals acquired a turquoise colour, in contrast to the colourless of undoped ZnS crystals.

Diffusion of Co was performed under conditions in which the impurity concentration

in the source remained virtually constant. In this case, the solution of Fick's diffusion equation for the one-dimensional diffusion has the form

$$C(x,t) = C_0\left(1 - erf\frac{x}{\sqrt{4Dt}}\right), \qquad (1)$$

where C_0 is the activator concentration at the surface and the symbol "*erf*" denotes the error function (the Gaussian function).The optical density D^* spectra were measured using a MDR-6 monochromator with 1200, 600, and 325 grooves/mm diffraction grates. The first grate was used to analyze the absorption spectra in the 3.8-1.6 eV photon energy range, the second, in the 1.6-0.6 eV one, and third, in the 0.6-0.4 eV one. A FEU-100 photomultiplier was used as a light flow receiver in the visible spectral region, while FR-1P photoresistor working in the alternating current mode in the IR region. The optical density spectra were measured at 77 and 300 K.

When measuring the diffusion profile of the Fe impurity, a thin plate of the crystal (0.2–0.4 mm) was cleaved in the plane parallel to the direction of the diffusion flux. The measurement of the profile of optical density of the Fe-doped crystals was performed using an MF-2 microphotometer. This device allowed us to measure the magnitude of optical density with a step of 10 μm in the direction of the diffusion flux. In this case, the integrated optical density was measured in the spectral range of 2.8–2.4 eV.

ANALYSIS OF OPTICAL DENSITY SPECTRA

The spectra of optical density of undoped ZnS crystals at 77K are feature an absorption edge with energy of 3.75 eV (Fig. 1, curve 1). In the range 0.40-3.6 eV, no features of the absorption spectra of undoped crystals are found.

Doping of crystals with cobalt leads in the absorption edge shift towards lower energies (Fig. 1, curves 2-3). The shift value increases with annealing temperature and is due to the interimpurity Coulomb interaction. The band gap width variation ΔE_g (in meV) as a function of impurity concentration depending on concentration of introduced impurities is determined in [4] by the relation:

$$\Delta E_g = 2\cdot 10^5\left(\frac{3}{\pi}\right)^{1/3}\frac{eN^{1/3}}{4\pi\varepsilon_0\varepsilon_s}, \qquad (2)$$

where e is electron charge, N, impurity concentration in cm^{-3}, $\varepsilon_s = 8.3$ is ZnS dielectric constant, ε_0, electric constant. The cobalt concentration in the studied crystals was calculated from band gap width changing (see Table 1). The maximum Co concentration ($3\cdot 10^{19}$ cm^{-3}) for the crystals annealed at 1270 K.

Table 1.

Optical characteristics of ZnS:Cr crystals in the absorption edge region

Sample No	Type of the crystal	E_g, eV	ΔE_g, meV	N, cm^{-3}
1	ZnS starting	2.75	---	---
2	ZnS:Co, annealing 1170 K	2.74	10	$4\cdot 10^{16}$
3	ZnS:Co, annealing 1220 K	2.68	70	$8\cdot 10^{18}$
4	ZnS:Co, annealing 1270 K	2.64	110	$3\cdot 10^{19}$

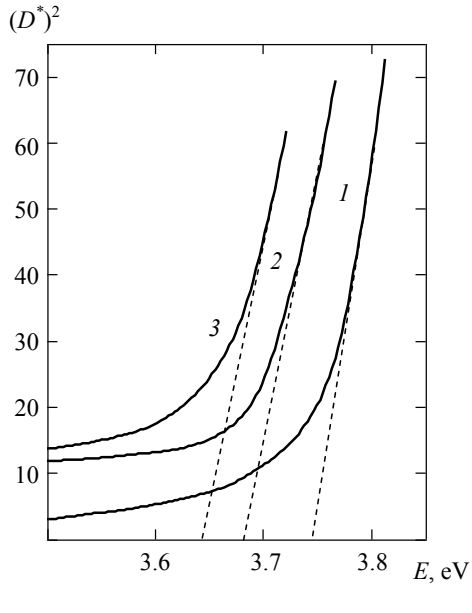

Fig. 1. Spectra of optical density of ZnS (*1*) and ZnS:Co samples 3 (*2*) and 4 (*3*).

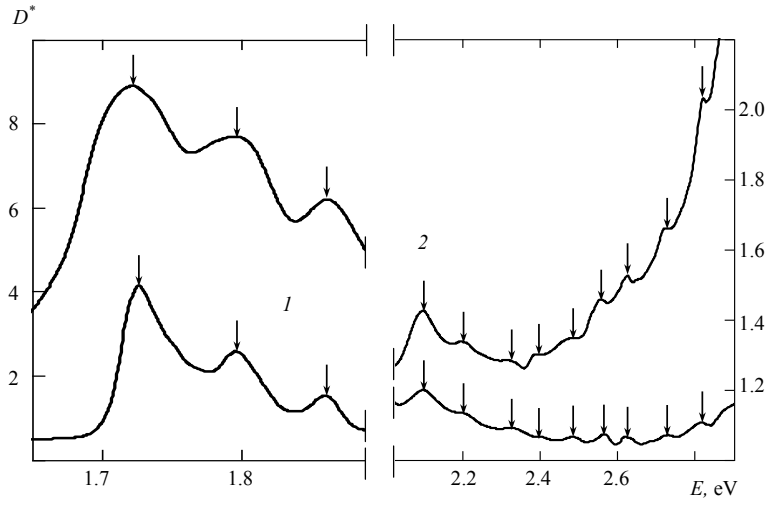

Fig. 2. Spectra of optical density of ZnS:Cr crystals in the visible region. Samples (*1*) 3 and (*2*) 4

In the visible spectral region, the spectra of the optical density of the ZnS:Co crystals involve a series of poorly resolved lines (Fig. 2). The absorption of the light in this region increases as the cobalt concentration. In the absorption spectrum of the lightly-doped ZnS:Co crystals obtained at 1170 K, twelve absorption lines can be distinguished, namely, at 2.82, 2.73, 2,61, 2.55, 2.48, 2.39, 2.32, 2.19, 2.09, 1.86, 1.8, 1.73 eV (Fig. 2, curve 1). As the doping level increased, the location of these lines remained unchanged (Fig. 2, curve 2). Studies of optical density in the temperature range 77-300 K showed that the location of these lines remained unchanged. Such conduct is characteristic for the absorption lines conditioned by the optical transitions of electrons within the impurity ion limits [5]. In the Table 2, the energies of optical transitions in the limits of the Co^{2+} ion and their identification are given. This table is constructed based on our experimental results and our calculations of the Co^{2+} ion energy states in ZnS lattice performed on the Tanabe-Sugano diagrams [6]. It is achieved the best accordance of experiment and theory at the parameters of the crystalline field of Δ=4000 cm^{-1} and B=750 cm^{-1}. Values of Δ and B parameters correspond with the results of the calculations performed in [7]. Lines of absorption at 2.73, 2.61, 2.55 eV was observed before in [8,9]. The energy of $^4A_2(F)\rightarrow{}^4T_1(P)$ transition corresponds with energy position of $^4T_1(P)$ level, calculated in [10].

Table 2.

Optical transitions in the limits of Co^{2+} ion.

Line no.	E_{exp}, eV	E_{calc}, eV	Transition
1.	2.82	2.85	$^4A_2(F)\rightarrow{}^2E(D)$
2.	2.73	2.82	$^4A_2(F)\rightarrow{}^2T_2(D)$
3.	2.61	2.81	$^4A_2(F)\rightarrow{}^2T_1(P)$
4.	2.55	2.58	$^4A_2(F)\rightarrow{}^2E(H)$
5.	2.48	2.42	$^4A_2(F)\rightarrow{}^2T_1(H)$
6.	2.39	2.40	$^4A_2(F)\rightarrow{}^2T_2(H)$
7.	2.32	---	---
8.	2.19	2.21	$^4A_2(F)\rightarrow{}^2T_1(H)$
9.	2.09	2.06	$^4A_2(F)\rightarrow{}^2A_1(G)$
10.	1.86	1.81	$^4A_2(F)\rightarrow{}^2T_2(G)$
11.	1.8	1.78	$^4A_2(F)\rightarrow{}^2T_1(G)$
12.	1.73	1.72	$^4A_2(F)\rightarrow{}^4T_1(P)$
13.	1.48	1.48	$^4A_2(F)\rightarrow{}^2E(G)$
14.	0.89	---	---
15.	0.84	0.85	$^4A_2(F)\rightarrow{}^4T_1(F)$
16.	0.77	---	---
17.	0.43	0.4	$^4A_2(F)\rightarrow{}^4T_2(F)$

In the near IR-region the spectra of optical density of ZnS:Co crystals are characterized by the broad absorption band at 1.48 eV. The optical density of the crystals increased with cobalt concentration growth. The location of this band was unchanged under the temperature varying from 77 to 300 K and cobalt temperature varying. According to our calculations (see Table 2), the absorption band at 1.48 eV can be explained by $^4A_2(F) \rightarrow {}^2E(G)$ transitions occurring in the limits of Co^{2+} ion.

In the middle IR-region, the spectra of optical density of the crystals involve the absorption bands at 0.89, 0.84, 0.76 and 0.43 eV (Fig. 3). The optical density of the crystals increased as the cobalt concentration increased. The location of this band was unchanged as the temperature and the cobalt concentration varied. According to our calculations (see Table 2), the absorption band at 0.84 eV are related to the $^4A_2(F) \rightarrow {}^4T_1(F)$ transitions. Two other bands can be conditioned by the presence of the spin-orbit splitting of $^4T_1(F)$ state of Co^{2+} ion.

The absorption band at 0.43 eV was observed by us before in ZnS:Co, ZnSe:Co and ZnTe:Co crystals [11-13]. According to our calculations and calculations [10] this absorption band is conditioned by $^4A_2(F) \rightarrow {}^4T_2(F)$ transitions between $^4A_2(F)$ ground state and $^4T_2(F)$ first excited state of Co^{2+} ion.

It should be noted that, as the doping level of the crystals increased, the absorption bands broadened. A similar broadening of the structure of the lines takes place in the absorption spectra in the visible spectral region. This is apparently associated with manifestation of the impurity–impurity interaction of the Co^{2+} ions.

DETERMINATION OF THE COBALT DIFFUSIVITY IN THE ZnS CRYSTALS

The presence of characteristic cobalt-absorption lines in the visible region of the spectrum indicates that it is possible to determine the impurity-diffusion profile by measuring the relative optical density (Δ^*). This quantity is a function of the coordinate x in the direction of the diffusion flux and is defined by the expression

$$\Delta^* = \frac{D^*(x) - D^*(\infty)}{D^*(0) - D^*(\infty)}, \qquad (3)$$

where $D^*(x)$ is the crystal's optical density as a function of the coordinate x, $D^*(0)$ is the optical density of the crystal in the surface layer with the coordinate $x = 0$, and $D^*(\infty)$ is the optical density of the crystal in the region, where the cobalt concentration is negligible (the crystal is not doped). The chosen definition of relative optical density makes it possible to compare the dependence $\Delta^*(x)$ with the impurity concentration profile $C(x)/C_0$ calculated by formula (1). By choosing the value of the diffusivity in Eq. (1), we managed to obtain good agreement between the relative optical density and cobalt concentration profiles in the crystals (Fig. 4). The diffusivities of Co in ZnS crystals at temperature 1170-1270 K were calculated similarly. The temperature dependence of diffusivity $D(T)$, presented in inset to Fig. 4, is described by Arrhenius equation

$$D(T) = D_0 \exp\left(-\frac{E}{kT}\right), \qquad (4)$$

where the factor D_0=2.39 cm^2/s, while the activation energy of diffusion E=2.34 eV. At the crystals annealing temperature of 1270 K the diffusivities of chromium is 10^{-9} cm^2/S. This value is a few orders less than cobalt diffusivity in ZnSe crystals, which we determined according to the procedure described in [12].

CONCLUSIONS

The study allows a number of conclusions. These are as follows:

1. The method of cobalt diffusion doping of ZnS single crystals was developed. The maximum concentration of cobalt impurity determined by the shift of the absorption edge in ZnS:Co crystals was $3 \cdot 10^{19}$ cm^{-3}.
2. The nature of absorption lines of ZnS:Co crystals in the visible and IR regions of the spectrum was identified.

3. The diffusivities of cobalt in ZnS crystals in the temperature range 1170-1270 K were calculated for the first time. Analysis of the temperature dependence *D(T)* allowed us to determine the coefficients in Arrhenius equation: D_0=2.39 cm^2/s and *E*=2.34 eV. At 1270 K the diffusivity of Co is 10^{-9} cm^2/s.

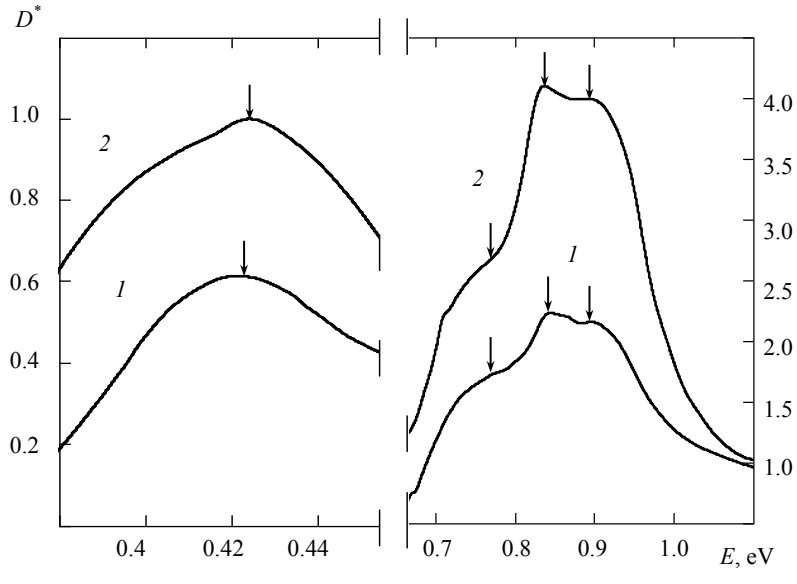

Fig. 3. Spectra of optical density of ZnS:Co crystals in the IR-region. Samples (*1*) 3 and (*2*) 4.

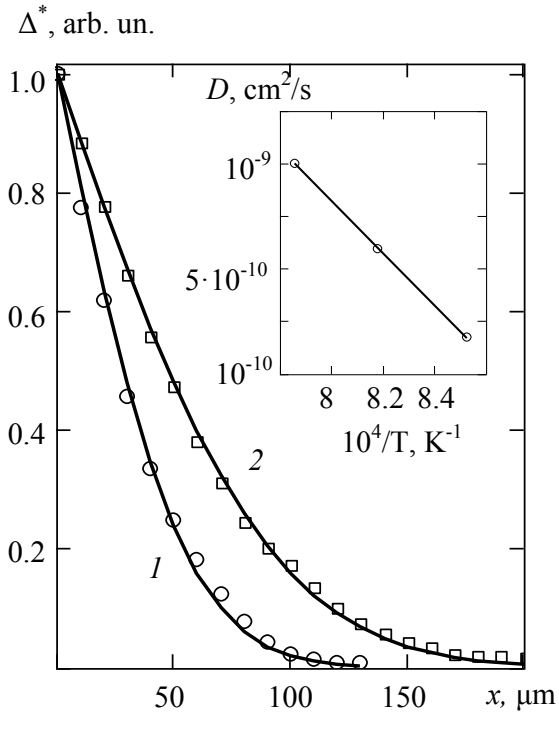

Fig. 4. Profiles of relative optical density (points in the curve) and diffusion profiles of Co (solid lines) of ZnS:Co crystals, samples (*1*) 3 and (*2*) 4. The temperature dependence of the Co diffusivity in ZnS crystals is in the inset.

REFERENCES

1. *Sims R. A.; Kernal J.; Fedorov, V. V.; Mirov, S. B.* Characterization of cobalt doped ZnSe and ZnS crystals as saturable absorbers for alexandrite lasers. Solid State Lasers XV: Technology and Devices. Edited by Hoffman H. J., Shori R. K. Proceedings of the SPIE. — 2006. — V. 61. — P. 216-225.
2. *Tsai T.-Y., Milton B.* Characteristics of Co^{2+}:ZnS saturable absorber Q-switched neodymium lasers at 1.3 μm // J. Appl. Phis. — 2001. — V. 89, № 4. — P. 2009-2016.
3. *Korostelin Yu. V., Kozlovsky V. I., Nasibov A. S., Shapkin P. V.* Vapour growth of II-VI solid solution single crystals // J. Cryst. Growth. — 1999. — V. 159. — P. 181-185.
4. *Ukhanov Yu. I.* Optical Properties of Semiconductors. — Moscow: Nauka. — 1999. — P. 366 .
5. *Агекян В. Ф.* Внутрицентровые переходы ионов группы железа в полупроводниковых матрицах типа A_2B_6 (Обзор) // ФТТ. — 2002. — Т. 44, №. 11. — С. 1921-1999.
6. *Huheey J. E.* Inorganic chemistry, New York: Harper & Row. — 1999. — P. 696.
7. *Wray E. M., Allen J. W.* Crystal field spectra of $3d^n$ impurities in zinc selenide // J. Phys. C: Solid State Phys. — 1999. — V. 4. — P. 512-516.
8. *Noras J. M., Szawelska H. R., Allen J. W.* Energy levels of cobalt in ZnSe and ZnS // J. Phys. C: Solid State Phys. — 1981. — V. 14. — P. 3255-3268.
9. *Соколов В. И., Мамедов А. Н., Суркова Т. П., Чукичев М. В., Кулаков М. П.* Энергетические состояния кобальта в селениде и сульфиде цинка // Оптика и спектроскопия. — 1999 — Т. 62, № 4. — С. 805-811.
10. *Zunger A.* 3d transition atom impurities in semiconductors // Solid State Physics. — 1986. — V. 39. — P. 276-464.
11. *Vaksman* ***Yu. F., Nitsuk Yu. A., Pavlov V. V., Purtov Yu. N., Nasibov A. S., Shapkin P. V.*** Optical properties of ZnS single crystals doped with cobalt // Photoelectronics. — 2007.— № 16. — P. 33-36.
12. *Ваксман Ю. Ф., Павлов В. В., Ницук Ю. А., Пуртов Ю. Н., Насибов А. С., Шапкин П. В.* Получение и оптические свойства монокристаллов ZnSe, легированных кобальтом // ФТП. — 2006. — Т. 40, № 7. — С. 815-818.
13. *Ваксман Ю. Ф., Ницук Ю. А., Павлов В. В., Пуртов Ю.Н., Насибов А. С., Шапкин П. В.* Оптические свойства моно-кристаллов ZnTe, легированных кобальтом // ФТП. — 2007. — Т. 41, В 6. — С. 679-682.

UDC 621.315.592

Yu. A. Nitsuk, Yu. F. Vaksman, Yu. N. Purtov

OPTICAL ABSORPTION AND DIFFUSION OF COBALT IN ZnS SINGLE CRYSTALS

Abstract

ZnS:Co single crystals obtained by diffusion doping are investigated. The spectra of optical density in the energy range 0.4-3.8 eV are investigated. On absorption edge shift of investigated crystals the cobalt concentration is calculated. Nature of optical transitions determining optical properties of ZnS:Co single crystals in the visible and IR-region of spectrum is identified.

The diffusion profile of the Co dopant is determined via measurement of the relative optical density of the crystals in the visible spectral region. The Co diffusivities in the ZnS crystals at 1170-1270 K are calculated. The Co diffusivity at 1270 K equals 10^{-9} cm^2/s.

Key words: zinc sulfide, diffusion doping, cobalt impurity, optical density, diffusivity.

УДК 621.315.592

Ю. А. Ницук, Ю. Ф. Ваксман, Ю. М. Пуртов

ОПТИЧЕСКОЕ ПОГЛОЩЕНИЕ И ДИФФУЗИЯ КОБАЛЬТА В МОНОКРИСТАЛЛАХ ZnS

Резюме

Исследованы монокристаллы ZnS:Co, полученные методом диффузионного легирования. Исследованы спектры оптической плотности в области энергий 0.4-3.8 эВ. По величине смещения края поглощения определена концентрация кобальта в исследуемых кристаллах. Идентифицирована природа оптических переходов, определяющих оптические свойства монокристаллов ZnS:Co в видимой и ИК-области спектра.

Диффузионный профиль примеси кобальта определен путем измерения относительной оптической плотности кристаллов в видимой области спектра. Рассчитаны коэффициенты диффузии кобальта в кристаллах ZnS при температурах 1170-1270 К. При 1270 К коэффициент диффузии кобальта составляет 10^{-9}см^2/с.

Ключевые слова: сульфид цинка, диффузионное легирование, примесь кобальта, оптическая плотность, коэффициент диффузии.

УДК 621.315.592

Ю. А. Ніцук, Ю. Ф. Ваксман, Ю. М. Пуртов

ОПТИЧНЕ ПОГЛИНАННЯ І ДИФУЗІЯ КОБАЛЬТУ В МОНОКРИСТАЛАХ ZnS

Резюме

Методом дифузійного легування отримані монокристали ZnS:Co. Досліджено спектри оптичної густини в області енергій 0.4-3.8 еВ. За величиною зсуву краю поглинання визначена концентрація хрому в досліджуваних кристалах. Ідентифіковані оптичні переходи, що визначають спектр поглинання монокристалів ZnS:Co в видимій та ІЧ області спектру.

Дифузійний профіль домішки Co визначався за вимірюваннями відносної оптичної густини кристалів у видимій області спектру. Вперше розраховано коефіцієнти дифузії кобальту в кристалах ZnS при температурах 1170-1270 К. При 1270 К коефіцієнт дифузії кобальту становить 10^{-9} см^2/с.

Ключові слова: сульфід цинку, дифузійне легування, домішка кобальту, оптична густина, коефіцієнт дифузії.

UDC 539.187

A. V. Loboda, T. B. Tkach

Odessa State Environmental University, 15, Lvovskaya str., Odessa, Ukraine
e-mail: andmolec@mail.ru

ELECTRON-COLLISIONAL SPECTROSCOPY OF ATOMS AND MULTICHARGED IONS IN PLASMA: Ne ATOM AND Be-LIKE IONS

The generalized relativistic energy approach with using the Debye shielding model is used for studying spectra of plasma of the multicharged ions and determination of electron-impact cross-sections and other spectral parameters for Ne-atom and Be-, Ne-like ions.

1. Introduction

Optics and spectroscopy of laser-produced hot and dense plasmas, known as laser plasma, has drawn considerable attention over the last two decades through the recent laser-fusion studies [1-24]. Similar interest is also stimulated by importance of these data for correct description of parameters characteristics for plasma in thermonuclear (tokamak) reactors, searching new mediums for X-ray range lasers. In recent years the X-ray laser problem has stimulated a great number of papers devoted to the development of theoretical methods for modelling the elementary processes in collisionally pumped plasma (see [1-16] and Refs. therein). There are constructed first lasers with using plasma of Li-, Ne-like ions as an active medium. The laser effects have been discovered on the transitions of Ni-like and other ions. An important application of the theory of atomic spectra in plasma is search of the optimum plasma excitation condition for lasing and discovery of new pumping approaches. In addition, these investigations are important to understand the plasma processes themselves. Different atomic levels are populated in a plasma by different physical processes. This results in a different dependence of the each line intensity on the plasma parameters. In most plasma environments the properties are determined by the electrons and the ions, and the interactions between them. The electron-ion collisions play a major role in the energy balance of plasmas. For this reason, modelers and diagnosticians require absolute cross sections for these processes. Cross sections for electron-impact excitation are needed to interpret spectroscopic measurements and for simulations of plasmas using collisional-radiative models.

In many papers the calculations of various atomic systems embedded in Debye plasmas have been performed (as example, see [13-19]). Different theoretical methods have been employed along with the Debye screening to study plasma environments. Two principal theoretical problems must be solved in order to develop a code adequate to predict the plasma parameters for many applications, i.e. accurate estimate of electron-collisional parameters for processes in plasma and kinetics calculations to find level inversions, gain coefficients at definite plasma parameters. Earlier [19-25] we developed a new generalized relativistic energy approach combined with the relativistic many-body perturbation theory (RMBPT) for multi-quasiparticle (QP) atomic systems for studying spectra of plasma of the multicharged ions and electron-ion collisional parameters. The method is based on the Debye shielding model and energy approach [4-8,21-25]. Here some new results on oscillator strengths and energy shifts due to the plasma environment effect, collisional excitation cross-sections for atom of neon and some Be, Ne-like ions are presented for different plasma parameters.

2. Energy approach in scattering theory and the Debye shielding model

The generalized relativistic energy approach combined with the RMBPT has been in details described in Refs. [21-24]. It generalizes earlier

developed energy approach by Ivanov-Ivanova et al [4-8]. Here we briefly present the key moments of our method. Namely, the key idea is in calculating the energy shifts D*E* of degenerate states that is connected with the secular matrix *M* diagonalization [4-6]. To construct *M*, one should use the Gell-Mann and Low adiabatic formula for D*E*. The secular matrix elements are already complex in the PT second order (the first order on the inter-electron interaction). The whole calculation is reduced to calculation and diagonalization of the complex matrix *M* .and definition of matrix of the coefficients with eigen state vectors $B^{K}_{ie,iv}$ [4-6,19]. To calculate all necessary matrix elements one must use the basis's of the 1QP relativistic functions. In many calculations of the atomic elementary process parameters it has been shown that their adequate description requires using the optimized basis's of wave functions. In [6] it has been proposed "ab initio" optimization principle for construction of cited basis's. There is used the minimization of the gauge dependent multielectron contribution of the lowest QED PT corrections to the radiation widths of atomic levels. In the fourth order of QED PT there appear diagrams, whose contribution into the ImdE accounts for the polarization effects. This contribution describes collective effects and it is dependent upon the electromagnetic potentials gauge (the gauge non-invariant contribution dE_{ninv}). The minimization of functional $ImdE_{ninv}$ leads to an integral differential equation, that is numerically solved. In result one can get the optimal one-electron basis of the PT [21-23]. As an example, consider the collisional de-excitation of the Ne-atom:

$$((2j_{iv})^{-1}3j_{ie}[J_iM_i],\ \varepsilon_{in})\rightarrow(\Phi_o,\ \varepsilon_{sc}). \qquad (1)$$

Here Φ_o is the state of the ion with closed shells (ground state of the Ne-like ion); J_i is the total angular moment of initial target state; indices *iv, ie* are related to initial states of vacancy and electron; indices ε_{in}, ε_{sc} are the incident and scattered energies respectively to incident and scattered electrons. The initial state of the system «atom plus free electron» can be written as

$$|I>= a^{+}_{in}\sum_{m_{iv},m_{ie}} a^{+}_{ie}a_{iv}\Phi_o C^{J_i,M_i}_{m_{ie},m_{iv}} \qquad (2)$$

Here $C^{J_i,M_i}_{m_{ie},m_{iv}}$ is the Clebsh-Gordan coefficient. Final state is as follows: where Φ_o is the state of an ion with closed electron shells (ground state of Ne-like ion), $|I>$ represents the 3QP state, and $|F>$ represents the 1QP state. The justification of the energy approach in the scattering problem is in details described in [4-6,21-23]. For the state (2) a scattered part of energy shift ImdE appears first in the second order of the atomic perturbation theory. The collisional de-excitation cross section is defined as follows:

$$\sigma(IK\rightarrow 0)=2\pi\sum_{j_{in},j_{sc}}(2j_{sc}+1)$$
$$\{\sum_{j_{ie},j_{iv}}<0\,|\,j_{in},j_{sc}\,|\,j_{ie},j_{iv},J_i>B^{IK}_{ie,iv}\}^2 \qquad (3)$$

The amplitude like combination in (3) has the following form:

$$<0\,|\,j_{in},j_{sc}\,|\,j_{ie},j_{iv},J_i>=\sqrt{(2j_{ie}+1)(2j_{iv}+1)}$$
$$(-1)^{j_{ie}+1/2}\times\sum_{\lambda}(-1)^{\lambda+J_i}\times \qquad (4)$$
$$\times\{\delta_{\lambda,J_i}/(2J_i+1)Q_\lambda(sc,ie;iv,in)+$$
$$+\begin{bmatrix} j_{in}\ldots j_{sc}\ldots J_i \\ j_{ie}\ldots j_{iv}\ldots.\lambda\end{bmatrix}Q_\lambda(ie;in;iv,sc)\},$$

where $Q_\lambda = Q_\lambda^{\mathrm{Qul}} + Q_\lambda^{\mathrm{Br}}$ is, as a rule, the sum of the Coulomb and Breit matrix elements.

Further consider the Debye shielding model. It is known (see [10-14,19] and refs. therein) in the classical theory of plasmas developed by Debye and Hückel, the interaction potential between two charged particles is modelled by a Yukawa - type potential as follows:

$$V(r_i,\ r_j) = (Z_aZ_b/|r_a-r_b|\}exp\ (-\mu|r_a-r_b|), \qquad (5)$$

where r_a, r_b represent respectively the spatial coordinates of particles A and B and Z_a,Z_b denote their charges. A difference between the Yukawa type potential and standard Coulomb potential is in account for the effect of plasma, which is modeled by the shielding parameter μ [1]. The parameter μ is connected with the plasma parameters such as the temperature *T* an d the charge density n as follows: $\mu\sim\sqrt{e^2n/k_BT}$. Here, as usually, e is the electron charge and κ_B is the

Boltzman constant. The density n is given as a sum of the electron density N_e and ion density N_k of the k-th ion species having the nuclear charge q_k : $n = N_e + \sum_k q_k^2 N_k$. Under typical laser plasma conditions of T~1keV and n~10^{22} cm^{-3} the parameter μ is of the order of 0.1 in atomic units [13,14]. If the Debye radius limits to 0, or a parameter μ becomes very large, the Debye approximation doesn't be true. If the parameter μ becomes very small, the plasma screening effect on the plasma-embedded atomic systems is not significant. But, even in this case it is practically useful to apply the formulas of the Debye shielding model. By introducing the Yukawa-type e-N and e-e interaction potentials, an electronic Hamiltonian for N-electron multicharged ion in a plasma is in atomic units as follows [19]:

$$H = \sum_i [\alpha cp - \beta mc^2 - Z\exp(-\mu r_i)/r_i] + \sum_{i>j} \frac{(1-\alpha_i\alpha_j)}{r_{ij}} \exp(-\mu r_{ij}) \quad (6)$$

A difference between our model Hamiltonian (6) and analogous model Hamiltonian with the Yukawa potential of Refs. [13,14] is in using the relativistic approximation, which is obviously necessary for adequate description of such relativistic systems as the high-Z multicharged ions. To describe the electron-ionic core interaction we use the optimized Dirac-Fock potential (for Be-like ions) or optimized model potential by Ivanova et al (for Ne-like ions) with one parameter [8], which calibrated within the special ab initio procedure within the relativistic energy approach [6]. The modified PC numerical code 'Superatom" is used in all calculations. Other details can be found in Refs. [4-8, 19-24].

3. Results

We applied our approach to calculate the radiative and collisional characteristics (energy shifts, oscillator strengths, electron-ion cross-sections and collision strengths) for the neon atom and Be-, Ne-like ions embedded to the plasma environment. Firstly, we present our results on energy shifts and oscillator strengths for transitions $2s^2$-$2s_{1/2}2p_{1/2,3/2}$ in spectra of the Be-like Ni and Kr. The corresponding plasma parameters are as follows: n_e=10^{22}-10^{24}cm^{-3} , T=0.5-2 keV (i.e. m~0.01-0.3). In table 1 and 2 we list the results of calculation of the energy shifts DE (cm^{-1}) for $2s^2$-$[2s_{1/2}2p_{1/2,3/3}]_1$ transitions and oscillator strengths changes for different plasma parameters (the electron density and temperature). There are also listed the available data by Li etal and Saha-Frische: the multiconfiguration Dirac-Fock (DF) calculation results and ionic sphere (I-S) model simulation data (from [13,19] and refs. therein). The analysis shows that the presented data are in physically reasonable agreement, however, some difference can be explained by using different relativistic orbital basises and different models for accounting of the plasma screening effect. From the physical point of view, the behavior of the energy shift is naturally explained, i.e by increasing blue shift of the line because of the increasing the plasmas screening effect. The electron-ion collisional characteristics of the Be-like ions are of a great importance for such applications as diagnostics of astrophysical, thermonuclear plasma and also EBIT plasma [1-13]. In the last case the characteristic values of electron density are significantly lower as the considered above on several orders. In [16,17] it is performed the MEIBEL (merged electron-ion beams energy-loss) experiment. The experimental data (dots) are listed for Be-like ion of oxygen in figure 1, where the cross-section of electron-impact excitation of $[2s^2\,{}^1S$ -$(2s2p\,{}^1P)]$ transition for Be-like oxygen is presented. In figure 1 there are also presented the theoretical results for the cross-section (in 10^{-16} cm^3), obtained by calculation on the basis of the 3-configuration R-matrix theory and our data [16,25]. The analysis shows that for energies lower 20eV there is a physically reasonable agreement between data of both theories and experiment. For energies higher 20eV there is a large disagreement of our data and R-matrix data.

It is provided by different degree of accounting for the correlation effects (configuration interaction) and different basises of relativistic wave functions. In table 3 there are listed our theoretical results and experimental data by Khakoo et al [23] for integral electron-impact cross-sections (in 10^{-19}cm^2) of excitation of the neon atom to the $2p^53s[3/2]^o_2$, $2p^53s[1/2]^o_0$ states

of the $2p^5 3s$ configuration. The full data for neutral Ne are in Ref. [25]. Further we present results of studying collisional parameters of ions in collisionally pumping plasma of the Ne-like ions with parameters T_e= 20-40eV and density $n_e = 10^{19\text{-}20}$ cm^{-3}. This system is of a great interest for generation of laser radiation in the short-wave range of spectrum [4].

Table 1. Energy shifts DE (cm^{-1}) for $2s^2$-$[2s_{1/2}2p_{3/2}]_1$ transition in spectra of the Be-like Ni and Kr for different values of the n_e (см$^{-3}$) and T (in eV) (see explanations in text)

	n_e	10^{22}	10^{23}	10^{24}	10^{22}	10^{23}	10^{24}
Z	kT	Li et al	Li et al	Li et al	Our data	Our data	Our data
NiXXV	500	31.3	292.8	2639.6	33.8	300.4	2655.4
	1000	23.4	221.6	2030.6	25.7	229.1	2046.1
	2000	18.0	172.0	1597.1	20.1	179.8	1612.5
	I-S	8.3	86.6	870.9			
KrXXXIII	500	21.3	197.9	2191.9	27.2	215.4	2236.4
	1000	15.5	150.5	1659.6	21.3	169.1	1705.1
	2000	11.5	113.5	1268.0	16.9	128.3	1303.8

Table 2. Oscillator strengths gf for $2s^2$-$[2s_{1/2}2p_{3/2}]_1$ transition in Be-like Ni and Kr for different values of the n_e (см$^{-3}$) and T (in eV) (gf_0 –the gf value for free ion)

n_e		10^{22}	10^{23}	10^{24}		10^{22}	10^{23}	10^{24}
kT	Li etal	Li etal	Li etal	Li etal	gf_0-our	our data	our data	our data
500	0.1477	0.1477	0.1478	0.1487	0.1480	0.1480	0.1483	0.1495
1000		0.1477	0.1477	0.1482		0.1480	0.1483	0.1495
2000		0.1477	0.1477	0.1481		0.1479	0.1482	0.1493
I-S		0.1477	0.1477	0.1479				

Figure 1. Cross-section of electron-impact excitation of [$2s^2$ ^{1}S -($2s2p$ ^{1}P)] transition for Be-like oxygen with the MEIBEL experiment data (dots); theory — R-matrix theory (continuous line) [16,17]; our theory (dotted line).

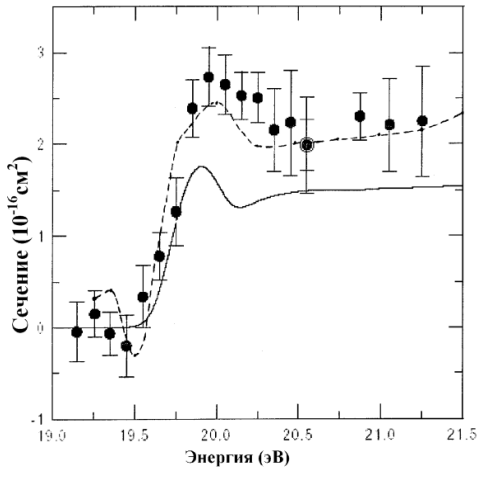

Table 3. Theoretical (Th.; our) and experimental (Exp.) data by Khakoo et al [23] for integral electron-impact cross-sections (in 10^{-19}cm^2) of excitation of neon atom to the $2p^5 3s[3/2]^o_2$, $2p^5 3s[1/2]^o_0$ states of the $2p^5 3s$ configuration. (E_0,eV) [10,11,19]

E_0	Exp.- $2p^5 3s[3/2]^o_2$	Exp.- $2p^5 3s[1/2]^o_0$	Th. - $2p^5 3s[3/2]^o_2$	Th.- $2p^5 3s[1/2]^o_0$
20	14.6	2.7	14.9	2.9
30	9.7	1.7	9.9	1.8
40	4.9	1.1	5.1	1.15
50	4.0	0.9	3.9	0.8
100	0.5	0.1	0.4	0.13

It is obviously more complicated case in comparison with previous one. Here an accurate account of the excited, Rydberg, autoionization and continuum states plays a critical role. In table 4 we present the theoretical values of the collisional excitation rates (CER) and collisional de-excitation rates (CDR) for Ne-like argon transition between the Rydberg states and from the Rydberg states to the continuum states (see details in [5,19]). Speech is about the Rydberg states which converge to the corresponding lower boundary of continuum -e_0 (figure 2). As it is indicated in [5,19], the parameter -e_0 is the third parameter of the plasma

environment (together with electron density and temperature). In fact it defines the thermalized energy zone of the Rydberg and autoionization states which converge to the ionization threshold for each ion in a plasma. Usually value e_0 can be barely estimated from simple relation: $e_0=0.1\times T_e$. In the consistent theory the final results must not be dependent on the model parameters, so the concrete value of e_0 is usually chosen in such way that an effect of its variation in the limits $[0.01\times T_e, 0.1\times T_e]$ (for Ne-like ions) doesn't influence on the final results. Usually few subzones can be separated in the zone of Rydberg states (figure 2) [5]. In tables 4 and 5 we list the theoretical collisional excitation (CER) and de-excitation (CDR) rates for Ne-like Ar in plasma with $n_e=10^{19\text{-}20}cm^{-3}$, T_e =20eV (table 4) and 40 eV (table 5). For comparison there are listed data by Ivanov etal (RMPPT without shielding effect [4,5]).

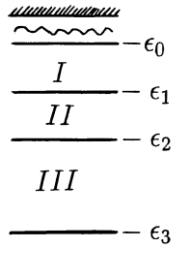

Figure 2. Rydberg states zones (Ne-like ion: [Ne,i],nl); e_0 is a boundary of thermalized zone, neighboring to continuum; e_3 -ionization potential for states nl=3s; $e_2=(e_0+e_3)/2$, $e_1=(e_0+e_2)/2$

This effect plays an important role for Debye plasma. An account for exchange-correlation effects and superposition of the highly-lying excited states are quantitatively important for adequate description of the collision parameters. In our scheme the optimal 1-QP basis is used. The PT first order correction is calculated exactly, the high-order contributions are taken into account for effectively: polarization interaction of the above-core QPs and effect of their mutual screening (correlation effects). The calculations encourage us to believe that using energy approach combined with the optimized relativistic Debye-model many-body PT is quite consistent and effective tool from point of view of the theory correctness and exactness. Obviously, the presented approach can be used in theory of other collisional processes and, in general speaking, other systems (see [24] and refs. therein). Its using is very perspective when the experimental data on corresponding properties and systems are very scarce or absent.

Table 4. The collisional excitation (CER) and de-excitation (CDR) rates (in cm^3/s) for Ne-like argon in plasma with parameters: $n_e= 10^{19\text{-}20}\ cm^{-3}$ and temperature T_e =20eV.

		RMPPT			Our data		
Parameters	n_e, cm^{-3}	T_e = 20eV	T_e = 20eV	T_e = 20eV	T_e = 20eV	T_e = 20eV	T_e= 20eV
Transition		1→2	1→3	2→3	1→2	1→3	2→3
CDR (i→i ;k)	1.0+19	5.35-10	1.64-10	1.13-09	5.77-10	1.92-10	1.28-09
	1.0+20	5.51-10	1.60-10	1.12-09	5.94-10	1.78-10	1.25-09
Transition		2→1	3→1	3→2	2→1	3→1	3→2
CER (i→i ;k)	1.0+19	5.43-10	5.39-12	2.26-11	5.79-10	1.88-12	2.64-11
	1.0+20	3.70-10	8.32-12	2.30-11	4.85-10	1.13-11	2.78-11

Table 5. Collisional excitation (CER) and de-excitation (CDR) rates (in cm^3/s) for Ne-like argon in plasma with parameters: $n_e= 10^{19\text{-}20}\ cm^{-3}$ and temperature T_e =40eV (our data)

Parameters	n_e, cm^{-3}	T_e =40 eV	T_e =40 eV	T_e =40 eV
Transition		1→2	1→3	2→3
CDR (i→i ;k)	1.0+19	3.18-10	8.45-11	6.81-10
	1.0+20	5.02-10	1.56-10	4.99-10
Transition		2→1	3→1	3→2
CER (i→i ;k)	1.0+19	5.33-10	5.63-10	7.11-11
	1.0+20	7.67-10	6.94-11	8.93-11

References

1. Oks E., Stark Broadening of Hydrogen and Hydrogenlike Spectral Lines in Plasmas: The Physical Insight (Oxford: Alpha Science International).— 2006.

2. Griem H R, Spectral Line Broadening by Plasmas (New York: Academic Press).-1974.
3. Oks E., Relation between Theories, Experiments, and Simulations of Spectral Line Shapes//Int. Journ. Spectroscopy. — 2010. —Vol. 10. — P. 852581.
4. Ivanova E. P., Grant I., Oscillator strength anomalies in Ne iso-electronic sequence with applications to X-ray laser modeling// J. Phys.B:At.Mol.Phys.— 1998 — Vol. 31. — P. 2871-2883
5. Ivanov L. N., Ivanova E. P., Knight L., Energy Approach to consistent QED theory for calculation of electron-collision strengths/ //Phys.Rev.A. — 1993. — Vol. 48. — P. 4365-4374.
6. Glushkov A. V., Ivanov L. N., Radiation Decay of Atomic States: atomic residue and gauge non-invariant contributions// Phys. Lett.A. — 1992. — Vol. 170 (1). — P. 33-38.
7. Glushkov A. V., Ivanov L. N., DC Strong-Field Stark-Effect: consistent quantum-mechanical approach//J.Phys. B: At. Mol.Phys. — 1999. — Vol. 26. — P.L379-386.
8. Ivanov L. N.,Ivanova E. P., Extrapolation of atomic ion energies by model potential method: Na-like spectra/ // Atom.Data Nucl.Data Tab. — 1999. — Vol. 24. — P. 95-121.
9. Badnell N. R., Calculations for electron-ion collisions and photoionization processes for plasma modeling// J. Phys. CS.— 2007. — Vol. 88. — P. 012070 (12p.).
10. Khakoo M. A., Wrkich J., Larsen M., Kleiban G., Kanik I., Trjmar S., Brubger M. J. et al, Differential cross-sections and cross-sections ratios for the electron-impact excitation of the neon $2p^5 3s$ configuration//Phys.Rev.A.— 2002. — Vol. 65. — P. 062711.
11. Khakoo M. A., Vandeventer P., Childers J.G. etal, Electron-impact excitation of argon $3p^5 4s$ configuration: Differential cross-sections and cross-sections ratios// J. Phys. B: At. Mol. Phys.—2004.— Vol. 37.— P. 247-281.
12. Griffin D., Balance C., Mitnik D., Berengut J., Dirac *R*-matrix calculations of electron-impact excitation of Ne-like Kr//J. Phys.B:At.Mol.Opt.Phys. — 2008.— Vol. 41.— P. 215201.
13. Yongqiang Li, JianhuaWu, Yong Hou, Jianmin Yuan, Influence of hot and dense plasmas on energy levels and oscillator strengths of ions: Be-like ions for Z = 26–36// J. Phys. B: At. Mol. Opt. Phys. — 2008. — Vol. 41. — P. 145002.
14. Okutsu H., SakoI., Yamanouchi K., Diercksen G., Electronic structure of atoms in laser plasmas: Debae shielding approach// J.Phys. B: At. Mol.Phys. — 2005 — Vol. 38. — P. 917-927.
15. Nakamura N., Kavanagh A., Watanabe H, Sakaue H., Li Y., Kato D., Curell F, Ohtani S., Relativistic effects on resonant interactions between electrons and highly charged ions// J.Phys.CS. — 2007. — Vol. 88. — P. 012066 (6p).
16. Bannister M., Djuric N., Woitke O., Dunn G., Chung Y., Smith A., Wallbank B., Berrington K., Absolute cross-sections for near-threshold electron-impact excitation of Be-like C^{2+},N^{3+},O^{4+} ions//Int. Journ. of Mass Spectrometry. — 1999. — Vol. 192. — P. 39-48.
17. Smith A., Bannister M., Chung Y., Djuric N., Dunn G., Wal-lbank B., Woitke O., Near-threshold electron-impact excitation of multiply-charged Be-like ions//Phys.Scr. — 1999. — Vol. T 80 — P. 283-287.
18. Talukder, M. R., Electron impact total ionization cross sections of beryllium and boron isoelectronic ions// Applied Phys. Lasers and Opt. — 2008.— Vol. 93. — P. 576-574.
19. Malinovskaya S. V., Glushkov A. V., Khetselius O. Yu., Perelygina T. B., Svinarenko A., Loboda A.V., Lopatkin Yu.M., Nikola L.V., Generalized energy approach to calculating electron collision cross-sections for multicharged ions in a plasma: Debye shielding model// Int. Journ. Quant.Chem 2011. — Vol.111. — P. 288-296.
20. Glushkov A. V., Khetselius O. Yu.,

Gurnitskaya E. P., Loboda A.V., Florko T. A., Sukharev D. E.,.Lovett L., Gauge-invariant QED perturbation theory approach to calculating nuclear electric quadrupole moments, hfs constants for heavy atoms and ions// Frontiers in Quantum Systems in Chem. and Phys. (Springer). — 2008. — Vol. 18. — P. 505-522
21. Glushkov A. V., Ambrosov S. V., Loboda A. V., Gurnitskaya E.P., Prepelitsa G. P., Consistent QED approach to calculation of electron-collision excitation cross-sections and strengths: Ne-like ions//Int. Journ. Quant.Chem. — 2005. —Vol. — 104.— № 4. — P. 562-569.
22. Glushkov A. V., Malinovskaya S. V., Loboda A. V., Shpinareva I. M., Gurnitskaya E. P., Korchevsky D. A., Diagnostics of the collisionally pumped plasma and search of the optimal plasma parameters of x-ray lasing: Calculation of electron-collision strengths and rate coefficients for Ne-like plasma// Journ. Physics: CS. — 2005. — Vol. 11. — P. 188-198.
23. Florko T., Loboda A., Svinarenko A., Sensing forbidden transitions in spectra of some heavy atoms and multicharged ions: New scheme//Sensor Electr. & Microsys.Tech. — 2009. — № 3. — P. 10-15.
24. Loboda A. V., The electron capture processes in the ion-atomic collision system structure: Energy approach// Sensor Electr. and Microsyst. Techn. — 2009.— № 2. — P. 21-25
25. Loboda A. V., Electron-collisional spectroscopy of neutral neon atom for low and middle collision energies//Preprint of OSENU, N1.-2012.-24P.

UDC 539.187

A. V. Loboda, T. B. Tkach

ELECTRON-COLLISIONAL SPECTROSCOPY OF ATOMS AND MULTICHARGED IONS IN PLASMA: Ne ATOM AND Be-LIKE IONS

Abstract. The generalized relativistic energy approach with using the Debye shielding model is used for studying spectra of plasma of the multicharged ions and determination of electron-impact cross-sections and other spectral parameters for Ne-atom and Be-, Ne-like ions.

Key words: electron-collisional spectroscopy, relativistic energy approach

УДК 539.187

А. В. Лобода, Т. Б. Ткач

ЭЛЕКТРОН-СТОЛКНОВИТЕЛЬНАЯ СПЕКТРОСКОПИЯ АТОМОВ И МНОГОЗАРЯДНЫХ ИОНОВ В ПЛАЗМЕ: АТОМ Ne, Be-ПОДОБНЫЕ ИОНЫ

Резюме. На основе обобщенного релятивистского энергетического подхода с использованием модели экранирования Дебая выполнено изучение спектра плазмы многозарядных ионов и рассчитаны столкновительные сечения возбуждения и другие параметры для атома неона и Be-, Ne-подобных ионов.

Ключевые слова: электрон-столкновительная спектроскопия, энергетический подход

УДК 539.187

А. В. Лобода, Т. Б. Ткач

СПЕКТРОСКОПІЯ ЗА РАХУНОК ЕЛЕКТРОННИХ ЗІТКНЕНЬ АТОМІВ ТА БАГАТОЗАРЯДНИХ ІОНІВ У ПЛАЗМІ: АТОМ Ne, Be-ПОДІБНІ ІОНИ

Резюме. На основі узагальненого релятивістського енергетичного підходу з використанням моделі екранювання Дебая виконано вивчення спектру плазми багатозарядних іонів і розраховані перерізи збудження за рахунок зіткнень і інші спектральні параметри для атома неону і Be- ,Ne-подібних іонів.

Ключові слова:електронна спектроскопія за рахунок зіткнень, енергетичний підхід

UDC 537. 311. 33: 622. 382.33

I. R. Iatsunskyi

Odessa I. I. Mechnikov National University, Department of Experimental Physics,
65023 Ukraine, Odessa, Pastera, 42. e-mail: yatsunskiy@gmail.com

EVOLUTION OF STRUCTURAL DEFECTS IN SILICON CAUSED BY HIGH-TEMPERATURE OXIDATION

The dislocation self-organization processes in near-surface silicon layers of Si-SiO_2 during high temperature oxidization have been investigated. It was observed the complex destruction of these layers caused by relaxation of mechanical stresses. We have proposed the defect formation mechanism of near-surface layers in Si-SiO_2 structure. For self-organization processes to be explained, the synergetic method was applied. It was shown that the formation of periodical dislocation structures at the interface is a consequence of the spatial instability of the dislocation distribution in the crystal, their self-organization due to correlation effects between the oxygen diffusing along structural defects and an ensemble of dislocations.

1. INTRODUCTION

Structures Si-SiO_2 are widely used in modern micro and nano – electronics. Electrophysical parameters of these structures depend on many factors. The property of initial semiconductor, silicon dioxide parameters, and the presence of structural defects on the interface can have an effect on the quality of devices based on the Si-SiO_2 structure [1]. Despite a huge number of articles related to this problem, interest in the study and production of the Si-SiO_2 structure is increasing. Due to transition of the active devices elements to nanoscale the quality of the Si-SiO_2 interface plays an important role in electrical processes. Even existence of one dislocation in space-charge zone of the device leads to catastrophic degradation of ten thousands nanoscale elements and as a consequence causes a reduction in quality of functional units [2, 3].

Dislocations in silicon and other semiconductors have been well studied both theoretically and experimentally. Properties of dislocations were under investigation since the initial observations of these extended defects in crystalline semiconductors. Complexity of the investigations was related to large variety of dislocation structures and to strong interaction of dislocations with impurities and other defects [1]. Moreover, previously applied methods for introduction of dislocations to the bulk of the crystal, i.e. plastic deformation, indentation, oxide precipitation etc., were not capable of well-controlled fabrication of dislocations regarding their structure, electro-optical properties, location and state of decoration with impurities. As a result, many important properties of dislocations still remain under discussion. Namely, relations of optical and electrical properties of dislocations with their microscopic structure were not yet well established.

On the other hand, the complex defect structure is formed at near-surface Si-SiO_2 interface during high-temperature oxidization. The disordered silicon layer and the dislocation network layer are both present in this structure. Also, the additional chemical treatment of dislocation networks allowed us to obtain nanostructured silicon surface which fluoresces in a visible spectrum range [4]. Such a periodical structure as a dislocation network is a consequence of self-organization processes of defects at near-surface silicon layers of the Si-SiO_2 interface.

The self-organization of ordered structures is a recurring theme in physics, chemistry, and biology. Spatially periodic patterns, in particular, are observed at length scales ranging from the atomic to the astronomical. Self-organized patterns are rarely perfect; topological defects, such as dislocations and disclinations, are an intrinsic element of their phenomenology.

This paper is devoted to studying of dislocation self-organization processes in silicon during high temperature oxidization. We have been tasked with investigating on the complex defect structure of the Si-SiO_2 interface and to determine the mechanism of self-organization processes of dislocations.

2. EXPERIMENTAL RESULTS

The experiments were carried out on p-type Si samples cut from the Czochralski grown wafers. The initial wafers were doped with boron ($N_B \sim 10^{15}$ cm^{-3}). The silicon wafers were oxidized in dry oxygen at 1150C (the oxide thicknesses were about 0.1 – 1.5 μm) followed by etching in a hydrofluoric (HF) acid solution and treatment of the silicon surface by selective etchants (SE). To reveal the deformation-induced defects (dislocations), the surface of samples was selectively etched by the Secco-etchant and the Sirtl-etchant for the (100) and (111) surfaces, respectively.

The following techniques and equipment were used for examination of the silicon surface upon chemical treatment:

- Scanning electron microscopes (SEM) (Cam-Scan 4-D with a Link-860 system of an energy dispersion analyzer; REM-104);
- Auger electron spectroscopy (AES) («Riber» Las-300 spectrometer);
- Optical methods using an MMR-2R microscope;
- X-Ray analysis.

During investigations of near-surface silicon layers of the Si-SiO_2 interface the complex defect structure was revealed. Directly below the silicon dioxide there was a layer of disordered silicon. A pattern of the silicon surface upon removed a 1 μm thick dioxide is shown in Figure 1. The tendency is clearly seen for the absence of etch pits typical for a crystalline structure. The irregularly shape pits can be associated with the oxide formed under enhanced diffusion of oxygen along structural defects. We were unable to view the silicon surface using an SEM since the surface was heavily charged. This made it impossible to obtain a reflected electron beam. These results enabled us to conclude that the silicon surface had a highly disordered structure close to a fine-polycrystalline or even an amorphous. X-Ray analysis allowed us to calculate the average sizes of silicon grain. The sizes were about 0.3 – 1 μm and depend on oxidization conditions, the structural defect density and dioxide thickness [5].

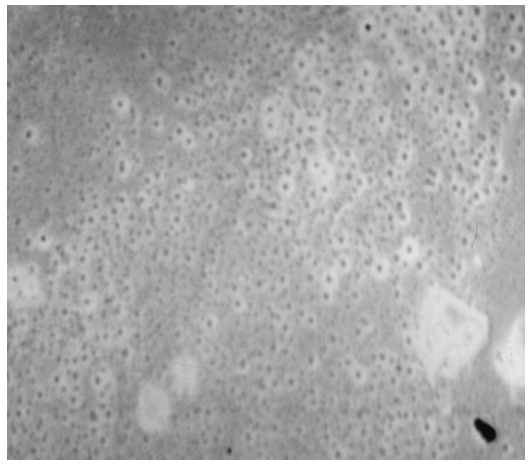

Figure 1. Optical image of the silicon surface after removal of an oxide layer (1 x 1000).

With further 5 minutes of SE, dislocation networks were formed on the silicon surface (Figure 2 (a, b)). The dislocation networks were decorated by SiO_x. This observation is supported by the fact that further etching can be performed without an oxidant. This is also confirmed by an X-Ray analysis and Auger spectroscopy analysis (Table 1). Given the SE velocity is about 3 μm/min ; the depth of dislocation networks was calculated to be about 30 μm for an oxide thickness of 1 μm . The thickness of the silicon layer with dislocation networks was about 10 μm .

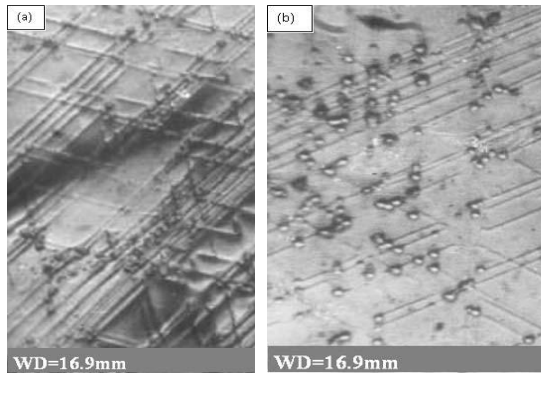

Figure 2. (a) SEM image of a typical dislocation network pattern upon selective etching in the Sirtl-etchant for 10 min. (b) SEM image of a typical dislocation network pattern upon selective etching in the Sirtl-etchant for 15 min.

Table 1. Calculations of Auger-spectra of elements in the dislocation network.

Element	Amount, % [atomic percent]
K	0.00
C	0.452
Na	0.04
Si	95.245
O	3.742

The dislocation networks occur at the disordered silicon – crystalline silicon interface and disappear at the interface between the two nearest silicon layers (Figure 3) [6]. In case of the absence of layered structure, dislocation networks transform in the single dislocations (Figure 4).

Figure 3. A typical SEM image of the silicon wafer cleavage with a layered structure.

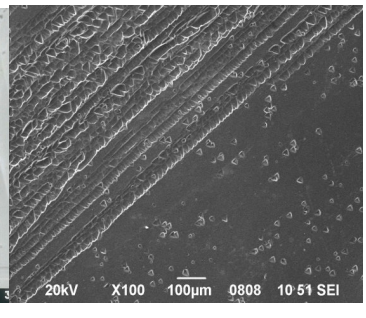

Figure 4. A typical SEM image of single dislocations on the silicon wafer cleavage.

It is known, that dislocations which are generated under the influence of diffusion impurity, form the flat dislocation network that are parallel to the solidification front. Stresses lead to plastic deformations due to a difference of atomic radius of the dopant and silicon (for example: R_{Si} = 1.17 Å, R_B = 0.88 Å, R_P = 1.10 Å). The Wegard's law describes the deformation if the dopant atom penetrates into the crystal (taking into account the sp^3 hybridization) [7]

$$\varepsilon = \omega N, \qquad (1)$$

where ω - Vegard's coefficient (depends on a type of impurity atoms and their lattice position), N – impurity concentration. Besides, stresses in the crystal due to the penetration of atoms with another radius are described by the following equation [8]

$$\sigma = 2 \cdot \omega \cdot \mu \cdot \frac{1+\nu}{1-\nu}(N_0 - \frac{1}{a}\int_0^a N(y)dy), \qquad (2)$$

where μ – shear modules, ν – Poisson ratio, y – the interior plane of the crystal and limited by planes situated at a given distance. Calculations have shown that the stresses (concentration of the impurity) required for Boron at which plastic deformation occurs are about 10^{18} cm^{-3} [9]. A pattern of the dislocation network which was generated under the influence of Boron is shown in Figure 5.

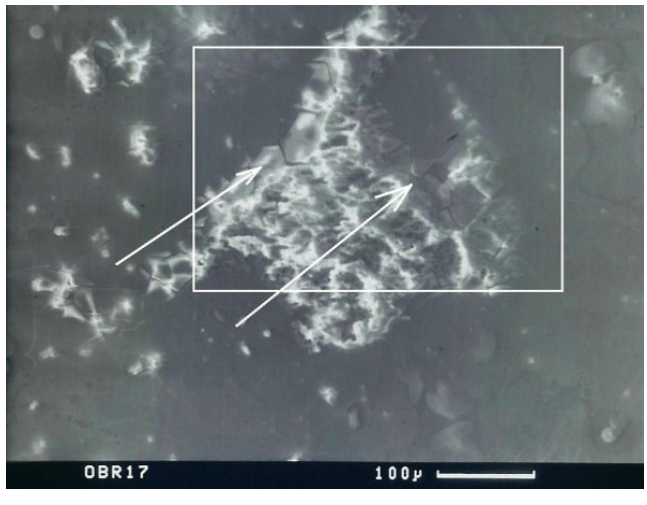

Figure 5. SEM image of a typical dislocation network pattern (concentration of the Boron is 3 10^{18} cm^{-3}).

We can explain the generation of dislocation networks at the silicon in the same initial analysis. The ionized oxygen overcomes the potential barrier at silicon surface and penetrates into the interstices of silicon crystal lattice. The knocking out processes of silicon atoms of the crystal lattice are begun when oxygen ions reach the saturation stage. Silicon atoms diffuse into the bulk due to the impossibility to fill the interstices occupied by oxygen. This process is accompanied by a rapid diffusion of oxygen along the lines of structural defects, thereby raising the level of mechanical stress. Thus, the increasing of mechanical stresses

in the surface layer of silicon at the early stage of oxidation leads first to the elastic deformation and then to plastic deformation respectively. Stresses in silicon layers cause the different types of defects depending on these stresses values. The layer of maximum oxygen concentration is becoming the silicon dioxide with an amorphous structure. Next layer of silicon has highly disordered structure of oxygen-rich nonstoichiometrical oxides. And last layer consists of dislocation networks decorated by oxygen and nonstoichiometrical oxides. It should be noted that the boundary between disordered silicon and dislocation networks is relative because of the disordered silicon consists of grain boundary dislocations.

3. THEORETICAL MODEL

Unfortunately, this empirical theory failed to explain why, in some cases, the dislocations are organized in a strictly periodic structure. For this structuring of the silicon surface to be clarified, we applied synergetic method.

The formation of defect structures like dislocation networks is the consequence of spatial instability of the distribution of dislocations in the crystal and their self-organization. There are two different conditions of behavior of the defect ensemble during plastic deformation. The plastic flow regime takes place for insignificant stresses and low defects density. This regime of plastic flow is carried out autonomously by external influences. At a certain magnitude of the stress, the coherent regime takes place, and the correlations effects between dislocations begin to appear [10-12].

Let us consider the following model (Figure 6). A semi-infinite plane X0Y is an interface Si-SiO_2. Let us fix some plane at a certain depth Z_1.

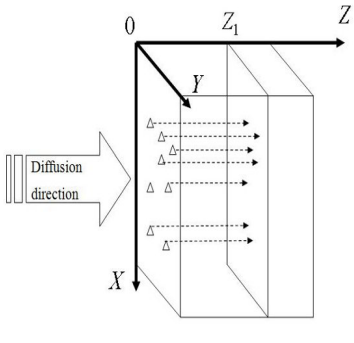

Figure 6. Diffusion model (triangles — dislocations on the surface, dash lines — directions of enhanced diffusion of oxygen).

During high-temperature oxidation in a given plane will be the processes that lead to the formation of structural defects, and to their annihilation. The kinetic equation for the dislocation density N_d in the given plane is

$$\frac{dN_d}{dt} = AN_d - BN_d^2 + CN_dN_o, \qquad (3)$$

where A is a constant characterizing the sources of the generation of structural defects, B is a constant characterizing the sources of the annihilation of dislocations, and here is characterized by a quadratic law [11], C is a constant characterizing the generation of dislocations due to stresses caused by the oxygen penetrated along the dislocation, N_o is an oxygen concentration.

It is obvious, that the concentration of oxygen in the given plane depends on the density of structural defects, along which occurs the enhanced diffusion. Thus, a case of self-consistency between the dislocation density and oxygen concentration takes place. If we assume that the interface XY is a constant source of oxygen then obviously the kinetic equation takes the form

$$\frac{dN_o}{dt} = D\,N_d - EN_o + FN_dN_o, \qquad (4)$$

where D is a constant characterizing the concentration of oxygen diffusing along dislocations, E is a constant characterizing the annihilation channels, F is a constant characterizing the increasing of oxygen concentration due to the generation of new dislocations. Coherent (autocatalytic) regime requires equality sign of the last term in (3) and (4), namely it must be positive to comply with the positive feedback.

We faced with nonlinear system (3)-(4) which does not have an analytical solution. Let us write the equations in dimensionless form

$$\frac{dN_d}{dt} = \frac{N_d}{t_1}\left(1 + \frac{N_o}{\nu} - \frac{N_d}{\theta}\right), \qquad (5)$$

$$\frac{dN_o}{dt} = \frac{1}{t_2}\left(\frac{N_d}{\eta} - N_o\left(1 - \frac{N_d}{\xi}\right)\right), \qquad (6)$$

where $t_1 \equiv 1/A$, $t_2 \equiv 1/D$ are characteristic times of the autonomous change the density of defects;

scales terms $\theta = A/B$ and $\eta = D/\varepsilon$ determine the density of dislocations without oxygen; characteristic densities $\nu = A/C$ and $\xi = D/F$ determine the intensity of the relative influence of defects. Let us introduce the dimensionless density of defects $y = N_d/\xi$, $x = N_o/\nu$ and dimensionless time $z = t/t_2$. Such parameter as $\alpha = t_2/t_1$ determines the ratio of characteristic times $\beta = \xi/\theta$ determines the intensity ratio of the generation and annihilation of defects and $\gamma = \xi/(\nu\eta)$ determines the relative intensities of the relative influence of dislocations and oxygen. In dimensionless quantities the system becomes

$$\frac{dy}{dz} = \alpha y(1 + x - \beta y), \qquad (7)$$

$$\frac{dx}{dz} = -x(1 - y) + \gamma y. \qquad (8)$$

As a matter of fact, the nonlinear equations (7)-(8) have the opportunity to be analyzed qualitatively for different values of the parameters α, β, γ. In order to generation rate of defects was greater than their annihilation, the following conditions $\beta > 1$, $\gamma < \left(\sqrt{\beta} - 1\right)^2$ must be met. The phase portrait is shown in Figure 7. Phase curves converge to the point Σ (coherent regime) which has an asymptote $N_d = (\xi/\nu)\left[(t_1/t_2) + (\xi/\theta)\right]^{-1} N_o$. On the one hand, the coherent regime is carried out by a high concentration of oxygen (the bottom of phase portrait). On the other hand, the coherent regime is carried out by increasing of dislocations (the top of phase portrait). However, it requires an initial density of defects (dislocations) exceeding a critical value which depends on many microparameters.

4. CONCLUSIONS

Thus, as shown by experimental investigations, the near-surface layers of silicon at the silicon — dioxide interface has a complex structure and consist of polycrystalline silicon region and dislocation network region. Generation of dislocation networks can be explained by accelerated thermodiffusion of oxygen atoms along initial structural defects that are present in silicon before high-temperature oxidation. In order to explain the generation of such periodical dislocation structure, it was applied the synergetic method.

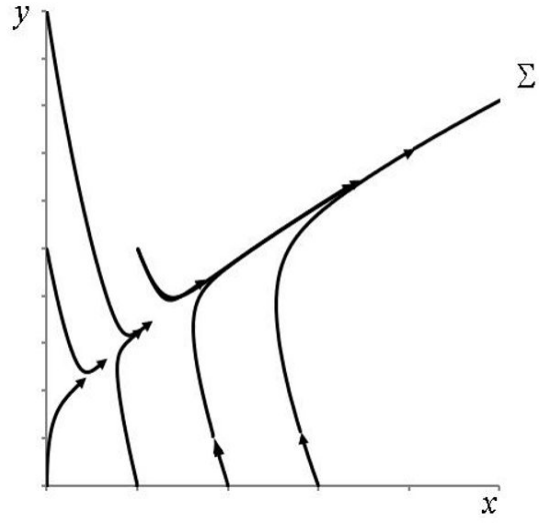

Figure 7. Phase portrait (dimensionless density of defects: y — dislocations, x — oxygen; Σ — coherent regime).

The formation of periodical dislocation structures at the interface is a consequence of the spatial instability of the dislocation distribution in the crystal and their self-organization due to correlation effects (coherent regime) between the oxygen atoms diffusing along structural defects and an ensemble of dislocations. The coherent regime could take place in the case of increasing of dislocations or a high concentration of oxygen.

REFERENCES

1. Tsybeskov L., Kamenev B. V., Sirenko A. A., McCaffrey J. P. and Lockwood D. J., Strain-induced lateral self-organization in Si/SiO_2 nanostructures // Appl. Phys. Lett. — 2010. — Vol. 96. — P. 013105.
2. Stesmans A., Nouwen B., Afanasyev V. V., Structural degradation of thermal SiO_2 on Si by high-temperature annealing: Defect generation // Phys. Rev. B. — 2002. — Vol. 66. — P. 045307.
3. Hideki Tsuya, Present Status and Prospect of Si Wafers for Ultra Large Scale Integration // Jpn. J. Appl. Phys. — 2004. — Vol. 43. — P. 4055.
4. Smyntyna V. A., Kulinich O. A., Iatsun-

skyi I. R., Marchuk I. A., Pavlenko N. N. Fractal analysis of nanostructured silicon surfaces // Photoelectronics. — 2011. — №. 20. — P. 63-66.
5. Yatsunskiy I. R. and Kulinich O. A., Complex destruction of near-surface silicon layers of Si-SiO structure // Semiconductor Physics, Qûantum Electronics and Optoelectronics. — 2010. —Vol. 13. — P. 418-421.
6. Kulinich O. A., The mechanism of formation and properties of stratified-inhomogeneity defects in silicon // Russian Physics Journal. — 2006. Vol. 49. — P. 233-238.
7. Ravi K. V., Imperfections and impurities in semiconductor silicon, NY: Wiley, 1981.
8. H. F. Matare., Defect Electronics in Semiconductors, Willey-Interscience, New York, 2000.
9. Kulinich O. A. and Glauberman M. A., Correlation between the parameters and structural perfection of silicon pin-photodetectors // Russian Physics Journal. — 2004. — Vol. 47. — P. 1268-1275.
10. Katsnelson A. and Olemskoi A., Microscopic Theory of nonhomogeneous structures, Amer. Inst of Physics, 1990.
11. Olemskoi A. I., Theory of structure in nonequilibrium Condensed Matter, NY: Nova Science, 1999.
12. Malygin G. A., Dislocation self-organization processes and crystal plasticity// Physics-Uspekhi. — 1999. — Vol. 42. — P. 887.

UDC 537. 311. 33: 622. 382.33

I. R. Iatsunskyi

EVOLUTION OF STRUCTURAL DEFECTS IN SILICON CAUSED BY HIGH-TEMPERATURE OXIDATION

Abstract

The dislocation self-organization processes in near-surface silicon layers of Si-SiO_2 during high temperature oxidization have been investigated. It was observed the complex destruction of these layers caused by relaxation of mechanical stresses. We have proposed the defect formation mechanism of near-surface layers in Si-SiO_2 structure. For self-organization processes to be explained, the synergetic method was applied. It was shown that the formation of periodical dislocation structures at the interface is a consequence of the spatial instability of the dislocation distribution in the crystal, their self-organization due to correlation effects between the oxygen diffusing along structural defects and an ensemble of dislocations.

Key words: dislocations, self-organization, Si-SiO_2 structure.

УДК 537. 311. 33: 622. 382.33

И. Р Яцунский

ЭВОЛЮЦИЯ СТРУКТУРНЫХ ДЕФЕКТОВ В КРЕМНИ, ВЫЗВАННОЕ ВЫСОКОТЕМПЕРАТУРНЫМ ОКИСЛЕНИЕМ

Резюме

Процессы самоорганизации дислокаций в приповерхностных слоев кремния в Si-SiO_2 при высокотемпературном окислении были исследованы в данной работе. Было определено, что появление сложной дефектной структуры вызвано релаксацией механических напряжений.

Было предложено механизм образования дефектов в приповерхностных слоях Si-SiO_2. Процессы самоорганизации объясняется, в рамках синергетического метода. Было показано, что формирование периодической структуры дислокации на границе является следствием пространственной неустойчивости распределения дислокаций в кристалле, их самоорганизации за счет корреляций между кислородом, который распространяется вдоль структурных дефектов и ансамбля дислокаций.

Ключевые слова: дислокации, самоорганизация, структура Si-SiO_2

УДК 537. 311. 33: 622. 382.33

І. Р Яцунський

ЕВОЛЮЦИЯ СТРУКТУРНИХ ДЕФЕКТІВ В КРЕМНІЇ, ЯКЕ ВИКЛИКАНЕ ВИСОКОТЕМПЕРАТУРНИМ ОКИСЛЕННЯМ

Резюме

Процеси самоорганізації дислокацій в приповерхневих шарів кремнію в Si-SiO_2 при високотемпературному окисленні були досліджені в даній роботі. Було визначено, що поява складної дефектної структури викликано релаксацією механічних напружень. Було запропоновано механізм утворення дефектів у приповерхневих шарах Si-SiO_2. Процеси самоорганізації пояснюється, в рамках синергетичного методу. Було показано, що формування періодичної структури дислокації на границі є наслідком просторової нестійкості розподілу дислокацій в кристалі, їх самоорганізації за рахунок кореляцій між киснем, що поширюється уздовж структурних дефектів та ансамблю дислокацій.

Ключові слова: дислокації, самоорганізація, структура Si-SiO_2.

UDC 621.315.539

V. A. Smyntyna, V. M. Skobeeva, N. V. Malushin

[1] Odessa National I. I. Mechnikov University, 65026, Odessa, Ukraine, Dvoryanskaya, 2,
e-mail: smyntyna@onu.edu.ua
[2] Research Institute of Physics, Odessa National I. I. Mechnikov University, 65026, Ukraine, Odessa, 27, Pasteur .* Phone. +38 048 7230329,
e-mail: v_skobeeva@ukr.net

INFLUENCE OF THE SURFACE ON THE SPECTRUM OF LUMINESCENCE OF CdS NANOCRYSTALS IN GELATINE MATRIXS

This paper investigates the optical absorption and luminescence of CdS nanocrystals (NCs) of varying size obtained by colloidal chemistry in an aqueous solution of gelatin. In NCs with a radius of 1.8 nm only long-wavelength luminescence with λ_{max} = 580 nm was observed, which is explained by the surface defects. In NCs of larger size (3.5 nm), the contribution of the recombination with the participation of the surface defects decreases. There is a redistribution of recombination channels to the advantage of recombination of nonequilibrium carriers in the volume of cadmium sulfide nanocrystals, which in that case exhibit intensive exciton band in their luminescence spectra.

1. INTRODUCTION

Phosphors based on semiconductor nanocrystals are promising functional materials for use as fluorescent markers for biochemical and biomedical applications. Compared to traditional organic phosphors nanocrystals have a high absorption coefficient, high brightness and high photostability of radiation [1-7].

Practical application of nanocrystalline semiconductor compounds is made possible by the development of new technologies that will produce nanosystems in a “wet” chemistry - for example, by colloidal chemistry (by sol-gel technology) through a series of simple chemical reactions in solution of the reagents in the presence of stabilizers. The stabilizer prevents the coagulation of particles and their further growth. Colloid-chemical synthesis of nanoparticles is affected by a large number of factors, including the concentration of the starting materials, the type and concentration of the stabilizer, temperature, pH of the solution, kinetics of the chemical reactions.

The most commonly used stabilizers include organic compounds such as polyphosphates [8-11], trioctylphosphine oxide [12] and thiols [13]. Characteristics of semiconductor materials obtained in the above stabilizers are given in [14]. The choice of the stabilizer is determined by many factors. The main factor is its ability to prevent the coagulation of the particles, preventing their further growth. This property is determined by the mechanism of interaction of the stabilizer with the surface of the particles. Adsorption of the molecular groups of the stabilizer on the surface of the nanocrystal leads to the passivation of the surface states that changes the surface potential and decreases the concentration of non-radiative recombination centers. It should be noted that organic compounds are often toxic substances, and the synthesis requires a high temperature and special safety precautions.

In this regard, a topical and emerging technologies nanoparticles are those that use eco-friendly and non-toxic materials.

From this point of view, a suitable stabilizer may be, well-established in the production of photographic materials, natural polymer — gelatin [15]. Gelatin is a high-molecular compound, elementary unit of which is presented in the isoelectronic state as H_2N-R_1-COOH, consisting of amino (H_2N), carboxyl (COOH), polar and non-polar basic and acidic groups (R_1). Gelatin

is a good medium for the dispersion of nano - and microparticles. Solution containing ions of the metal and chalcogen quickly penetrate into gelatin. Gelatin solutions can form gels, which after polymerization result in films that are sufficiently transparent and durable. However, the distinctive features of gelatin are not limited to colloid protective functions. Thanks to their acid-base properties of gelatin can take a positive or negative charge. For example, with increasing of pH solution COOH groups dissociate into H^+ and COO^- gelatin molecule acquires a negative charge, which can significantly affect the adsorption interaction with the surface of particles dispersed in it.

From the foregoing, it is of interest to obtain and study the cadmium sulfide nanocrystals obtained by sol-gel technology using gelatin solution as a stabilizing agent, and to explore the effect of size on the NC luminescence spectra.

2. MATERIALS AND FLUORESCENCE MEASUREMENTS

Investigated NC CdS were synthesized by colloidal chemistry. In aqueous solution of gelatin (5%) containing a solution of cadmium salt - $Cd(NO_3)_2$ the salt sulfur — Na_2S solution was injected under continuous stiring. Molar concentration of cadmium salt was 0.025 M and the concentration of sodium sulfide — 0.05 M and 0.5 M. The synthesis of cadmium sulfide happened as a result of exchange chemical reaction between these compounds. The process was carried out at 40 ± 1°C. Colloidal solution of the product was applied to a glass substrate and polymerized by the drying air temperature of 35 ± 2°C. Produced samples correspond to the film with thickness 5-10 microns with nanocrystals of cadmium sulfide dispersed in a gelatin matrix. The thickness of the film depended on the amount of deposited material and the surface tension of the solution.

For spectroscopic studies of quantum dots of cadmium sulfide (light transmission, luminescence) used a spectrometer facility KSVU — 12, based on an MDR — 12 with a resolution at a wavelength of 600 nm 0.1nm.

Luminescence was excited by the solid-state samples pulsed laser with the following specifications: maximum average power of 5 mW, pulse duration at 1 kHz ~ 1 ns, pulse energy at 1 kHz ~ 20 μJ, the emission wavelength of 355 nm. The luminescence was registered with the detector PMT-106, which has a maximum spectral sensitivity in the range of 400-440 nm.

3. DETERMINATION OF THE SIZE OF CdS NC

The average radii of cadmium sulfide nanoparticles were estimated using optical absorption spectra of colloidal solutions of these nanoparticles.

Interband absorption of nanoparticles has a spherical shape and the absorption spectrum is given by a series of discrete lines [15,17]. The threshold value is given by

$$\hbar\omega_{01} = E_g + \frac{\hbar^2\pi^2}{2\mu a^2}, \qquad (1)$$

where E_g — band gap of the bulk crystal;
a — the average radius of the nanocrystal;
$\hbar$ — Planck's constant;

$\mu = \frac{m_e m_h}{m_e + m_h}$ — is the reduced mass of the electron and hole.

This implies the law by which the energy of the first optical transition (effective band gap) increases with the decreasing radius of the nanopaticles.

The values of the constants used in the calculations are given by E_g = 2,5 эВ [18], $m_e = 0{,}205\, m_o$ и $m_h = 0{,}7\, m_o$ [19].

4. RESULTS AND DISCUSSION

Fig. 1. shows the spectral dependence of the optical density of the quantum dots for the two samples grown under the same conditions, at different ratio of cadmium salts and sulfur. Sample number 1 corresponded to a lower concentration Na_2S (0,05M) and number 2 to the larger (0.5 M). Curve 1 in this figure corresponds to the absorption of an aqueous solution of gelatin. It can be seen that the spectrum of the gelatin is almost transparent and its absorption spectrum does not

affect the absorption of NC. It is noticeable that the transparency of the two samples are significantly different, and the beginnign of the absorption is shifted to short-wavelength region compared with the absorption spectrum of a cadmium sulfide bulk crystal. According to equation (1), such behavior is characteristic for nanoscale objects and corresponds to the presence of quantum - size effect. Magnitude of the shift of the spectrum with respect to the bulk crystal of nanocrystals depends on the size of the nanocrystals. We estimate that the sample number 1 has an average radius NC 1,8 ±0.1 nm, and the sample number 2 - 3,5 ± 0,1 nm. This clearly shows the dependence of the QD size on the reagent concentrations.

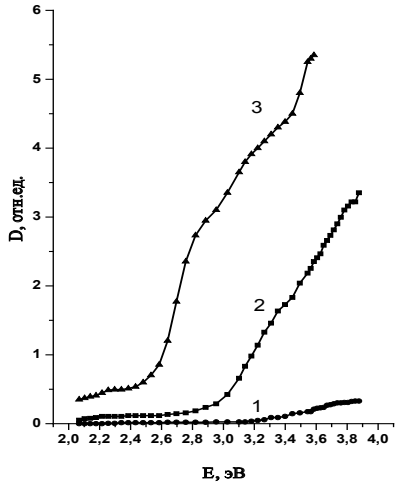

Fig. 1. Absorption spectrums of gelatinous solution (1) and NC of sulfide of cadmium samples: N 1 (2); N 2 (3).

Note that in nanocrystals ratio of surface area to volume of the nanocrystal varies considerably depending on their radius, therefore, changes and number of non-compensated valence atoms leaving the surface. Moreover, the interaction of the gelatin molecules with the surface of the nanocrystals can depend on their size due to the influence of steric factors. Thus, there is every reason to expect the effect of surface defects on the properties that are sensitive to surface recombination of charge carriers, for example, the fluorescent characteristics of NC.

Let us discuss the influence of the surface defects on the photoluminescence characteristics of NC various sizes. Fig. 2. shows the luminescence spectra of CdS QDs (sample number 1) for different powers of the exciting light P, MW: 26.6 (1) 19.5 (2) 45.0 (3). It can be seen that the emission intensity increases with increasing power, but regardless of its size nanocrystals have one broad band with a maximum λ_{max} = 580 nm. The nature of this band is associated with deep centers and radiation appears in the nanocrystals with a high density of defects, including surface [20-22] and this luminescence is called “defective.” It should be noted that the localization of the maxima of the luminescence bands on deep centers depends on the nature of the defects, that is to the energy of ionization. According to our observations [20,21] and the analysis of references [23,24], the long-wavelength region of the spectrum has three luminescence bands that are located at λ_{max} = 580, 670 and 750 nm. The contour of the luminescence bands observed by different authors depends on the technology of the nanocrystals and consists of either one elementary band or emission band formed from the total contribution of the few bands.

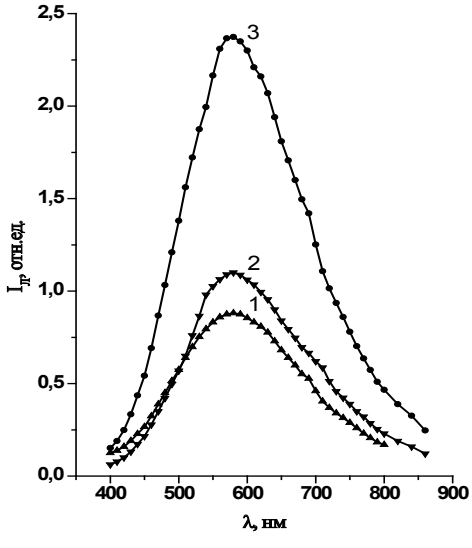

Fig. 2. Luminescence spectrums of NC CdS (sample № 1) at various excitation power, mWt: 26,6 (1) 19,5 (2); 45,0 (3).

Thus, in our case in the sample N 1 we register «defective» emission band and do not observed radiation with energies close to the forbidden band, which is a sign of the dominant role of the luminescence associated with surface defects. The fact that the position of the maximum emission of these samples is independent of the excitation power is indirect evidence of the radiative recombination that is caused by one type of defect.

In contrast, in the spectra of the sample number 2, along with the long-wave radiation, there is a narrow and short-wavelength luminescence band with λ_{max} = 480 nm (Fig. 3), the nature of which is due to the exciton luminescence [25].

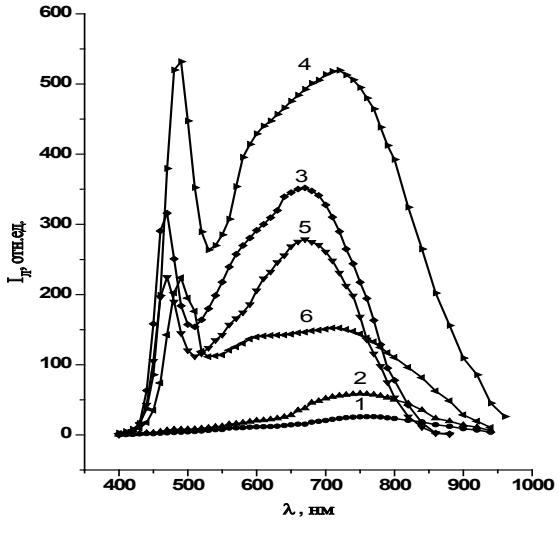

Fig. 3. Luminescence spectrums of NC CdS (sample № 2) at various excitation power, mWt: 19,5 (1); 26,0 (2); 32,0 (3); 42,0 (4); 45,0 (5); 26,6 (6).

The presence of such a band indicates the competitive advantage of the recombination channel, which is associated with the recombination in the cadmium sulfide nanocrystals volume.

It was found that intensity and contour defect luminescence emission of the sample N 2 depend on the power. Thus, the intensity of the bands increases with increasing excitation power luminescence from 19.5 mW to 42 mW, and the ratio of the intensities of the bands that form the total loop «defect» luminescence changes with power. Due to the latter fact there is a possibility of observing the longer wavelengths of several luminescence bands with peaks localized in the wavelength: λ_{max} = 580, 670 and 750 nm. The dependence of the contour on the power of the excitation luminescence is likely to be due to the different parameters of emission centers, and may be the subject of further research.

Conclusion

In this paper we have established a novel dependency of the luminescence spectrum of CdS NC on their size that is associated with different contribution of surface defects in NC of different sizes. In particular the luminescence of NC with an average radius of 1.8 nm is dominated by long-wavelength light with λ_{max}= 580 nm, caused by one type of surface defects. Such NC do not exhibit band-band or exciton luminescence. In NC of larger size (3.5 nm), the contribution of surface recombination is reduced, and the presence of short-wavelength band λ_{max} = 480 nm demonstrates that the dominating recombination channel is due to nonequilibrium carriers in the volume of nanocrystals of cadmium sulfide.

References

1. Bruchez M, Moronne M, Gin P, Weiss S, Alivisatos A. P. Semiconductor nano-crystals as fluorescent biological labels // *Science* — 1998. — Vol. 281, № 5385. — P. 2013–2016.
2. Gao X, Cui Y, Levenson R M, Chung LWK, Nie S. In vivo cancer targeting and imaging with semiconductor quantum dots // *Nat. Biotechnol*. — 2004. — Vol. 22, № 8. — P. 969 – 976.
3. X. Michalet, F. F. Pinaud, L. A. Be-ntolila, J. M. Tsay, S. Doose, J. J. Li, G. Sundaresan, A. M. Wu, S. S. Gambhir, S. Weiss. Quantum Dots for Live Cells, in Vivo Imaging, and Diagnostics // *Science* — 2005. — Vol. 307. — P. 538 — 544.
4. Fabien Pinaud, Xavier Michalet, Laurent A. Bentolila, James M. Tsay, Soren Doose, Jack J. Li, Gopal Iyer, and Shimon Weiss Advances in fluorescence imaging with quantum dot bio-probes // *Biomaterials* — 2006. — Vol. 27, № 9. — P. 1679–1687.
5. J. M. Klostranec, W.C.W. Chan. Quantum Dots in Biological and Biomedical Research:Recent Progress and Present

Challenges // *Advanced Materials* — 2006. Vol. 18, № 15. — P. 1953-1964.
6. Parvesh Sharma, Scott Brown, Glenn Walter, Swadeshmukul Santra, Brij Moudgil. Nanoparticles for bioimaging // *Advances in Colloid and Interface Science* — 2006. — Vol. 123–126. — P. 471–485.
7. Yunqing Wang, Lingxin Chen, Quantum dots, lighting up the research and development of nanomedicine Nanomedicine — // *Nanotechnology, Biology, and Medicine* — 2011. — Vol. 7. — P. 385–402.
8. A. Henglein. Photochemistry of colloidal cadmium sulfide // *J. Phys. Chem.* 1999. — V. 86. — P. 2291-2299.
9. L. E. Brus. A simple model for the ionization potential, electron affinity, and aqueous redox potentials of small semiconductor crystallites // *J. Chem. Phys*. — 1999. — Vol. 79. — P. 5566-5571.
10. L. Brus. Electronic wave functions in semiconductor clusters: experiment and theory // *J. Phys. Chem*. 1999. — Vol. 90. — P. 2555-2560.
11. Mews, U. Banin, A. V. Kadavanich, A. P. Alvisators, B. Bunsenges Struktur e Determination and Homogeneous Optical Properties of CdS/HgS Quantum Dots // *J. Phys. Chem*. — 1997. — Vol. 101. — P. 1621-1625.
12. C. B. Murray, D. J. Noris, M. G. Bawendi. Synthesis and charac-terization of nearly monodisperse CdE (E = sulfur, selenium, tellurium) semiconductor nanocrystallites // *J. Am. Chem. Soc.* — 1999. — V. 115. — P. 8706- 8715.
13. Lubomir Spanhel, Markus Haase, Horst Weller, and Arnim Henglein. Photochemistry of Colloidal Semiconductors. 20. Surface Modification and Stability of Strong Luminescing CdS Particles // *J. Am. Chem. Soc*. — 1987. — Vol. 109. — P. 5649-5655.
14. A. Eychmuller. Structure and Photophysics of Semiconductor Nanocrystals. // *J. Phys. Chem.,* B. — 2000. — Vol. 104. — P. 6514-6528.
15. Т. Джеймс. *Теория фотографического процеса*. — Л.: Химия. 1999. — 672 с.
16. Эфрос Ал. Л., Эфрос А. Л. Межзонное поглощение света в полупроводниковом шаре. — *Физ. и техн. полупроводников. //* — 1999. — Т. 16, № 7. — С. 1209-1214.
17. Кулиш Н. Р., Кунец В. П., Лисица М. П.. Оптические методы определения параметров нанокристаллов в квазинульмерных полупроводниковых структурах // *Украинский физический журнал*. — 1996. — Т. 41, № 11-12. — С. 1075-1081.
18. Madelung O., Martienssen,W., Eds; Landolt — Bornstein. *Numerical data and functional relationships in science and tech-nology*. Springer — Verlag: Berlin. — 1998. — Vol. III — 17b. — P. 166-194.
19. В. И. Гавриленко, Д. В. Корбутяк, В. Г. Литовченко. *Оптические свойства полупроводников. Справочник*. — Наукова думка, 1999. — 608 с.
20. Воронцова М. М., Малушин Н. В., Скобеева В. М., Смынтына В. А. Оптические и люминесцентные свойства нанокристаллов сульфида кадмия // *Фотоэлектроника.* — 2002. — № 11. — С. 104-106.
21. В. А. Сминтина, В. М. Скобєєва, М. В. Малушин. Вплив границі розділу на оптичні та люмінесцентні властивості квантових точок сульфіду кадмію у полімері // *Фізика і хімія твердого тіла.* — 2011. — Т. 12. № 2. -
22. Abhijit Mandal, Jony Saha, Goutam De Stable CdS QDs with intense broadband photoluminescence and high quantum yields // *Optical Materials.* — 2011. — Vol. 34. — P. 6–11
23. S. R. Cordero, P. J. Carson, R. A.Estabrook, G. F. Strouse, and Buratto. Pho-

to-Activated Luminescence of Quantum Dot Monolayers // *J.Phys.Chem. B*. — 2000. — Vol. 104. — P. 12137-12142.
24 C. Ricollean, I. Vasilevsky, M. I. M. Gomes. Microstructure and Photoluminescence of CdS — Doped Silica Films Gown by RF Magneton Sputtering // *Phys. stat. sol. (b)* — 2002. — Vol. 232. — №.1. — P. 44-49.
25. N. V. Bondar, M. S. Brodyn Evolution of excitonic states in two-phase systems with quantum dots of II–VI semiconductors near the percolation threshold // *Physica E*. — 2010. — Vol. 42. — P. 1549–1554.

UDC 621.315.539

V. A. Smyntyna, V. M. Skobeeva, N. V. Malushin

INFLUENCE OF THE SURFACE ON THE SPECTRUM OF LUMINESCENCE NC CdS IN GELATINE MATRIX

Abstract

The optical absorption and luminescence of nanocrystals (NCs) CdS different sizes obtained by colloidal chemistry in an aqueous solution of gelatin investigated. In NCs with a radius of 1.8 nm was observed only with long-wavelength luminescence λ_{max} = 580 nm due to surface defects. In NCs larger (3.5 nm), the contribution of surface recombination decreases, there is a redistribution of recombination channels. Recombination of nonequilibrium carriers in the volume of cadmium sulfide nanocrystals is primary and their luminescence spectra contains intensive exciton band.

Keywords: nanocrystals CdS, absorption, luminescence

УДК 621.378.35

В. А. Сминтина, В. М. Скобєєва, М. В. Малушин

ВПЛИВ ПОВЕРХНІ НА СПЕКТР ЛЮМІНЕСЦЕНЦІЇ НК CDS В ЖЕЛАТИНОВІЙ МАТРИЦІ

Анотація

Досліджувалося оптичне поглинання і люмінесценція нанокристалів (НК) CdS різного розміру, отриманих методом колоїдної хімії у водному розчині желатини. У НК, що мали розмір з радіусом 1,8 нм спостерігається лише довгохвильове світіння з $\lambda_{макс}$ = 580 нм, яке обумовлене поверхневими дефектами. У НК більшого розміру (3,5 нм) вклад рекомбінації за участю поверхневих дефектів зменшується, відбувається перерозподіл каналів рекомбінації на користь рекомбінації нерівноважних носіїв в об'ємі нанокристалів і спектрі їх люмінесценції реєструється інтенсивна смуга випромінювання екситона.

Ключові слова: нанокристали CdS, поглинання, люмінесценція

УДК 621.378.35

В. А. Смынтына, В. М. Скобеева, Н. В. Малушин

ВЛИЯНИЕ ПОВЕРХНОСТИ НА СПЕКТР ЛЮМИНЕСЦЕНЦИИ НК CDS, В ЖЕЛАТИНОВОЙ МАТРИЦЕ

Аннотация

Исследовалось оптическое поглощение и люминесценция нанокристаллов (НК) CdS разного размера, полученных методом коллоидной химии в водном растворе желатины. В НК с радиусом 1,8 нм наблюдается только длинноволновое свечение с $\lambda_{макс}$ = 580 нм, обусловленное поверхностными дефектами. В НК большего размера (3,5 нм) вклад рекомбинации с участием поверхностных дефектов уменьшается, происходит перераспределение каналов рекомбинации в пользу рекомбинации неравновесных носителей в объеме нанокристаллов сульфида кадмия и спектре их люминесценции регистрируется интенсивная экситонная полоса свечения.

Ключевые слова: нанокристали CdS, поглощение, люминесценция

UDC 539.192

G. P. Prepelitsa, V. M. Kuzakon, V. V. Buyadzhi, E. P. Solyanikova, A. A. Karpenko, D. A. Korchevsky

Odessa National Polytechnical University, 1, Shevchenko av., Odessa, Ukraine
Odessa State Environmental University, 15, Lvovskaya str., Odessa, Ukraine
International Humanitarian University, 33, Fontanskaya dor., Odessa, Ukraine
Odessa Computer Academy, Odessa, Ukraine e-mail: quantpre@mail.ru

NONLINEAR STOCHASTIC DYNAMICS GOVERNING FOR QUANTUM SYSTEMS IN EXTERNAL FIELD: CHAOS THEORY AND RECURRENCE SPECTRA ANALYSIS

Nonlinear method of chaos theory and the recurrence spectra formalism are used to study quantum stochastic futures and chaotic elements in dynamics of atomic systems in the external electromagnetic (laser) field. Some illustrations regarding the recurrence spectra and chaos dynamics of lithium and magnesium atoms in the crossed electric and magnetic and laser fields are presented.

1. Introduction

In last years a great interest attracts studying a dynamics of quantum systems in external electric and magnetic field [1-18]. It has been discovered that dynamics of these systems in external electromagnetic fields has features of the random, stochastic kind and its realization does not require the specific conditions. The importance of studying a phenomenon of stochasticity or quantum chaos in dynamical systems is provided by a whole number of technical applications, including a necessity of understanding chaotic features in a work of different electronic devices and systems, including the nano-optical ones. New field of investigations of the quantum and other (geophysical, chemical, biological, social etc) systems has been provided by a great progress in a development of a chaos theory methods [1,2] (c.f. review part in Refs.[19-22]).

Rydberg atoms in strong external fields have been shown to be real physical examples of non-integrable systems for studying the quantum manifestations of classical chaos both experimentally and theoretically. To describe these phenomena, one has to make calculating and interpreting the recurrence spectra which is the Fourier transformation of a photo absorption spectrum [2,13,14]. Consequently, the recurrence spectrum provides a quantum picture of classical behaviour. Studies of recurrence spectra have led to observations of the creation of new orbits through bifurcation's, the onset of irregular behaviour through core scattering and symmetry breaking in crossed fields [1-7,17,18]. In the past, many researchers have calculated the recurrence spectra of a Rydberg atom in an external field. But they only calculated the spectra in static electric or magnetic fields. In a recent experiment, the absorption spectrum of the lithium atom in a static electric field plus a weak oscillating field was measured and Haggerty and Delos gave some explanation for it theoretically (c.f.[2,13,14]). But as to the influence of an oscillating electric field on the absorption spectrum of the Rydberg atom in static magnetic field, none has given the calculation both experimentally and theoretically, besides the first classical estimate [14]. In previous our papers we have given a review of this approach in analysis of different systems of quantum physics, electronics and photonics. In this paper we have used the nonlinear method of chaos theory and the recurrence spectra formalism to study quantum stochastic futures and chaotic elements in dynamics of atomic systems in the external electroomagnetic fields.

2. Nonlinear analysis of quantum system dynamics in a field and a chaos theory methods

Following refs. [21,22] we briefly consider an analysis of nonlinear dynamics of some system in a field by means of a chaos theory

methods. Usually some dynamical parameter $s(n) = s(t_0 + n\mathrm{D}t) = s(n)$, where t_0 is the start argument (for example, time), Dt is the argument step, and is n the number of the measurements. In a general case, $s(n)$ is any time series, particularly the amplitude level. Since processes resulting in the chaotic behaviour are fundamentally multivariate, the reconstruction results in a certain set of d-dimensional vectors $\mathbf{y}(n)$ replacing the scalar measurements. The standard method of using time-delay coordinates is usually used to reconstruct the phase space of an observed dynamical system. The direct use of the lagged variables $s(n + \mathrm{t})$, where t is some integer, results in a coordinate system in which a structure of orbits in phase space can be captured. Using a collection of time lags to create a vector in d dimensions,

$$\mathbf{y}(n) = [s(n), s(n + \mathrm{t}), s(n + 2\mathrm{t}), \ldots, s(n + (d\text{-}1)\mathrm{t})], \quad (1)$$

the required coordinates are provided. In a nonlinear system, the s(n + jt) are some unknown nonlinear combination of the actual physical variables that comprise the source of the measurements. The dimension d is also called the embedding dimension, dE. If any time lag t is chosen too small, then the coordinates s(n + jt) and s(n + (j + 1)t) are so close to each other in numerical value that they cannot be distinguished from each other. Similarly, if t is too large, then s(n + jt) and s(n + (j + 1)t) are completely independent of each other in a statistical sense. Also, if t is too small or too large, then the correlation dimension of attractor can be under- or overestimated respectively. It is therefore necessary to choose some intermediate (and more appropriate) position between above cases. First approach is to compute the linear autocorrelation function

$$C_L(\delta) = \frac{\frac{1}{N}\sum_{m=1}^{N}[s(m+\delta) - \bar{s}][\, s(m) - \bar{s}]}{\frac{1}{N}\sum_{m=1}^{N}[s(m) - \bar{s}]^2} \quad (2)$$

where $\bar{s}$ is an averaged value and to look for that time lag where C_L(d) first passes through 0. This gives a good hint of choice for t at that $s(n + j\mathrm{t})$ and $s(n + (j + 1)\mathrm{t})$ are linearly independent. However, a linear independence of two variables does not mean that these variables are nonlinearly independent. It is therefore preferably to utilize approach with a nonlinear concept of independence, e.g. the average mutual information. Let there are two systems, A and B, with measurements a_i and b_k. The mutual information I of two measurements a_i and b_k is symmetric and nonnegative, and equals to zero if only the systems are independent. The average mutual information between any value a_i from system A and b_k from B is the average over all possible measurements of $I_{AB}(a_i, b_k)$,

$$I_{AB}(\tau) = \sum_{a_i, b_k} P_{AB}(a_i, b_k) I_{AB}(a_i, b_k)\,. \quad (3a)$$

To place this definition to a context of observations from a certain physical system, let us think of the sets of measurements $s(n)$ as the A and of the measurements a time lag t later, $s(n + \mathrm{t})$, as B set. The average mutual information between observations at n and $n + \mathrm{t}$ is then

$$I_{\mathbf{B}}(\tau) = \sum_{a_i, b_k} P_{\mathbf{B}}(a_i, b_k) I_{\mathbf{B}}(a_i, b_k)\,. \quad (3b)$$

Now we have to decide what property of I(t) we should select, in order to establish which among the various values of t we should use in making the data vectors $\mathbf{y}(n)$. It is necessary to choose that t where the first minimum of I(t) occurs.

The goal of the embedding dimension determination is to reconstruct a Euclidean space R^d large enough so that the set of points d_A can be unfolded without ambiguity. According to the embedding theorem, the embedding dimension, d_E, must be greater, or at least equal, than a dimension of attractor, d_A, i.e. $d_E > d_A$. There are standard approaches to reconstruct the attractor dimension, for example, the correlation integral method. It was shown in refs. [23,24] in studying chaos in the vibrations dynamics of the autogenerators and similar analysis for geophysical systems [19-21, 24, 25], the low, non-integer correlation dimension value indicates on an existence of low-dimensional chaos. The embedding phase-space dimension is equal to the number of variables present in the evolution of the system. To verify data obtained by the correlation integral analysis, it is often used a surrogate data method.

This an approach makes use of the substitute data generated in accordance to the probabilistic structure underlying the original data [19-21]. The next step is an estimating of the Lyapunov exponents (LE). These parameters are the dynamical invariants of the nonlinear system and defined as asymptotic average rates. So, they are independent of the initial conditions, and therefore they do comprise an invariant measure of attractor. In fact, if one manages to derive the whole spectrum of LE, other invariants of the system, i.e. Kolmogorov entropy and attractor's dimension can be found. The Kolmogorov entropy, *K*, measures the average rate at which information about the state is lost with time. An estimate of this measure is the sum of the positive LE. The inverse of the Kolmogorov entropy is equal to an average predictability. The estimate of the dimension of the attractor is provided by the Kaplan and Yorke conjecture: $d_L = j + \sum_{\alpha=1}^{j} \lambda_\alpha / |\lambda_{j+1}|$, where *j* is such that $\sum_{\alpha=1}^{j} \lambda_\alpha > 0$ and $\sum_{\alpha=1}^{j+1} \lambda_\alpha < 0$, and the LE l_a are taken in descending order. The known approach to computing the LE is based on the Jacobin matrix of the system function [3]. The detailed description of the whole approach (our version) to analysis a nonlinear dynamics of chaotic systems can be found in refs. [19-25].

3. The recurrence spectra for atomic systems in an electromagnetic fields: Sensing chaos

For quantum systems in an external field there is very useful method, based on the analysis of the recurrence spectra. To calculate the energy spectra of atomic systems in the electric and magnetic fields one should use an approach, which combines solution of the 2D Schrödinger equation [16-18] for atomic system in crossed fields and operator perturbation theory [8,9]. The detailed description of such an approach is presented in these refs.[8,17,18], so here we briefly discuss the key moments. For definiteness, we consider a dynamics of the non-coulomb atomic systems in a static magnetic field and oscillating electric filed. The Hamiltonian of the system in a static magnetic field and an oscillating electric field is (in atomic units) is as follows:

$$H = 1/2(p_\rho^2 + l_Z^2/\rho^2) + \gamma l_Z/2 + (1/8)\gamma^2\rho^2 + \\ + (1/2)p_Z^2 + F_1 z \cdot \sin(\omega t) + V(r) \quad (4)$$

where the electric field and magnetic field B are taken along the z-axis in a cylindrical system; $g=B/2.35\times10^5$; $V(r)$ is a one-electron model potential, which is as follows:

$$V(r) = -1/r + (2/Zr)[1 - \exp(-2b_1 r)(1+r)]. \quad (5)$$

Here Z is a nuclear charge, and *b* is a free length parameters, which are chosen to give the energy spectrum of free atom. In fact, the second term in (5) is the corresponding potential of the K-shell (in a case of the Li atom). We consider only the m=0 state, thus $l_z=0$. The Hamiltonian obeys a classical scaling rule and can be written as:

$$\tilde{H} = \tilde{p}^2/2 + (1/8)\tilde{\rho}^2 + \\ + f \cdot \tilde{z} \cdot \sin(\tilde{\omega} \cdot \tilde{t}) + V(r) = E(t)\gamma^{-2/3} \quad (6)$$

Here $\tilde{r} = r\gamma^{2/3}$, $\tilde{p} = p\gamma^{-1/3}$, $\tilde{f} = F_1\gamma^{-4/3}$, $\tilde{l} = l\gamma$, $\tilde{\alpha}_i = \alpha_i\gamma^{-2/3}$ and $\tilde{\omega} = \omega\gamma^{-1}$.

In the oscillating field, the electron energy *E(t)* is not constant. We define $e=E^{out}g^{-2/3}$ as it leaves the atom. The useful method is a scaled recurrence spectroscopy, which allows to analyse the photo absorption amplitude as a function of the parameter $g^{-1/3}$ while varying the external fields frequency simultaneously in such a way that *e* and *f* remain constant. To account for an electric field (under supposition that an electric field is quite weak) one can use the perturbation theory. For solution of the Schrödinger equation the finite differences scheme is usually used. To find the resonances width and absorption spectrum one should use the golden Fermi rule (see details in refs. [2,3,8]).

4. Some results and discussion

We have studied a dynamics of the lithium atom in a crossed electric and magnetic fields. The transition from the lithium 3s state to final states corresponding to the principle quantum

numbers around n =125 and m =0 is considered. Following to ref. [14,16-18], because the ionic core produces important dynamical effects, we can split the whole space into two characteristic spatial regions: (1) The core region, where the laser field and the ionic core potential dominate while the external magnetic field can be eliminated. It should be noted here that the standard semi classical closed orbit theory provides an efficient treating the motion of a Rydberg electron far from the nucleus, but it fails when the electron is close to the nucleus. Because this region extends for only a few Bohr radii around the atomic nucleus, one must deal with this region by using a quantum method; (2)

The external region typically lies beyond 30 Bohr radii from the nucleus, so one can treat this region using standard semi classical methods or approximations to quantum approaches [14-18]. Using equation (4-6), we calculate the photo absorption spectrum of lithium in a magnetic field plus an oscillating electric field, with B =4.7T, F_1 =10V/cm and w=10^8 Hz. The corresponding data are presented in figure 1. In figure 2 we present the data on the photoabsorption spectrum of the LiI in a magnetic field without electric field. One should conclude that, when the oscillating field was added, the photo absorption spectrum was weakened greatly. This is fully corresponding the analysis within the standard closed orbit semiclassical calculation [5,14]. In figures 3(b),(d) we list the results of calculating the recurrence spectra of the Li atom in a magnetic field plus an oscillating field, with e=-0.03,v=0.32 ,$g^{-1/3}$ in the range 35–50 and f= 0.0035 and 0.07, respectively.

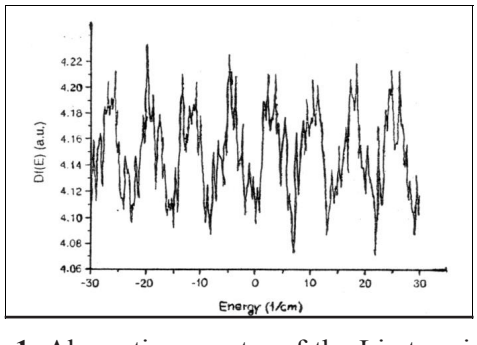

Figure 1. Absorption spectra of the Li atom in magnetic field plus an oscillating electric field

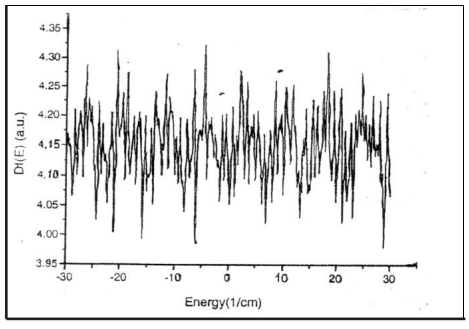

Figure 2. Absorption spectra of the Li atom in magnetic field, B =4 7 T.

This data are similar to parameters of the semiclassical approximation analysis [17]. As analysis of received data shows, when the value of f increases, the strength of all the peaks decreases. Some recurrences dropped rapidly and vanished as f increased; others remained even at much higher f. As the oscillating field gets stronger, some of the peaks re-appear, some more than once. Because when the oscillating field is strong, one can not consider it as a perturbation, the method described in this paper [14] is no longer suitable. Note that besides the semi-classical closed-orbit theory in versions [2-6,13,14], the other standard methods, for example, based on the perturbation theory [2,3], are not also acceptable for large values of field strengths. At the same time, the approach applied can be used even in a case of strong field. Availability of multiple resonances with little widths in atomic spectra in external fields is described within quantum chaos theory and provided by interference and quantum fluctuations, which characterize chaotic systems [1,9]. The chaos theory analysis fully confirms this conclusion. The mutual information approach, the correlation integral analysis, the false nearest neighbour algorithm, the LE analysis were used in analysis. The main conclusion is that the system exhibits a nonlinear behaviour and low-D chaos. The LE analysis supported this conclusion. Really, the first two LE have the following positive values: l_1=0.0242; l_2=0.0039. In conclusion, let us note that there is of a great interest to perform the similar analysis of chaotic dynamics and recurrence spectra for more heavy alkali systems in a microwave field. In conclusion we present also another remarkable example of the chaos

phenomenon for quantum systems in an external electromagnetic (laser) field, namely, the multi-photon above threshold ionization (ATI) process for magnesium atom (from the ground state).

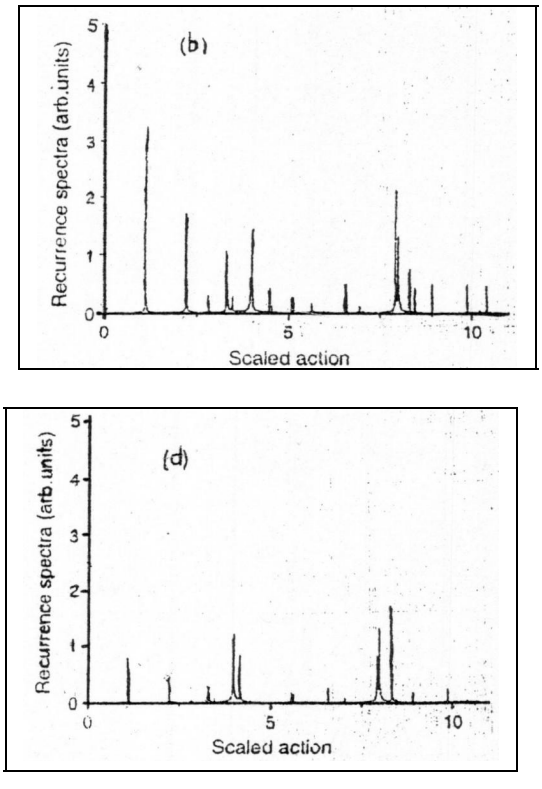

Figure 3. The recurrence spectra of Li in magnetic field plus an oscillating electric field: (b) scaled field f =0 0035; (d) scaled field f =0 07.

In ref.[9] it has presented the detailed theoretical description of the cited process and listed the data about the theoretical spectrum of two-photon ATI to final states with J=2 (figure 4). The laser radiation photons energies w in the range of 0,28-0,30 a.u. are considered, so that the final autoionization state (AS) is lying in the interval between 123350 см$^{-1}$ and 131477см$^{-1}$. First photon provides the AS ionization, second photon can populate the Rydberg resonance's, owning to series *4snl,3dnl,4pnp* с J=0 and J=2 [9,25]. In a case of $^1S_0$ resonance's there is observed an excellent identification of these resonance's. Situation is drastically changed in a case of spectrum of two-photon ATI to final states with J=2. Only three resonance's are identified.

Other resonance's and ATI in a whole demonstrate non-regular behavior. Studied system is corresponding to a status of quantum chaotic system.

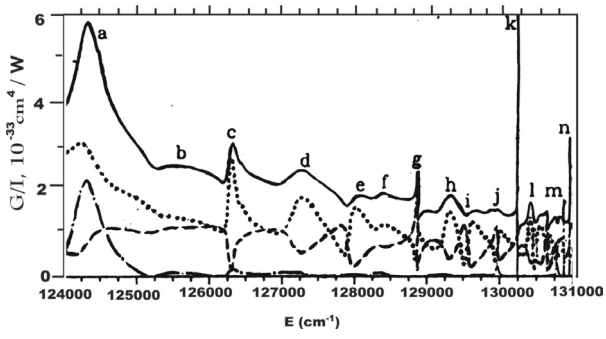

Figure 4. Two-photon ATI from the ground state Mg to states J=2; The full cross-section s/I (solid line) and partial cross-sections, corresponding to ionization to 3sed (dashed line) or to 3pep opened channels (dotted line). Identification of the $^1D_2$ resonance: a-4p4p; b-3d4d; c-4s5d;d-3s6d;e-4s6d;f-3d5d; g-4s7d; h-3d7s; i-4s8d; j-4s9d; k-4s10d; l-4s11d; m-4s14d; n-4s15d;

It realizes through the electromagnetic field induction of the overlapping (due to random interference and fluctuations) resonance's in spectrum, their non-linear interaction, which lead to a global stochasticity and quantum chaos phenomenon. Spectrum of resonance's is divided on three intervals: 1). the interval, where states and resonance's are clearly identified and not strongly perturbed; 2) quantum-chaotic one, where there is a complex of the overlapping and strongly interacting resonance's; 3). shifted one on energy, where behavior of energy levels and resonance's is similar to the first interval. Analysis shows that the resonance's distribution in the second quantum-chaotic interval is satisfied to the Wigner distribution $W(x)=x\exp(-px^2/4)$, however, in the first interval the Poisson distribution is valid. The chaos theory analysis fully confirms this conclusion.

References

1. Gutzwiller M.,Chaos in Classical and Quantum Mechanics.— N. — Y.: Springer-Verlag, 1990. — 720p.
2. Kleppner D., Chun-Ho I., Welch G. R., Irregular Atomic Systems and Quantum Chaos, Ed. J.C.Gay, N-Y.: Kluwer, 1999. — P. 21-48.
3. Dupret K., Zakrzewski J., Delande D., Resonances in the diamagnetic rydberg spectrum: order and chaos// Europhys.

Lett. — 1995. — V. 31(5). — P. 251-256.
4. Gasati G., Guarneri I., Mantica G., Classical Stabilization of periodically kicked hydrogen atoms// Phys.Rev.A. — 1999. — V. 50(6). — P. 5018-5024.
5. Dando P. A., Monteiro T. S. Atoms in static fields: Chaos or difraction// In: Photonic, Electro-nic, Atomic Collisions, Eds.W.Aumyr, H.Winter.-World Sci. Pub., Singapore. — 1997.— P. 621-630
6. Benvenuto F., Casati G., Shepelyansky D. L., Rydberg Stabilization of atoms in strong fields: «magic»mountain in chaotic sea// Z.Phys.B. — 1999. — V. 94. — P. 481-486.
7. Glushkov A. V., Ivanov L. N., DC Strong-Field Stark-Effect: consistent quantum-mechanical approach // J.Phys.B:At.Mol.Opt.Phys. — 1999. — V. 26. — P.L379-388.
8. Glushkov A. V., Ambrosov S. V. et al, Resonances in Quantum Systems in strong external fields: Consistent Quantum Approach// Journ. Techn. Phys. — 1999. — V. 37(2). — P. 215-218.
9. Glushkov A. V., Khetselius O. Yu., Svinarenko A. A., Prepelitsa G. P., Energy approach to atoms in a laser field and quantum dynamics with laser pulses of different shape//In: Coherence and Ultrashort Pulsed Emission, Ed. Duarte F. J. (Intech, Vienna). — 2011. — P. 159-186.
10. Glushkov A. V., Prepelitsa G. P., Svinarenko A. A. Sensing the stochastic laser pulse structure and chaotic and photon-correlation effects in the non-linear multi-photon atomic dynamics in laser and DC electric field// Sensor Electr. & Microsyst. Techn. — 2004. — № 2. — P. 8-14.
11. Popov V. S., Karnakov B. M., Moor V. D., Ionization of atoms in electric and magnetic field and method of imaginary time// JETP. — 1998. — V. 113(5). — P. 1579-1605.
12. Ivanov M. V., Schnelcher P., Ground States of H,He,…,Ne and their singly positive ions in strong magnetic fields: the high-field regime// Phys.Rev.A.— 2000. — V. 61.— P. 2251-2263.
13. Cheng T., Liu J., Chen S., Guo H. Rydber atoms in parallel microwave and magnetic fields- Classical dynamics// Phys.Lett.A. — 2000. — V. 265. — P. 384-390.
14. Wang D., Din S., Liu S. Influence of oscillating electric field on the recurrence spectra of a Li Rydberg atom in strong magnetic field// J.Phys.B:At.Mol.Opt. Phys. — 2003. — V. 36. — P. 4225-4232.
15. Glushkov A. V., Lepikh Ya. I., Svinarenko A. A., Prepelitsa G. P., Ambrosov S., Bakunina E., Loboda A. V., Physics of laser-photoionization atomic processes in isotopes and gases separator devices: new optimal schemes//Sensors Electr. and Microsyst.Techn. — 2011. — Vol. 2(8). — P. 27-35.
16. Glushkov A. V., Loboda A. V., Khokhlov V. N., Prepelitsa G. P. Numerical modelling a population differences dynamics of resonant levels of atoms in nonrectangular form laser pulse: Optical bistability effect// Laser and Fiber-Optical Networks Modeling. — 2006. — P. 428-430.
17. Rusov V. D., Glushkov A. V., Vaschenko V. N., Korchevsky D. A., Ignatenko A. V. Stochastic dynamics of the atomic systems in the crossed electric and magnetic field: the rubidium atom recurrence spectra//Kiev Nat. Univ. Sci. Bull. Ser.Phys. — Math.. — 2004. — № 4. — P. 433-438.
18. Korchevsky D. A., Shpinareva I. M., Ignatenko A. V., Sensing stochasticity of atomic systems by analysis of recurrence spectra in an crossed dc magnetic and ac electric fields // Sensor Electr. & Microsyst. Techn. — 2005. — № 1. — P. 21-26.
19. Glushkov A. V., Khokhlov V. N., Tsenenko I. A., Atmospheric teleconnection patterns and eddy kinetic energy content: wavelet analysis//Nonlinear Proc.in Geophys. — 2004. — Vol. 11.—P. 285-293.

20. Glushkov A. V., Khokhlov V. N., Svinarenko A. A., Bunyakova Yu. Ya., Prepelitsa G. P., Wavelet analysis and sensing the total ozone content in the Earth atmosphere: MST «Geomath»//Sensor Electr. and Microsyst.Techn. — 2005. — № 3. — P. 43-48.
21. Glushkov A. V., Khokhlov V. N., Loboda N. S., Bunyakova Yu. Ya., Short-range forecast of atmospheric pollutants using non-linear prediction method// Atmosph. Environment (Elsevier).— 2008. — Vol. 42. — P. 7284–7292
22. Glushkov A. V., Prepelitsa G. P., Khetselius O. Yu., Kuzakon V. M., Solyanikova E. P., Svinarenko A. A., Modeling of interaction of non-linear vibrational systems on basis of temporal series analyses (application to semiconductor quantum generators)// Dynamical Systems — Theory and Applications.— 2011. — P. BIF-110 (8p.).
23. Serbov N. G., Kuzakon' V. M., Khetselius O. Yu., Prepelitsa G. P., Solyanikova E. P., Non-linear analysis methods of signal's temporal series in modeling of interactions in the non-linear vibrational systems of the quantum generators type// Photoelectronics. — 2011. — Vol. 20. — P. 117-123.
24. Rusov V., Glushkov A., Prepelitsa G., Loboda A., Khetselius O., Khokhlov V., Svinarenko A., On possible genesis of fractal dimensions in the turbulent pulsations of cosmic plasma- galactic-origin rays-turbulent pulsation in planetary atmosphere system// Advances in Space Research.— 2008. — Vol. 42, № 9.— P. 1614-1617.
25. Luc-Koenig E., Lyras A., Lecomte J.-M., Aymar M. Eigenchannel R-matrix study of two-photon processes in magnesium// J.Phys. B: At. Mol. Opt. Phys. — 1997. — Vol. 30. — P. 5213-5232.

UDC 539.192

G. P. Prepelitsa, V. M. Kuzakon, V. V. Buyadzhi, E. P. Solyanikova, A. A. Karpenko, D. A. Korchevsky

NONLINEAR STOCHASTIC DYNAMICS GOVERNING FOR QUANTUM SYSTEMS IN EXTERNAL FIELD: CHAOS THEORY AND RECURRENCE SPECTRA ANALYSIS

Abstract.

Nonlinear method of chaos theory and the recurrence spectra formalism are used to study quantum stochastic futures and chaotic elements in dynamics of atomic systems in the electromagnetic (laser) field. Some illustrations regarding the recurrence spectra and chaos dynamics of lithium and magnesium atoms in the crossed electric and magnetic and laser fields are presented.

Key words: atomic system, electromagnetic field, chaos, recurrence spectrum

УДК 539.192

Г. П. Препелица, В. М. Кузаконь, В. В. Буяджи, Е. П. Соляникова, А. А Карпенко, Д. А. Корчевский

НЕЛИНЕЙНАЯ СТОХАСТИЧЕСКАЯ ДИНАМИКА КВАНТОВЫХ СИСТЕМ ВО ВНЕШНЕМ ПОЛЕ: АНАЛИЗ НА ОСНОВЕ ТЕОРИИ ХАОСА И РЕКУРРЕНТНЫХ СПЕКТРОВ

Резюме.

На основе нелинейных методов теории хаоса и формализма рекуррентных спектров изучены квантово-стохастические особенности и элементы хаоса в динамике атомных систем во внешнем электромагнитном (лазерном) поле. В качестве примера приведены данные по рекуррентным спектрам и хаотической динамике атомов лития и магния в скрещенных электрическом и магнитном.а также лазерном полях.

Ключевые слова: атомная система, электромагнитное поле, хаос, рекуррентный спектр

УДК 539.192

Г. П. Препелица, В. М. Кузаконь, В. В. Буяджи, О.П. Соляникова, А. А Карпенко, Д. О. Корчевський

НЕЛІНІЙНА СТОХАСТИЧНА ДИНАМІКА КВАНТОВИХ СИСТЕМ У ЗОВНІШНЬОМУ ПОЛІ: АНАЛІЗ НА ОСНОВІ ТЕОРІЇ ХАОСУ ТА РЕКУРЕНТНИХ СПЕКТРІВ

Резюме.

На підставі нелінійних методів теорії хаосу та формалізму рекурентних спектрів досліджені квантово-стохастичні особливості та елементи хаосу в динаміці атомних систем у зовнішньому електромагнітному (лазерному) полі. В якості приклада наведені дані по рекурентним спектрам та хаотичній динаміці атомів літію та магнію у схрещених електричному та магнітному, а також лазерному полях.

Ключові слова: атомна система, електромагнітне поле, хаос, рекурентний спектр

UDC 535.37

G. M. Burlak, L. N. Vilinskaya

The Odessa State Academy of Building and Architecture
4 Didrikhson str., Odessa 65029, Ukraine

LUMINESCENT PROPERTIES OF OXIDE FILMS ALUMINUM AND TANTALUM IN CONTACT WITH AN ELECTROLYTE

The results of the study of the photoluminescence spectra, electroluminescence and luminescence excited ions of the electrolyte, oxide films of aluminum and tantalum, obtained by the electrochemical method are presented. It is shown that the emission of oxide films, appearing in contact with the electrolyte, due to the processes occurring on the surface of the sample.

Recently, we have showed the possibility of storing the lightsum by oxides when they interact with water vapor as a result of its dissociation on a solid surface [1]. It was assumed that the emission of a number of semiconductor materials in contact with the electrolyte is determined by the energy parameters of the centers formed by adsorbed on the surface of the hydroxyl ions, acting as donors, and the localized electrons on them. [2]

To confirm that the observed emission of a number of semiconductor materials in contact with the electrolyte occurs in the surface layer of phosphorus, we studied the luminescence, excited by the ions of the electrolyte (LEIE), photoluminescence (PL) and electroluminescence (EL).

In this work Al_2O_3 and Ta_2O_5 film thickness of 50 microns, obtained by electrolytic oxidation of aluminum and, accordingly, a tantalum foil in a 0.5% water solution of sorrel acid in 30 minutes on an alternating voltage of 70 V. (PL), (EL) and (LEIE), recorded at room temperature in the spectral range from 400 to 600 nm. The spectra were measured for the same sample and in the same electrolyte. To measure the EL spectra of oxide films of aluminum and tantalum sample was constant voltage anodic or cathodic polarization. As a counter used a film tin dioxide applied by pyrolytic decomposition of $SnCl_2$ on a glass substrate. The electrolyte is a water solution of salts of sodium chloride and manganese (pH=5,5). Luminescence emission was focused on the entrance slit of the monochromator. Emission coming out of the monochromator was detected by a photoelectronic multiplier operating in the mode of counting single photons in the 300-850 nm spectral sensitivity. The signal from the anode of the photoelectronic multiplier was fed to an amplifier and then to the input of the recording device, namely, the frequency counter. In the case of spectra LEIE the sample was applied alternating voltage insufficient to excite the EL.

Fig. 1 shows the curves of the spectral distribution of the PL (1), electroluminescence (2) and LEIE (3) aluminum oxide films in contact with the electrolyte. As can be seen from the figure, the spectrum LEIE has fundamental and additional emission bands for PL and EL.

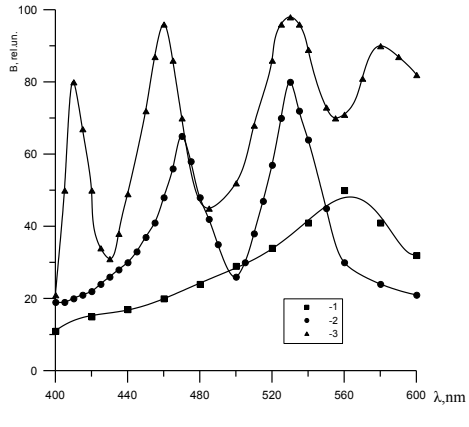

Fig. 1. Spectral distribution of the PL (1), electroluminescence (2) and LEIE (3) aluminum oxide films in contact with the electrolyte.

Maximum of the band in the PL spectrum are located at 560 nm. In EL spectra bands with peaks are located by about 470 and 530 nm. In the spectrum of LEIE bands with peaks are located by about 410, 460, 530 and 580 nm. Obviously, the band of 560 nm for the PL band and 530 nm for EL and LEIE are principal because their appearance is independent of way the excitation of luminescence.

The band at about 580 nm is observed in the spectra LEIE matter in which the electrolyte was measured and does not occur in the photoluminescence and electroluminescence. This additional band, apparently due to the centers of «biographical» nature contained in a certain amount in the phosphor [3], and does not appear in the sample with other types of luminescence, besides luminescence excited by ions of the electrolyte.

The appearance of a band at about 410 nm depends essentially on the nature of the electrolyte in contact with which is film Al_2O_3. Accoding to the electron theory of chemisorption and catalysis, the appearance of such additional band can be explained by the appearance on the film surface chemisorption luminescence centers due to the adsorption of ions of the electrolyte, in contact with which LEIE is observed.

Fig. 2 shows the curves of the spectral distribution of the PL (1), electroluminescence (2) and LEIE (3) Ta_2O_5 films in contact with the electrolyte. As seen from the curves of the spectral distribution emission of the films Ta_2O_5, LEIE spectrum as well as the spectrum of the films Al_2O_3, has fundamental and additional emission bands with the spectra of PL and EL.

Bands with maxima at 430 and 540 nm in the PL spectrum of tantalum oxide films are observed, which is similar to the PL spectra of aluminum oxide film. In the spectrum of the EL tantalum oxide films bands with maxima at 430, 460 and 540 nm are also observed. In the spectral distribution of the LEIE, bands with maxima at 430, 460, 490, 540 and 580 nm are allowed.

Obviously bands with maxima at about 430 and 540 nm can be attributed to the fundamental, as they are observed as in the case of LEIE, as in the case of the PL and EL. The band at about 580 nm is observed in the spectra LEIE in any of the used electrolytes and is not observed under light or

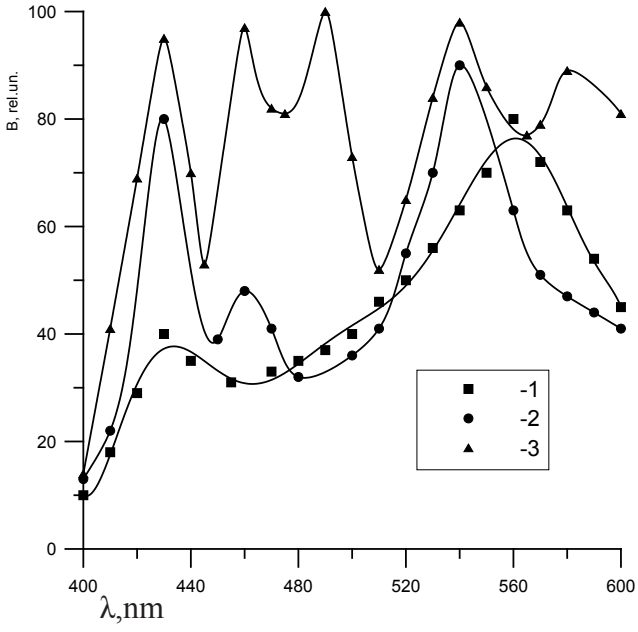

Fig. 2. Spectral distribution of the PL (1), electroluminescence (2) and LEIE (3) Ta_2O_5 films in contact with the electrolyte.

field excitation. Apparently, this band is due to the presence on the surface of the film centers «biographical» nature. Band with a maximum at 490 nm is observed only in certain electrolytes and its position depends on the nature of the electrolyte, in contact with which is film. Obviously, this additional band is related to the arising on Ta_2O_5 film surface emission adsorption centers.

In the spectrum LEIE tantalum oxide film, as well as in aluminum oxide film spectrum LEIE a band at about 460 nm is observed. This additional band, apparently, of the chemiluminescent nature and is explained by reaction occurring at radical recombination of H^+ and OH^- on the surface of the oxide film [4]. By chemiluminescent nature of this band is meant to initiate a catalytic surface of the film chemiluminescent reactions that may take place near the surface of the oxide film in contact with the electrolyte.

Oxidation of aluminum or tantalum films with manganese or being oxide films after oxidation in water solution of manganese results in an appearance of a band at about 600 nm. Obviously, the appearance of this band is caused by the presence of manganese in the film. This band is observed for the same film in different electrolytes, which indicates that it is not related to chemiluminescent reactions on the film surface and the surface centers of «biographical» nature, which are contained in the film are responsible for its origin

Change of surface modification, by treating it before measuring spectra in different electrolytes, changes the properties of the layer of oxide films, and these changes occur in a layer about 10^{-9}m. To fix such surface changes in the study of electroluminescence and also photoluminescence impossible. Since the electrochemical obtained of aluminum and tantalum oxide layers are of variable thickness [5], the PL spectrum is due to the average thickness of the physical and chemical characteristics of these films. In the case of electroluminescence electric field is concentrated in the electrode layers thickness of about 10^{-8} m, and therefore, electroluminescence spectrum is determined by properties of the film of the same order of thickness.

It is established, that only the spectra of LEIE, are sensitive to the nature of the sample and the electrolyte in contact with which it is, that is evidence in favour of what we observed emission is due to the processes occurring on the surface of the sample. This is the evidence that by the emission spectra, occuring in the contact of oxide films of Al_2O_3 and Ta_2O_5 with electrolyte we can judge adout physical and chemical properties luminofores surface.

REFERENCES

1. Михо В. В., Денисова Г. М., Тоцкая А. В. Исследование люминесценции пленок Al_2O_3 в электролите // Химическая физика — 1999. — Т. 11, № 9. — С. 1232-1234.
2. Micho V. V., Vilinskaya L. N., Koleboshin V. Ya. Phenomena arising by interaction of metal oxide with water and ammonia vapours // Workshop sensors springtime in Odessa. — 1998. — P. 50.
3. Михо В. В., Белов В. Т. Использование метода термовы-свечивания для изучения анодного оксида Al // Журн. прикл.химии. — 1999.— Т. 31.— С. 271.
4. L. N. Vilinskaya, G. M. Burlak. Sensors on the basis of aluminium metal — oxide films // Photoelectronics. № 18, 2009, P. 92-94.
5. Вилинская Л. Н., Бурлак Г. М. Влияние перекиси водорода на интенсивность люминесценции полупроводниковых пленок // Сенсорна електроніка і мікросистемні технології. — 2008 — № 4. — С. 53-56.

UDC 535.37

G. M. Burlak, L. N. Vilinskaya

LUMINESCENT PROPERTIES OF OXIDE FILMS ALUMINUM AND TANTALUM IN CONTACT WITH AN ELECTROLYTE

Abstract

The results of the study of the photoluminescence spectra, electroluminescence and luminescence excited ions of the electrolyte, oxide films of aluminum and tantalum, obtained by the electrochemical method are presented. It is shown that the emission of oxide films, appearing in contact with the electrolyte, due to the processes occurring on the surface of the sample.

Key word:uminescence, oxide films, electrolyte

УДК 535.37

Бурлак Г. М., Вілінська Л. М.

ЛЮМІНЕСЦЕНТНІ ВЛАСТИВОСТІ ОКСИДНИХ ПЛІВОК АЛЮМІНІЮ І ТАНТАЛУ В КОНТАКТІ З ЕЛЕКТРОЛІТОМ

Резюме

Приведені результати вивчення спектрів фотолюмінесценції, електролюмінесценції та люмінесценції, яка збуджується іонами електроліту, оксидних плівок алюмінію та танталу, отриманих електрохімічним методом. Показано, що світіння оксидних плівок, яке виникає у контакті з електролітом, обумовлено процесами, що відбуваються на поверхні досліджуваного зразка.

Ключові слова: люмінесценція, оксидні плівки, електроліт.

УДК 535.37

Бурлак Г. М., Вилинская Л. Н.

ЛЮМИНЕСЦЕНТНЫЕ СВОЙСТВА ОКСИДНЫХ ПЛЕНОК АЛЮМИНИЯ И ТАНТАЛА В КОНТАКТЕ С ЭЛЕКТРОЛИТОМ

Резюме

Приведены результаты изучения спектров фотолюминесценции, электролюминесценции и люминесценции, возбуждаемой ионами электролита, оксидных пленок алюминия и тантала, полученных электрохимическим методом. Показано, что свечение оксидных пленок, возникающее в контакте с электролитом, обусловлено процессами, происходящими на поверхности исследуемого образца.

Ключевые слова: люминесценция, оксидные пленки, электролит.

UDC 539.182

A. A. Svinarenko

Odessa National Polytechnical University, 1, Shevchenko av., Odessa, Ukraine
e-mail: quantsvi@mail.ru

SPECTROSCOPY OF AUTOIONIZATION RESONANCES FOR THE LANTHANIDES ATOMS: THULLIUM SPECTRUM, NEW DATA AND EFFECTS

We applied a generalized energy approach (Gell-Mann and Low S-matrix formalism) combined with the relativistic multi-quasiparticle (QP) perturbation theory (PT) with the Dirac-Kohn-Sham zeroth approximation to studying autoionization resonances (AR) in heavy atoms, in particular, energies and widths for the Tm AR with accounting for exchange-correlation and relativistic effects.

Traditionally an investigation of spectra, spectral, radiative and autoionization characteristics for heavy and superheavy elements atoms and multicharged ions is of a great interest for further development atomic and nuclear theories and different applications in the plasma chemistry, astrophysics, laser physics, etc. (look Refs. [1–10]). Theoretical methods of calculation of the spectroscopic characteristics for heavy atoms and ions may be divided into a few main groups [1-6]. First, the well known, classical multi-configuration Hartree-Fock method (as a rule, the relativistic effects are taken into account in the Pauli approximation or Breit hamiltonian etc.) allowed to get a great number of the useful spectral information about light and not heavy atomic systems, but in fact it provides only qualitative description of spectra of the heavy and superheavy ions. Second, the multi-configuration Dirac-Fock (MCDF) method is the most reliable version of calculation for multielectron systems with a large nuclear charge. In these calculations the one- and two-particle relativistic effects are taken into account practically precisely. In this essence it should be given special attention to two very general and important computer systems for relativistic and QED calculations of atomic and molecular properties developed in the Oxford group and known as GRASP («GRASP», «Dirac»; «BERTHA», «QED») (look [1-5] and refs. therein). In particular, the BERTHA program embodies a new formulation of relativistic molecular structure theory within the framework of relativistic QED. This leads to a simple and transparent formulation of Dirac-Hartree-Fock-Breit (DHFB) self-consistent field equations along with algorithms for molecular properties, electron correlation, and higher order QED effects. The DHFB equations are solved by a direct method based on a relativistic generalization of the McMurchie-Davidson algorithm [4].

In this paper we applied a new relativistic approach [11-15] to relativistic studying the autoionization characteristics of the Tm atom. New approach in optics and spectroscopy of heavy atomic systems is the combined the generalized energy approach and the gauge-invariant QED many-QP PT with the Dirac-Kohn-Sham (DKS) «0» approximation (optimized 1QP representation) and an accurate accounting for relativistic, correlation, nuclear, radiative effects. [17-20]. The generalized gauge-invariant version of the energy approach has been further developed in Refs. [12,13]. In relativistic case the Gell-Mann and Low formula expressed an energy shift ΔE through the QED scattering matrix including the interaction with as the photon vacuum field as the laser field. The first case is corresponding to definition of the traditional radiative and autoionization characteristics of multielectron atom. The wave function zeroth basis is found from the Dirac-Kohn-Sham equation with a potential, which includes the ab initio (the optimized model potential or DF potentials, electric and polarization po-

tentials of a nucleus; the Gaussian or Fermi forms of the charge distribution in a nucleus are usually used) [5]. Generally speaking, the majority of complex atomic systems possess a dense energy spectrum of interacting states with essentially relativistic properties. Further one should realize a field procedure for calculating the energy shifts ΔE of degenerate states, which is connected with the secular matrix *M* diagonalization [8-12]. The secular matrix elements are already complex in the second order of the PT. Their imaginary parts are connected with a decay possibility. A total energy shift of the state is presented in the standard form:

$$\Delta \mathrm{E} = \mathrm{Re}\,\Delta E + i\,\mathrm{Im}\,\Delta E \qquad \mathrm{Im}\,\Delta E = -\Gamma/2, \quad (1)$$

where Γ is interpreted as the level width, and the decay possibility $\mathrm{P} = \Gamma$. The whole calculation of the energies and decay probabilities of a non-degenerate excited state is reduced to the calculation and diagonalization of the *M*. The *jj*-coupling scheme is usually used. The complex secular matrix *M* is represented in the form [9,10]:

$$M = M^{(0)} + M^{(1)} + M^{(2)} + M^{(3)}. \quad (2)$$

where $M^{(0)}$ is the contribution of the vacuum diagrams of all order of PT, and $M^{(1)}$, $M^{(2)}$, $M^{(3)}$ those of the one-, two- and three-QP diagrams respectively. $M^{(0)}$ is a real matrix, proportional to the unit matrix. It determines only the general level shift. We have assumed $M^{(0)} = 0$. The diagonal matrix $M^{(1)}$ can be presented as a sum of the independent 1QP contributions. For simple systems (such as alkali atoms and ions) the 1QP energies can be taken from the experiment. Substituting these quantities into (2) one could have summarized all the contributions of the 1QP diagrams of all orders of the formally exact QED PT. However, the necessary experimental quantities are not often available. So, the optimized 1-QP representation is the best one to determine the zeroth approximation. The correlation corrections of the PT high orders are taken into account within the Green functions method (with the use of the Feynman diagram's technique). All correlation corrections of the second order and dominated classes of the higher orders diagrams (electrons screening, polarization, particle-hole interaction, mass operator iterations) are taken into account [10-14]. In the second order, there are two important kinds of diagrams: polarization and ladder ones. Some of the ladder diagram contributions as well as some of the 3QP diagram contributions in all PT orders have the same angular symmetry as the 2QP diagram contributions of the first order [10-12]. These contributions have been summarized by a modification of the central potential, which must now include the screening (anti-screening) of the core potential of each particle by two others. The additional potential modifies the 1QP orbitals and energies. Then the secular matrix is : $M \to \tilde{M}^{(1)} + \tilde{M}^{(2)}$, where $\tilde{M}^{(1)}$ is the modified 1QP matrix (diagonal), and $\tilde{M}^{(2)}$ the modified 2QP one. $\tilde{M}^{(1)}$ is calculated by substituting the modified 1QP energies), and $\tilde{M}^{(2)}$ by means of the first PT order formulae for $M^{(2)}$, putting the modified radial functions of the 1QP states in the interaction radial integrals. Let us remind that in the QED theory, the photon propagator D(12) plays the role of this interaction. Naturally, an analytical form of D depends on the gauge, in which the electrodynamic potentials are written. In general, the results of all approximate calculations depended on the gauge. Naturally the correct result must be gauge invariant. The gauge dependence of the amplitudes of the photoprocesses in the approximate calculations is a well known fact and is in details investigated by Grant, Armstrong, Aymar-Luc-Koenig, Glushkov-Ivanov [1,2,5,9]. Grant has investigated the gauge connection with the limiting non-relativistic form of the transition operator and has formulated the conditions for approximate functions of the states, in which the amplitudes are gauge invariant. These results remain true in an energy approach as the final formulae for the probabilities coincide in both approaches. In ref. [16] it has been developed a new version of the approach to conserve gauge invariance. Here we applied it to get the gauge-invariant procedure for generating the relativistic DKS orbital bases (abbreviator of our method: GIRPT). The autoionization width is defined by the square of interaction matrix element [9]:

$$V^{\omega}_{1234} = [(j_1)(j_2)(j_3)(j_4)]^{1/2} \sum_{\lambda\mu} (-1)^{\mu} \begin{pmatrix} j_1 j_3 & \lambda \\ m_1 - m_3 & \mu \end{pmatrix} \times \mathrm{Re}\, Q_{\lambda}(1234) \quad (3)$$

The real part of the interaction matrix element can be expanded in terms of Bessel functions [5,8]:

$$\frac{\cos|\omega| r_{12}}{r_{12}} = \frac{\pi}{2\sqrt{r_1 r_2}} \sum_{\lambda=0} (\lambda) J_{\lambda+1/2}(|\omega| r_<) J_{-\lambda-1/2}(|\omega| r_>) P_{\lambda}(\cos \mathbf{r}_1 \mathbf{r}_2). \quad (4)$$

The Coulomb part $Q_{\lambda}^{\mathrm{Qul}}$ is expressed in the radial integrals R_{λ}, angular coefficients S_{λ} as follows:

$$\mathrm{Re}\, Q_{\lambda}^{\mathrm{Qul}} \sim \mathrm{Re}\{R_l(1243) S_{\lambda}(1243) + R_{\lambda}(\tilde{1}243\tilde{3}) S_{\lambda} (\tilde{1}243\tilde{3}) + R_{\lambda}(1\tilde{2}43) S_{\lambda}(1\tilde{2}43) + R_{\lambda}(\tilde{1}\tilde{2}43\tilde{3}) S_{\lambda}(\tilde{1}\tilde{2}43\tilde{3})\} \quad (5)$$

where $\mathrm{Re}Q_{\lambda}(1243)$ is as follows:

$$\mathbf{Re}\, R_{\lambda}(1243) = \iint dr_1 r_1^2 r_2^2 f_1(r_1) f_3(r_1) f_2(r_2) f_4(r_2) Z_{\lambda}^{(1)}(r_<) Z_{\lambda}^{(1)}(r_>). \quad (6)$$

where f is the large component of radial part of the 1QP state Dirac function and function Z is :

$$Z_{\lambda}^{(1)} = [2/|\omega_3|\alpha Z]^{\lambda+1/2} J_{\lambda+1/2}(\alpha|\omega_3|r)[r^{\lambda}\Gamma(\lambda+3/2)] \quad (7)$$

The angular coefficient is defined by standard way as above [3]. The calculation of radial integrals $\mathbf{Re}R_{\lambda}(1243)$ is reduced to the solution of a system of differential equations:

$$\left.\begin{aligned} y_1' &= f_1 f_3 Z_{\lambda}^{(1)}(\alpha|\omega|r) r^{2+\lambda}, \\ y_2' &= f_2 f_4 Z_{\lambda}^{(1)}(\alpha|\omega|r) r^{2+\lambda}, \\ y_3' &= [y_1 f_2 f_4 + y_2 f_1 f_3] Z_{\lambda}^{(2)}(\alpha|\omega|r) r^{1-\lambda}. \end{aligned}\right\} \quad (8)$$

In addition, $y_3(\infty)=\mathbf{Re}R_{\lambda}(1243)$, $y_1(\infty)=X_{\lambda}(13)$. The system of differential equations includes also equations for functions $f/r^{|æ|-1}$, $g/r^{|æ|-1}$, $Z_{\lambda}^{(1)}$, $Z_{\lambda}^{(2)}$. The formulas for the autoionization (Auger) decay probability include the radial integrals $R_{\alpha}(\alpha k \gamma \beta)$, where one of the functions describes electron in the continuum state. When calculating this integral, the correct normalization of the function ψ_k is a problem. The correctly normalized function should have the following asymptotic at $r \to 0$:

$$\left.\begin{matrix} f \\ g \end{matrix}\right\} \to (\lambda\omega)^{-1/2} \begin{cases} [\omega + (\alpha Z)^{-2}]^{-1/2} \sin(kr + \delta), \\ [\omega - (\alpha Z)^{-2}]^{-1/2} \cos(kr + \delta). \end{cases} \quad (9)$$

When integrating the master system, the function is calculated simultaneously:

$$N(r) = \{\omega_k [f_k^2 [\omega_k + (\alpha Z)^{-2}] + g_k^2 [\omega_k + (\alpha Z^{-2})]]\}^{-1/2} \quad (10)$$

It can be shown that at $r \to \infty$, $N(r) \to N_k$, where N_k is the normalization of functions f_k, g_k of continuous spectrum satisfying the condition (9). Other details can be found in refs.[10-13,16-20].

Further we present the results on the Tm AR spectrum. Let us note that the positions of 2 nearly lying ionization limits $4f^{13}6snl$ (with states of the QP vacancy in the $4f^{14}$ core: $4f_{7/2}^{-1} \mid 4f_{5/2}^{-1}$) provide two main type of the AR decay [10,11]: i).the Beutler-Fano decay (*BFD*) channel:

$4f^{1}{}_{5/2}$ 6s1/2 (J12) nl - $4f^{1}{}_{7/2}$ 6s1/2 [J12'] Tm^{+} + leje,

n>7, J12=2;3, J12'=3;4

ii). the Letokhov-Ivanov reorientation decay *(ROD)* channel:

$4f^{1}j$ 6s1/2 (J12) nl - $4f^{1}j$ 6s1/2 [J12'] Tm^{+} + leje)

n>25 J12=3, J12'=2;4 j=5/2,7/2,

In table 1 we list the theoretical (the experimental data are absent) results for energies and widths (in cm^{-1}) of different Tm $4f^{13}6sn_Rs$, $4f^{13}6sn_Rp$ states: E_1, Γ_1 — data by Ivanov etal (RPTMP) [10,11]; E_2, Γ_2 — our data (GIRPT). An analysis shows quite physically reasonable agreement between the values of energies E_1 and E_2. However, the widths Γ_1, Γ_2 differ more significantly. In our opinion, this fact is explained by different accuracy of estimates of the radial integrals, using the different type basises (gauge invariance conservation or a degree of accounting for the exchange-correlation effects) and some other additional calculation approximations. In the GIRPT there are used more optimized basises of the orbitals. In table 2 we list similar (as in table 1) our data for the AR widths of the Tm $4f^{13}6sn_Rs$ and $4f^{13}6sn_Rp$ (1/2,5/2), (3/2,5/2) states.

Table 1. The energies and widths of the Tm $4f_{5/2}^{13}6s_{1/2}np_j[J]$ states (j=3/2, J=3/2, n=10-50).

n	Γ_1 (ROD)	Γ_1 (BFD)	E_1	Γ_2 (ROD)	Γ_2 (BFD)	E_2
	RPTMP	RPTMP	RPTMP	GIRPT	GIRPT	GIRPT
10	-	3.69E-3	56163	-	3.79E-3	56184
20	-	5.23E-4	58429	-	5.32E-4	58438
25	4.72E-1	2.45E-4	58597	4.86E-1	2.54E-4	58609
30	2.94E-1	1.32E-4	58678	3.05E-1	1.41E-4	58690
40	1.35E-1	5.01E-5	58753	1.46E-1	5.20E-5	58764
45	9.73E-2	3.38E-5	58772	9.89E-2	3.49E-5	58781
50	7.24 E-2	2.39E-5	58785	7.40E-2	2.48E-5	58794

Table 2. The AR widths (in cm^{-1}; our data) of the Tm $4f_{5/2}^{13}6s_{1/2}np_j[J]$ states (n=10-50).

j,J	(1/2,5/2)		(3/2,5/2)	
n	ROD	BFD	ROD	BFD
10	-	6.72E-3	-	2.36E-3
20	-	5.61E-4	-	3.25E-4
25	4.01E-2	2.57E-4	4.42E-1	1.62E-4
30	3.61E-2	1.39E-4	2.65E-1	8.51E-5
40	3.16E-2	5.04E-5	9.47E-2	3.49E-5
45	4.84E -2	2.55E-5	5.02E-2	3.28E-5
50	1.93E-2	1.98E-5	5.45E-2	2.16E-5

In ref. [14] (see also [5,12]) it has been predicted a new spectral effect of the giant changing of the AS ROD width in a sufficiently weak electric field (for two pairs of the Tm, Gd AR). Following to [5], let us remind that any two states of different parity can be mixed by the external electric field. The mixing leads to redistribution of the autoionization widths. In the case of degenerate or near-degenerate resonances this effect becomes observable even at a moderately weak field. In the Tm one could deal with ROD *ns* and *np* series, converging to the same ionization limit, i.e. they are nearly degenerate states of different parity. Among them one can find some pairs of *ns* and *np* states with widths Γ, differing by several orders. We have quantitatively estimated a value of the changing the studied AR (n>25) width at the weak electric field with strength up to 150 V/cm and found that the corresponding effect is about one order of the AR width for the maximal field strength considered.

References

1. Grant I. P., Relativistic Quantum Theory of Atoms and Mole-cules. — Oxford, 2008. — 650P.
2. Wilson S., Handbook on Molecular Physics and Quantum Chemistry.— Wiley, 2003.— 680P.
3. Quiney H., Relativistic Quantum Mechanics of Atoms and Molecules//New Trends in Quantum Systems in Chemistry and Physics (Springer). — 2002. — Vol. 6. — P. 135–173.
4. Bell K. L., Berrington K., Crothers D., Hibbert A., Taylor K. T., BERTHA: 4-Component Relativistic Molecular Quantum Mechanics// Supercomputing, Collision Processes, and Application, Series: Physics of Atoms and Molecules (Springer). — 2002.—P. 213–224.
5. Glushkov A. V., Relativistic Quantum Theory. Quantum, mechanics of Atomic Systems. — Odessa: Astroprint, 2008. — 900P.
6. Safronova U. I., Safronova M. S., Third-order relativistic many-body calculations of energies, transition rates, hyperfine constants, and blackbody radiation shift in $^{171}Yb^{+}$//Phys. Rev. A. — 2009. — Vol. 79.— P.022512.
7. Bieron J, Froese-Fischer C., Fritzsche S., Pachucki K., Lifetime and hyperfine structure of $^3D_2$ state of radium//J. Phys.B:At.Mol.Opt.Phys. — 2004. — Vol. 37. — P.L305-311.
8. Ivanov L. N., Ivanova E. P., Extrapolation of atomic ion energies by model potential method: Na-like spectra/ // Atom. Data Nucl.Data Tab. — 1999. — Vol. 24. — P. 95-121.

9. Bekov G. I., Vidolova-Angelova E., Ivanov L. N.,Letokhov V. S., Mishin V. I., Laser spectroscopy of low excited autoionization states of the ytterbium atom// JETP. — 1981.— Vol. 80.—P. 866-878.
10. Vidolova-Angelova E., Ivanov L. N., Autoionizing Rydberg states of thulium. Re-orientation decay due to monopole interaction// J.Phys.B:At.Mol.Opt. Phys.— 1999. — Vol. 24. — P. 4147-4158
11. Ivanov L. N., Letokhov V. S. Spectroscopy of autoionization resonances in heavy elements atoms// Com.Mod. Phys.D.:At.Mol.Phys. — 1999. — Vol.4. — P. 169-184.
12. Glushkov A. V., Ivanov L. N., Ivanova E. P., Radiation decay of atomic states. Generalized energy approach// Autoionization Phenomena in Atoms. — M.: Moscow State Univ. — 1986.
13. Glushkov A. V., Ivanov L. N. Radiation decay of atomic states: atomic residue and gauge non-invariant contributions // Phys. Lett.A. — 1999. — Vol. 170. — P. 33-38.
14. Glushkov A. V., Ivanov L. N. DC Strong-Field Stark-Effect: consistent quantum-mechanical approach// J.Phys.B: At. Mol. Opt. Phys. — 1999. — Vol. 26. — P.L379-386.
15. Glushkov A. V., Khetselius O. Yu., Svinarenko A. A., Relativistic theory of cooperative muon-gamma-nuclear processes: Negative muon capture and metastable nucleus discharge// Advances in the Theory of Quantum Systems in Chemistry and Physics (Springer). — 2012. — Vol. 22. — P. 51-70.
16. Glushkov A. V., Khetselius O. Yu., Loboda A. V., Svinarenko A. A., QED approach to atoms in a laser field: Multiphoton resonances and above threshold ionization//Frontiers in Quantum Systems in Chemistry and Physics (Springer). — 2008. — Vol. 18. — P. 541-558.
17. Glushkov A. V., Svinarenko A. A., Ignatenko A. V., Spectroscopy of autoionization resonances in spectra of the lanthanides atoms//Photoelectronics. — 2011. — Vol. 20. — P. 90-94.
18. Svinarenko A. A., Nikola L. V., Prepelitsa G. P., Tkach T., Mischenko E., The Auger (autoionization) decay of excited states in spectra of multicharged ions: Relativistic theory//Spectral Lines Shape. — 2010. — Vol. 16. — P. 94-98
19. Malinovskaya S. V., Glushkov A. V., Khetselius O. Yu., Svinarenko A., Bakunina E., Florko T., Optimized perturbation theory scheme for calculating interatomic potentials and hyperfine lines shift for heavy atoms in buffer inert gas//Int. Journ. Quant. Chem. — 2009. — Vol. 109. — P. 3325-3329.
20. Svinarenko A. A., Mischenko E. V., Loboda A. V., Dubrovskaya Yu. V., Quantum measure of frequency and sensing the collisional shift of the ytterbium hyperfine lines in medium of helium gas// Sensor Electronics and Microsystem Techn. — . № 1. — P. 25-29.

UDC 539.183

A. A. Svinarenko

SPECTROSCOPY OF AUTOIONIZATION RESONANCES FOR THE LANTHANIDES ATOMS: THULLIUM SPECTRUM, NEW DATA AND EFFECTS

Abstract. We applied a generalized energy approach (Gell-Mann and Low S-matrix formalism) combined with the relativistic perturbation theory with the Dirac-Kohn-Sham zeroth approximation to studying autoionization resonances in heavy atoms, in particular, energies and widths for the Tm autoionization resonances with accounting for exchange-correlation and relativistic effects.

Key words: spectroscopy of autoionization resonances, relativistic energy approach

УДК 539.183

А. А. Свинаренко

СПЕКТРОСКОПИЯ АВТОИОНИЗАЦИОННЫХ РЕЗОНАНСОВ ДЛЯ АТОМОВ ЛАНТАНИДОВ: СПЕКТР ТУЛЛИЯ, НОВЫЕ ДАННЫЕ И ЭФФЕКТЫ

Резюме.

Обобщенный энергетический подход (S-матричный формализм Гелл-Мана и Лоу) и релятивистская теория возмущений с дирак-кон-шэмовским нулевым приближением применены к изучению автоионизационных резонансов в тяжелых атомах, в частности, на его основе с учетом обменно-корреляционных и релятивистских эффектов оценены энергии и ширины автоионизационных резонансов в туллии.

Ключевые слова: спектроскопия автоионизационных резонансов, релятивистский энергетический подход

УДК 539.183

А. А. Свинаренко

СПЕКТРОСКОПІЯ АВТОІОНІЗАЦІЙНИХ РЕЗОНАНСІВ ДЛЯ АТОМІВ ЛАНТАНІДІВ: СПЕКТР ТУЛІЯ, НОВІ ДАНІ ТА ЕФЕКТИ

Резюме.

Узагальнений енергетичний підхід (S-матричний формалізм Гелл-Мана та Лоу) и релятивістська теорія збурень з дірак-кон-шемівським нульовим наближенням застосовані до вивчення автоіонізаційних резонансів у важких атомах, зокрема, на його основі з урахуванням обмінно-кореляційних і релятивістських ефектів оцінені енергії та ширини автоіонізаційних резонансів у тулії.

Ключові слова: спектроскопія автоіонізаційних резонансів, релятивістський енергетичний підхід

UDC 621.315.592

V. A. Borschak

Odessa I. I. Mechnikov National University
2, Dvoryanskaya str., Odessa, 65062, Ukraine
Phone: +380(48)7266356, Fax: +380(48)7233461, e-mail: borschak_va@mail.ru

APPLICATION OF A SENSOR ON THE HETEROJUNCTION CdS-Cu_2S BASIS

A novel image sensor has been developed for measuring weak optical signals. The optical information is stored as the charge of the non-equilibrium carriers trapped in the space-charge region of the heterojunction. In the visible range of the spectrum a response of 10^{-6} lx is achieved. In this work the opportunity to obtain the image in X-ray beams was investigated. It is established that investigated sensor is sensitive to soft X-ray radiation. Memory and accumulation of a signal at a room temperature, which is characteristic of the sensor at registration of images in visible beams, take place for the images obtained in X-ray range, too, that makes it possible to apply such sensor in medicine and in crystallography.

We have fabricated and investigated a novel sensor based on the non-additive formation of current [1]. The special properties of this novel sensor are an ability for long-term signal storage at room temperature and the large area of the operating surface. Even the first fabricated samples have an imaging area of 10 cm^2, which exceeds the area of typical CCDs by a factor of 15-20. For example, the imaging area of the TC 241 CD camera (Texas Instruments) is 8.6 mm × 6.5 mm.

It was established that there is no image-signal smearing with time and this quality is based upon the principle of image formation. The latent image in the sensor has been formed by the non-equilibrium charge trapped in the deep levels at the interface of the heterojunction. This permits a time-stable image to be obtained with the sensor.

Experimental curves that characterize the process of signal storage at room temperature for various levels of illumination of the heterojunction surface has been obtained. Such dependencies are well known for photographic emulsions. It should be noted that the applied bias is zero during the exposure. Before the adsorption of the photons the system is in equilibrium and it can be in this state for any period of time. Therefore, under minimum illumination levels the signal increase is not distorted by thermally generated carriers.The good stability of the latent image signal and, therefore, its ability for prolonged storage has been determined.

The sensor was based on a CdS-Cu_2S heterojunction. A thin-film sandwich arrangement is deposited by vacuum evaporation on a glass substrate. A thin Cu film and a transparent conducting $Sn0_2$ layer provide the integral contacts to the p- and n-sides of the heterojunction, respectively. A 256 level video-signal readout is obtained by scanning the surface of the sensor with a point IR probe. Our computer set-up provides the output data in two formats: 128x128 pixels with 16 grey levels and 250x250 pixels with 32 grey levels.

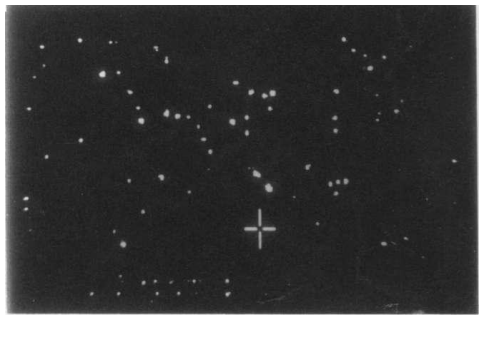

FIG. 1. Image of artificial stars given by the sensor (250x250 pixels)

The spatial resolution is also an important feature of image sensors. The theoretical analysis of the resolution of the detector gives a value of about 1 μm. We have not been able to focus a light spot within such small dimensions. For visible light, the maximum measured spatial resolution is 2-3 μm. Such a high resolution is obtained because of the small lifetime of the minority non-equilibrium current carriers in non-ideal heterojunctions and, consequently, their very small diffusion length. Experimental data for the sensor are listed in Table 1. Fig. 1 represents an image of artificial stars produced by the sensor. High resolution of point objects is seen in the case of an image shape of 250x250 pixels.

Parameters of the detector, based on a non-ideal heterojunction

Imaging area	50 mm×30 mm
Maximum of sensitivity	10^{-6} lx
Spatial resolution	<50 μm
Maximum period of signal storage	2 h

It is known that the effect of X-rays, like visible beams, leads to appearance of non-equilibrium carriers and it can be used to obtain images in X-rays. In this case, as in [2,3], image, in fact, should be shaped by non-equilibrium positive charge, captured at hole traps in space charge area of cadmium sulphide. So, there are the reasons to suppose that it shall have the same properties like the images obtained in the visible range of spectrum. At the same time, it is known that operating sensors of X-ray radiation have the thickness of sensitive absorbing layer not less than 100 μm. And it should not forget that cadmium as component absorbs X-rays successfully. But, the thickness of cadmium sulphide layer, obtained by electro-hydro-dynamic spray of liquid, is not more than 10 (im, so the problem to use the given transducer in X-ray range leaves open.

To clear up this problem we use the sample, in which the layer of cadmium sulphide was obtained by the above mentioned procedure. Medical plant, giving soft X-ray radiation, was used as a source. The doze obtained by means of this plant was not more than 100 millirentgen. As the test-subject, which partially screened X-ray radiation, we used the absorbing wedge consisted of aluminium foil strips with thickness of 100 (μm each. After exposure the sample was scanned, and the shadow of wedge with increasing density being clearly seen on the obtained image. It shows the principal possibility to indicate X-ray images.

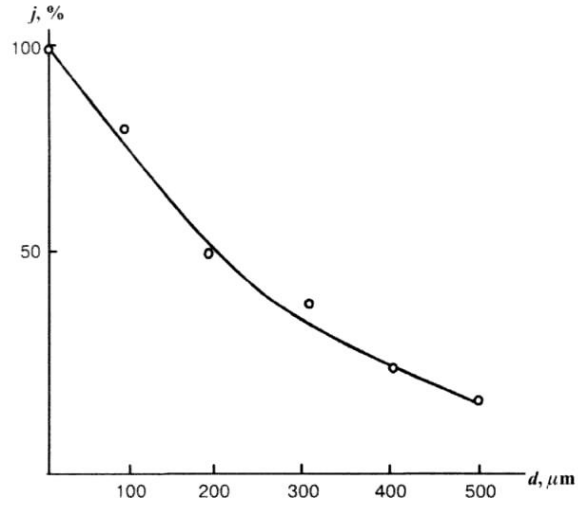

FIG. 2. Dependence of video-signal amplitude on the thickness of absorbing layer

Fig. 2 shows the curve for dependence of photo- response on thickness of absorbing layer d, which is different for various wedge parts. It is seen clearly that signal value falls exponentially under increase of absorbing layer thickness. It is seen that absorbing layer reduce signal in ratio 1.37. Exponential shape of curve indicates good linearity for dependence of signal on doze of X-ray radiation (because increase of absorbing layer thickness by stated value always leads to the same drop in signal level). It is clearly seen from Fig. 3.

Besides, since the signal being used to construct the plot was taken from different surface points, the obtained curve indicates the sufficient homogeneity of sensitivity to X-rays along the surface.

To investigate the abilities of the sample to be used as sensor of X-ray image, the ordinary IC with standard plastic package was taken. Under the repeated scanning, which was carried out in 30 minutes after the foregoing one, it was found out that in this case there was no spread too, and the quality of image remained satisfactory, de-

spite the signal relaxation in time. So, the positive properties, such as memory and signal accumulation characteristic of our sensor under image indication in visible beam, take place for the images obtained in X-ray range.

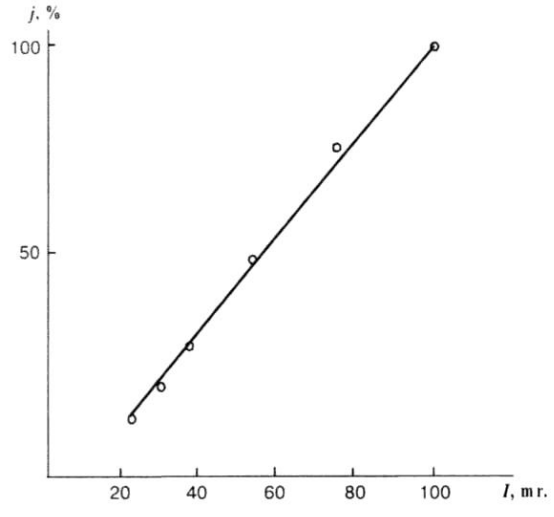

FIG. 3. Dependence of video-signal amplitude on the doze of incident X- ray radiation

So, resting on the above described investigation, one can say with certainty, that our sensor is sensitive to soft X-ray radiation. This makes possible to use such sensor in medicine, and also in crystallography.

Summarizing the main properties of the novel image sensor, we conclude that the detector is также very suitable for applications in astronomy. The use of adaptive optics with astronomical instruments allows the influence of atmospheric turbulence to be decreased. In these conditions an increase of exposure increases the power of the telescope-sensor system that is necessary for the imaging of faint objects, such as galaxies. The use of the sensor to obtain large-format electronic photographs of subtle lunar and planetary details with high resolution is also of great interest. In our first astronomical experiment [4] we obtained a lunar image as well as an image of 5-magnitude (5^m) stars. The future applications of the novel sensor are associated with the possibility of high-quality long-term image processing by means of active and adaptive optics.

References

1. Borschak V. A., Smyntyna V. A., Brytavskyi Ie. V., Balaban, A. P., Zatov= skaya N. P.// Dependence of conductivity of an illuminated nonideal heterojunction on external bias. Semiconductors, v.45, no.7, 2011 July, P.894-899
2. Borschak V. A., Brytavskyi Ie. V., Smyntyna V. A., Lepikh Ya. I., Balaban A. P., Zatovskaya N. P. In-fluence of internal parameters on the signal value in optical sensor based on the non-ideal heterostructure CdS-Cu_2S / Semiconductor Physics, Quantum Electronics & Optoelectronics, 2012, V.15, № 1. P. 41-43
3. V. A. Smyntyna, M. I. Kutalova, N. P. Zatovskaya, V. A. Borschak, Yu. N. Karakis, Investigation of current transfer on the boundaries and in volume of semiconductor barrier structures to develop the effective optical and X-ray image sensors // Photoelectronics, 9, P 8–12 (2000)
4. D. L. Vassilevski and V. A. Borschak, The utilization of a sensor based on a heterojunction for astronomy, ICO-16 Satellite Conf. Active and Adaptive Optics., Garching, Germany, 2-5 Aug. 1999.

UDC 621.315.592

V. A. Borschak

APPLICATION OF A SENSOR ON THE HETEROJUNCTION CdS-Cu_2S BASIS

Abstract

A novel image sensor has been developed for measuring weak optical signals. The optical information is stored as the charge of the non-equilibrium carriers trapped in the space-charge region of the heterojunction. In the visible range of the spectrum a response of 10^{-6} lx is achieved. In this work the opportunity to obtain the image in X-ray beams was investigated. It is established that investigated sensor is sensitive to soft X-ray radiation. Memory and accumulation of a signal at a room temperature, which is characteristic of the sensor at registration of images in visible beams, take place for the images obtained in X-ray range, too, that makes it possible to apply such sensor in medicine and in crystallography.

Keywords: astronomy, heterojunction, image sensor, X-ray image.

УДК 621.315.592

В. А. Борщак

ВИКОРИСТАННЯ СЕНСОРА НА ОСНОВІ ГЕТЕРОПЕРЕХОДУ CdS-Cu_2S

Резюме

Був розроблений новий сенсор зображення для слабких оптичних сигналів. Оптична інформації зберігається у вигляді нерівноважного заряду локалізованого на пастках в області просторового заряду гетеропереходу. У видимій області спектру чутливість досягає 10^{-6} лк. У роботі також показана можливість отримання зображення в рентгенівській області. Встановлено, що сенсор чутливий до м'якого рентгенівського випромінювання. Ефекти пам'яті і накопичення сигналу при кімнатній температурі, що є характерним для датчика при реєстрації зображень у видимих променях, притаманні йому і при реєстрації зображень в рентгенівському діапазоні, що робить можливим застосування таких датчиків в медицині і в кристалографії.

Ключові слова: астрономія, гетероперехід, сенсор зображення, рентгенівських сенсор

УДК 621.315.592

В.А.Борщак

ПРИМЕНЕНИЕ СЕНСОРА НА ОСНОВЕ ГЕТЕРОПЕРЕХОДА CdS-Cu_2S

Резюме

Был разработан новый сенсор изображения для слабых оптических сигналов. Оптическая информации хранится в виде неравновесного заряда локализованного на ловушках в области пространственного заряда гетероперехода. В видимой области спектра чувствительность достигает 10^{-6} лк. В работе также показана возможность получения изображение в рентгеновской области. Установлено, что сенсор чувствителен к мягкому рентгеновскому излучению. Эффекты памяти и накопления сигнала при комнатной температуре, что является характерным для датчика при регистрации изображений в видимых лучах, присущи ему и при регистрации изображений в рентгеновском диапазоне, что делает возможным применение таких датчиков в медицине и в кристаллографии.

Ключевые слова: астрономия, гетеропереход, сенсор изображения, рентгеновский сенсор.

UDC 539.84

O. Yu. Khetselius

Odessa State Environmental University, 15, Lvovskaya str., Odessa, Ukraine
e-mail: nuckhet@mail.ru

OPTICS AND SPECTROSCOPY OF COOPERATIVE ELECTRON-GAMMA-NUCLEAR PROCESSES IN HEAVY ATOMS

It is presented an estimate of probability of the cooperative electron-γ-nuclear processes in some heavy atoms within of earlier developed consistent relativistic approach. The approach is based on S-matrix Gell-Mann and Low formalism combined with relativistic many-body perturbation theory and provides opening new field of cooperative atomic-nuclear quantum optics.

1. Introduction

This paper goes on our work on studying the cooperative electron-gamma-nuclear processes [1-4]. The important example of the cooperative e-g-N process is so called NEET (nuclear excitation by electron transition) one [5-7]. The similar NEEC (nuclear excitation by electron capture) process should be reminded too. In both NEEC and NEET, which are at the borderline between atomic and nuclear physics, electronic orbital energy is converted directly into nuclear energy. These effects offer therefore the possibility to explore the spectral properties of heavy nuclei through the typical atomic physics experiments. In fact, the NEET is a fundamental but rare mode of decay of an excited atomic state in which the energy of atomic excitation is transferred to the nucleus via a virtual photon. This process is naturally possible if within the electron shell there exists an electronic transition close in energy and coinciding in type with nuclear one. In fact the resonance condition between the energy of nuclear transition w_N and the energy of the atomic transition w_A should be fulfilled. Obviously, the NEET process corresponds to time-reversed bound-state internal conversion. Let us remind that firstly the NEET and NEEC effects have been postulated in 1973 by Morita and Goldanskii–Letokhov-Namiot (see also review [1] and Refs. [5-20]). Unlike the NEEC effect, the NEET process has been observed experimentally in $^{197}_{79}Au$ by Kishimoto et al (Institute of Material Structure Science, KEK, and Japan Synchrotron Radiation Research Centre, Japan) and in $^{189}_{76}Os$ by Ahmad et al (Argonne National Laboratory, USA) [10-14]. Below in table 1 we present a summary of the experimental works on the NEET in $^{189}_{76}Os$. It should be noted that each of the experimental techniques has certain inherent difficulties. Analysis of this problem has been presented in Refs. [1,13,14]. It explains quite large difference between the results of different experiments. Saying briefly, the cited difficulties are reduced to the problem of revealing a NEET signal among the surrounding other effects. Really, using electron beam can cause direct Coulomb excitation of a nucleus. In this case it is hardly possible to distinguish this component from that due to the NEET process. Using a broad continuous spectral distribution of synchrotron or bremsstrahlung X-rays leads to contribution into the nuclear state from direct nuclear photoabsorption or into a range of nuclear levels that can feed that state or the lower-lying metastable state. Theoretical NEET effect models were developed in Refs. [1,5-17] (see more [1]). Many of early estimates involved using simple approximations that led to results at considerable variance. More lately Tkalya [17] proposed a model for description of the NEET process near the K-shell ionization threshold of an atom. The QED PT with empirical estimating the nuclear and electron matrix elements and the Dirac-Fock code by Band-Fomichev (with account for finite nuclear size) were used.

Table 1. Experimental data on the NEET probabilities P_{NEET} (M1) for the isotope of $^{189}_{76}Os$.

Exp.group	year	Experimental techniques	P_{NEET}
Otozai et al	1973	e^- bombardment 75-85 keV	1×10^{-6}
Otozai et al	1978	e^- bombardment 72-100 keV	$(1.7\pm0.2)\times10^{-7}$
Saito et al	1981	200 keV bremsstrahlung	$(4.3\pm0.2)\times10^{-8}$
Shinohara etal	1987	„white« synchrotron radiation	$(5.7\pm1.7)\times10^{-9}$
Lakosi et al	1995	300 keV bremsstrahlung	$(2.0\pm1.4)\times10^{-8}$
Ahmad et al	2000	monochromatic 100-keV X rays	$<9.5\times10^{-10}$

New theoretical approach by Ahmad et al [13] is based on using the time-dependent amplitude coupled equations. These authors calculated electron wave functions using the GRASP code and tabulated values of the nuclear transition matrix elements. Thus, the theoretical models involved the use of different consistency level approximations led to results at quite considerable variance. It is obvious that more sophisticated relativistic many-body methods should be used for correct treating the NEET effect. Really, the nuclear wave functions have the many-body character. The correct treating the electron subsystem processes requires an account of the relativistic, exchange-correlation and nuclear effects. Really, the nuclear excitation occurs by electron transition from the M shell to the K shell. So, there is the electron-hole interaction and it is of a great importance a correct account for the many-body correlation effects, including inter-shell correlations, the post-act interaction of the removing electron and hole, possibly the continuum pressure etc [1,17-20]. In this paper we have used earlier developed generalized relativistic energy approach [1-5] to calculation of probabilities of the electron-gamma-nuclear process in some heavy atoms ($^{189}_{76}Os$, $^{193}_{77}Ir$).

2. Relativistic energy approach to cooperative electron-gamma-nuclear process

The relativistic energy approach is based on the S-matrix Gell-Mann and Low formalism combined with the relativistic many-body PT [1,19-24]. Let us remind that in atomic theory, a convenient field procedure is known for calculating the energy shifts ΔE of degenerate states [20,24]. Secular matrix M diagonalization is used. In constructing M, the Gell-Mann and Low adiabatic formula for ΔE is used. A similar approach with the electro-dynamical scattering matrix, is applicable in the relativistic theory [1-5,19-24]. In contrast to the non-relativistic case, the secular matrix elements are already complex in the PT second order. Their imaginary parts relate to radiation decay probability. The total energy shift is as:

$$\Delta E = \mathrm{Re}\Delta E + \mathrm{i}\ \mathrm{Im}\Delta E, \quad (1)$$

$$\mathrm{Im}\ \Delta E = -\mathrm{G}/2, \quad (2)$$

where G is interpreted as the level width, and the decay possibility $P=G$. The whole calculation of energies and decay probabilities of a non-degenerate excited state is reduced to calculation and diagonalization of the complex matrix M. To start with the Gell-Mann and Low formula it is necessary to choose the PT zero-order approximation. Usually, the one-electron Hamiltonian is used, with a central potential that can be treated as a bare potential in the formally exact PT [21]. The total probability of radiative decay (excitation, de-excitation) is connected with imaginary part of ΔE of the system «atom plus field» [9,18-21]. The corresponding corrections of the PT for $\mathrm{Im}\Delta E$ can be represented as a sum on the virtual states. In the lowest PT the separated terms of these sums correspond to the additive contributions of different physical channels into the total decay probability. The fundamental parameter of the cooperative NEET process is a probability P_{NEET} (cross-section) of the nuclear excitation by electron transition. In fact it can be defined as the probability that the decay of the initial excited atomic state will result to the excitation of and subsequent decay from the nuclear state. Within the energy approach a

decay probability is linked with Im D*E* for system (nuclear subsystem plus electron subsystem) excited state. An imaginary part of the excited state energy shift in the lowest PT order is as [1]:

$$\mathrm{Im}\,\Delta E = e^2\,\mathrm{Im}\,i\cdot\lim_{\gamma\to 0}\iint d^4x_1 d^4x_2 e^{\gamma(t_1+t_2)}$$

$$\cdot\{D(r_{N1t1}, r_{N2t2}) < \Psi_I\,|\,(\hat{J}_N(x_1)\hat{J}_N(x_2))\,|\,\Psi_I > +$$

$$J_N(x_2))\,|\,\Psi_I > + \qquad (3)$$

Here $D(r_1t_1,r_2t_2)$ is the photon propagator (for example, in the Lorenz gauge); $\hat{J}_N$, $\hat{j}_e$ — are the 4-dimensional components of a current operator for the nuclear and electron (hole) subsystems; $x=(r_n,r_e,\ t)$ is the 4D space-time coordinate of the particles, respectively; g- is an adiabatic parameter. The nuclear current can be written as follows:

$$J^P(R,t) = \psi^+_{N*}\hat{J}^P\psi_N\,, \qquad (4)$$

where $\hat{J}^P$ is operator of an nuclear electromagnetic transition, ψ_N is a nuclear wave function. The current operator for electron is

$$\overline{j}^{\mu}_e = \hat{\overline{\psi}}_e\gamma^{\mu}\hat{\psi}_e\,, \qquad (5)$$

where γ^{μ} are the Dirac matrices. The Hamiltonian of the interaction of the electronic hole current j^{μ}_{fi} and the nuclear current $J^{\nu}_{fi}(R)$ is written as :

$$\mathrm{H_{int}} = \int\ d^3r\,d^3R\ j^{\mu}_{fi}\ D_{\mu\nu}(\mathrm{x}_N,\ r\text{-}R)\ J^{\nu}_{fi}(R)\,. \qquad (6)$$

The energy shift can be further represented as the PT set. After transformations the final expression for Im D*E* is written sum of the corresponding N-electron (hole) contributions:

$$\mathrm{Im}\,\Delta E = \mathrm{Im}\,E_e + \mathrm{Im}\,E_N\,,$$

$$\mathrm{Im}\,E_a = -\frac{z_a^2}{4\pi}\sum_F\iint dr_{e1}dr_{e2}\iint dr_{N1}dr_{N2}\cdot \qquad (10)$$

$$\cdot\,\Psi^*_I(1)\Psi^*_F(2)\,\frac{\sin(\omega_{IF}r_{a12})}{r_{a12}}\,\Psi_F(1)\Psi_I\,,$$

Here $r_{a12} = |r_{a1} - r_{a2}|$, ω_F is the energy of transition between the initial *I* and final *F* states; sum on *F* means the summation on the final states of a system. Naturally, the form of operator in (10) is defined by a gauge of photon propagator (see discussion in Refs. [9, 21]). In zeroth approximation dependence $\Psi_F\,\Psi_I$ on nuclear and electron coordinates (R_N, $R_{e(h)}$) is factorized ($\sim\Phi_e\Phi_N$). Thus, the combined electron (hole)- nuclear one-photon transitions occur as each of the operators T_N, T_e in (10) contains the combination of nuclear and electron variables. After factorization and transformations the expression (10) can be presented in the following form:

$$\mathrm{Im}\,E_a = -\frac{z_a^2}{4\pi}\sum_{F_eF_N}\iint dR_{N1}dR_{N2}\iint dR_{e1}dR_{e2}\ \Phi^*_{Ie}(R_{e1})\Phi^*_{IN}(R_{N1})\Phi^*_{Fe}(R_{e2})\cdot$$

$$\cdot\,\Phi^*_{FN}(R_{N2})\,\frac{\sin\omega_{IF}R_{a\,12}}{R_{a12}}\,\Phi_{Fe}(R_{e1})\Phi_{FN}(R_{N1})\Phi_{Ie}(R_{e2})\Phi_{IN}(R_{N2}). \qquad (11)$$

The expansion of the operator $\frac{\sin(\omega_{IF}R_{a12})}{R_{a12}}$ on the spherical harmonics generates the decay probability multipole expansion. It can be written in the following known form:

$$\frac{\sin|\omega|R_{12}}{R_{a12}} = \frac{\pi}{2\sqrt{R_1R_2}}\sum_{\lambda=0}^{\infty}(\lambda)J_{\lambda+1/2}(|\omega|R_{a1})J_{\lambda+1/2}$$

$$(|\omega|R_{a2})P_{\lambda}(\cos R_{a1}R_{a2}) \qquad (12)$$

where *J* is the Bessel function of the first kind and (l)=2l+1.

In fact this expansion coincides with the known power expansion; naturally the strict decreasing contribution on multipolarity corresponds to them. In our problem the power expansion parameters are the combinations $\omega^a_F R_e$, $\omega^N_F R_N$. Further the effects of purely nuclear transition, purely electron-(hole) transition and combined electron – nuclear transition in (11) can be distinguished. The corresponding technique of work with these expansions is well developed [8,19-21] and often used in our previous papers (look [1-5]). In the expression for $\mathrm{P_{NEET}}$ there is the square modulus of the Hamiltonian of the electron hole current-nuclear current interaction, averaged over initial states and summed over the final states and written (say, for $\mathrm{M_I}$ – K transition) as:

$$M^2_{\mathrm{int}} = 4\pi e^2\omega_N^{2(\lambda+1)}\,\frac{(j_i\,\frac{1}{2}\,\lambda O\,|\,j_f\,\frac{1}{2})^2}{[\,2\lambda+1)\,!]^2}$$

$$\left|R^{E/M}_{\lambda}(\omega_N)\right|^2 B(E/M\lambda; J_i\to J_f) \qquad (13)$$

Here $B[E/(M)\lambda;\ J_i\text{-}J_f\,]$ is the reduced nuclear probability, $\left|R^{E/M}_{\lambda}(\omega_N)\right|$ are the atomic radial

matrix elements of electric (magnetic) [E/M] multipolarity λ; $j_{i,f}$ and $J_{i,f}$ are the angular momenta of the electronic and nuclear states correspondingly. The atomic radial matrix elements $\left|R_\lambda^M(\omega_N)\right|$ of [E/M] multipolarity λ are expressed by means the integral:

$$\int_0^\infty dr r^2 \left[\frac{2}{|\omega|\alpha Z}\right]^{\lambda+1/2} \frac{J_{\lambda+1/2}(\alpha|\omega|r)}{r^\lambda \Gamma(\lambda+3/2)} [g_i(r)f_f(r)+f_i(r)g_f(r)], \quad (15)$$

where *f(r)* and *g(r)* are the large and small components of the Dirac electronic wave functions. Other details can be found in Refs. [1-5,18-24].

3. Results and conclusions

In concrete calculation of the NEET probabilities for different systems one should calculate the corresponding matrix elements. As we will consider below M1 (E2) transition from the ground state to the first excited state in the nuclei $^{189}_{76}Os$ and $^{193}_{77}Ir$, it should be noted that the values of $B[E/(M)l; J_i\text{-}J_f]$ are usually taken from the Nuclear Data tables or can be estimated according the known formula (see Ref. [1]). To calculate the electronic wave functions and matrix elements we used the relativistic many-body PT formalism [1-4,18,22]. It allows take into account accurately the relativistic, exchange-correlation, nuclear, radiative corrections (code «Superatom»). The zeroth approximation electronic wave functions are found from the Dirac (or Dirac-Kohn-Sham) equation with potential, which includes the SCF potential, the electric and polarization potentials of a nucleus. As an account of the finite nuclear size has a sensitive effect on the energy levels of the bound electron, one should use the Fermi function of the charge distribution in a nucleus. The correlation corrections of the second and high orders are taken into account within the Green functions method (with the use of the Feynman diagram's technique). There have taken into account all correlation corrections of the second order and dominated classes of the higher orders diagrams [18]. The magnetic inter-electron interaction is accounted in the lowest (on a^2 parameter; a is the hyperfine structure constant). The QED corrections are accounted effectively: the Lamb shift self-energy part - within the generalized Ivanov-Ivanova non-perturbative procedure and the polarization part - in the generalized Uehling-Serber approximation [18]. The important feature of the whole method is using the optimized one-quasiparticle representation in the zeroth approximation, which is constructed within the method [9]. The nuclear part of the method includes a set of the nuclear shells models, including the relativistic mean-field approach and Dirac-Bloumkvist-Wahlborn and Dirac-Woods-Saxon models [2, 26-28]. Our data on the NEET probability for ($^{189}_{76}Os$, $^{193}_{77}Ir$), atoms together with the alternative theoretical (by Tkalya & Ahmed et al) [13,16,17] and experimental data (see [11-13] and Refs. therein) are listed in table 2. Let us note that in $^{189}_{76}Os$ during the NEET process the initial K-vacancy state decays via an electronic transition from the M shell. The KM_I (70.822 keV, M1) KM_{IV} (71.840 keV, E2) and KM_V (71.911keV, E2) atomic transitions can give the contribution. The corresponding nuclear state at 69.535 keV can be excited via M1 or E2 transitions from the 3/2$^-$ nuclear ground state. The following energy parameters w_N=69.535 keV, $w_A=E_{MI}\text{-}E_K$=70.822 keV, G_K=42.6 eV, G_M=12.8 eV are used for $^{189}_{76}Os$ atom. The energy parameters for $^{193}_{77}Ir$: w_N=73.04 keV, w_A=72.937 keV, G_K =45 eV, G_M =12.8 eV. Analysis of all presented theoretical data shows that these results are consistent with each other and are in the physically reasonable agreement with the recent experimental results.

Table 2. Theoretical and experimental probabilities P_{NEET} (M1) for $^{189}_{76}Os$ and $^{193}_{77}Ir$

Nucl.	Nuclear excitation energy (keV)	Experiment. values	Theory by Tkalya	Theory by Ahmed etal	Our theory
$^{189}_{76}Os$	69.535	$<9.5\times10^{-10}$	1.2×10^{-10}	1.3×10^{-10}	1.9×10^{-10}
$^{193}_{77}Ir$	73.04	$(2.8\pm0.4)\times10^{-9}$	2.0×10^{-9}	-	2.7×10^{-9}

In conclusion note that above presented method with some modifications can be reformulated in a case of the multi-nucleon nuclear system with

using potentials [26-28]. Generally speaking, the approach used can be applied in studying the whole spectra of the cooperative electron-other particle-g-nuclear processes in atomic/nuclear systems [2-17,28-36] and thus provides opening a new field of cooperative atomic/nuclear quantum optics.

References

1. Khetselius O. Yu., Relativistic energy approach to cooperative electron-gamma-nuclear processes: NEET effect// Advances in Theory of Quantum Systems in Chemistry and Physics, Series: Progress in Theor. Chem. and Physics (Springer). — 2012. — Vol. 26 — P. 57-70.
2. Glushkov A. V., Khetselius O. Yu., Malinovskaya S. V., Optics and spectroscopy of cooperative laser-electron nuclear processes in atomic and molecular systems — New Trend in Quantum Optics// Europ. Phys. Journ. — 2008. — Vol. 160.— P. 195-204.
3. Glushkov A. V., Khetselius O. Yu., Malinovskaya S. V., Spectroscopy of cooperative laser-electron-g-nuclear effects in multiatomic molecules// Molec. Phys. (UK). — 2008. — Vol. 106.-P.1257-1260.
4. Glushkov A. V., Khetselius O. Yu., Malinovskaya S. V., New laser-electron nuclear effects in the nuclear g transition spectra in atomic and molecular systems// Frontiers in Quantum Systems in Chemistry and Physics, Series: Progress in Theoretical Chem. and Physics (Springer). — 2008. — Vol. 18. — P. 523-540.
5. Morita M., Nuclear excitation by electron transition//Progr.Theor.Phys. — 1999. — Vol. 49. — P. 1574-1586.
6. Goldanskii V. I., Letokhov V. S., On problem of g laser on nuclear transitions//JETP.-1999. — Vol. 67. — P. 513-524
7. Goldanskii V. I., Namiot V. A., On excitation of isomeric nuclear levels by laser radiation through inverse internal electron con-version//Phys.Lett.B. — 1976. — Vol. 62. — P. 393-394.
8. Ivanov L. N., Letokhov V. S., Spectrum of electron-nuclear gamma transitions of a nucleus in an atom//JETP. — 1999. — Vol. 68. — P. 1748-1760.
9. Glushkov A. V., Ivanov L. N. Radiation decay of atomic states: atomic residue and gauge non-invariant contributions // Phys. Lett.A. — 1992. — Vol. 170. — P. 33-38.
10. Shinohara A.,Saito T., Shoji M., Yokoyama A., Baba H., Ando M.,Taniguchi K., Nuclear excitation in ^{189} Os with synchrotron radiation// Nucl.Phys.A.— 1987. —Vol. 472.— P. 151–160
11. Shinohara A., Saito T., Shoji M., Yokoyama A., Baba H., Ando M., Taniguchi K., Nuclear excitation in ^{189} Os with synchrotron radiation//Nucl. Phys.A. — 1999. — Vol. 472. — P. 151-160.
12. Kishimoto S., Yoda Y., Seto M., Kobayashi Y., Kitao S., Haruki R., Kawauchi T., Fukutani K., Okano T., Observation of nuclear excitation by electron transition in ^{197}Au with synchrotron X-rays and avalanche photodiode//Phys.Rev. Lett. — 2000. —Vol. 85. — P. 1831-1834.
13. Kishimoto S., Yoda Y., Kobayashi Y., Kitao S., Haruki R., Masuda R., Seto M., Nuclear excitation by electron transition on ^{197}Au by photoionization around the K-absorption edge// Phys.Rev.C. — 2006. — Vol. 74. — P. 031301 (8p).
14. Ahmad I., Dunfird R., Esbensen H., Gemmell D., Kanter E., Run U., Siuthwirth S., Nuclear excitation by electron transition in ^{189}Os// Phys.Rev.C. — 2000. — Vol. 61. — P. 051304.
15. Morel P., Daugas J. M., Gosselin G., Méot V., Gogny D., Nuclear excitation by electronic processes: NEEC and NEET effects//Nucl.Phys.A. — 2004. — Vol. 746. — P. 608-612.
16. Harston M. R., Carroll J.J., Nuclear excitation and de-excitation in resonant

electronic transitions// Laser Phys. — 2004. — Vol. 14. — P. 1452–1456.
17. Tkalya E. V., Theory of the nuclear excitation by electron transition process near the K edge//Phys.Rev.A. — 2007. — Vol. 75. — P. 022509
18. Khetselius O. Yu., Relativistic perturbation theory calculation of hyperfine structure para-meters for some heavy-element isotopes//Int.J.Quant.Chem. — 2009. — Vol. 109. — P. 3330-3335
19. Glushkov A. V., Ivanov L. N., Ivanova E. P., Radiation decay of atomic states. Generalized energy approach// Autoionization Phenomena in Atoms. — M.: Moscow State Univ. — 1986.
20. Ivanov L. N., Letokhov V. S., Spectroscopy of autoionization resonances in heavy elements atoms/ //Com.Mod. Phys.D: At.Mol.Phys. — 1985 — Vol. 4 — P. 169-184
21. Glushkov A. V., Khetselius O. Yu., Loboda A. V., Svinarenko A. A., QED approach to atoms in a laser field: Multiphoton resonances and above threshold ionization/ // Frontiers in Quantum Systems in Chemistry and Physics, Series: Progress in Theoretical Chemistry and Physics (Springer). — 2008. — Vol. 18. — P. 541-558.
22. Khetselius O. Yu., Relativistic calculating the hyperfine structure parameters for heavy-elements and laser detecting the isotopes and nuclear reaction products// Physica Scripta. — 2009. — Vol. T 135. — P. 014023.
23. Glushkov A. V., Ivanov L. N., DC strong-field Stark-effect: new consistent quantum-mechanical approach// J. Phys. B: At. Mol. Opt. Phys. — 1993. — Vol. 26. — P.L379-386.
24. Ivanov L. N., Ivanova E. P. Storm orbital technique in calculation of physical characteristics of atomic and ionic emissions//JETP. — 1996. — Vol. 110. — P. 483-498.
25. Glushkov A. V., Rusov V. D., Ambrosov S., Loboda A., Resonance states of compound super-heavy nucleus and EPPP in heavy nucleus collisions//New Projects and New Lines of Research in Nuclear Physics. Eds. G.Fazio, F.Hanappe, Singapore: World Sci.. — 2003. — P. 142-154.
26. Serot B. D., Walecka J. D., Advances in Nuclear Physics: The Relativistic Nuclear Many Body Problem. — N.-Y.: Plenum Press. — 1999. — Vol. 16. — P. 3-216
27. Yang F., Hamilton J., eds, Fundamentals of nuclear models.-Singapore: World Sci. — 2010.
28. Glushkov A. V., Lovett L., Khetselius O. Yu., Gurnitskaya E. P., Dubrovskaya Y. V., Loboda A. V., Generalized multiconfiguration model of decay of multipole giant resonances applied to analysis of reaction (m-n) on the nucleus ^{40}Ca//Int. Journ. of Modern Phys.: A. Particles, Fields, Nuclear Phys. — 2009. — Vol. 24.— P. 611-615.
29. Basov N. G., Letokhov V. S., Optical frequency standards//Sov.Phys. — Uspekhi. — 1969. — Vol. 11. — P. 855-880.
30. Letokhov V. S., Using lasers in atomic, nuclear and molecular physics// Apllication of Lasers in Atomic, Nuclear and Molecular Physics. Eds. Prokhorov A. M., Letokhov V. S. — Moscow: Nauka,1999. — P. 405-414.
31. Glushkov A. V., Ivanov L. N., Shift and deformation of radiation atomic lines in the laser emission field. Multiphoton processes//Preprint ISAN-RAN.-Moscow, 1992 — N92-3-AS.
32. Glushkov A. V., Ivanov L. N., Letokhov V. S., Nuclear quantum optics//Preprint ISAN-RAN. — Moscow, 1999 — N92-4-AS.
33. Vysotskii V. I., The problem of controlled spontaneous nuclear gamma-decay: theory of controlled excited and radioactive nuclei g-decay//Phys.Rev.C — 1998. — Vol. 58. — P. 337-350.
34. Palffy A., Sheid W., Harman Z., Theory

of nuclear exci-tation by electron capture for heavy ion// Phys.Rev.A. — 2006. — Vol. 73. — P.012715.
35. Shahbaz A., Muller C., Staudt A., Burvenich T. J., Keitel C.H., Nuclear quantum optics with X-ray laser pulses// Phys.Rev.Lett. — 2007. — Vol.98. — P.263901.
36. Glushkov A. V., Khetselius O. Yu., Lovett L., Electron-b-nuclear spectroscopy of atoms and molecules and chemical environment effect on b-decay parameters//Adv. in Theory of Atomic and Molecular Systems: Dynamics, Spectroscopy, Clusters, Nanostructures, Series: Progress in Theoretical Chem. and Physics (Springer). — 2010. — Vol. 20. — P. 125-152.

UDC 539.84

O. Yu. Khetselius

OPTICS AND SPECTROSCOPY OF COOPERATIVE ELECTRON-GAMMA-NUCLEAR PROCESSES IN HEAVY ATOMS

Abstract. It is presented an estimate of probability of the cooperative electron-g-nuclear processes in some heavy atoms within of earlier developed consistent relativistic approach. The approach is based on S-matrix Gell-Mann and Low formalism combined with relativistic many-body perturbation theory and provides opening new field of cooperative atomic-nuclear quantum optics.

Key words: cooperative optics, electron-g-N processes, relativistic theory

УДК 539.84

О. Ю. Хецелиус

ОПТИКА И СПЕКТРОСКОПИЯ КООПЕРАТИВНЫХ ЭЛЕКТРОН-ГАММА-ЯДЕРНЫХ ПРОЦЕССОВ В ТЯЖЕЛЫХ АТОМАХ

Резюме. На основе ранее развитого последовательного релятивистского энергетического подхода, базирующегося на S-матричном формализме Гелл-Мана и Лоу и релятивистской многочастичной теории возмущений, выполнена оценка вероятностей кооперативных электрон-g-ядерных процессов в тяжелых атомах.

Ключевые слова: кооперативная оптика, электрон-g-N процессы, релятивистская теория

УДК 539.84

О. Ю. Хецеліус

ОПТИКА І СПЕКТРОСКОПІЯ КООПЕРАТИВНИХ ЕЛЕКТРОН-ГАММА-ЯДЕРНИХ ПРОЦЕСІВ У ВАЖКИХ АТОМАХ

Резюме. На основі раніше розвинутого послідовного релятивістського енергетичного підходу, який базується на S-матричному формалізмі Гелл-Мана та Лоу і релятивістській багаточастинковій теорії збурень, виконано оцінку ймовірностей кооперативних електрон - g-ядерних процесів у важких атомах.

Ключові слова: кооперативна оптика, електрон-g-N процеси, релятивістська теорія

UDC 539.125.5

Karakis Yu. N., Kutalova M. I., Zatovskaya N. P.

Odessa National University, Pasteur Str.,42; ph. 726 63 56
e-mail:waz@mail.ru

OPTIMYZATION IN CONDITIONS FOR CdS-Cu_2S HETEROPHOTOCELL SHAPING

We carried out the investigation in photoelectric properties of photoconverter on conditions that shaped each level of its structure. Cadmium sulphide layers doped with zinc ($Zn_xCd_{1-x}S$, $x \leq 0,2$) obtained by electrohydrodynamic spray procedure on glass substrates coated with tin dioxide by the practice described in [--] were used as the basic ones.

The thickness of these layers is 3...4 μm. The layer of CuC1 was applied by thermal sputtering on surface of cadmium sulphide one being under room temperature. Then, Cu_2S layer is shaped under heating as the result of substitution reaction in solid phase

$$2Cu_{1-\gamma}Cl + Cd_{1-\delta}CdS \leftrightarrow (1 - \delta)Cu_{1-\gamma}$$

where γ and δ – the numbers described the deviation degree from stoichiometry for CdS and CuC1, correspondingly. The compound $CdCl_2$ obtained as reaction outcome can be wasted by washing in distilled water. The deposition of copper contact was the crown stage to form the converter.

The introduction of Zn into CdS layer to increase open-current voltage (U_{oc}) leads simultaneously to increase in base resistance and respectively to decay of short-circuit current (I_{sc}). So, the decrease of resistivity was the first stage to optimize the conditions for heterojunction shaping. $Zn_xCd_{1-x}S$ newly-made layers were thermally treated on air and in vacuum with different time intervals and under various temperatures. The dependencies of U_{oc} and I_{sc} on vacuum annealing temperature within the range 470 K – 770 K are presented in Figure 1. The given curves show that the maximum values of U_{oc} and I_{sc} can be reached within the annealing range 710...740 K.

Such higher temperature value is connected with recrystallization processes in $Zn_xCd_{1-x}S$ layer. The optimal annealing time is 25 minutes. One should take into account that the decrease of sulphur surface concentration and desorption oxygen adsorbed under growth are the important processes in vacuum annealing because oxygen in $Zn_xCd_{1-x}S$ base level increases its resistivity and hampers the reaction of Cu_xS shaping. As the annealing result cadmium sulphide surface became enriched in cadmium.

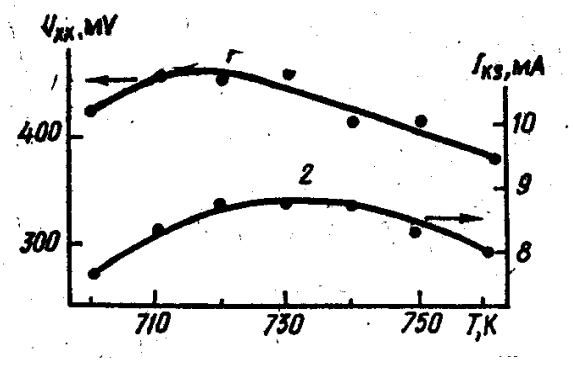

Figure 1. Photoconverter dependence of U_{oc} (*1*) and I_{sc} (*2*)on $Zn_xCd_{1-x}S$ vacuum annealing temperature (AM- 1,5).

The base surface should be depleted with sulphur accordingly to chemical reaction to obtain Cu_xS of stoichiometric composition. The stoichiometric composition of Cu_xS is necessary to obtain photovoltaic effect observed only in chalcocite phase (Cu_2S). Vacuum annealing will improve the efficiency of elements when $Zn_xCd_{1-x}S$ surface is enriched with sulphur that has been observed in our case.

The fact that vacuum annealing agrees with production technology of (ZnCd)S/Cu_2S photoconverters (by substitution process in solid

phase) should be referred to the positive aspects in thermal treatment of $Zn_xCd_{1-x}S$ layer. Such annealing is carried out before deposition of cuprum chloride and is one of the stages to shape heterostructure in the united technological process.

The annealing of base layers in air slightly improves photoconverter parameters. This can be explained as follows: oxygen and sulphur are not removed during such annealing, and surface parameters are not applicable to shape effective heterojunction.

The determination of optimal conditions to create cuprum sulphide layer that provides high efficiency of photoconverter is seemed to be important. The data [] showed that Cu_xS was grown by epitaxy on CdS and sulphur sublattice remain unchanged. Only cuprum and cadmium atoms diffuse during the reaction. The deviation in CuC1 and CdS stoichiometry will be represented in cuprum sulphide stoichiometry. So, we have paid our particular attention to grow CuC1 layer of stoichiometric composition. One knows that CuCl is not stable composition and can pass into $CuC1_2 \cdot 2H_20$ crystalline hydrate phase. When this material is applied in deposited layer of cuprum chloride the impurity in the form of $CuC1_2$ or $CuCl_2\ 2H_20$ will be present and the composition Cu_xS that differs significantly from Cu_2S is determined. So, CuC1 powder (newly-prepared or cleaned) was used for deposition of cuprum chloride layer, and evaporator was covered by copper chip to saturate chlorine ions with it fully. This resulted in cuprum chloride layer that the nearest to stoichiometric one.

When temperature of substrate with $Zn_xCd_{1-x}S$ and CuCl increases higher that 370 K copper began to diffuse from CuCl to the growing surface of cuprum sulphide, and at the same time cadmium diffuses from cadmium sulphide to the growing surface of $CdCl_2$. As the rates of copper and cadmium diffusion depend on vacancy concentration, there will be the dynamic equilibrium between diffusant concentrations. During the most period of reaction the diffusion of Cu and Cd will take place through the mixtures of cuprum chloride and cadmium chloride, on the one side, and through the mixtures of cuprum sulphide and cadmium sulphide, from the other side. At the start of reaction vacancy concentrations will be significant and diffusion through thin areas of mixtures will be easy. As reaction follows the areas of mixtures become thicker and thicker and diffusion through the whole width becomes hampered. So, when thickness (d) of $CdCl_2$ layer increases, diffusion of cooper from CuCl will decrease sharply. It follows that thickness of cuprum chloride layer influences considerably on kinetics of Cu_xS formation.

To determine the optimal thickness (d) of CuCl layer we studied the dependence of photocell parameters on the mentioned value. The thickness of cuprum chloride layer was varied by changes in amount of powder charged into evaporator.

Curves *1* and *2* (Fig. 2) demonstrate the changes in open-current voltage and short-circuit current of the samples from thickness (d) of CuCl layer. The given curves were measured under light intensity that corresponded to atmospheric mass AM 1,5. Figure 3 shows that maximum values of parameters and $I_{кз}$ can be reached at values $d \sim 0{,}4...0{,}6$ μm. When thickness d decreases, the thickness of growing Cu_xS layer is not sufficient to absorb completely the incident radiation, so short-circuit current decreases, but at its increase the diffusion of cooper ions is blocked by the growing layer of cadmium chloride and the reaction results in formation of cuprum sulphide layer with higher deviation from stroichiometry.

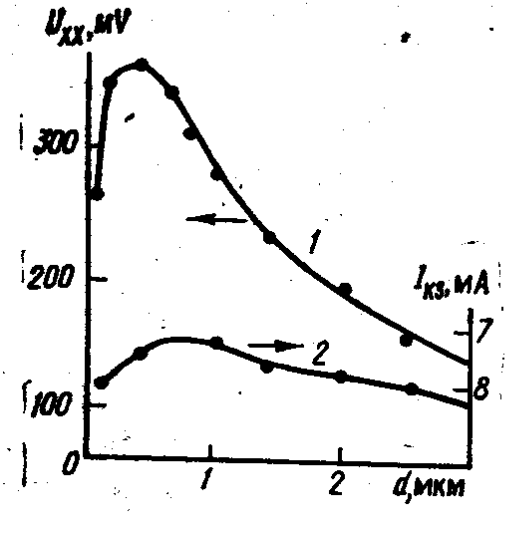

Figure 2. Photoconverter dependence of U_{oc} (1) и I_{sc} (2) on thickness (d) of CuC1 layer (AM1,5).

Temperature of substitution process is rather significant to obtain Cu_xS being similar to the stoichiometric composition. The substrates with $Zn_xCd_{1-x}S$ and CuC1 layers were placed over the heater that increased temperature up to 440…460 K and withstand it during $t \sim (5...35)$ min.

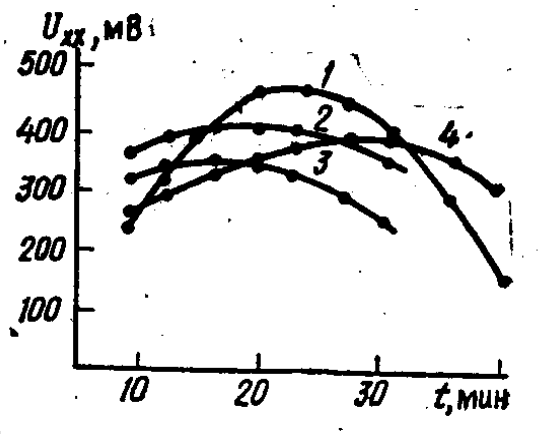

Figure 3. U_{oc} dependence of photoconverter on formation time of Cu_xS layer at temperatures: 1 — 440; 2 — 460; 3 — 480; 4 — 500 K

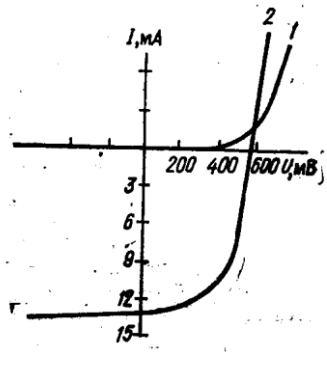

Figure 4. CVC of $Zn_xCd_{1-x}S$ — Cu_2S heterojunction at AM1,5

The results for U_{oc} measurements on heating time are presented in Figure 3. All curves have the maximum, and the higher T, the maximum value U_{xx} reaches early. But the highest photovoltage value is reached at $\boldsymbol{T}$ = 440 K. At higher and lower temperatures these values decrease.

The optimal conditions of layer formation are $T \sim 440$ K and t= 20 min.

Experimental current-voltage characteristics (CVC) for $Zn_xCd_{1-x}S$-Cu_2S photoconverter made according to the optimized procedure are presented in Figure 4.

Under AM 1,5 the efficiency of photoconverter with square 1 cm^2 is 6,0% under open-circuit voltage U_{oc} = 510 mV and short-circuit current I_{sc} = 15 mA/cm^2, CVC occupation coefficient is equal to = 0,61.

The described investigation determined the optimal conditions shape $Zn_xCd_{1-x}S$-Cu_2S heterojunction for high-effective converters of solar energy into electric one.

REFERENCES:

1. Ю. Н. Каракис, М. И. Куталова, Н. П. Затовская, В. В. Зотов, «Особенности релаксации фототока в кристаллах сульфида кадмия с запорными контактами» 1-а Українська наукова конференція з фізики напівпровідників. Одеса, 10-14 вересня 2002 р. Тези доповідей. Т.2. С.138.

2. A. A. Dragoev, A. V. Muntjanu, Yu. N. Karakis, M. I. Kutalova «Calculation for migration-dependent changes in near-contact space-charge regions of sensitized crystals». «Photoelectronics», v. 19. Odessa «Astroprint» 2010. P. 74-78.
3. M. A. Novikova, Yu. N. Karakis, M. I. Kutalova «Particularities of current transfer in the crystals with tw types of Recombination centers». «Photoelectronics», 2005, v.14, P. 58-61.
4. Melnik A. S., Karakis Y. N. Kutalova M. I., Cheme-resjuk G. G. «Features of thermo-optical transitions from the recombination centers excited states». «Photoelectronics», v. 20. Odessa «Astroprint» 2011. P. 23-28.

UDC 539.125.5

Karakis Yu. N., Kutalova M. I., Zatovskaya N. P.

OPTIMYZATION IN CONDITIONS FOR CdS-Cu_2S HETEROPHOTOCELL SHAPING

Abstract

CdS-Cu_2S thin film structures are prospective to be the base for high-efficient converters of solar energy to electric one. The theoretical efficiency of these elements is 27 %. But the complexity to obtain all components of the system with optimal parameters confines to reach such higher efficiency in practice.

Key words: optimization, geterophotocell, thin film structures.

УДК 539.125.5

Караис Ю. Н., Куталова М. И., Затовская Н. П.

ОПТИМИЗАЦИЯ УСЛОВИЙ ФОРМИРОВАНИЯ ГЕТЕРОФОТОЭЛЕМЕНТА CdS-Cu_2S

Резюме

Тонкопленочные структуры CdS-Cu_2S – являются перспективными для создания на их основе высокоэффективных преобразователей солнечной энергии в электрическую. Теоретический к.п.д. этих элементов составляет 27 %. Однако практическое достижение такого высокого коэффициента полезного действия ограничивается сложностью получения всех компонент системы с оптимальными параметрами.

Ключевые слова: оптимизация, гетерофотоэлемент, тонкоплёночные структуры.

UDC 535.42, 539.184

S. V. Ambrosov, A. P. Fedchuk, A. V. Glushkov, Ya. I. Lepikh

I. I. Mechnikov Odessa National University, 2, Dvoryanskaya str., Odessa, Ukraine
Odessa National Polytechnical University, 1, Shevchenko av., Odessa Ukraine
Odessa State Environmental University, 15, Lvovskaya str., Odessa, Ukraine
e-mail: serambr@mail.ru

LASER-PHOTOIONIZATION METHOD OF SEPARATION OF THE ISOTOPES: RADIATIVE PARAMETERS FOR ALKALI ELEMENTS

It is proposed an optimal scheme of the separating isotopes alkali elements, which is based on the selective laser excitation of the isotope atoms into excited Rydberg states and further DC electric field ionization. Some radiative parameters data are evaluated for the alkali elements.

The AVLIS (atomic vapour laser isotope separation) and MLIS (molecular laser isotope separation) methods, based on the atomic photoionization and molecular photoionization and photodissociation processes, are well known now and actively developing [1-10]. The laser photoionization method is one of the most perspective methods for the separating isotopes, nuclear isomers and nuclear reactions products [1-20]. The standard laser ionization sensor scheme is usually realized with using a scheme of the multi-step excitation and ionization of atoms by laser pulse. The scheme of selective ionization of atoms, based on the selective resonance excitation of atoms by laser radiation into states near ionization boundary and further photo-ionization of the excited states by additional laser radiation, has been at first proposed and realized by Letokhov et al (look refs. [1,2]). Naturally, this scheme represents a great interest for laser separation of isotopes and nuclear isomers. However, a significant disadvantage of the two-step selective ionization of atoms by laser radiation method is a great difference between cross-sections of resonant excitation σ_{exc} and photo-ionization σ_{ion} ($[\sigma_{exc}/\sigma_{ion}]>10^4\div10^8$). It requires a using very intensive laser radiation for the excited atom ionization. The situation is more simplified for autoionization resonances in the atomic spectra because of the advanced energy parameters, however, the detailed data about characteristics of these atomic states are often absent. Here the main problems are connected with difficulties of theoretical studying and calculating the autoionization resonance characteristics. An account of complex relativistic and correlation effects (continuum states, self-energy diagrams contributions etc.) by means of the traditional quantum-mechanical methods became obligatorily.

In a number of papers (look refs. [10,11,17-21]) a possibility of the selective ionization of atoms, based on the selective resonance excitation of atoms by laser radiation into states near ionization boundary and further ionization decay of excited atoms by external electric field, has been considered. Electric field changes the electron spectra so that the part of discrete spectra levels (near the ionization boundary) part moves into continuum and other levels become by the autoionization ones. The probability of their autoionization decay quickly increases with growth of the main quantum number. The most optimal situation is when atom is excited to state, which has the autoionization probability more than the radiation decay one. To receive an accurate information about optimal laser photoionization sensor scheme, it is necessary to carry the accurate calculation of the process of sequent atomic excitation by laser field (it is the standard task) and probability of ionization of the atoms in the highly excited states (au-

toionization levels) by electric field. Now the accurate calculations of elementary atomic processes in different calculation schemes are intensively carried out, including calculation of characteristics of decay of the autoionization resonances [8-21]. As a rule, non-relativistic approximation has been used [1]. More consistent approach to this problem must be based on the relativistic models [11,17-21], as the most interesting elements for laser isotope separation are heavy ones and a role of relativistic corrections is often very dramatic.

We present a new optimal scheme of the separating isotopes, which is based on the selective laser excitation of the isotopes atoms into excited Rydberg states and further DC electric field ionization. Some radiative parameters data are obtained for alkali elements. It should be noted that the excitation and ionization cross-sections of ground and low excited state for these atoms by laser pulse are as follows: the excitation cross-section $\sigma_{exc} = \sigma_1 \sim 10^{-13}$-$10^{-11}$ cm^2, ionization cross-section from excited state: $\sigma_{ion} = \sigma_2 \sim 10^{-18}$-$10^{-17}$cm^2, from ground state $\sigma_2 \sim 10^{-19}$cm^2 [1]. For selective photoionization scheme with excitation to Rydberg *ns, np* states with n = 10-50 and further ionization by the DC electric field (see below) the calculated cross-section values are as follows: $\sigma_2 \sim \times 10^{-15 \div 12}$ cm^2. It means that the selective photoionization scheme with using the Rydberg states (autoionization resonances) and ionization by external electric field is quite effective for studied isotopes of alkali atoms from the energetic point of view. But it is arisen a problem with the ionization output (here it may be less than 100%, so it is necessary to search the optimal levels). The corresponding theory of determination of the excitation and ionization cross-sections and radiative probabilities in a laser field is in details given in ref. [5, 11,17-20].

The important aspect of theoretical studying laser photoionization isotope separation process is linked with calculating probabilities of the autoionization resonance decay in the external DC electric field [11,17]. In a case of atomic ionization by the pulsed field, a probability of this process is determined by the following expression:

$$W(nlm) = \sum_{n2} (a^{nlm}_{n1n2})^2 W(n_1 n_2 m) \qquad (1)$$

Here $W(n_1 n_2 m)$ is the state decay probability; a are the coefficients of expansion of the $\psi(nlm)$ functions on the parabolic functions $\psi(n_1 n_2 m)$. In real multi-electron atom it is necessary to account for the influence of the electron shells, which results in the changing the potential barrier and wave functions. Usually in order to take into account an influence of the electron shells one should use the corresponding model potentials. The detailed description of the «best» model potentials and corresponding schemes can be found, for example, in Refs.[8,10,22].

To define the wave functions and electron state energies in an electric field, one needs to carry out the diagonalization of energy matrice, calculated between states with the same n [11]. The diagonalization of the complex energy matrix leads to complex energy correction:

$$\mathrm{Re}E - i\Gamma/2 , \qquad (2)$$

where Re E is the level shift and Γ is the level width, including the radiation and autoionization widths simultaneously. If the effects of the autoionization resonance decay are included in the matrix M, then Γ presents only the autoionization width of the state. Only Re M is diagonalized. The imaginary part is converted by means of the matrix of eigen-vectors $\{C_{mk}\}$. The eigen vectors are obtained by diagonalization of ReM:

$$\mathrm{Im}\, M_{ik} = \sum_{ij} C^*_{mi} M_{ij} C_{jk} . \qquad (3)$$

The other details of calculation procedure are given in refs. [5, 11,17- 21].

As example, we present some characteristic results of numerical calculating the ionization characteristics for the alkali elements isotope (the rubidium). In table 1 the characteristics of the quickly decayed states of the Rb atom (electric field strength: $E = 3 \times 10^4$ V/cm) are given for states with fundamental quantum number n=7-12 (our data). In fig.1 we present the calculation results on critical electric field strength E in depen-

dence on effective quantum number n^* for atoms of Rb, Na (dots- experimental data; line 1 is theoretical estimate on the basis of classical model $E\sim 1/16n^4$ without an account of the Stark shift and electron tunneling effect [1]; line 2 is calculation result on basis of the H-like non-relativistic model [2]; dashed line is corresponding to our relativistic data). It is stressed that the hydrogen-like approximation gives an inaccuracy ~15-20% [17]. However, consistent relativistic calculation has given the results in an excellent agreement with experiment.

Table 1. Characteristics of the quickly decayed states of the Rb atom
(E =3×10^4 V/cm; n=7-12)

n	7	8	9	10	11	12
E, cm (-1)	31405	31904	32229	32456	32614	32761
n_2^*	4,7	5,8	7,0	8,0	8,9	9,0
a_f^2	0,28	0,27	0,13	0,13	0,011	0,12
a_s^2	<10(-6)	<10(-6)	<10(-5)	<10(-5)	5 10(-5)	0,022
a_p^2	<10(-6)	8.8 10(-6)	2,5 10(-5)	0,00016	0,0024	0,15
a_d^2	0,00027	0,0006	0,0033	0,015	0,045	0,008

The next step is modelling the optimal parameters of the laser photoionization separating scheme. As usually [16-18], the optimization procedure of the laser photoionization sensor scheme is in a searching the optimal form of the laser pulse to provide a maximum of excited particles in the gases separation scheme (naturally this is one of the possible versions). The separation process is described by the density matrice equations system (c.f. [12,13]). We considered a scheme for laser separation and sensing Na, Rb isotopes. At the first step of the laser photoionization scheme δ-pulse provides a maximally possible level of excitation for the up state. At the last step an external DC electric field ionization must be realized earlier than the parasitic spontaneous relaxation processes (resonant re-charging etc.[1]) begin to destroy and change achieved excitation level of atoms. Using DC electric field ionization scheme sharply increases the output of charged particles, improve in whole energetics of the laser photoionization scheme and its optimality. It is possible to accept the special measures to provide very high ionization output (up to 95%) that requires using specially separated autoionization levels. The analysis shows that creation of laser photoionization scheme on the basis of considered scheme is more perspective in comparison to traditional two- and three-step laser photoionization schemes with an atomic ionization by laser pulse at the final step [1,2].

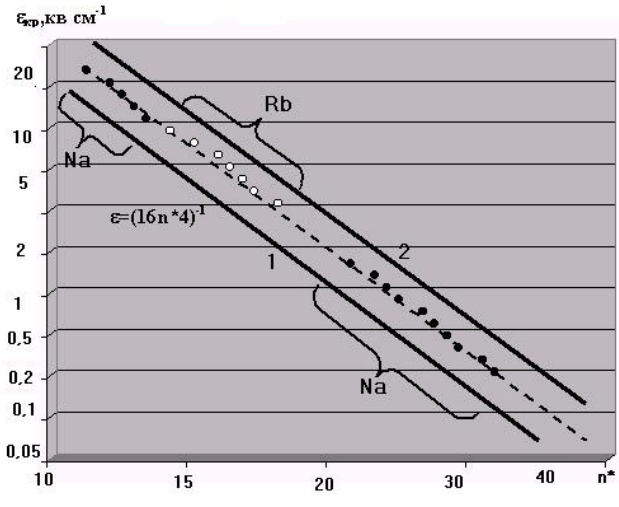

Fig.1. Critical electric field strength in dependence upon effective quantum number n^* for atoms of Na, Rb: dots – experiment (see [1]); solid line 1 – theoretical estimate on the basis of classical model; solid line 2 – calculation within the H-like approximation; dotted line –our data (eq.(1))

So, we considered the alkali elements isotopes separation scheme, which is based on the selective laser excitation of the isotopes atoms into excited Rydberg states and further DC electric field ionization, and evaluated some important radiative parameters. The final presentation of the optimal parameters for the whole scheme requires more detailed search of the optimal laser and DC electric pulses characteristics and solving the task of the optimal governing [16-18].

References:

1. Basov N. G., Letokhov V. S., Optical frequency standards//Sov.Phys. — Uspekhi. — 1999. — Vol. 11. — P. 855-880.
2. Letokhov V. S., Laser isotope separation// Nature. — 1999. — № 277. — P. 605-610.
3. Bokhan P. A., Buchanov V. V., Fateev N. V., Kalugin M. M., Kazaryan M. A., Prokhorov A. M., Zakrevskў D., Laser Isotope Separation in Atomic Vapor- WILEY-VCH Verlag, 2006.
4. Bagratashvili V. N., Letokhov V. S., Makarov A. A., Ryabov E. A. Multiple Photon infrared Laser Photophysics and Photochemistry.-N-Y, Harwood Acad. Publ.1999.
5. Glushkov A. V., Ivanov L. N. DC Strong-Field Stark-Effect: consistent quantum-mechanical approach// J.Phys.B: At. Mol. Opt. Phys. — 1999. — Vol. 26. — P.L379-L386.
6. Ryabov E. A. Laser separation of isotopes on the basis of IR multi-photon dissociation of molecules//Usp.Phys. Nauk. — 2004. — Vol.174. — P. 684-688.
7. Baldwin G. G., Salem J. C., Goldanskii V. I., Approaches to the development of gamma ray lasers // Rev.Mod. Phys. — 1981.-Vol.53.-P.687-742
8. Ivanov L. N., Letokhov V. S. Spectroscopy of autoionization resonances in heavy elements atoms// Com.Mod. Phys.D.:At.Mol.Phys. — 1999. — Vol. 4. — P. 169-184.
9. Goldanskii V. I., Letokhov V. S. Effect of laser radiation on nuclear decay processes// Sov. Phys. JETP. — 1999 — Vol. 67.-P. 513-516.
10. Glushkov A. V., Atom in an electromagnetic field.-Kiev: KNT, 2005.
11. Glushkov A. V., Khetselius O. Yu., Svinarenko A. A., Pre-pelitsa G.P., Energy Approach to Atoms in a Laser Field and Quantum Dynamics with Laser Pulses of Different Shape//In: Coherence and Ultrashort Pulsed Emission, Ed. Duarte F. J. (InTech). — 2011. — P. 159-186.
12. Karlov N.,Orlov A., Petrov Y., Prokhorov A. M. Laser governing by diffusion stream of gases to vacuum through obstacle with developed surface // Izv. AS USSR.Phys-1999Vol.49-P.500-505.
13. Solatz R. W., May C. A., Carlson L. R. et al, Detection of Rydberg states in atomic uranium using time-resolved stepwise laser photoionization//Phys.Rev.A. — 1999. — Vol. 14, № 3.—P. 1129-1148.
14. Stoll W. Present Status of industrial Isotope separation by laser technology// Atomic and Molecular Pulsed Lasers.-Tomsk: SO RAN, 2001. — P. 71.
15. Buchanov V. V., Kazaryan M., Kalugin M., Prokhorov A. M. Laser separation of Silicon Isotopes by the AVLIS Technology// Atomic and Molecular Pulsed Lasers. — Tomsk: SO RAN, 2001. — P. 72.
16. Glushkov A. V., Ambrosov S. V., Shpinareva I. M. Non-linear Selective Photoprocesses in Atoms and Molecules and their Optimal Governing. Optimized Isotope Separation Schemes// Atomic and Molecular Pulsed Lasers. — Tomsk: SO RAN, 2001. — P. 70.
17. Glushkov A. V., Khetselius O. Yu., Svinarenko A. A., Prepelitsa G. P., Energy Approach to Atoms in a Laser Field and Quantum Dynamics with Laser Pulses of Different Shape//In: Coherence and Ultrashort Pulsed Emission, Ed. Duarte F. J. (Intech, Vienna). — 2011. — P. 159-186..
18. Glushkov A., Lepikh Ya., Svinarenko A., Prepelitsa G., Ambrosov S., Bakunina E., Loboda A., Physics of laser-photoionization atomic processes in isotopes and gases separator devices: New optimal schemes//Sensors Electr. and Microsyst.Techn. — 2011. — Vol. 2 (8), № 1. — P. 27-35.
19. Glushkov A. V., Prepelitsa G. P., Ambrosov S. V., Loboda A. V., Gurnitskaya E. P., Consistent QED approach to cal-

culation of electron-collision excitation cross-sections and strengths: Ne-like ions // Int. Journ.Quant.Chem. — 2005. — Vol. 104, № 4. — P. 562-569.
20. Glushkov A. V., Ambrosov S. V., Fedchuk P. O., Fedchuk O. P., Stark effect and resonances in the ionization continuum for hydrogen atom and Wannier-Mott excitons in DC electric field// Journ. Phys.Stud. — 2003. — V. 7, № 3. — P. 121-125.
21. Glushkov A. V., Lepikh Ya. I., Ambrosov S. V., Khetselius O. Yu., New optimal schemes of laser photoionization technologies for cleaning the semiconductor materials and preparing the films of pure composition at atomic level//Ukrainian Journ. Physics.-2008. — Vol. 53, № 10. — P. 1017-1022.
22. Glushkov A. V., Fedchuk P. A., Fedchuk A. P., Loboda A. V., New general approach in electron theory of catalytic processes on semiconductors and binary metallic materials// Photoelectronics.-2004. — № 13. — P. 19-22.

UDC 535.42, 539.184

S. V. Ambrosov, A. P. Fedchuk, A. V. Glushkov, Ya. I. Lepikh

LASER-PHOTOIONIZATION METHOD OF SEPARATION OF THE ISOTOPES: RADIATIVE PARAMETERS FOR ALKALI ELEMENTS

Abstract.

We present an optimal scheme of the separating alkali elements isotopes, which is based on the selective laser excitation of the isotopes atoms into excited Rydberg states and further DC electric field ionization. Some radiative parameters data are obtained for alkali elements.

Key words: laser photoionization method, isotopes separation, radiative parameters

УДК 535.42, 539.184

С. В. Амбросов, А. П. Федчук, А. В. Глушков, Я. И. Лепих

ЛАЗЕРНО-ФОТОИОНИЗАЦИЙ МЕТОД РАЗДЕЛЕНИЯ ИЗОТОПОВ: РАДИАЦИОННЫЕ ПАРАМЕТРЫ ДЛЯ ЩЕЛОЧНЫХ ЭЛЕМЕНТОВ

Резюме.

Представлена оптимальная схема лазерного разделения изотопов щелочных элементов, базирующаяся на лазерном возбуждении атомов изотопов в ридберговские состояния и дальнейшей ионизации внешним постоянным электрическим полем. Определены некоторые радиационные параметры для щелочных элементов.

Ключевые слова: лазерный фотоионизационный метод, разделение изотопов, радиационные параметры

УДК 535.42, 539.184

С. В. Амбросов, О. П. Федчук, О. В. Глушков, Я. І. Лепих

ЛАЗЕРНО-ФОТОІОНІЗАЦІЙНИЙ МЕТОД ПОДІЛЕННЯ ІЗОТОПІВ: РАДІАЦІЙНІ ПАРАМЕТРИ ДЛЯ ЛУЖНИХ ЕЛЕМЕНТІВ

Резюме.

Представлена оптимальна схема лазерного поділення ізотопів лужних елементів, яка базується на лазерному збудженні атомів ізотопів у рідбергівські стани та подальшій іонізації зовнішнім сталим електричним полем. Визначені декотрі радіаційні параметри для лужних елементів.

Ключові слова: лазерний фотоіонізаційний метод, поділення ізотопів, радіаційні параметри

UDC 621. 315. 592

A. V. Kiss, V. A. Smyntyna, S.V. Zubritskiy

Odessa National University named after I. I. Mechnikov, Odessa,. Pasteur, 42, 65000
Kiss, A., tel. 0934280155,
e-mail: akiss@inbox.ru, Smyntyna V.A, tel. 0674806610, e-mail: smyntyna@onu.edu.ua

INFLUENCE OF NANOCRYSTALLITE SIZES ON THE ABSORPTION SPECTRUM OF CDS NANOCRYSTALS

Recently, special attention is paid to the magnetic and semiconducting nanomaterials, and the interest in them is increasing. This is due to the enormous practical importance of these classes of materials for the development of information, medical, chemical, and electronic technology. Nanomaterials based on semiconductors (eg, $A_{II}B_{VI}$ and $A_{IV}B_{VI}$) have unique optical properties and are promising materials for the active elements of nonlinear optics and nanoelectronics devices.

In this paper, the synthesis of nanocrystals was performed by two different methods: the first is with the introduction dopped aqueous solution of sodium sulfide in an aqueous solution of cadmium nitrate, the second is by blowing hydrogen sulfide in a container with an aqueous solution of cadmium nitrate. The technology of obtaining nanocrystalline structures with colloidal solutions by both methods were worked, we've found conditions and reagent concentrations necessary to produce nanocrystals of a given size. The characteristic size of the nanocrystals on the optical absorption spectra. With the help of the data was calculated energy level spectrum, characteristic of these objects. The good agreement between the values obtained with the theoretical data podtverdaet possibility of approximation of the form of a spherical semiconductor nanocrystal quantum dots.

We investigated the cadmium sulfide nanocrystals obtained by two independent methods: the first method nanocrystals formed by a chemical reaction of colloidal solutions of cadmium nitrate (Cd $(NO_3)_2$) and sodium sulfide (Na_2S) in aqueous solution photo jelly (14 g gelatin in 100 ml of water, 14%). Gelatin has the properties of isolated nanoparticles in the volume and acts as a dielectric matrix. Chemical reactions was performed on formula:

$$Cd\left(NO_3\right)_2 + Na_2S \rightarrow CdS + 2NaNO_3 \qquad (1)$$

In the course of chemical reactions in aqueous solution Cd $(NO_3)_2$) (0.007 g, 0.06 g and 0.05 g per 50 ml of distilled water) mixed with an aqueous solution of gelatin in 1:1, with continuous stirring, drip (droplet diameter 3 mm), with a period of dropping τ = 3-4 sec. (for uniform response components), an aqueous solution of Na_2S (300 drops). Throughout the time of preparation of the samples, the temperature of the solution was kept constant of 60 ± 5 °C (was fixed by thermometer).

The second method as an alternative method for making nanocrystals used technology in which cadmium sulfide nanocrystals prepared by blowing hydrogen sulfide in a container with a solution of cadmium nitrate. The chemical reaction of the synthesis:

$$Cd(NO_3)_2 + H_2S \rightarrow CdS\downarrow + 2HNO_3 \qquad (2)$$

Cadmium is a source of hydrated Cd $(NO_3)_2 \cdot 4H_2O$ c concentration of 0.007 grams per 50 ml of water. As a stabilizer used 9% of photographic gelatin.

Hydrogen sulfide is obtained by decomposition of concentrated aqueous sodium sulphide by the 30% solution of the orthophosphoric acid. We slowly dripped acid (100, 200 and 300 drops) to a solution of sodium sulfide.

Was synthesized two series of samples, one for each method, each with three samples with different concentrations of reagents: the first one was 0.007, 0.06 and 0.05 g of Na_2S per 50 ml of water in 14% aqueous solution of gelatin in the first method, the second one was with 0.007 g Cd (NO3) 2 in 50 ml of water with a 9% aqueous content photo gelatin for the second method.

Usually, we obtain reducing the size of the nanocrystals shifts the fundamental absorption edge to shorter wavelengths [1, 2]. The shape of the absorption band depends on the conditions of synthesis of nanocrystals and the number of initial reagents. The absorption spectra obtained by the first method, are shown in Fig. 1:
The absorption spectra for the second alternative method of obtaining CdS nanocrystals are shown in Fig. 2:

The absorption spectra of the second series in Fig. 2, obtained by the second method has more complex structure than the absorption spectrum on Fig. 1. This indicates the presence of different types of optical transitions.

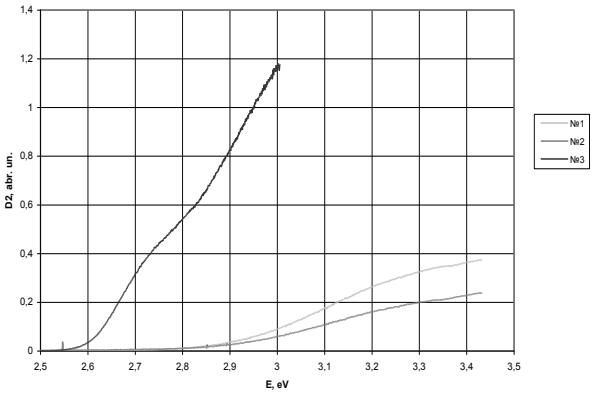

Fig. 1. Spectra of absorption of nanocrystals CdS (№ 1 - 0.06 g of $Cd(NO_3)_2$ in 50 ml of water, 300 drops of Na_2S with concentration 0.1 g of Na_2S per 50 ml water, 14% aqueous solution of gelatin; № 2 - 0.06 g of $Cd(NO_3)_2$ in 50 ml of water, 300 drops of Na_2S with concentration of 0.05 g of Na_2S per 50 ml water, 14% aqueous solution of gelatin; № 3 -0.007 g $Cd(NO_3)_2$, 300 drops of Na_2S with concentration of 0,05 g of Na_2S per 50 ml water, 14% aqueous solution of gelatin)

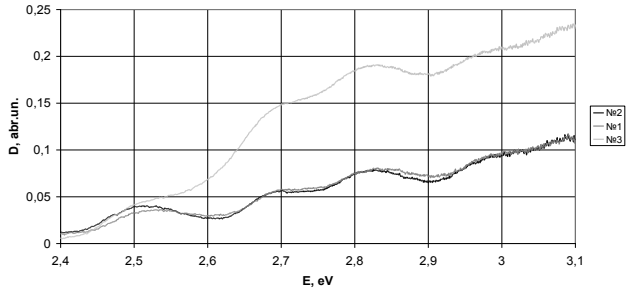

Fig. 2. The absorption spectra of the samples with 9% concentration of gelatin (№ 1 - 0.007 g Cd (NO3) 2, 50 ml of water, 100 drops of H 2 S, 9% gelatin, № 2 - 0.007 g Cd (NO3) 2 in 50 ml of water, 200 drops of H2S, 9% gelatin № 3 - 0.007 g Cd (NO3) 2) in 50 ml of water, 300 drops of H 2 S, 9% gelatin)

To better define the edge of the fundamental absorption bands were calculated first derivative of the absorption spectra of Fig. 2. They are shown in Fig. 3. The fundamental absorption edge is defined as the highest peak:

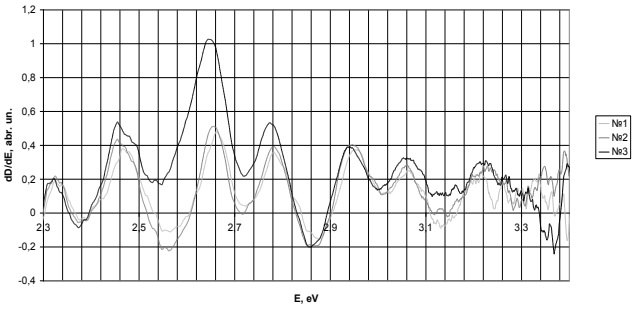

Fig. 3. The first derivatives of the absorption spectra of 9% concentration of gelatin (№ 1 - 0.007 g of Cd $(NO_3)_2$, 50 ml of water, 100 drops of H_2S, 9% of gelatin, № 2 - 0.007 g of $(NO_3)_2$ in 50 ml of water, 200 drops of H_2S, 9% of gelatin № 3 - 0.007 g of Cd $(NO_3)_2$) in 50 ml of water, 300 drops of H_2S, 9% of gelatin)

Values of the effective band gap, determined by the maximum extremum in Fig. 3 (№ 1-2.64 eV, № 2-2.66 eV, № 3-2.67 eV) were obtained by extrapolation of the absorption edge to the energy axis, into the eq. (3) [1] to find the effective size of the nanocrystals:

$$R = \sqrt{\frac{\hbar^2 \varphi_{1n}^2}{2\mu(E_{eff} - E_g)}} \qquad (3)$$

where R- the radius of the nanocrystal, m

To determine allowed optical transitions of different types are necessary to build second derivative of the absorption spectra of Fig. 2, which are shown in Fig. 4:

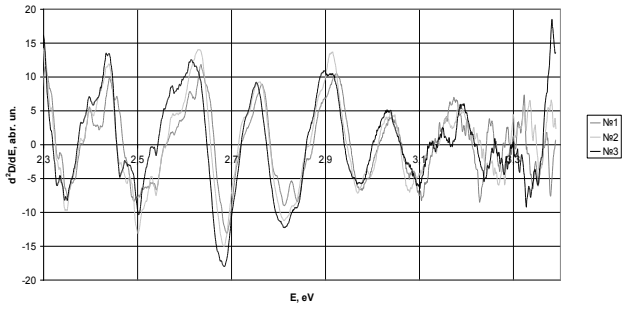

Fig. 4. The second derivatives of the series with a 9% of gelatin content gelatin (№ 1 - 0.007 g of Cd $(NO_3)_2$, 50 ml of water, 100 drops of H_2S, 9% of gelatin, № 2 - 0.007 g of $(NO_3)_2$ in 50 ml of water, 200 drops of H_2S, 9% of gelatin № 3 - 0.007 g of Cd $(NO_3)_2$) in 50 ml of water, 300 drops of H_2S, 9% of gelatin)

Table 1

Number of transition →	1s	1p	1d	1f	1g	2s
$E_{trans,theor}$, eV	2.68	2.82	3.06	3.25	3.68	3.16
$E_{trans,e\div p}$, eV	2.68	2.8	2.97	3.24	--	3.16
Number of nuclons	2	6	10	14	18	2

Thus, in this paper, the necessary conditions for the formation and concentration of reagents to prepare nanocrystals of a specific size were obtained. Displacement measurement edge of the main absorption band in the short wavelength region with decreasing the size of the nanocrystals [5] allowed us to calculate the effective size of the objects. A comparison of the radii, calculated theoretically and experimentally obtained from the optical absorption spectra confirms the theoretical assumption about the shape of the spherical nanocrystals as quantum dots [6, 7].

Conclusion. Based on these data the energy-level diagram (Fig. 5), which can be interpreted as single-particle states of infinite square well for several values of l <6 and n. This shows that with the increase of the well depth levels are dropping. Also the decreasing of the energy level occurs with increasing width of the well, i. e., the parameter *R*. Table 1. shows that the course of the levels in a square well reproduces the first two magic numbers 2 and 8. Number 2 corresponds filled 1s-state, the number of 8 corresponds filled 1s-and 1p-states. We can assume that also played a third magic number of 20, because the levels of 1d and 2s Rural location close to each other. In this case, the number 20 corresponds to the filling of 1s-, 1p-, 1d-and 2s-states. The numbers 28, 50, 82 and 126 can not be obtained by filling a rectangular well nucleons levels without spin-orbit interaction.

REFERENCES

[1] Al. L. Efros, AL Efros, Interband absorption of light in a semiconductor sphere, — FTP — 1999. — T. 16, B. 7, P. 1209-1214.

[2] A. A. Sirenko, V. I. Belitsky, T. Ruf, M. Cardona, A. I. Ekimov, S. Trallero, Phys. Rev. — 1999 — B. 58, 4. 2077

[3] A. I. Ekimov A. A. Onuschenko, quantum size effects in the optical spectra of semiconductor microcrystals — 2002. — T. 16. 7. P. 1215-1219.

[4] A. I. Ekimov A. A Onuschenko, size quantization of the energy spectrum of electrons in microscopic — 1999 — JETP Letters, v.40, in. 8., P. 337-339.

[5] Chang Q. Sun, Size dependence of nanostructures: Impact of bond order deficiency — 2007 — Prog. Solid State Chem., Vol. 35, P. 1-159.

[6] NE Kaputkina, YE Lozovik, «ball» of quantum dots. — 1998 — Solid State, Vol 40. In. 11., P. 2134-2135.

[7] A. V. Kiss, V. A. Smyntyna, S. V. Zubritskiy, Influence of Size Effects on Absorbtion and Raman Spectra of CdS nanocrystals, — 2011 — 16th international conference on transdusers, devices and Microsystems «Transdusers — 2011.»

UDC 621. 315. 592

A. V. Kiss, V. A. Smyntyna, S.V. Zubritskiy.

INFLUENCE OF NANOCRYSTALLITE SIZES ON THE ABSORPTION SPECTRUM OF CDS NANOCRYSTALS

Abstract

Recently, special attention is paid to the magnetic and semiconducting nanomaterials, and the interest in them is increasing. This is due to the enormous practical importance of these classes of materials for the development of information, medical, chemical, and electronic technology. Nanomaterials based on semiconductors (eg, $A_{II}B_{VI}$ and $A_{IV}B_{VI}$) have unique optical properties and are promising materials for the active elements of nonlinear optics and nanoelectronics devices.

In this paper, the synthesis of nanocrystals was performed by two different methods: the first is with the introduction dopped aqueous solution of sodium sulfide in an aqueous solution of cadmium nitrate, the second is by blowing hydrogen sulfide in a container with an aqueous solution of cadmium nitrate. The technology of obtaining nanocrystalline structures with colloidal solutions by both methods were worked, we've found conditions and reagent concentrations necessary to produce nanocrystals of a given size. The characteristic size of the nanocrystals on the optical absorption spectra. With the help of the data was calculated energy level spectrum, characteristic of these objects. The good agreement between the values obtained with the theoretical data podtverdaet possibility of approximation of the form of a spherical semiconductor nanocrystal quantum dots.

Keywords: nanocrystals, absorption, energy bands.

УДК 621. 315. 592

Кисс А. В., Смынтына В. А., Зубрицкий С. В.

ВЛИЯНИЕ РАЗМЕРОВ КРИСТАЛЛИТОВ НА СПЕКТРЫ ПОГЛОЩЕНИЯ НАНОКРИСТАЛЛОВ CDS

Резюме

В последнее время особое внимание уделяется магнитным и полупроводниковым наноматериалам, причем интерес к ним постоянно возрастает. Это связано с огромной практической значимостью этих классов материалов для развития информационных, медицинских, химических, электронных технологий. Наноматериалы на основе полупроводников (например, $A_{II}B_{VI}$ и $A_{IV}B_{VI}$) обладают уникальными оптическими свойствами и являются перспективными материалами для активных элементов нелинейной оптики и устройств наноэлектроники.

В данной работе синтез нанокристаллов проведен двумя различными методами: первый — с помощью покапельного введения водного раствора сульфида натрия в водный раствор нитрата кадмия, второй — путем продувки сероводорода в емкости с водным раствором нитрата кадмия. Отработана технология получения нанокристаллических образований с коллоидных растворов по двум методам, найдены условия и необходимые концентрации реагентов для получения нанокристаллов заданного размера. Определены характерные размеры нанокристаллов по спектрам оптического поглощения. С помощью полученных данных был рассчитан энергетический спектр уровней, характерных для данных объектов. Хорошее совпадение полученных значений с теоретическими данными подтвердает возможность использования приближения о форме нанокристаллов как сферических полупроводниковых квантовых точках.

Ключевые слова: нанокристаллы, поглощение, энергетические зоны.

УДК 621. 315. 592

Кисс А. В., Сминтина В. А., Зубрицький С. В.

ВПЛИВ РОЗМІРІВ КРИСТАЛІТІВ НА СПЕКТРИ ПОГЛИНАННЯ НАНОКРИСТАЛІВ CDS

Резюме

Останнім часом особлива увага приділяється магнітним і напівпровідниковим наноматеріалам, причому інтерес до них постійно зростає. Це пов'язано з величезною практичною значущістю цих класів матеріалів для розвитку інформаційних, медичних, хімічних, електронних технологій. Наноматеріали на основі напівпровідників (наприклад, $A_{II}B_{VI}$ та $A_{IV}B_{VI}$) володіють унікальними оптичними властивостями і є перспективними матеріалами для активних елементів нелінійної оптики і пристроїв наноелектроніки.

У даній роботі синтез нанокристалів проведений двома різними методами: перший - за допомогою покапельного введення водного розчину сульфіду натрію в водний розчин нітрату кадмію, другий - шляхом продувки сірководню в ємность з водним розчином нітрату кадмію. Відпрацьована технологія отримання нанокристалічних утворень з колоїдних розчинів за двома методами, знайдені умови і необхідні концентрації реагентів для отримання нанокристалів заданого розміру. Визначено характерні розміри нанокристалів за спектрами оптичного поглинання. За допомогою отриманих даних був розрахований енергетичний спектр рівнів, характерних для даних об'єктів. Гарний збіг отриманих значень з теоретичними даними подтвердает можливість використання наближення про форму нанокристалів як сферичних напівпровідникових квантових точках.

Ключові слова: нанокристали, поглинання, енергетичні зони.

UDK 678.01+539.3

V. V Kovalchuk

Odessa State Environmental University, 15, Lvovskaya str., Odessa, Ukraine
e-mail: lslvv@rambler.ru

NANOELECTRONIC'S MATERIAL FOR OPTIC SYSTEM

The theoretical approach of quantum-dimensional system we have discussed. Our results are important for visualization and generation nanodimensional parts of the optical system.

An semiconductor surface is specific surface disordered phase (SDP) and the main peculiarities of modern nanoelectronic devices depend on the individual parameters of the surface phase. Furthermore, the reactions of atomic hydrogen (H), fluorine (F), chlorine (Cl) and bromine (Br) with Si surface were widely studied experimentally and many investigators have observed the semiconductor SDP directly [**1-3**]. For a quantitative analyses of nanostructures like nanoclusters (NC) creation in Si and other solid materials the clusters distribution along the surface is necessary.

On the other hand, the recent progress in the combination of visualization with simulation techniques have concurred to obtain spectacular results in the investigation of chemical reaction mechanisms as well [**4**]. The traditional quantum chemical ab initio methods, based on the Hartree-Fock scheme have become well established in studies of the electronic and geometrical structure of the solid NC [**1**]. Therefore, the surface NC as real objects and model in the nanoelectronic's material for intelectual system is great interest.

Our Model Molecular Graphics Package (MMGP) which is specially designed so as to allow for high-level computerized visualization in molecular science. MMGP contains many interfaces with quantum chemical programs such as the semiempirical and molecular surface geometry generation, which is based on the interatomic potential (for example, Modified Stillinger-Weber (MSW)).

In the paper development and applications of the MMGP to the Si-NC was demonstrated. The MMGP generates detailed and easily interpretable and aesthetically appealing graphics representing models of molecular structures and related properties. The package offers a high level of interactivity through the use of the mouse and via a large set of menus and submenu, organized in such a way so as to enable users to learn rapidly the basic operations leading to efficient visualization (see **Fig 1,2.**).

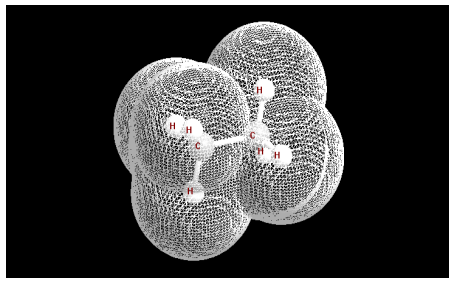

Fig 1.
Map of the density electron distribution for the nanocluster

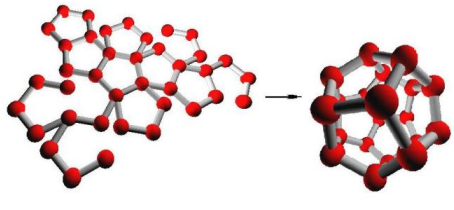

Fig.2.
3D-representation of the
nanoparticle's formation from nanocluster

For all the menu items, a help facility has been implemented. Various representation options and attributes may be selected for adapting the visual output to personal needs and preferences:

the molecular structures may be represented as discrete dots, and the global appearance may be modified via attributeS such as back ground appearance, perspective or orthogonal projection and others. The purpose of the MMGP is the interactive visual representation of three-dimensional (3D) models of molecular structures and properties for research. Due to the flexibility of the data- and program-structure, various chemical systems ranging from small compounds (clusters) to large macromolecules may be investigated; additional interfaces and tools can easily be implemented. The MMGP contains the tools which are neccessary for the investigation and visualization of the results generated by the calculation program-package contains:

- Modified IEHT-α method.

This is for semiempirical calculations of one-electron level energies, wave functions and other parameters of electronic structure of NC. The estimation of the total energy of clusters which has different size is follows:

$$E_{tot} = \sum_{A \neq B} \frac{Q_A(\vec{r}_{AB}) - Q_A^*(\vec{r}_{AB})}{r_{AB}} + \\ + \sum_i g_i E_i - (E_{ee} + E_{exc}) \quad (1)$$

$$E_{exc} = \sum_{A \neq B,}^{all} \sum_{\mu \neq \nu}^{occ} \frac{1}{r_{AB}} \nu_{AB} S_{\mu\nu}^2 \quad (2)$$

υ_{AB} is the fitting parameter.

→POTENTIAL package.

This is simulation programme for calculations based on different types of interaction potentials. One of them is modified Stillinger-Weber-type potential [2]. Hamiltonian is follows:

$$H(\vec{r}_1, \vec{r}_2 \ldots \vec{r}_N, \vec{p}_1, \vec{p}_2 \ldots \vec{p}_N) = \sum_{i=1}^{N} \frac{p_i^2}{2m} + \\ + \sum_{i<j}^{N} V_{\text{int}}^{(2)}(\vec{r}_{ij}) + \sum_{i<j<k}^{N} V_{\text{int}}^{(3)}(\vec{r}_{ij}, \vec{r}_{ik}, \vec{r}_{jk}) \quad (3)$$

$\vec{r}_1, \vec{r}_2 \ldots \vec{r}_N$ are coordinates of the atoms. $V_{(2)int}$ is the twin potential (4); $V_{(3)int}$ tree-part *SW*-potential :

$$V_{\text{int}}^{(2)}(\vec{r}_{ij}) = \left\{ A\left(B\frac{1}{r_{ij}^p} - 1\right) \exp\left(\frac{\Lambda}{r_{ij} - a}\right) \right\}, \vec{r}_{ij} < 2{,}5\sigma_{AB} \\ 0, others \quad (4)$$

$$V_{\text{int}}^{(3)}(\vec{r}_{ij}, \vec{r}_{ik}, \vec{r}_{jk}) = \Pi_{ijk} + \Pi_{kij} + \Pi_{jki}$$

$$\Pi_{ijk} = \Lambda\left(\cos\theta_{jik} + \frac{1}{3}\right)^2 \exp\left(\frac{\delta_{ijk}}{r_{ij} - a} + \frac{\delta_{ijk}}{r_{ik} - a}\right) \quad (5)$$

Θ_{ijk} is angle, $\vec{r}_{ij}$ and $\vec{r}_{jk}$, $\vec{r}_{ij} = \left|\vec{r}_i - \vec{r}_j\right|$ is the vector between i and j atoms in units of the equilibrium distance between nearest atoms in the structure ($\vec{r}_0$). For *Si* $\vec{r}_0$ *= 2,351A (*modified SW*),* and $\vec{r}_0$*=2,0951A* (original SW). The energy unit equal *E = 2,1675* eV *i.e* $E_{Si\text{-}Si}$ in the crystal *Si* . The parameters of the modified SW-potential are present in the [3].

→Graphic Package is a geometrical program based on *3D*-representation of the investigation of NC.

We will report the results of test calculation for adsorption processes**,** optics properties of the closely packed and ball-like Si NC. Real surface objects may be built by introducing stereochemistry, i.e., the 3D atomic positions, and it is important to visualize them as molecular models with the usual rendering techniques leading to 3D perception. MMGP visualization allows investigators to emphasize at length the different aspects of molecular structure of surface: chemical topology, conformational details, etc.

We applied the MMGP to the Si-SDP. With the appearance of semiempirical methods the calculation of the equilibrium geometry and visualization of quite large model became possible (*N=125* Atoms). The calculation bond lengths of some surface are given in ref. [5-7].

As one can see from these data the calculated interatomic are in a quite good agreement with the experimental ones. Especially, the changes of the Si - Si bond, going from a small Si -NC (2-10 atoms) to big are accurately described. We find the energies of NC, binding energy per atom and interection energy of the systems «NC-SDP» are

obtained for more stable geometry. Furthermore, the energetic positions and equilibrium distances as well as of silicon are described rather well.

Other example of the adsorption process and chemical reactions on semiconductor surfaces is the interaction with halogen-atoms [6]. When using the model to represent the SDP, a choice has to be made about the NC size, that is, the number of atoms which are treated explicity in the calculation, and the level of precision of the required computation. Fortunately, the chemisorption of atoms on SDP seems to be of local character. This fact is greately supported by ab initio model calculations, and particularly by the calculations for the chemisorption of F and Cl on Si-SDP.

In our calculation the single NC contains 10-100 Si atoms, representing the first four layers of the Si-SDP. We regard this model as hypothetical molecules (quasimolecules) and do try to compare the computed results (for example, magic numbers) directly to experimental data of the corresponding impurities in the solids or chemisorbed systems [1]. The mass spectra of charged NC, where magic numbers are observed [3].

Take into account the internal structure of the ball-like Si NC we investigate theoretically the adsorbtion and scattering of light by ones. The theory for the interaction of electromagnetic fields with local charge-carrier near boundary of the small spherical semiconductor microcrystals was presented in [8]. In the [5,8] the dipole moments of NC (using MMGP) and transition dipole moments for local bulk states and local exterior surface states were calculated. It was shown that the dipole moments of the transitions for local states of the Si NC are large compared to the typical values of transition dipole moments for Si - NC.

Conclusion. We have shown that the calculated energy and geometrical characteristics by MMGP are in satisfactory agreement with the experiment and others ab initio calculations [1-8]. The present calculations show that the MMGP can be used to obtain a detailed and reasonably accurate description of various aspects of the small halogen-Si-NC. In view of interest of a physicist for the visualization of such NC, one may foresee that the data banks that represent the major types of stable systems will soon be available. Therefore, it is important for a physicist to have at hand the computer tools allowing visualization and generation of computational information. The combination MMGP with molecular dynamics in connection with technique of simulated annealing, makes it a very useful tool for the determination of geometries of large NC. Reconstruction processes at Si SDP or amorphous solids can be studied also in this way

References

1. Keghelian P., Melinon P., Perez A. Properties of silicon and silicon-carbon cluster assembled films // Nano structured materials.— 2009. — v. 12. — p.277-280
2. Dresselhaus M. S., Dresselhaus G., Eklund P. Science of fullerenes and carbon nanotubes: san diego:Academic press, 2006.— P.. 24-229
3. Marsen B., Lonfat M., Scheier P., Sattler K. The energy gap of pristine silicon clusters // J.Electr.Spectr.Rel.Phenom.— 2008. — v. 109. — p.157-168
4. Calculation of Molecules, Clusters and Solids with DFT-LDA Scheme / Blaudeck P., Freuenheim Th., Seifert G. and others. // J. Phys.: Condensed Matter. — 2012. — vol. 4. — P. 6368-6371.
5. Kovalchuk V. V., Dolinska L. V. Principles of research of the devices providing of nanomeasuring // Metrology and devices. — 2010. — № 4(24). — C.49-59
6. Kovalchuk V. V. Cluster morphology of silicon nanoparticles // Semiconductor physics, quantum electronics & Optoelectronics. — 2007. — v. 10, № 4. P. 81-86
7. Kovalchuk V. V. Cluster modification semiconductor's heterostructures. — Kiyv: Hi-Tech, 2007. — 309 p.
8. Kovalchuk V. V. The optical properties, stability and reactivity of solid nanocluster subsystem // Photoelectronics. — 2011.—№ 20. — P. 53-58.

UDC 678.01+539.3

Kovalchuk V. V

NANOELECTRONIC'S MATERIAL FOR OPTIC SYSTEM

Abstract

The theoretical approach of quantum-dimensional system we have discussed. Our results are important for visualization and generation nanodimensional parts of the optical system.

Key words: visualization, optic, system

УДК 678.01+539.3

Ковальчук В. В.

НАНОЕЛЕКТРОННІ МАТЕРІАЛИ ДЛЯ ОПТИЧНИХ СИСТЕМ

Резюме

Наведені теоретичні підходи вивчення квантово-розмірних систем. Результати є важливим для візуалізації та створення нанорозмірних складових оптичних систем.

Ключові слова: візуалізація, оптика, система

УДК 678.01+539.3

Ковальчук В. В.

НАНОЕЛЕКТРОННЫЕ МАТЕРИАЛЫ ДЛЯ ОПТИЧЕСКИХ СИСТЕМ

Резюме

Приведены теоретические подходы изучения квантово-размерных систем. Результаты могут быть использованы для визуализации и создания наноразмерных составляющих оптических систем.

Ключевые слова: визуализация, оптика, система

UDC 539.186

Yu. A. Kruglyak, D. A. Korchevsky, Yu. G. Chernyakova, T. A. Florko

Odessa State Environmental University, 15, Lvovskaya str., Odessa, Ukraine
Odessa Computer Academy, Odessa, Ukraine
e-mail: quantumnet@mail.ru

RELATIVISTIC MODEL DIRAC-FOCK APPROACH TO STUDYING Fe PLASMA EMISSION SPECTRA IN A LOW INDUCTIVE VACUUM SPARK

There are presented the results of theoretical calculation for transition probabilities of the Fe plasma Li-like satellite lines on the basis of the relativistic perturbation theory (PT) with the Dirac-Fock model zeroth approximation and accounting for correlation and radiative corrections. With using the calculated values for relation of intensities of the dielectronic satellites lines and resonant lines of He-like ions, it is carried out an estimate of the plasma electron temperature and density.

At present time a great attention is turned to problems of experimental and theoretical study of high temperature multi-charged ions plasma and developing the new diagnostics methods (c.f. [1-12]). Similar interest is also stimulated by importance of carrying out the approaches to determination of the characteristics for multi-charged ions plasma in thermonuclear (tokamak) reactors, searching new mediums for X-ray range lasers. The X-ray laser problem has stimulated a great number of papers devoting to development of theoretical methods for the modelling the elementary processes in a collisionally pumped plasma. The current trend is to study high Z (Z is a charge of a nucleus of ions). There is a hope to find lasing effects on the transitions in plasma of the Li-, Ne-, Ni-like ions. Very shocking example is a scheme for accomplishing tabletop x-ray lasing in Li-like ion of Ne at 98 Å in an optically ionized plasma during recombination in the transient regime. At the same time, low temperature plasma sources are more efficient and less expensive devices. They show promise for producing lasing in the vacuum ultraviolet and soft X-ray region. Preliminary investigations of capillary spark discharge were made (c.f.[5-9]), which show the possibility of their use as effective plasma sources for the generation of a soft-X-ray or extreme ultraviolet amplified spontaneous emission. A great progress in development of laser technique, tokamak and accelerator experiments resulted to a new class of problems in the plasma physics and correspondingly diagnostics of their parameters. The electron temperatures and particle confinement times in tokamak plasmas permit the ionization of the heavy impurity elements up to the helium-like (eventually hydrogen-like) charge state. High resolution spectroscopy of the line emission of these ions has become a powerful technique for determining the electron and ion temperatures T_e and T_i ,the macroscopic plasma movement and dynamics of the plasma impurity transport. Experimental measurements have beer carried out at several large tokamaks: Ti^{20+} and Fe^{24+} (Princeton Large Torus), Cr^{22+} (tokamak de Fontenau-aux-Roses=TFR) etc. The TFR measurements of the plasma parameters and wavelengths, atomic characteristics of satellite spectrum of the He-like ions from Ar^{16+} to Mn^{23} (Ar, Sc, V,Cr, Mn) are accurately carried out and presented in ref. [3].

In ref. [1-3] a new, effective relativistic version of the PT for calculations of the spectroscopic characteristics of the multicharged ions in plasma have been developed It is based on the fundamental formalism of the QED perturbation theory [10-14]. It has been used for developing

high resolution theoretical spectroscopy schemes for sensing and diagnostics the tokamak plasma parameters [1]. We carried put the estimates of the tokamak plasma parameters (electron temperature etc.) and presented the calculation results for wavelengths and other atomic characteristics of satellite spectrum of the He-like ions from Ar^{16+} to Mn^{23} [4]. However some theoretical non-consistency remained because of the non-account so-called QED corrections in theoretical scheme. For ions of the Ar^{16+} , Sc^{+21} there is got a good agreement with the tokamak de Fontenau-aux-Roses (TFR) and other measurements [5-9], but it is obvious that this scheme must be significantly improved for a case of plasma of more heavy elements. Here we present the results of theoretical calculation of the Fe plasma Li-like satellite lines on the basis of the relativistic perturbation theory with account for correlation and radiative corrections. With using the calculated values for relation of intensities of the dielectronic satellites lines and resonant lines of He-like ions, it is carried out an estimate of the plasma electron temperature which is equal 2,4keV under electron density of $10^{23}sm^3$.

Now we describe the key moments of our theoretical scheme. The details of the whole consistent QED version for studying and spectroscopic characteristics of the multicharged ions in plasma have been earlier presented in refs. [2,3] and based on the gauge invariant QED energy approach [1,10-12] and correct account of the finite nuclear size and QED effects (the Lamb shift, including self-energy part and vacuum polarization part).

The wave functions zeroth basis is found from the Dirac equation solution with potential, which includes core ab initio potential, electric, polarization potentials of nucleus (gaussian form for charge distribution in the nucleus is accepted). All correlation corrections of the PT second and high orders (electrons screening, particle-hole interaction etc.) are accounted for. The nuclear potential is provided by choice of charge distribution in the nucleus. The Coulomb potential for spherically symmetric density $\rho(r|R)$ is:

$$V_{nucl}(r|R) = -((1/r)\int_0^r dr' r'^2 \rho(r'|R) + \int_r^\infty dr' r' \rho(r'|R)$$

Let us consider the Li-like ion as example. One can write the DF-like equations for a three-electron system $1s^2nl$j. Formally they fall into one-electron Dirac equations for the orbitals *1s,nlj* with potential:

$$V(r)=2V(r|1s)+V(r|nlj)+V_{ex}+V(r|R).$$

This potential includes the electrical and polarization potentials of the nucleus. The part V_{ex} accounts for exchange inter-electron interaction. The main exchange effect will be taken into account if in the equation for the *1s* orbital we assume $V(r)=V(r|1s)+V(r|nlj)$ and in the equation for the *nlj* orbital $V(r)=2V(r|1s)$. The rest of the exchange-correlation effects are accounted for in the first two PT orders by the total inter-electron interaction. The core electron density is defined by iteration algorithm within gauge invariant QED procedure [12]. Other details of the calculation procedure, including definition of the matrix elements of the QED PT with effective account of the exchange-correlation effects can be found in refs. [1,10-12]. The details of calculational procedure are described in ref. [1-3]. Here we only note the following: in order to construct the optimal PT zeroth approximation we use ab initio quantum electrodynamics (QED) procedure [12]. The lowest order multielectron effects contribution, in particular, the gauge dependent radiative contribution for the certain class of the photon propagator calibration is minimized. Such a minimization results in the construction of the optimal one-electron basis.

In the Fe plasma in full similarity with the K, Cu plasma in a law inductive vacuum spark [2,7] one could observe the resonant lines $1snp\text{-}1s^2$ of the He- like ions with ground quantum number n from 3 to 6. The satellite lines $1s^22l\text{-}1s2lnl$ with n=3,4 are situated nearly.

In [2,4] we present the measured values of wavelengths (in Å) of the *Li*-like lines dielectronic satellites to $1s^{21}S_0\text{-}1s3p^1P_1$ emission line in the K plasma in a law inductive vacuum spark. We also present theoretical data on wavelengths, obtained on the basis of calculation within different theoretical approaches: PT on the 1/Z, relativistic PT with model zeroth approximation for three-quasiparticle atomic systems with effective

Transitions	Probability			Wavelength			Wave-length [7]
	B	C	D	B	C	D	
$1s^2 2p^2 P_{3/2} - 1s2p3p^2 D_{5/2}$	61,26	59,65	59,70	1,5933	1,5932	1,5934	1,5930± 0,0005
$1s^2 2p^2 P_{1/2} - 1s2p3p^2 D_{3/2}$	33,76	27,39	26,60	1,5931	1,5929	1,5935	
$1s^2 2p^2 P_{3/2} - 1s2p3p^4 S_{3/2}$	4,88	7,56	14,68	1,5947	1,5945	1,5948	
$1s^2 2p^2 P_{3/2} - 1s2p3p^4 P_{3/2}$	-----	5,48	-----	-----	1,5953	---	
$1s^2 2p^2 P_{3/2} - 1s2p3p^4 D_{5/2}$	-----	7,57	-----	-----	1,5952	---	

Table 1. The transitions probabilities (P, in 10^{13} s^{-1}) for Li-like lines of dielectronic satellites to $1s^{21}S_0$-$1s3p^1P_1$ emission line in the Fe plasma: (B)- PT on 1/Z, C- relativistic PT with model "0"-approximation for 3-quasi-particle atomic systems with effective account for correlation and radiative corrections (present work), D-method AUTOJOLS [2,7].

account for correlation and radiative QED corrections, method AUTOJOLS, optimized Dirac-Fock method with account QED corrections [2,7]. Table 1 lists the theoretical data on energies and transitions probabilities (in 10^{13} s^{-1}), which are corresponding Li-like lines of dielectronic satellites to $1s^{21}S_0$-$1s3p^1P_1$ emission line in the Fe plasma.

As in a case of calculating dielectronic satellites to emission line $1s^{21}S_0$-$1s3p^1P_1$ for K plasma in a low inductive vacuum spark [2,7], theoretical and experimental values of wavelengths for satellite lines in a whole are sufficiently well agreed with each other. However, values for the transition probabilities, calculated by different theoretical methods, are significantly disagreed with each other. Our work has shown that new ab initio version of the relativistic PT with correct account of correlation, relativistic and radiative effects for three-particle atomic systems is to be waited for a powerful theoretical tool for studying complex spectra and spectral characteristics of the plasma emission as in a law inductive vacuum spark as other plasma sources. It should be noted also that our approach is in a great degree oriented on the classical tasks of spectroscopy of free multicharged ions and spectroscopy of plasma. The last fact is especially valuable from the point of view of the realizing spectroscopic diagnostics of the hot plasma etc.

To define the electron density and temperature of a plasma one needs the correct data on the intensities of dielectronic satellites to resonant lines and the corresponding set of atomic constants (coefficients of dielectronic recombination, velocities of impact excitation, probabilities of radiation decay and autoionization etc. [2-7,13-17]. In our case the plasma electron temperature and its electron density can be defined using the relationship between the dielectronic satellites intensities, say, *j,k,* and resonant line. The intensity of resonant line of the He- like ion is defined as follows (c.f. [2,7]):

$$I_R = N_e < v\sigma >_{1s-2p} \int_0^{\tau} N_{He} dt$$

where N_{He} is a concentration of the He-like ions, $<vs>$ is an averaged cross-section of the impact excitation *1s-2p*; *t* is a time of the hot plasma. The relationship between the resonant lines satellites intensities of the He- like ions, say, Fe, Cl ions, is as follows:

$$W = I_{R_{Cl}} / I_{R\,Fe} = < v\sigma >_{1s-2p} \int_0^{\tau} N_{He_{Cl}} dt \{ < v\sigma >_{1s-2p} \int_0^{\tau} N_{He_{Fe}} dt \}^{-1}$$

With using the method of ref. [7], theoretical data of present paper, it is possible to evaluate the value of *W* in dependence upon the electronic temperature for given electron density: N_e=10^{23} cm^3. In result we predict the electron temperature 2400 eV that is in an reasonable agreement with experimental data [7]. The presented theory has to be very effective tool in treating the atomic (multicharged ions) spectroscopic characteristics in the laser-produced plasma, where studying of the elementary atomic processes is of a great interest and importance (see, for example, [18,19]).

References

1. Glushkov A. V., Gurnitskaya E. P., Florko T. A. et al, Gauge-invariant QED perturbation theory approach to calculating nuclear electric quadrupole moments, hyperfine structure constants for heavy atoms and ions// Frontiers in Quantum Systems in Chemistry and Physics (Springer).— 2008. — Vol.18. — P. 505-522.
2. Turin A. V., Chernyakova Yu. G., Prepelitsa G. P., Characteristic features of the emission spectra of K plasma in a law inductive vacuum spark: Relativistic calculation//Phys. Aerodisp.Syst. — 2003. — Vol40. — P. 327-332.
3. Chernyakova Yu. G., Ignatenko V. M.,Vitavetskaya L. A., Sensing the tokamak plasma parameters by means high resolution x-ray theoretical spectroscopy method: New scheme// Sensor Electr. and Microsyst. Techn. — 2004. — N2. — P. 20-24.
4. Chernyakova Yu. G., High resolution X-ray spectroscopy approach to determination of the Tokamak plasma parameters// Photoelectronics. — 2006. — Vol.15. — P. 71-78.
5. Koshelev K. N., Sidel'nikov Yu. V., Vikhrov V. V., Ivanov V. V., Micropinches in law inductive vacuum spark and radiative pressing// In: Spectroscopy of multicharged ions..— Moscow: Nauka, 1991. — P. 163-198.
6. Safronova U. I., Aglitsky E. V., Spectroscopy of autoionization states. — Moscow: Atomizd., — 1999.
7. Aglitskii E. V., Panin A. S., Safronova U. I. etal Theoretical and experimental investigation of satellite structure of $1s1s^{21}S0\text{-}1s3p^{1}P_{1}$ line in He-like ions// Journ.de Phys.— 1999.— Vol.49. — P. 267-269.
8. Yongqiang Li, JianhuaWu, Yong Hou, Jianmin Yuan, Influence of hot and dense plasmas on energy levels and oscillator strengths of ions: Be-like ions for $Z = 26–36$//J. Phys. B: At. Mol. Opt. Phys. — 2008. — Vol.41. — P. 145002.
9. Mandelstam S. L., Aglitsky E. V., Antsiferov P. S., Panin A. M. X-ray spectra of Ne-like Ba, La, Ce and Pr ions// Canad. Journ.of Phys.1999. — Vol.62, N10. — P. 1923-1930.
10. Glushkov A.V., Relativistic quantum theory. Quantum mechanics of atomic systems, Odessa: Astroprint, 2008.-700P.
11. Glushkov A. V., Ivanov L. N. Radiation decay of atomic states: atomic residue and gauge non-invariant contributions // Phys. Lett.A. — 1999. — Vol.170. — P. 33-38.
12. Glushkov A. V., Loboda A. V., Chernyakova Yu. G. et al, QED theory of the superheavy elements ions: energy levels, radiative corrections, and hyperfine structure for different nuclear models// Nuclear Phys.A— 2004. — Vol. 734. — P. 21-28.
13. Dyall K. G. Introduction to relativistic quantum theory.-Oxford, 2007. — 590P.
14. Mocken G. R., Keitel C. H., Bound atomic dynamics in the MeV regime// J.Phys. B: At. Mol. Opt. Phys.— 2004. — Vol.37.— P.L.275-283.
15. Rosmej F. B., Hoffman D. H., Geissel M. et al, Advanced X-ray diagnostics based on an observation of high-energy Rydberg transitions from auto ionizing levels in dense laser-produced plasmas// Phys. Rev.A.— 2001 — Vol.63. — P.063409-063418.
16. Trabert E., Saathoff G., Wolf A., M1/E2 decay rates in CoXI, NiXII, CuXIII measured at heavy-ion storage ring//J. Phys.B.:At.Mol.Opt.Phys. — 2004. — Vol.37. — P.945-952
17. Oks E., Relation between theories, experiments, and simulations of spectral line shapes//Int. Journ. of Spectroscopy. — 2010. —Vol.10. — P. 852581.
18. Gurnitskaya E. P., Korchevsky D. A., Loboda A. V., Sensing the optimal plasma parameters for x-ray lasing: calculation of electron-collision excitation cross-sections for Ar-like plasma ions// Sensor Electr. and Microsyst. Techn. — 2006. — N1. — P. 18- 22.
19. Malinovskaya S. V., Glushkov A. V., Loboda A. V. et al, Generalized energy approach to calculating electron collision cross-sections for multicharged ions in a plasma: Debye shielding model// Int. Journ. Quant. Chem. — 2011. — Vol.111. — P.288-296.

UDC 539.186

Yu. A. Kruglyak, D. A. Korchevsky, Yu. G. Chernyakova, T. A. Florko

RELATIVISTIC MODEL DIRAC-FOCK APPROACH TO STUDYING FE PLASMA EMISSION SPECTRA IN A LOW INDUCTIVE VACUUM SPARK

Abstract. There are presented the results of theoretical calculation for transition probabilities of the Fe plasma Li-like satellite lines on the basis of the relativistic perturbation theory with the Dirac-Fock model zeroth approximation and accounting for correlation and radiative corrections. With using the calculated values for relation of intensities of the dielectronic satellites lines and resonant lines of He-like ions, it is carried out an estimate of the plasma electron temperature and density.

Key words: Fe plasma Li-like satellite lines, relativistic perturbation theory

УДК539.186

Ю. А. Кругляк, Д. А. Корчевский, Ю. Г. Чернякова, Т. А. Флорко

РЕЛЯТИВИСТСКИЙ МОДЕЛЬНЫЙ ПОДХОД ДИРАКА-ФОКА К ИЗУЧЕНИЮСПЕКТРА ИЗЛУЧЕНИЯ ПЛАЗМЫ Fe В МАЛОИНДУКТИВНОЙ ВАКУУМНОЙ ИСКРЕ

Резюме. Проведено изучение параметров Li-подобных сателлитных линий плазмы Fe на основе расчета методом релятивистской теории возмущений с дирак-фоковским модельным нулевым приближением и учетом корреляционных и радиационных поправок. С использованием рассчитанных значений отношения интенсивностей диэлектронных и резонансных линий He- подобных ионов получена оценка величин электронной температуры и плотности плазмы.

Ключевые слова: Li-подобные сателлитные линии, плазма Fe, релятивистская теория возмущений

УДК539.186

Ю. О. Кругляк, Д. О. Корчевський, Ю. Г. Чернякові, Т. О.Флорко

РЕЛЯТИВІСТСЬКИЙ МОДЕЛЬНИЙ ПІДХІД ДІРАКА-ФОКА ДО ВИВЧЕННЯ СПЕКТР ВИПРОМІНЮВАННЯ ПЛАЗМИ Fe У МАЛОІНДУКТИВНІЙ ВАКУУМНІЙ ІСКРІ

Резюме. Виконано вивчення параметрів Li-подібних сателітних ліній плазми Fe на основі розрахунку методом релятивістської теорії збурень з дірак-фоківським модельним нульовим наближенням і урахуванням кореляційних та радіаційних поправок. З використанням розрахованих значень відношення інтенсивностей діелектронних й резонансних ліній He- подібних іонів виконано оцінку величини електронної температури та густини плазми.

Ключові слова: Li-подібні сателітні лінії, плазма Fe, релятивістська теорія збурень

UDC 621.315.592

Dragoev A. A., Ilyashenko A. S., Babinchuk V. S., Karakis Yu. N., Kutalova M. I.

Odessa National University, Pasteur Str.,42; ph. 723-34-61
e-mail: : wadz@mail.ru

FEATURES OF PHOTOCURRENT RELAXATION IN SENSOR-BASED CdS CRYSTALS OR FEATURES OF PHOTOCURRENT RELAXATION IN CRYSTALS WITH FAST AND SLOW RECOMBINATION CENTRES

The fast relaxation of the photocurrent associated with electronic processes has been explored. The external factors effect has been investigated. It was shown that in contrast to the accepted view of the phenomena, the of carriers' transitions mechanism includes thermal excitation in sensitivity centers, and only then transition to the free state.

The study of semiconductor devices operating in the infrared part of the spectrum attracts attention in connection with their applications for communication, diagnostics, radiation sensors, in technological processes, for data-transmission systems, in medicine, in military science, etc.

One of the most promising materials for the production of such electronic devices are semiconductors of A^2B^6 group due to cheapness of the substances used, well-designed fabrication technologies, and also due to high photosensitivity of the devices based on such materials.

One of the typical specimen of these binary compounds is cadmium sulfide. For many years, CdS crystals are of considerable interest owing to high photoresponse (the ratio of light to dark conductivity up to eight orders of magnitude), the optimal (~ 5.7 nm) lattice constant, the comparative ease of electrical contacts plating, as well as to a significant solubility coefficient for most doping agents. Due to well-established properties, in some cases, such crystals are used as a model material to clarify the nuances of photoelectric processes.

At the same time this semiconductor belongs to a class of large-gap semiconductors. Its band gap width (2.42 eV), providing the most part of the positive operating properties, including the above, significantly limits range of spectral sensitivity. Even at the expense of its improper excitation it can be extended to long wave region only up to 980 - 1000 nm. Further extension up to 1600 nm (twofold) can be achieved for crystals doped both with fast and slow recombination centers.

The specific feature of such samples is a presence of the photocurrent infrared blanking effect through the joint operation of the recombination centers. The elements' sensitivity does not decrease, as it usually happens with direct current measurements, but also can significantly increase as the relative change of the current is measured instead of the current itself.

The photocurrent infrared blanking reduces current magnitude formed by the free carriers, excited by light from the proper absorption region, when sample is additionally subjected to long wavelength lighting.

The wave length of suppressing light is usually in an infrared part of the spectrum. Therefore the effect is called photocurrent infrared blanking. For the first time this mechanism was suggested by A.Rouz.

The A.Rouz' model is based on the process of a charge carriers release from traps. In this case, after the light excitation from the local center, nonequilibrium carrier does not participate in the current formation immediately. Depending on the applied electric field and temperature, it stays for some time in the vicinity of the center. It is energetically favorable for such carrier,

of course, to return into the trap. The change of trap's charge state after the excitation event also promotes this process. Such free-capture oscillations, probably repeated, do not affect measured electric current, as the spatial position of such charge carriers is unchanged. For this reason, these stages of excitation remained unexplored.

As a tool to study these oscillations we chose the photocurrent infrared blanking effect.We believe that this approach has several advantages.

First, if the crystals under consideration are sufficiently saturated with S- and R-centers, the distance between these centers is small. In this case, holes, knocked by infrared light from centers of slow recombination, after passing only a few crystal lattice cells will hit the S-centers and affect the current. Moreover, if the S-and R-centers are distributed uniformly, the free path length will be more or less fixed. In ordinary situation, these processes are concealed by scattering, random trap captures, other channels of recombination, etc.

In addition, the features of the infrared blanking allow to change independently both parameters of current-forming self light, and the intensity and spectral composition of the infrared light, responsible only for the holes release.

Finally, the effect of IR-blanking allows identifying and investigating the mechanism of carriers' emission from a specific class of the centers, whereas in the usual case we have to deal with a range of traps, depletion processes of which obscure each other.

These features of the infrared blanking make it a sensitive and flexible method for studying the fine details of improper carriers photoexcitation.

The present study aims to investigate features of the carriers excitation from bound to the conductive state using the photocurrent IR blanking effect and the features of current formation.

In the paper [1] the long-time relaxation of the photocurrent (about 10^5 - 10^4 seconds per day) in short samples of cadmium sulfide with IR-blanking under illumination by their proper light is described. A model that explains such relaxation is also suggested there. When crystals are stored in the dark for a long term deep R-centers (1.1 eV), gradually losing charge, are retracted by barriers field into the spatial charge region of electrical contacts and accumulate there. At the subsequent illumination they diffuse towards the crystal center. In this case, the photosensitivity of this region increases, photocurrent increases as well.

We also observed a similar relaxation which authors [1] associated with migration of ions in the crystal. In accordance with the techniques proposed in this article, measures to eliminate such change of the photocurrent were implemented in the sample preparation. The samples were kept for a long time on their proper light.

In the article [2] the middle-time (10^3-10^2 seconds, tens of minutes) relaxation of proper current was studied. The complicated form is explained by additional mechanism of the electrical contacts' spatial charge region shape change due to external voltage applied. However, as before, it was supposed that the photocurrent formation is controlled by the spatial redistribution of the crystal impurities.

In this regard, it is interesting to study the photocurrent change for the periods, excluding influence of ionic processes — 10^1-10^2 sec (tens of seconds, up to several minutes). In this case, the sample is illuminated by its proper light of varying intensity (Fig. 1A). For ease of comparison, all graphs are shifted to the

$t = 0$.

Usually photocurrent relaxation is measured from the initial state, i.e. darkness, to completely steadied value, i.e. saturation on graph I_{ph} (t). In this case, only one value of light intensity is used.

It is clear that the process of electrical current change includes at least two fundamentally different phases. In the initial phase, the photoexcitation of free carriers occurs, most of which fills existing traps and recombination centers. In our case, there are, at least, effective R-centres for this purpose.

The nonequilibrium charge capture process dominates for small values of light intensity, when the number of absorbed photons is less than traps concentration. Conditions are unfavorable for the formation of the photocurrent. On the contrary, the final stages of relaxation occur already in conditions of quasi-equilibrium for capture-

emission processes. In our samples, it happens not less, than in four channels: besides always present sticky centers, recombination at the S-centers occurs, as well as captures and emissions from ground and excited states of R-centers and intracenter transitions as shown in Fig.2b.

Exactly this complex ensemble of interactions was a main subject of research. Therefore, measurements were carried out in the conditions of already existing intensity of proper light and steady photocurrent during the transition to the higher intensity. The additional lighting switching on is considered t = 0 (Figure 1A).

Observations were compared with the reverse process, when the intensity decreased to the base value. In this case, the competing process determines the system behavior — centers are depleted. Indeed, at measurements in low lighting conditions, we observed rather widened relaxation region on the $I_{ph}(t)$ graph. At the same time, the reverse relaxation appeared faster.

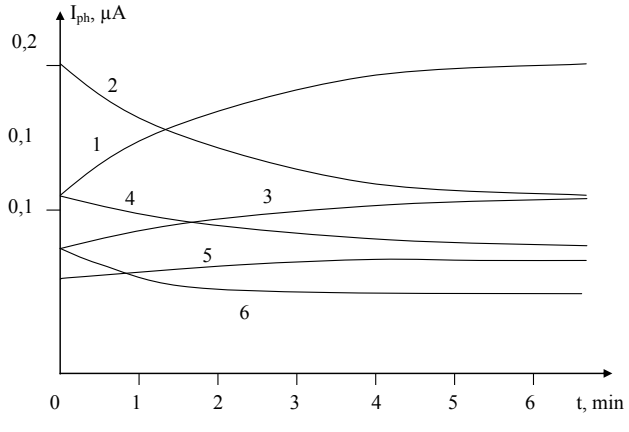

Fig. 1A. A photocurrent relaxation during the change of proper light intensity: 1. — from 4.25 to 9.8 lux; 2. — from 9.8 to 4.25 lux; 3. — from 1.35 to 4.25 lux; 4. — from 4.25 to 1.35 lux; 5. — from 0.6 lux to 1.35 lux; 6. — from 1.35 to 0.6 lux.

For the transitions from low to high lighting conditions at large luminous fluxes, in addition to the natural increase of the photocurrent absolute values, the increase of the growing component over time was insignificant, due it's being determined not by lighting parametres, but the presence of empty states in the traps. The declining component of the $I_{ph}(t)$ dependence was delayed to a bigger extent, as it is determined by the greater charge stored in the traps.

Finally, for the relatively high light intensities, as shown in Figure 1A, the photocurrent magnitude itself depended on intensity of used light. Dynamics of its change — both increase and decrease, starting with two minutes, appeared identical. By superimposing the graphs it can be shown, that these parts of the curves coincide.

In addition to this, the relaxation time from the initial value for the decrease to the initial value for the growth (Fig. 1A) also increased with light intensity increase.

Note that the method of photocurrent relaxation analysis in the separate measurement of the stepwise light intensity is used for the first time.

The short time region, that is less than 2 minutes, appeared dependent on the temperature at which the measurement was made. The essential curve shapes are shown as Figure 1B.

Graphs on Figure 1b were normalized to the saturation point. That is, for the convenience of comparison, the value of the current in the saturation area in both cases was taken as 100% with the corresponding conversion of currents in other areas. Actual absolute values of a current decreased with temperature increase, value in the saturation area, and the current value both.

To avoid rapid reduction of currents associated with the effect of temperature blanking [3], which is not considered in this study, we used the temperature range below 50-60 ° C, typical for the beginning of T-blanking.

As seen in Figure 1B, the temperature increase leads to a noticeable rise of relaxation in 2-3 times. Taking into account approximately 1 sec durations of current evolutions, we related observed changes to electronic processes.

When proper light illuminates sample release of nonequilibrium charge carriers occurs. A certain number of them are involved in the photocurrent formation, but significant part, especially in the initial moments, are spent on filling of deep traps. It is obvious, that the amount of such carriers captured by traps is great at first, as traps were empty. But eventually it is reduced, as traps are filled.

This provides an increase of free state carriers, with the corresponding relaxational photocurrent increase.

At the same time the competing process occurs - as traps are filled at a given temperature the number of thermally emitted carriers increases.

In general, the presence of a plateau is characterized by approximate balance of carriers captured by and emitted from traps. With temperature growth at the same intensity of captures a number of thermal emissions increases. This provides faster saturation (see Fig. 1B).

To observe the photocurrent relaxation under influence of the long-wave radiation, wavelengths corresponding to the maxima of blanking - 960 and 1380 nm (fig. 2.A) were used. Optimal intensities of proper light and blanking light were set according to [4]

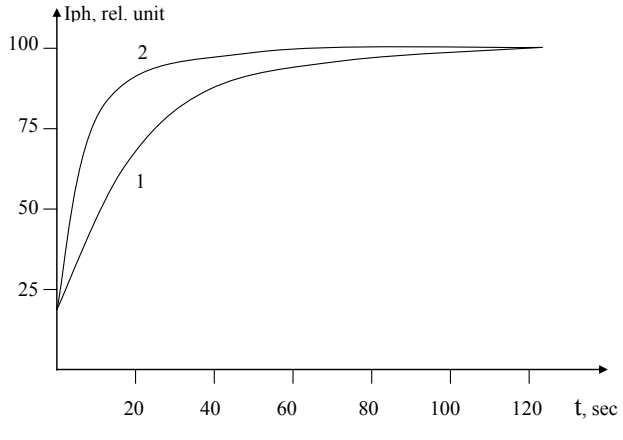

Fig. 1B. Plot of the short time current relaxation
1. — at t ° = 17.5 °C; 2. — at t ° = 43.5 °C.

Fig. 2.A. Temporal photocurrent changes in the blanking maxima.

With the constant exciting light after the relaxation of photocurrent I_0, the infrared illumination was turned on, preset on a wavelength of the corresponding blanking maximum and photocurrent l time dependence was measured.

Both curves start from the same point corresponding to the value of proper excitation. With the infrared lighting photocurrent blanking starts and the current decreases — the curve 1, corresponding to a wavelength of 960 nm, is above the curve 2 for the wavelength of 1380 nm and takes longer to reach saturation.

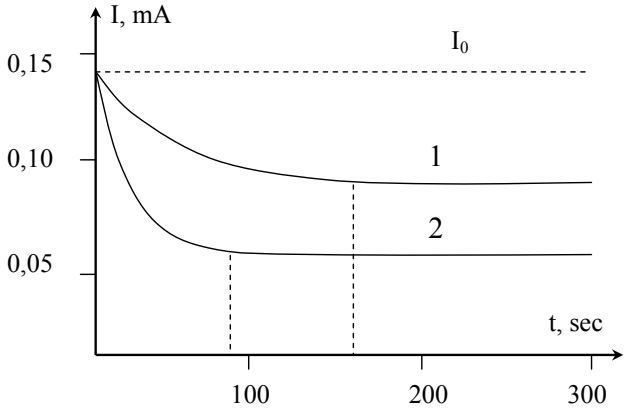

Fig. 2.A. Temporal photocurrent changes in the blanking maxima.

This is explained as follows. Figure 2.B shows the band diagram, where the transitions from the ground state of R-centers correspond to curve 1, and the transitions from the R ‘correspond to curve 2.

Since there is a thermal transition from level R to level R’, the probability of transition from level R’ is greater than from level R. This explains the fact that the curve 2, corresponding to the transition R’, is lower than curve 1, corresponding to the transition from the levels R.

As seen in Figure 2.A, curve 2 reaches saturation faster. This is due to only one process, namely the transitions from the R’. At the same time, curve 1 is due to transitions from the R and R’, plus the thermal transitions inside the sensitivity centers from the ground to the excited states. In addition, as noted above, there is a probability of inverse capture of a hole from the valence band by R centers. In general, the existence of such complex combination of processes accounts for more delayed front of the observed curve.

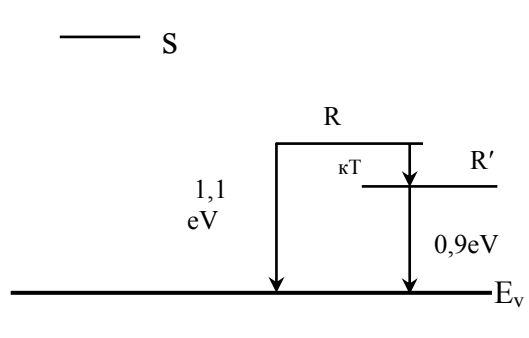

Fig. 2B. Model of phonon-photon transitions involving excited states of R — centers.

Thus, the considered model suggests greater holes population on R' levels due to the thermal transitions from the ground state of R-centers to R'. It contradicts with R.Bjub's zonal model [5] which is based on the opposite mechanism of holes release — intracenter optical excitation with activation energy 0.9 eV followed by thermal excitation in the band with energy of 0.2 eV.

These data provide additional evidence for alternative model presented in the paper [6].

REFERENCES

1. Ю. Н. Каракис, Н. П. Затовская, В. В. Зотов, М. И. Куталова «Особенности релаксации фототока в кристаллах сульфида кадмия с запорными контактами» 1-а Українська наукова конференція з фізики напівпровідників. Одеса, 10-14 вересня 2002 р. Тези доповідей. Т. 2. С. 138.
2. A. A. Dragoev, A. V. Muntjanu, Yu. N. Karakis, M. I. Kutalova «Calculation for migration-dependent changes in near-contact space-charge regions of sensitized crystals.» «Photoelectronics», n. 19. Odessa «Astroprint» 2010. P. 74-78.
3. В. В. Сердюк, Г. Г. Чемересюк «Фотоэлектрические процессы в полупроводниках», Киев, «Либідь», 1999, С.190 .
4. M. A. Novikova, Yu. N. Karakis, M. I. Kutalova «Particularities of current transfer in the crystals with two types of Recombination centers». «Photoelectronics», 2005, n.14, P. 58-61.
5. Р. Бьюб «Фотопроводимость твёрдых тел». Из-во ин. лит. М., 2002 г. С. 558.
6. Melnik A. S., Karakis Y. N., Kutalova M. I., Chemeresjuk G. G. «Features of thermo-optical transitions from the recombination centers excited states». «Photoelectronics», n. 20. Odessa «Astroprint» 2011. P. 23-28.

UDC 621.315.592

Dragoev A. A., Ilyashenko A. S., Karakis Yu. N., Kutalova M. I., Babinchuk V. S.

FEATURES OF PHOTOCURRENT RELAXATION IN SENSOR-BASED CdS CRYSTALS OR FEATURES OF PHOTOCURRENT RELAXATION IN CRYSTALS WITH FAST AND SLOW RECOMBINATION CENTRES

Abstract.

The fast relaxation of the photocurrent associated with electronic processes has been explored. The external factors effect has been investigated. It was shown that in contrast to the accepted view of the phenomena, the of carriers' transitions mechanism includes thermal excitation in sensitivity centers, and only then transition to the free state.

Key words: relacxation, photocurrent, recombination.

УДК 621.315.592

Драгоев А. А., Ильяшенко А. С., Каракис Ю. Н., Куталова М. И., Бабинчук В. С.

ОСОБЕННОСТИ РЕЛАКСАЦИИ ФОТОТОКА В КРИСТАЛЛАХ С ЦЕНТРАМИ БЫСТРОЙ И МЕДЛЕННОЙ РЕКОМБИНАЦИИ

Резюме.

Исследована быстрая релаксация фототока, связанная с электронными процессами. Изучено влияние на неё внешних факторов. Показано, что в отличие от действующих представлений, процесс перехода носителей включает в себя сначала термическую активацию на возбуждённые уровни центров чувствительности, а затем в свободное состояние.

Ключевые слова: релаксация, фототок, рекомбинация.

UDC 539.184

A. A. Kuznetsova, A. S. Kvasikova, A. N. Shakhman, L. A. Vitavetskaya

Odessa National Maritime Academy, Odessa, 4, Didrikhsona str., Odessa, Ukraine
K.D. Ushinsky South-Ukrainian Nat. Pedagogical University, 25, Staroportofrankovskaya str., Odessa, Ukraine
Odessa State Environmental University, 15, Lvovskaya str., Odessa, Ukraine
Kherson State University, Kherson, Ukraine
e-mail: quantkva@mail.ru

CALCULATING THE RADIATIVE VACUUM POLARIZATION CONTRIBUTION TO THE ENERGY SHIFT OF 2P-2S TRANSITION IN μ-HYDROGEN

Calculating the radiative contribution due to the vacuum polarization effect to energy shift for 2p-2s transition in muonic hydrogen has been carried out on the basis of gauge-invariant relativistic many-body perturbation theory.

Due to the significant progress in the modern experimental technologies now a great interest attracts studying spectra of heavy and super heavy elements atoms, exotic atomic systems, including hadronic and leptonic atoms [1-6]. Especial problem is connected with précised calculating the radiative corrections to the transition energies of the muonic atoms, namely, muonic hydrogen [1-5]. Naturally, it is provided by necessity of further developing the modern as atomic and as nuclear theories. From the other side, detailed information about spectra of the exotic atomic systems (kaonic, pionic, muonic atoms) can be very useful under construction of the new X-ray standards. One could remind a great importance of the muonic chemistry, muonic spectroscopy. Very attractive perspective of the thermonuclear fission through the mechanism of the muonic catalysis is still interesting and widely studied.

The standard Dirac approach is traditionally used as starting basis in calculations of the heavy ions [5]. The problem of accounting the radiative corrections, in particular, self-energy part of the Lamb shift and vacuum polarization contribution is mostly treated with using the perturbation theory (PT) on parameters $1/Z$, αZ (α is fine structure constant). It permits evaluations of the relative contributions of different expansion energy terms: non-relativistic, relativistic ones, as functions of Z. For high Z (Z is a nuclear charge) serious problems are connected with correct definition of the QED corrections: the Lamb shift, Lamb shift self-energy part, vacuum polarization, the nuclear finite size correction etc [6-13]. Further improvement of this method is linked with using gauge invariant procedures of generating relativistic orbital basises and more correct treating nuclear and QED effects [5-8,13-18].

In refs. [19-22] it has been proposed a new scheme to calculating spectra of heavy systems with account of nuclear and radiative effects, based on the relativistic many-body PT [13-18] (see also [3]) and advanced effective procedures for accounting the radiative corrections. Here we present the results of calculating the contribution due to the vacuum polarization effect to energy shift for 2p-2s transition in muonic hydrogen. The obtained result has to be more précised in comparison with our result [19].

The calculation of the radiative vacuum polarization shift in the muonic hydrogen can be performed using the relativistic Dirac approximation as a zeroth one. Further, the expectation value of the radiative vacuum polarization operator gives the corresponding correction. One can write the one-particle relativistic Dirac equation with a potential:

$$V(r)=V_n(r)+U(r). \qquad (1)$$

This potential includes the electrical V_n and polarization U(r) potentials of a nucleus. Further one could define the charge distribution in a nucleus, for example, by the Gaussian function (look details in Ref. [9]):

$$\rho(r|R) = \left(4\gamma^{3/2}/\sqrt{\pi}\right)\exp\left(-\gamma r^2\right). \quad (2)$$

Here $\gamma = 4/\pi R^2$; R is an effective nucleus radius. As usually, the Coulomb potential for spherically symmetric density $\rho(r|R)$ can be written as follows:

$$V_{nucl}(r|R) = -\left((1/r)\int_0^r dr' r'^2 \rho\left(r'\middle|R\right) + \int_r^\infty dr' r' \rho\left(r'\middle|R\right)\right). \quad (3)$$

The details of the determination of this potential can be, for example, found in ref. [9]. The vacuum polarization part is usually accounted in the first PT order by using the Uehling potential [1,8,16,17]:

$$U(r) = -\frac{2\alpha}{3\pi r}\int_1^\infty dt \exp\left(-2rt/\alpha Z\right)\left(1+1/2t^2\right)\frac{\sqrt{t^2-1}}{t^2} \equiv -\frac{2\alpha}{3\pi r}C(g),\ g = \frac{r}{\alpha Z}. \quad (4)$$

The corresponding expectation value of this operator gives the corresponding vacuum polarization correction. In the scheme [17] this potential is approximated by quite precise analytical function (see details in refs. [3,15,16]). The most advanced version of the such potential ($C \to \tilde{\tilde{C}}$) is presented as follows:

$$\tilde{\tilde{C}}(g) = \tilde{C}_1(g)\tilde{\tilde{C}}_2(g)/\left(\tilde{C}_1(g) + \tilde{\tilde{C}}_2(g)\right),$$
$$\tilde{\tilde{C}}_2(g) = \tilde{C}_2(g)\, f(g),$$
$$\tilde{C}_2(g) = -1.8801\exp(-g)/g^{3/2}$$
$$\tilde{C}_1(g) = h(g/2) + 1.410545 - 1.037837g,$$
$$f(g) = \left((1.1024/g - 1.3361)/g + 0.8027\right)$$

The using this formula permits one to decrease the calculation errors for this term down to ~0.1%. Error of usual calculation scheme is~10%. We carried out the calculation of the vacuum polarization contribution to the energy shift for 2p-2s transition in muonic hydrogen. It should be noted that the energy levels of muonic atoms are very sensitive to effects of QED, nuclear structure and recoil since the muon is about 206 times heavier than the electron. As usually the fundamental constants from the CODATA 1998 are used in the numerical calculations. The most QED effect for muonic atoms is the virtual production and annihilation of a single e^+e^- pair (the Uehling contribution). In table 1 we present our data for the generalized Uehling potential expectation values and results of other calculations [5,17]). The mixed muon-electron vacuum polarization correction is 0.00007 meV. Correction to the Lamb shift due to the anomalous magnetic moment has the value (accepted in literature value): -0.00002mev. The relativistic recoil correction is connected with the well known fact.

The centre of mass motion can be separated exactly from the relative motion only in the non-relativistic limit. Relativistic corrections have been calculated and its contribution to 2p-2s energy [1]: -0.00419 meV. To obtain total relativistic and recoil corrections, one must add the difference between the Uehling potential expectation calculated with relativistic and non-relativistic wave functions, giving total correction 0.0169meV. Two-photon recoil for μ- hydrogen is -0.04497 meV. Higher-order radiative recoil corrections give an additional contribution of -0.0096meV. The final result for the μ- hydrogen Lamb shift is 202.054 meV.

In conclusion we note that usually the radiative corrections are estimated in the light systems by means of the αZ expansion method and surely this approach is quite consistent in a case of the little values on nuclear charge. Obviously, the expansion method can not be used for studying the Lamb shift (polarization of vacuum effect) in more complicated and heavier muonic systems (than, say, hydrogen or the muonic hydrogen). At the same time our method is applicable to light atoms and more heavy ones as in free state as in an external field [21,22].

Table 1. The Uehling potential expectation value (R_p –proton radius in fm)

Point Nucleus		R_p=0,875 [5]		R_p=0,875 [19]		R_p=0,875 (our th.)	
$2p_{1/2}$-$2s_{1/2}$	$2p_{3/2}$-$2s_{1/2}$	$2p_{1/2}$-$2s_{1/2}$	$2p_{3/2}$-$2s_{1/2}$	$2p_{1/2}$-$2s_{1/2}$	$2p_{3/2}$-$2s_{1/2}$	$2p_{1/2}$-$2s_{1/2}$	$2p_{3/2}$-$2s_{1/2}$
205.0282	205.0332	205.0199	205.0250	205.0207	205.0256	205.0202	205.0254

References

1. Botham C., Martensson A. M., Sanders P. G. Relativistic effects in atoms and molecules. —Vancouver: Elseiver, 2001. — 550p.
2. Grant I. P., Relativistic Quantum Theory of Atoms and Mole-cules. — Oxford, 2008. — 650P.
3. Glushkov A. V., Relativistic quantum theory. Quantum mechanics of atomic systems, Odessa: Astroprint, 2008. — 700P.
4. Hayano R. S., Hori M., Horvath D., Widman E., Antiprotonic helium and CPT invariance//Rep. Prog. Phys.— 2007. —Vol.70. — P. 1995-2065.
5. Karshenboim S., Kolachevsky N., Ivanov V., Fischer M., Fendel P., Honsch T.,2s-Hyperfine Splitting in H-like Atoms// JETP. — 2006. — Vol.102. — P. 367-376.
6. Khriplovich I. V., Milstein A. I., Yelkhovsky A. S. Logarithmic corrections in the two-body QED problem// Phys. Scripta T. — 1999. — Vol. 46. — P. 252-261
7. Borie E., Lamb shift in muonic hydrogen// Phys. Rev. A. — 2005. — Vol.71. — P. 032508-1-8.
8. Mohr P. J. Quantum Electrodynamics Calculations in few-Electron Systems// Phys. Scripta. — 1999. — Vol. 46, N 1. — P. 44- 52.
9. Shabaev V. M., Tomaselli M., Kuhl T., Yerokhin V. A., Artemyev A. N., Ground state hyperfine splitting of high-Z hydrogen-like ions..// Phys.Rev.A. — 1999. — Vol. 56. — P. 252-262.
10. Schweppe J., Belkacem A., Blumenfeld L., Clayton N., Feinberg B., Gould H., Kostroum V.E., Levy L., Misawa S., Mowst J. R. and Priuor M. H. Measurement of the Lamb shift in lithiumlike uranium (U^{89+})// Phys.Rev.Lett. — 1999. — Vol. 66. — P. 1434-1437.
11. Schweppe J., Belkacem A., Blumenfeld L., Clayton N., Feinberg B., Gould H., Kostroum V., Levy L., Misawa S., Mowst J., Priuor M. H. Measurement of the Lamb shift in lithiumlike uranium (U^{89+})// Phys.Rev.Lett. — 1998 — Vol.66. — P.1434-1437.
12. Klaft I., Borneis S., Engel T., Fricke B., Grieser R., Huber G., Kuhl T., Marx D., Neumann R., Schroder S., Seelig P., Volker L. Precision laser spectroscopy of ground state hyperfine splitting of H-like $^{209}Bi^{82+}$// Phys.Rev.Lett. — 1999. — Vol.73. — P. 2425-2427
13. Khetselius O. Yu., Relativistic perturbation theory calculation of the hyperfine structure parameters for some heavy-element isotopes// Int. Journ. of Quantum Chemistry. — 2009. — Vol.109.— N 14. — P. 3330-3335.
14. Glushkov A. V., Rusov V. D., Ambrosov S. V., Loboda A. V., Resonance states of compound super heavy nucleus and EPPP in heavy nucleus collisions // New Projects and New Lines of Research in Nuclear Physics. Eds. Fazio G. and Hanappe F.-Singapore: World Sci., 2003. — P.142-154.
15. Glushkov A. V., Ivanov L. N. Radiation Decay of Atomic States: atomic residue and gauge non-invariant contributions // Phys. Lett.A. — 1999. — Vol. 170. — P. 33-38.
16. Ivanova E. P., Ivanov L. N., Aglitsky E. V., Modern trends in spectroscopy of multicharged ions// Phys.Rep. — 1991. —Vol. 166. — P. 315-390.
17. Glushkov A. V., Ambrosov S., Loboda A., Chernyakova Y. G., Khetselius O., Svinarenko A., QED theory of the superheavy elements ions: energy levels, radiative corrections, and hyperfine structure for different nuclear models//Nuclear Phys.A-2004.—Vol. 734. — P. 21-28.
18. Glushkov A. V., Khetselius O. Yu., Gurnitskaya E. P., Loboda A. V., Florko T. A., Sukharev D. E., Lovett L., Gauge-invariant QED perturbation theory approach to calculating nuclear electric quadrupole moments, hfs struc-

ture constants for heavy atoms and ions// Frontiers in Quantum Systems in Chem. and Phys.(Springer). — 2008. — Vol.18. — P. 505-522.
19. Glushkov A. V., Vitavetskaya L. A., Accurate QED perturbation theory calculation of structure of superheavy elements atoms and multicharged ions with account of nuclear size &QED corrections//Sci.Bull. Uzghorod Univ. Ser. Phys. — 2000. — Vol. 8.— C. 321-326.
20. Vitavetskaya L. A., Malinovskaya S. V., Dubrovskaya Yu., Advanced quantum calculation of beta decay probabilities// Low Energy Antiproton Phys. — 2005. — Vol. 796. — P. 201-205.
21. Gurnitskaya E. P., Khetselius O. Yu., Loboda A. V., Vitavetskaya L.A., Consistent quantum approach to quarkony energy spectrum and semiconductor superatom and in external electric field// Photoelectronics. — 2008. — N 17. — P. 127-130.
22. Kvasikova A. S., Ignatenko A. V., Florko T. A., Sukharev D. E., Chernyakova Yu. G., Photoeffect and spectroscopy of the hydrogen atom in the crossed dc electric and magnetic field//Photoelectronics. — 2011. — Vol. 20. — P. 71-75.

UDC 539.184

A. A. Kuznetsova, A. S. Kvasikova, A. N. Shakhman, L. A. Vitavetskaya

CALCULATING THE RADIATIVE VACUUM POLARIZATION CONTRIBUTION TO THE ENERGY SHIFT OF 2P-2S TRANSITION IN μ-HYDROGEN

Abstract. Calculating the radiative contribution due to the vacuum polarization effect to energy shift for 2p-2s transition in muonic hydrogen has been carried out on the basis of gauge-invariant relativistic many-body perturbation theory.

Key words: muonic hydrogen, energy shift, relativistic theory

УДК 539.184

А. А. Кузнецова, А. С. Квасикова, А. Н. Шахман, Л. А. Витавецкая

РАСЧЕТ РАДИАЦИОННОГО ВКЛАДА ЗА СЧЕТ ЭФФЕКТА ПОЛЯРИЗАЦИИ ВАКУУМА В СДВИГ ЭНЕРГИИ 2P-2S ПЕРЕХОДА В m- ВОДОРОДЕ

Резюме. Проведен расчет радиационного вклада за счет эффекта поляризации вакуума в сдвиг энергии 2p-2s перехода в мюонном водороде методом калибровочно-инвариантной релятивисткой теории возмущений.

Ключевые слова: μ — водород, энергетический сдвиг, релятивистская теория

УДК 539.184

Г. О. Кузнецова, Г. С. Квасикова, А. М. Шахман, Л. А. Вітавецька

РОЗРАХУНОК РАДІАЦІЙНОГО ВНЕСКУ ЗА РАХУНОК ЕФЕКТУ ПОЛЯРИЗАЦІЇ ВАКУУМУ У ЗСУВ ЕНЕРГІЇ 2P-2S ПЕРЕХОДУ У m- ВОДНІ

Резюме. Виконано розрахунок радіаційного внеску за рахунок ефекту поляризацій вакууму у зсув енергії 2p-2s переходу у мюонному водні методом калібровочно-інваріантної релятивістської теорії збурень

Ключові слова: μ — водень, енергетичний зсув, релятивістська теорія

UDC 621.315.592

O. O. Ptashchenko[1], F. O. Ptashchenko[2], V. R. Gilmutdinova[1], G.V Dovganyuk

[1] Odessa National I. I. Mechnikov University, Dvoryanska St., 2, Odessa, 65026, Ukraine,
[2]Odessa National Maritime Academy, Odessa, Didrikhsona St., 8, Odessa, 65029, Ukraine

EFFECT OF AMMONIA VAPORS ON THE BREAKDOWN CHARACTERISTICS OF Si AND GaAs P-N JUNCTIONS

The influence of ammonia and water vapors on *I-V* characteristics of the reverse currents in Si and GaAs p-n junctions was studied. At most of the studied samples, the ammonia- and water vapors lover the breakdown voltage. At some devices an opposite effect was observed. This difference is due to dominance of different surface centers, which have donor or acceptor properties. And some p-n junctions exhibit a fixed breakdown voltage independently on the presence of ammonia and water vapors. This is due to the bulk location of the breakdown in these samples. Thus, the influence of ammonia vapors on the breakdown voltage provides some information on the localization of the breakdown and on the charge state of surface centers.

Key words: p-n junction, gas sensor, reverse current, breakdown voltage, surface center.

1. INTRODUCTION

The gas sensitivity of the p-n junctions at reverse bias is much higher than at the forward bias. It was shown on GaAs-, AlGaAs- [1, 2], GaP- [3], InGaN- [4] and Si [5-7] p-n junctions. The forward current, due to ammonia and (or) water molecules adsorption, is shortened by the bulk injection current at the bias voltages of 0,5 – 2,5 Volts, depending of the band gap. And reverse currents caused by adsorption processes are much higher than the bulk current. This enables to apply to the sample relatively high reverse bias voltages that provide higher gas sensitivity. The upper limit for this voltage is due to breakdown [8]. Ammonia- and water molecules are donors in III-V semiconductors and in silicon. The gas sensitivity of studied *p-n* structures at reverse biases is due to forming of a surface conductive channel which shorts the *p-n* junction.

The adsorption of electrically active molecules can change the breakdown voltage, which is dangerous for the using of p-n structures as gas sensors at reverse biases.

The purpose of this work is a study of the influence of ammonia and water vapors on stationary *I–V* characteristics and on the breakdown voltage of GaAs and silicon p-n junctions.

2. EXPERIMENT

The measurements were carried out on GaAs and silicon p-n junctions with the structure described in previous works [1, 2] and [5, 6], respectively. *I-V* characteristics were measured with an automatic system. The effect of vapors over water solutions of several NH_3 concentrations and over distilled water was studied on stationary *I-V* characteristics, as well as on the current kinetics in p-n junctions. The currents in the samples were limited to <5 μA in order to prevent non-reversible breakdown.

I–V characteristics of the reverse current in a GaAs p-n junction are shown in fig 1. Curve 1, measured in dry air, has a section with a steep ascent due to avalanche breakdown at a voltage of 18 Volts. A measurement in saturated water vapors (at a partial pressure of 1.2 kPa) gives the breakdown voltage of 5 Volts, as shown in curve 2. The breakdown voltage non-monotonously changed with partial pressure of wet ammonia vapors as illustrated in curves 3–6. Curve 4, measured under ammonia pressure of 10 Pa, demonstrates that the breakdown voltage in this sample can increase due to adsorption of NH_3 molecules. Such behavior of the breakdown voltage in am-

monia vapors suggests that the breakdown in this sample is located at the surface of the crystal.

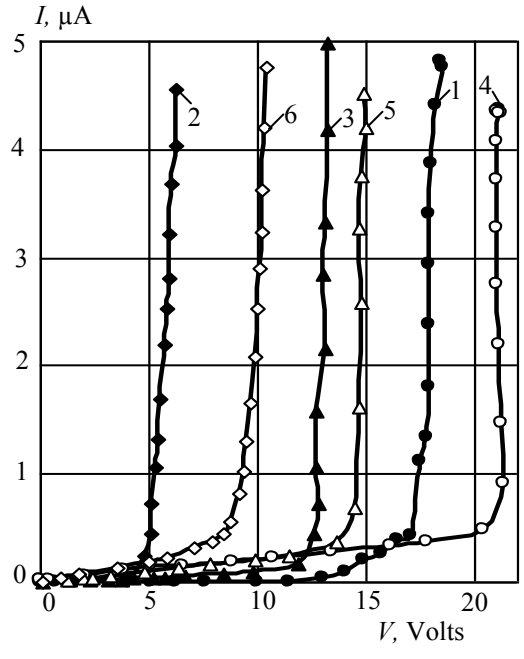

Fig. 1. *I-V* characteristics of the reverse current in a GaAs p-n junction, measured in dry air (curve 1) in water vapors (2) and in wet NH_3 vapors of several partial pressures, Pa: 3 — 1; 4 — 10; 5 — 20; 6 — 100.

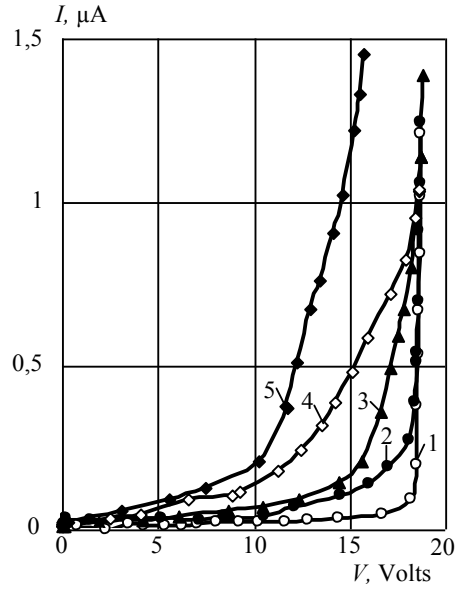

Fig. 2 presents *I-V* characteristics of the reverse currents in another GaAs p-n junction, measured in dry air and in NH_3 vapors of several partial pressures. As seen in this figure, the breakdown voltage in this sample is 18 Volts and does not change in ammonia vapors.

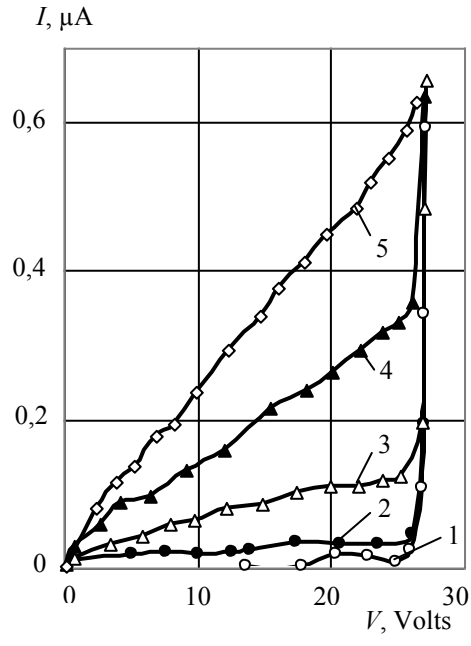

Fig. 3. *I-V* characteristics of the reverse current in a Si p-n junction, measured in dry air (curve 1) and in wet NH_3 vapors of several partial pressures, Pa: 2 – 5; 3 – 10; 4 – 20; 5 – 100; 6 –200.

Similar behavior is characteristic of some Si p-n junctions, as illustrated in fig. 3. It is evident from curves 5–6 in fig. 3 that the breakdown voltage in this Si p-n junction amounts to 28 Volts and does not change in water and ammonia vapors. This means that additional ionized donor centers due to adsorbed water- and ammonia molecules does not affect the electric field in the region of the depletion layer where the breakdown occurs. This argues that the avalanche breakdown in referred samples of GaAs and Si p-n junctions occurs in the crystal bulk and is not associated with the crystal surface.

3. DISCUSSION

The dependence of the avalanche breakdown voltage on the parameters of an asymmetrical abrupt p-n junction can be described as

$$V_B = 60(E_g/1{,}1)^{3/2}(N_B/10^{16})^{-3/4}, \quad (1)$$

where E_g is the band gap of the actual semiconductor; N_B denotes the impurity concentration in the region of lower doping in the p-n junction [9].

This expression can be used for an estimation of the impurity concentration in a p-n structure by using of the measured breakdown voltage as

$$N_B = 10^{16}(60/V_B)^{4/3}(E_g/1{,}1)^2 \,. \qquad (2)$$

The irregular change of the breakdown voltage with the ammonia concentration in the ambient atmosphere, illustrated in fig. 1, can be explained, as we assume the presence of several non-homogeneities with different local concentrations of donors and acceptors at the surface in this sample.

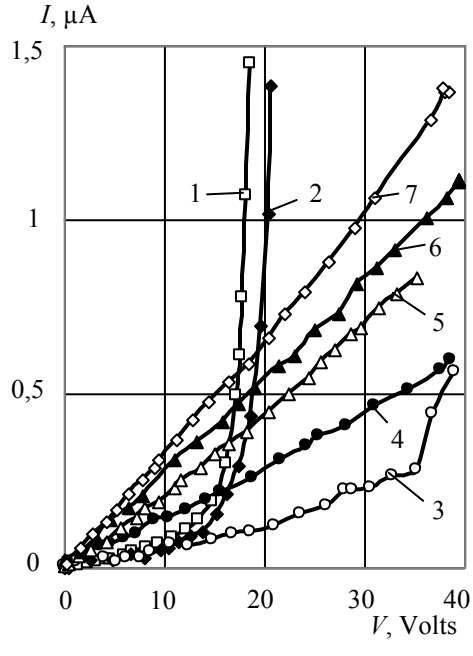

Fig. 4. *I-V* characteristics of the reverse current in a Si p-n junction, measured in dry air (curve 1), in water vapors (2) and in wet NH_3 vapors of several partial pressures, Pa: 3 — 1; 4 — 5; 5 — 10; 6 — 20; 7 — 100.

Fig. 4 presents *I-V* characteristics of the reverse current in a Si p-n junction, measured in dry air, in water vapors and in ammonia vapors of several partial pressures. Curve 1, obtained in dry air, exhibits a breakdown voltage of 17,8 Volts, that corresponds to an impurity concentration of $5{,}0\cdot10^{16}$cm^{-3}. As measured in water vapors of a H_2O partial pressure of 12 kPa, the breakdown voltage was 20 Volts, which yields for the impurity concentration an estimation $4{,}3\cdot10^{16}$cm^{-3}. A comparison of both this values, estimated from the measurements in dry air and in water vapors, suggests that the avalanche breakdown in this sample is located at the crystal surface. The adsorbed water molecules partly compensate the electrically active centers, which are responsible for the surface breakdown.

Curve 3 in fig. 4, measured in ammonia vapors with a partial pressure of 5 Pa, shows a breakdown voltage of 35,2 Volts, that corresponds to a concentration of electrically actives centers of $3{,}0\cdot10^{16}$cm^{-3}. The ammonia vapors of higher partial pressures give the further rise of the breakdown voltage. An analogues effect was observed on the breakdown voltage in GaAs p-n junctions.

The effect of ammonia vapors on the breakdown voltage in Si and GaAs p-n junctions is schematically illustrated in fig. 5. The model takes into account that water and NH_3 molecules are donors on the surface of Si and GaAs crystals. Fig 5*a* depicts the donors and acceptors distributions in a local section of p-n junction, which is responsible for the surface breakdown. The donor concentration N_D in the n-side of the depletion region of this p-n junction is much higher than the acceptor concentration N_A in the corresponding layer of this region:

$$N_D >> N_A. \qquad (3)$$

Therefore the breakdown voltage V_{B1} is controlled by the acceptor concentration at the p-side of the p-n junction. The value V_{B1} can be calculated from the expression (1), where

$$N_B = N_A. \qquad 4)$$

Fig. 5*b* illustrates the structure of the same local p-n junction at the crystal surface under presence of ammonia vapors in ambient atmosphere. Since adsorbed ammonia molecules are donors, they partly compensate the acceptors, which results in a widening of the local depletion region, as shown in fig. 5*b*. In this case the breakdown voltage is determined with the same formula (1), where

$$N_B = N_A - N_D^{\text{add}}, \qquad (5)$$

where N_D^{add} is an additional donor concentration due to ammonia molecules adsorption. It is evi-

dent from formulas (1) and (5), that an increase in N_D^{add} enhances the breakdown voltage.

An analysis of curves 1–3 in fig. 4 using relation (2) yields for N_D^{add} values $0{,}7\cdot10^{16}$cm^{-3} and $2\cdot10^{16}$cm^{-3}, respectively, for local donor concentrations, produced by water- and ammonia molecules (under a partial pressure of 5 Pa) adsorption.

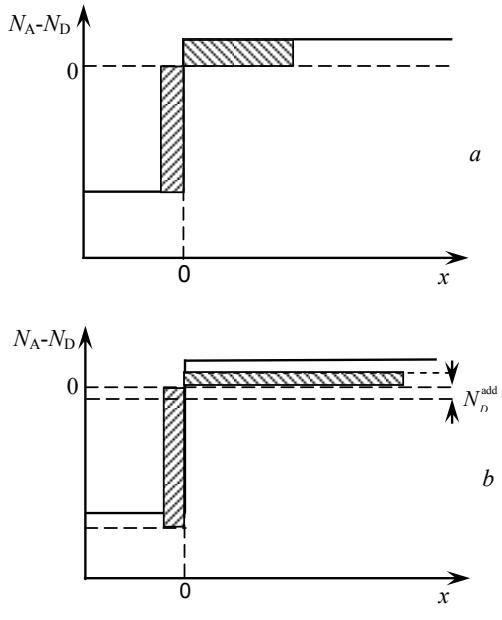

Fig. 5 The donors and acceptors distributions in a local section of p-n junction, which is responsible for the surface breakdown: *a*) — in dry air: *b*) — in wet ammonia vapors. The dashed areas correspond to the depletion region.

If an opposite to (3) inequality takes place in the non-homogeneity, an increase in the local donor concentration, due to donor molecules adsorption, lowers the breakdown voltage.

The samples of Si and GaAs p-n junctions with the breakdown located in the crystal bulk, as well as those with the breakdown voltage, enhanced by donor molecules adsorption, can be used as water- and ammonia vapors sensors, which can work at reverse biases, having higher sensitivity, than at forward biases.

The (absolute, current-) sensitivity of a gas sensor can be defined as

$$S_I = \Delta I/\Delta P, \qquad 6)$$

where ΔI is the change in the current (at a fixed voltage), which is due to a change ΔP in the corresponding gas partial pressure [10]. An analysis of the data in figs 2 and 3 yields for the maximum sensitivities of the corresponding GaAs and Si p-n junctions to ammonia vapors values of 60 μAPa^{-1} and 20 μAPa^{-1}, respectively.

4. CONCLUSIONS

The reverse bias is preferable for the gas sensors on Si and GaAs p-n junctions, as far as it provides a higher gas sensitivity, than the forward bias. The upper limit for the reverse bias voltage is due to breakdown voltage, which can depend on the partial pressure of the investigated vapors.

A simple model is proposed to explain the dependence of the p-n junction breakdown voltage on the ammonia partial pressure in the ambient atmosphere. In terms of this model the adsorbed ammonia molecules produce ionized donor centers, that partly compensate acceptors in local surface non-homogeneities, which are responsible for the breakdown. Depending on the donor- and acceptor local concentrations, this can result in either decrease or increase of the breakdown voltage.

The behavior of the breakdown voltage in ammonia vapors can be used for diagnostics of surface non-homogeneities in p-n junctions. Such diagnostics can be applied to a choose of samples, which can work as gas sensors under reverse biases, having higher sensitivity.

REFERENCES

1. Ptashchenko O. O., Artemenko O. S., Ptashchenko F. O. Vliyanie gazovoi sredy na poverhnostnyi tok v p-n geterostrukturakh na osnove GaAs-AlGaAs // Fisika i khimiya tverdogo tila. — 2001. — V. 2, № 3. — P. 481 — 485.
2. Ptashchenko O. O., Artemenko O. S., Ptashchenko F. O. Vplyv pariv amiaku na poverkhnevyi strum v p-n perekhodakh na osnovi napivprovidnykiv A^{3}B^5 // Journal of physical studies. — 2003. — V. 7, № 4. — P. 419 — 425.
3. Ptashchenko O. O., Artemenko O. S.,

Dmytruk M. L. et al. Effect of ammonia vapors on the surface morphology and surface current in p-n junctions on GaP. // Photoelectronics. — 2005. — No. 14. — P. 97 — 100.
4. Ptashchenko F. O. Effect of ammonia vapors on surface currents in InGaN p-n junctions. // Photoelectronics. — 2007. — No. 17. — P. 113-116.
5. Ptashchenko F. O. Vplyv pariv amiaku na poverkhnevyi strum u kremniyevykh p-n perekhodakh // Ptashchenko F. O. Visnyk ONU, ser. Fizyka. — 2006. — V. 11, №. 7. — P. 116-119.
6. Ptashchenko O. O., Ptashchenko F. O., Yemets O. V. Effect of ammonia vapors on the surface current in silicon p-n junctions. // Photoelectronics. — 2006. — No. 16. — P. 89-93.
7. Ptashchenko O. O., Ptashchenko F. O., Yemets O. V. Effect of ambient atmoswphere on the surface current in silicon p-n junctions // Photoelectronics. — 2009. — No. 18. — P. 28 — 32.
8. Ptashchenko O. O, Ptashchenko F. O. Gil'mutginova V. R., Dovganyuk G. V., Bogdan O. V. Effect of water- and ammonia vapors on the breakdown of *p-n* junctions // Sensor Electronics and Microsystem Technologies (SEMST-5). Odessa, June 4-8, 2012. Abstracts of the Reports. — P. 81.
9. Sze S. M. Physics of Semiconductor Devices. V. 1. — New York: A. Wiley-Interscience Publication, 1981. — 456 p.
10. Vashpanov Yu. A., Smyntyna V. A. Adsorbtsionnaya chuvstvitel'nost' poluprovodnikov. — Odessa: Astroprint, 2005. — 216 p.

UDC 621.315.592

O. O. Ptashchenko, F. O. Ptashchenko, V. R. Gilmutdinova, G.V Dovganyuk

EFFECT OF AMMONIA VAPORS ON THE BREAKDOWN CHARACTERISTICS OF Si AND GaAs P-N JUNCTIONS

Summary

The influence of ammonia and water vapors on *I-V* characteristics of the reverse currents in Si and GaAs p-n junctions was studied. At most of the studied samples, the ammonia- and water vapors lover the breakdown voltage. At some devices an opposite effect was observed. This difference is due to dominance of different surface centers, which have donor or acceptor properties. And some p-n junctions exhibit a fixed breakdown voltage independently on the presence of ammonia and water vapors. This is due to the bulk location of the breakdown in these samples. Thus, the influence of ammonia vapors on the breakdown voltage provides some information on the localization of the breakdown and on the charge state of surface centers.

Key words: p-n junction, gas sensor, reverse current, breakdown voltage, surface center.

УДК 621.315.592

О. О. Птащенко, Ф. О. Птащенко, В. Р. Гільмутдінова, Г. В. Довганюк

ВПЛИВ ПАРІВ АМІАКУ НА ХАРАКТЕРИСТИКИ ПРОБОЮ P-N ПЕРЕХОДІВ НА ОСНОВІ Si ТА GaAs

Резюме

Досліджено вплив парів аміаку та води на вольт-амперні характеристики зворотних струмів у p-n переходах на основі Si та GaAs. В більшості досліджених зразків пари аміаку та води зменшують напругу пробою. На деяких зразках спостерігався зворотний ефект. Ця різниця обумовлена домінуванням різних поверхневих центрів, які мають донорні або акцепторні властивості. Деякі p-n переходи мають фіксовану напругу пробою незалежно від присутності парів аміаку та води. Дана поведінка обумовлена локалізацією пробою в об'ємі кристалу в таких зразках. Таким чином, вплив парів аміаку на напругу пробою дає інформацію про локалізацію пробою і про зарядовий стан поверхневих центрів.

Ключові слова: p-n перехід, газовий сенсор, зворотний струм, напруга пробою, поверхневий центр.

UDC 621.315.592

О. О. Птащенко, Ф. О. Птащенко, В. Р. Гильмутдинова, Г. В. Довганюк

ВЛИЯНИЕ ПАРОВ АММИАКА НА ХАРАКТЕРИСТИКИ ПРОБОЯ P-N ПЕРЕХОДОВ НА ОСНОВЕ Si И GaAs

Резюме

Исследовано влияние паров аммиака и воды на вольт-амперные характеристики обратных токов в p-n переходах на основе Si и GaAs. В большинстве исследованных образцов пары аммиака и воды уменьшают напряжение пробоя. На некоторых образцах наблюдался обратный эффект. Это различие обусловлено доминированием различных поверхностных центров, имеющих донорные либо акцепторные свойства. Некоторые p-n переходы имеют фиксированное напряжение пробоя независимо от присутствия паров аммиака и воды. Такое поведение обусловлено локализацией пробоя в объеме кристалла в таких образцах. Таким образом, влияние паров аммиака на напряжение пробоя дает информацию о локализации пробоя и о зарядовом состоянии поверхностных центров.

Ключевые слова: p-n переход, газовый сенсор, обратный ток, напряжение пробоя, поверхностный центр.

UDC 539.3

O. V. Hrabovskiy, A. M. Klimenko, D. V. Lisovenko

State Institute of Measuring Technique (Odessa), tel. 0977163525; lslvv@rambler.ru

CALCULATION PROCEDURE FOR THE QUANTUM-DIMENSIONAL SYSTEMS

Calculations of structural phase transitions B1 - B2 under pressure in halcogenids Alkali and Metals are carried out on the basis of approach of the local functional density theory, using as adjustment designing of amendments to potential by means of the electronic density received in self-coordinated calculation using approximation of local density. The results has interest for nanosystems.

The standard calculation procedure of the energy of zoned structure E_k (for example, [**1**]) is used. In special points of Brillion's zone equation the secular was solved

$$\left[\frac{1}{2}\left(\vec{k}+\vec{g}\right)^2 - E_n\left(\vec{k}\right)\right] C_{n,\vec{k}}(\vec{g}) + \sum_{\vec{g}'} W(\vec{k}+\vec{g},\vec{k}+\vec{g}')\, C_{n,\vec{k}}(\vec{g}') = 0, \quad (1)$$

where $C_{n,\vec{k}}(\vec{g})$ are factors of decomposition of pseudo-wave function as a number of plane waves

$$\varphi_{n,\vec{k}} = \sum_{\vec{g}} C_{n,\vec{k}}(\vec{g}) \left|\vec{k}+\vec{g}\right\rangle, \quad (2)$$

n is then number of a zone, **k** is a wave vector in the first Brilluon's zone, **g**, **g**¢ - are vectors of a return lattice. The Furies-image of potential $W(\mathbf{k_1}, \mathbf{k_2})$ includes Furies -images potentials such as: W_H — Hartree, W_{xc} — exchange-correlation, W_{BHS} [**2**] — pseudo-potential which is named as Bachelet — Hamann — Schlüter.

Full energy using the density functional theory (DFT) is represented as

$$E = \frac{1}{N}\sum_{\vec{k}} E_{\vec{k}} - E_H + E_{xc} + E_{es} + \alpha_1 z, \quad (3)$$

where N is a number of atoms of various grades in an elementary cell, energy Hartree

$$E_H = \frac{\Omega}{2}\sum_{\vec{g}} \frac{4\pi}{g^2}\left|\rho\left(\vec{g}\right)\right|^2, \quad (4)$$

The exchange-correlation contribution is the following

$$E_{xc} = \Omega \sum_{\vec{g}} \left[\varepsilon_{xc}\left(\vec{g}\right) - W_{xc}\left(\vec{g}\right)\right]\rho\left(\vec{g}\right), \quad (5)$$

where W is the volume of an elementary cell, $e_{xc}(\mathbf{g})$ is the density of exchange -correlation energy, r(**g**) is a Furies -image of electronic density, z is the average number of the valent electrons on atom, E_{es} is electrostatic energy.

Non Coulomb part of electron-ionic interaction is the following

$$\alpha_1 = \lim_{\vec{g}\to 0}\left\{ W_{BHS}^{loc}\left(\vec{g}\right) + \frac{8\pi z}{\Omega g^2}\right\}. \quad (6)$$

The local density functional theory (LDFT) is the standard approximation methods of calculation of exchange-correlation energy (5). And the same lacks of this approach [**3**] are well-known. From the point of view of research of polymorphism we shall note some of them: underestimation of the forbidden zone; understating of parameters of a lattice; different influence LDFT on the calculation of different conditions, that especially strongly affects the size of the forbidden zone and details of a structure of electronic zoned structure. Some lacks are peculiar directly LDFT, others result from DFT.

Recently a number of methods both avoiding application LDFT is offered, and trying to remove existing lacks of frameworks LDFT. Among the last we shall note self-action corrected (SAC) pseudo-potentials [**4**]. SAC eliminates not physical self-action of every electron and reduces energy filled orbitals. Received in this approach power functional is noninvariant at unitary transformation filled orbitals it is possible to design a set of decisions too. Thus p-orbitals of an anion practically do not change, however d-orbitals of a cation can strongly be changed. It is necessary to note, that distortion of zoned structure is connected as with p-d-hybridization, which wrong estimates using LDFT, and to a wrong calculation of s-conditions which form a bottom of a zone of conductivity. Special interest can be shown to halcogenids of calcium because in Ca still there are no d-electrons. Calculation results sometimes to bad enough convergence of results in settlement circuits both not taking into account, and taking into account elimination of p-d-hybridization. Thus, the iterative decision of the equation (1) insufficiently precisely describes the located conditions because of not physical self-actions. Entering SAC pseudo-potentials [**5**]:

$$V_{ps}^{SIC} = V_{BHS} - V_H\left[\rho^{at}\right] - V_{xc}\left[\rho^{at}\right], \qquad (7)$$

unitary repeat calculation for electronic density of separate atoms r^{at}. Such pseudo-potentials cannot be used in solid-state calculations because of long interaction of Coulomb tails which should be compensated to introduction additional composed $1/r_{loc}$, which shifts a power scale and it is taken into account only in area $r < r_{loc}$.

The addition of additional contributions to pseudo-potential, which action could be counted «is destroyed'» in part or completely application LDFT further it is modeled by fit procedure. These contributions are designed from the electronic density received in LDFT-calculation. On each step of iterative procedure the density changes in view of correction factor which depends on volume of an elementary cell. That part which in [**5**] is received from nuclear calculations is modeled and kept r_{loc} as the second fitting parameter.

For research of polymorphism the self-coordinated calculation in 80 points for each connection in an interval 0,4 W_0-1,2 W_0 with a step 0,01 W_0 where W_0 is the experimental volume of an elementary cell in structure B1 was carried.

Results of calculation were adjusted under the equation using Berch's condition

$$P = \frac{3}{2} B_0 \left[\left(\frac{\Omega_0}{\Omega} \right)^{7/3} - \left(\frac{\Omega_0}{\Omega} \right)^{5/3} \right], \qquad (8)$$

where P is pressure, B_0 is the volumetric module of compression at P=0, W is the volume of an elementary cell, W_0 is the volume of an elementary cell at P=0.In structure B1 the calculation of W_0 and B_0 are adjusted under the corresponding experimental information, in structure B2 parameters determined full energy E_{tot} and B_0. Table 1 represents equilibrium volumes of elementary cells W_0, volumetric modules of compression B_0, deviations DW_0 and DB_0 from the corresponding experimental values, arising basically because of the limited word length of the parameters, full of energy E_{tot} and volumes of elementary cells at phase transition B1-B2 for structure B1. Table 2 contains the same data for structure B2. Deviations only with known experimental data (see [**6,7**] where are resulted as well results of calculations of other authors) are specified. Designations of volumetric characteristics: $W_{0\,B1}$, $W_{0\,B2}$ — equilibrium volumes of elementary cells in structures B1 and B2; $W_{pt\,1}$, $W_{pt\,2}$ — volumes at pressure of phase transition in corresponding structures are geven

$$\Delta\Omega = \Omega_{0B1} - \Omega_{0B2}; \Delta\Omega_{B1} = \Omega_{0B1} - \Omega_{pt1}; \Delta\Omega_{B2} = \Omega_{0B2} - \Omega_{pt2}. \qquad (9)$$

Table 1. Results of calculation in structure B1.

Connection	Ω_0, (a.u.)^3	$\Delta\Omega_0/\Omega_0$, %	B_0, GPa	$\Delta B_0/B_0$, %	E_{tot}, Ry	Ω_{pt}, (a.u.)^3
CaO	98,12	+4,3	113,01	0,0	-17,071	72,44
SrO	115,59	-0,3	90,29	-0,8	-16,996	90,02
CaS	155,91	+0,1	63,78	-0,3	-10,830	113,30
SrS	183,92	-0,1	57,90	-0,2	-10,537	149,93
BaS	219,28	-0,2	52,65	+1,3	-11,056	197,13
CaSe	175,21	-0,1	53,70	+5,3	-9,870	126,65
SrSe	205,25	-0,1	44,62	-0,8	-9,685	167,86
BaSe	242,81	+0,1	39,18	+0,5	-9,357	215,83
SrTe	249,34	+0,1	40,77	+1,9	-8,638	206,17
BaTe	289,42	-0,1	38,03	+0,1	-8,430	263,15

Table 2. Results of calculation in structure B2.

Connection	E_{tot}, Ry	B_0, GPa	Ω_0, $(a.u.)^3$	Ω_{pt}, $(a.u.)^3$
CaO	-17,029	138,74	84,62	64,85
SrO	-16,972	120,32	101,65	84,59
CaS	-10,790	59,68	138,66	99,70
SrS	-10,517	65,65	158,64	131,89
BaS	-11,045	44,74	195,12	173,44
CaSe	-9,832	46,71	158,09	111,32
SrSe	-9,671	59,94	183,39	155,88
BaSe	-9,349	37,85	220,56	194,96
SrTe	-8,631	49,27	235,61	200,27
BaTe	-8,424	46,14	265,09	243,79

Conclusion. In structure B1 the calculation of W_0 and B_0 are adjusted under the corresponding experimental information, in structure B2 parameters determined full energy E_{tot} and B_0. Table 1 represents equilibrium volumes of elementary cells W_0, volumetric modules of compression B_0, deviations DW_0 and DB_0 from the corresponding experimental values, arising basically because of the limited word length of the parameters, full of energy E_{tot} and volumes of elementary cells at phase transition B1-B2 for structure B1. Table 2 contains the same data for structure B2. Deviations only with known experimental data (see [**6,7**] where are resulted as well results of calculations of other authors) are specified.

Reference

1. Kovalchuk V. V. Cluster modidfication of the semiconductor's heterostructur Kiev: Hi-Tech Press. — 2007. — 309 p.
2. Calculation of Molecules, Clusters and Solids with DFT-LDA Scheme / Blaudeck P., Freuenheim Th., Seifert G. and others. // J. Phys.: Condensed Matter. — 2012. — vol. 4. — P. 6368 — 6371.
3. Encyclopedia of Computational Chemistry, Eds. P. Schleyer, H. Schaefer, N. Handy. Wiley, New York, — 1998. — P. 10-455.
4. M. W. Schmidt, K. K. Baldrige, J. A. Boatz et al., General atomic and molecular electronic structure system // J. Comp. Chem. **14**, p. 1347-1363 (1999)
5. E. F. Vansant, P. Van der Voort, K. C. Vrancken, Characterisation and Chemical Modification of Silica Durfaces. Elsevier, Amsterdam. — 2005. — P. 212-218
6. J. R. Chelikowsky, J. C. Phillips, Chemical reactivity and covalent-metallic bonding of Si_n^+ (n=11-25) clusters // Phys. Rev. Lett. 63. — 1999. — P. 1655-1656.
7. J. M. Garcia-Ruiz, E. Louis, P. Meakin, L. M. Sander, Growth patterns in physical sciences and biology / In: NATO ASI Series B: Physics **304**, Plenum, New York, 2003. — 344 p.

UDC 539.3

O. V. Hrabovskiy, A. M. Klimenko, D. V. Lisovenko

CALCULATION PROCEDURE FOR THE QUANTUM-DIMENSIONAL SYSTEMS

Abstract

Calculations of structural phase transitions B1 – B2 under pressure in halcogenids Alkali and Metals are carried out on the basis of approach of the local functional density theory, using as adjustment designing of amendments to potential by means of the electronic density received in self-coordinated calculation using approximation of local density. The results has interest for nanosystems.

Key words: phase, transition, density, optics

УДК 539.3

О. В. Грабовський, А. М. Клименко, Д. В. Лісовенко

РОЗРАХУНКОВА ПРОЦЕДУРА ДЛЯ КВАНТОВО-РОЗМІРНИХ СИСТЕМ

Резюме

Представлені результати розрахунку структурних параметрів фазових переходів типу B1 – B2 під тиском у халькогенідах лужних металів. Значення отримані у наближенні функціоналу електронної густини. Використано підгоночні параметри до потенціалів взаємодії щодо усереднення розподілу електронної густини за самоузгодженою схемою. Результати мають інтерес для наносистем.

Ключові слова: фаза, переходи, густина, оптика

УДК 539.3

О. В. Грабовский, А. М. Клименко, Д. В. Лисовенко

РАССЧЕТНАЯ ПРОЦЕДУРА ДЛЯ КВАНТОВО-РАЗМЕРНЫХ СИСТЕМ

Резюме

Представлены результаты расчетов структурных параметров фазовых переходов типа B1 – B2 под давлением в халькогенидах щелочных металлов. Значения получены в приближении функционала электронной плотности. Использованы подгоночные параметры к потенциалам взаимодействия для усреднения распределения электронной плотности в сасосогласованной схеме. Результаты интересны для наносистем.

Ключевые слова: фаза, переходы, плотность, оптика

ІНФОРМАЦІЯ ДЛЯ АВТОРІВ НАУКОВОГО ЗБІРНИКА «PHOTOELECTRONICS»

У збірнику «Photoelectronics» друкуються статті, які містять результати наукових досліджень та технічних розробок у таких напрямках:

- Фізика напівпровідників, гетеро- і низькорозмірні структури;
- Фізика мікроелектронних приладів;
- Квантова оптика і спектроскопія ядер, атомів, молекул та твердих тіл;
- Оптоелектроніка , квантова електроніка і сенсоріка;
- Фотофізика ядра, атомів, молекул;
- Взаємодія інтенсивного лазерного випромінювання з ядрами, атомними системами, речовиною.

Збірник включено до Переліку спеціальних видань ВАК України з фізико-математичних та технічних наук.

Рукописи надсилаються на адресу: відповід. секретарю Куталовій М. І., вул. Пастера, 42, Одеський національний університет ім.І. І. Мечникова, м. Одеса, 65026, http://www. photoelectronics.onu.edu.ua

Верстка — Карличук О. І.

Підп.до друку 27.12.2012. Формат 60×84/8. Гарн. Таймс. Умов.-друк.арк. 8,2. Тираж 100 прим.
Замов. № 563

Видавець і виготовлювач
«Одеський національний университет»
Свідоцтво ДК № 4215 від 22.11.2011 р.

65082, м. Одеса, вул. Єлісаветинська, 12, Україна
Тел.: (048) 723 28 39, e-mail: druk@onu.edu.ua